PB-250 545

THE HELICAL BEND COMBINED SEWER OVERFLOW REGULATOR

Richard H. Sullivan, et al

American Public Works Association

Prepared for:

Municipal Environmental Research Laboratory

December 1975

DISTRIBUTED BY:

NTIS
National Technical Information Service
U. S. DEPARTMENT OF COMMERCE

PB 250 545

REPRODUCED BY
NATIONAL TECHNICAL
INFORMATION SERVICE
U. S. DEPARTMENT OF COMMERCE
SPRINGFIELD, VA. 22161

RESEARCH REPORTING SERIES

Research reports of the Office of Research and Development, U.S. Environmental Protection Agency, have been grouped into five series. These five broad categories were established to facilitate further development and application of environmental technology. Elimination of traditional grouping was consciously planned to foster technology transfer and a maximum interface in related fields. The five series are:

1. Environmental Health Effects Research
2. Environmental Protection Technology
3. Ecological Research
4. Environmental Monitoring
5. Socioeconomic Environmental Studies

This report has been assigned to the ENVIRONMENTAL PROTECTION TECHNOLOGY series. This series describes research performed to develop and demonstrate instrumentation, equipment and methodology to repair or prevent environmental degradation from point and non-point sources of pollution. This work provides the new or improved technology required for the control and treatment of pollution sources to meet environmental quality standards.

This document is available to the public through the National Technical Information Service, Springfield, Virginia 22161.

TECHNICAL REPORT DATA

(Please read Instructions on the reverse before completing)

1. REPORT NO.
EPA-600/2-75-062

2.

3. RECIPIENT'S ACCESSION NO.
PB250545

4. TITLE AND SUBTITLE
The Helical Bend Combined Sewer Overflow Regulator

5. REPORT DATE
December 1975 (Issuing Date)

6. PERFORMING ORGANIZATION CODE

7. AUTHOR(S)
Richard H. Sullivan, Ralph R. Boericke, Morris M. Cohn, George Galina, Carl Koch, Fred E. Parkinson, T.M. Prus-Chacinski, James E. Ure

8. PERFORMING ORGANIZATION REPORT NO.

9. PERFORMING ORGANIZATION NAME AND ADDRESS

American Public Works Association
1313 East 60th Street
Chicago, Illinois 60637

10. PROGRAM ELEMENT NO. 1BB034
ROAP 21 ASY; TASK 107

11. CONTRACT/NO.
68-03-0272

12. SPONSORING AGENCY NAME AND ADDRESS

Municipal Environmental Research Laboratory
Office of Research & Development
U.S. Environmental Protection Agency
Cincinnati, Ohio 45268

13. TYPE OF REPORT AND PERIOD COVERED
Final

14. SPONSORING AGENCY CODE
EPA-ORD

15. SUPPLEMENTARY NOTES

16. ABSTRACT

A design procedure and method to calculate settleable solids retention efficiency has been prepared for a combined sewer overflow regulator, using the principle of developing helical flow in an enlarged, curved extension of a sewer. A curved side overflow weir is used to draw off the clarified combined sewer overflow.

Hydraulic and mathematical model studies were used in developing the helical flow concept and the design procedure. The reports of each model study are included.

The helical bend principle was originally investigated by Dr. Prus-Chacinski of London, England. A *second generation* regulator was constructed in 1971 in Nantwich, England. The present study modified the design to conform to American wastewater conditions and practices.

It was found that the helical bend combined sewer overflow regulator is capable of higher removal efficiencies with less hydraulic head loss than the swirl concentrator regulator, although the overall length of the helical unit appears to make it more expensive than the swirl concentrator.

The helical bend regulator requires the use of only a mechanical outlet gate and cleaning facilities; otherwise it is essentially non-mechanical.

This report is submitted by the American Public Works Association in partial fulfillment of Contract No. 68-03-0272, between the U.S. Environmental Protection Agency and the American Public Works Association.

17. KEY WORDS AND DOCUMENT ANALYSIS

a. DESCRIPTORS	b. IDENTIFIERS/OPEN ENDED TERMS	c. COSATI Field/Group
Combined sewers Overflows Storm sewers	Combined sewer overflow *Combined sewer regulator *Helical flow *Secondary motion Combined sewer overflow treatment	13B

18. DISTRIBUTION STATEMENT
RELEASE TO PUBLIC

19. SECURITY CLASS *(This Report)*
UNCLASSIFIED

20. SECURITY CLASS *(This page)*
UNCLASSIFIED

21. NO. OF PAGES
138

22. PRICE
$6.00-2.25

EPA Form 2220-1 (9-73)

PRICES SUBJECT TO CHANGE

☆ U.S. GOVERNMENT PRINTING OFFICE: 1975-657-695/5347 Region No. 5-11

EPA-600/2-75-062
December 1975

THE HELICAL BEND COMBINED SEWER OVERFLOW REGULATOR

By
Richard H. Sullivan
Ralph R. Boericke
Morris M. Cohn
George Galina
Carl Koch
Fred E. Parkinson
T. M. Prus-Chacinski
James E. Ure

American Public Works Association
Chicago, Illinois 60637

Contract No. 68-03-0272

Project Officer
Richard Field
Storm and Combined Sewer Section (Edison, N.J.)
Wastewater Research Division
Municipal Environmental Research Laboratory
Cincinnati, Ohio 45268

MUNICIPAL ENVIRONMENTAL RESEARCH LABORATORY
OFFICE OF RESEARCH AND DEVELOPMENT
U.S. ENVIRONMENTAL PROTECTION AGENCY
CINCINNATI, OHIO 45268

ia

DISCLAIMER

This report has been reviewed by the Municipal Environmental Research Laboratory, U.S. Environmental Protection Agency, and approved for publication. Approval does not signify that the contents necessarily reflect the views and policies of the U.S. Environmental Protection Agency, nor does mention of trade names or commercial products constitute endorsement or recommendation for use.

FOREWORD

Man and his environment must be protected from the adverse effects of pesticides, radiation, noise and other forms of pollution, and the unwise management of solid wastes. Efforts to protect the environment require a focus that recognizes the interplay between the components of our physical environment – air, water, and land. The National Environmental Research Centers provide this multidisciplinary focus through programs engaged in

- studies on the effects of environmental contaminants on man and the biosphere, and
- a search for ways to prevent contamination and to recycle valuable resources.

This report on the Helical Bend Combined Sewer Overflow Regulator presents the basis of design for an effective device to limit pollution of receiving waters from combined sewer overflows. Improvement of the quality of the overflow while regulating the quantity is an important performance specification. The use of a nonmechanical device utilizing fluid dynamics is particularly valuable in light of the importance of energy conservation.

ABSTRACT

A design procedure and method to calculate settleable solids retention efficiency has been prepared for a combined sewer overflow regulator, using the principle of developing helical flow in an enlarged, curved extension of a sewer. A curved side overflow weir is used to draw off the clarified combined sewer overflow.

Hydraulic and mathematical model studies were used in developing the helical flow concept and the design procedure. The reports of each model study are included.

The helical bend principle was originally investigated by Dr. Prus-Chacinski of London, England. A *second generation* regulator was constructed in 1971 in Nantwich, England. The present study modified the design to conform to American wastewater conditions and practices.

It was found that the helical bend combined sewer overflow regulator is capable of higher removal efficiencies with less hydraulic head loss than the swirl concentrator regulator, although the overall length of the helical unit appears to make it more expensive than the swirl concentrator.

The helical bend regulator requires the use of only a mechanical outlet gate and cleaning facilities; otherwise it is essentially non-mechanical.

This report is submitted by the American Public Works Association in partial fulfillment of Contract No. 68-03-0272, between the U. S. Environmental Protection Agency and the American Public Works Association.

TABLE OF CONTENTS

Page
Abstract iv
Section I Conclusions, Recommendations and Overview of the Studies 1
Section II The Study 5
Section III Design Factors for Helical Bend Regulator Separator Facilities 18
Section IV Implementation 46
SectionV Glossary of Pertinent Terms - Helical Bend Report 47
Section VI References 50
Appendix A Hydraulic Model Study 51
Appendix B Mathematical Model Study 81
Nomenclature 114
Appendix C Background Information on the Helical Bend 116

TABLES

Page
1. Velocities in Transitions 24
Helical Bend Regulator (Design Example) 28-32
2. Helical Bend Regulator Dimensions 33
3. Site Dimensions and Areas for Helical Bend and Swirl Concentrator Regulators 35
4. Typical Head Losses in Helical Bend and Swirl Concentrator Regulators 37
5. Construction Cost of Helical Bend Regulator 40
6. Swirl Concentrator Dimensions 41
7. Construction Cost – Swirl Concentrator 42
8. Comparison of Construction Costs – Helical Bend and Swirl Concentrator Regulators 44
9. Recovery Results – Modifications 1-8 57
10. Recovery Results – Modifications 9, 10, 12, 14-18 59
11. Recovery Efficiency at Various Bend Radii 114

FIGURES

Page
1. Isometric View of Helical Bend Regulator 3
2. Helical Bend Regulator, 1967 7
3. Photograph of Nantwich, England, Helical Bend Regulator 8
4. Helical Bend Regulator – Form 3 (Model Layout) 9
5. Discharge Measuring Weirs 10
6. Prototype Gradation for Grit and Settleable Organic Material 12
7. Particle Settling Velocities for Solids in Still Water 13
8. Gradation Curves for Gilsonite® and Petrothene® Used in Model 14
9. Prototype Grit Sizes Simulated by Gilsonite and Petrothene in Model 15
10. Prototype Settleable Organic Material Sizes Simulated by Gilsonite and Petrothene in Model 16
11. Predicted Prototype Grit Recovery vs Design Flowrate Ratio 18
12. Predicted Prototype Settleable Organic Material Recovery vs Design Flowrate Ratio 18
13. Recommended Transition Profile 19
14. Effect of Transition Slope 19
15. Design Flowrate vs Inlet Diameter 21
16. Recommended Plan Layout 22
17. Water Level in Regulator Above Weir 23
18. Recommended Cross Sections 25
19. Spillway Channel Profile 27
20. Site Requirements 34
21. Typical Cross Section – Helical Bend Regulator 38
22. Estimated Construction Costs – Helical Bend and Swirl Concentrator Regulators 43
23. Predicted Separation Efficiency vs Settling Velocity at Several Flowrates 45
24. Downstream View of Model 52
25. Upstream View of Model 52
26. Solids Injection Vibrator 53
27. Top and Bed Flow Angles 54
28. Floor Flow Angle Measuring Equipment 54
29. Bed Angle Relationships for Straight-Through Flow 55
30. Modification 6 – Tests 23-29 56
31. Modification 4 – Tapered Outlet 58
32. Modification 5 – Narrow Inlet 2D Wide 58
33. Modification 5 – Tapered Bend 58
34. Minimum Width Inlet, 1.5D Wide 59
35. Narrowest Bend, 1.5D Wide 59
36. Modification 9 – Tests 38-39 60
37. Modification 10 – Tests 40-41 60
38. Modification 12 – Tests 46-47 60
39. Modifications 14 & 15 – Tests 53-55 60
40. Petrothene Recovery in Model as Function of Bend Channel Width 61
41. Modifications 17 & 18 – Tests 60-61 61
42. Inlet Configurations Tested 62
43. Transition 10D Long 62
44. Petrothene Recovery in 60° Bend for Various Inlet Configurations 63
45. Transition 15D Long 64

FIGURES (Continued) Page

46. Scum Board Locations Tested 64
47. Petrothene Recovery in 50° Bend for Various Scum Board Locations 65
48. Petrothene Recovery in 60° Bend for Various Scum Board Locations 65
49. Floor Flow Angles with Scum Board D/2 Deep 65
50. Floor Flow Angles with Scum Board D/6 Deep 66
51. Cross Section of Offset Weir in Bend 66
52. 60° Bend with Offset Weir 67
53. Upstream View of Scum Board on Offset Weir 67
54. Downstream View of Bend and Offset Weir 67
55. Scum Board on Offset Weir 67
56. Petrothene Recovery in 60° Bend with Offset Weir
and Various Inlet Configurations 68
57. Proving Tests Layout 69
58. Solids Recovery in Model 70
59. Velocity Contours on 0° Cross Section 70
60. Velocity Contours on 10° & 20° Cross Sections 71
61. Velocity Contours on 30° & 40° Cross Sections 72
62. Solids Concentration Sampling Jig 73
63. Simultaneous Filling of Solids Sampling Bottles 73
64. Suspended Solids Concentrations on 0° Cross Section 74
65. Suspended Solids Concentrations on 10° & 20° Cross Sections 75
66. Suspended Solids Concentrations on 30° & 40° Cross Sections 76
67. Distribution of Solids Which Escape Over Weir 77
68. Floor Flow Angles 78
69. Comparative Average Floor Angles for Recommended Layout 80
70. Cylindrical Coordinate System 82
71. Definition of Surface Shape in Channel Cross Section 83
72. Coordinate Transformation 85
73. Mathematical Representation of Channel Cross Section 87
74. Channel Cross Section in Cartesian Coordinates 88
75. Transformation of Channel Cross Section to Rectangular Region 89
76. Rotation of Velocity Components 90
77. Computational Grid in Transformed Space 91
78. Fluid Flow Solution Summary 92
79. Location of Computational Grid Points for
Concentration Field Calculation 95
80. Particle Flow Solution Summary 97
81. Comparison of Measured and Predicted Velocity Profiles at 0° 103
82. Comparison of Measured and Predicted Velocity Profiles at 20° 104
83. Comparison of Measured and Predicted Velocity Profiles at 40° 105
84. Comparison of Measured and Predicted Flow Angles on Bottom
Along Channel Centerline 106
85. Measured Values of Relative Petrothene Concentration at 0° 107
86. Comparison of Measured and Predicted Relative
Petrothene Concentration at 20° 108

FIGURES (Continued) Page

87. Comparison of Measured Values of Relative Petrothene Concentration at 40° 109
88. Mass Flux Over Weir as a Function of Angular Position 111
89. Cumulative Mass Flux Over Weir as a Function of Angular Position 111
90. Comparison of Predicted and Measured Recovery Efficiencies at Discharges Greater than the Design Value 0.85 m^3/sec (Q_D = 30 cfs) 112
91. Predicted Separation Efficiency versus Settling Velocity at Several Flow Rates 113
92. Alternative Design for Future Investigation 121

ACKNOWLEDGEMENTS

The American Public Works Association is deeply indebted to the following persons and their organizations for the services they have rendered to the APWA Research Foundation in carrying out this study for the U. S. Environmental Protection Agency.

PROJECT DIRECTOR

Richard H. Sullivan

CONSULTANTS

Dr. Morris M. Cohn, P.E., Consulting Engineer
Paul B. Zielinski, P.E.

C. H. DOBBIE & PARTNERS

Dr. T. M. Prus-Chacinski

ALEXANDER POTTER ASSOCIATES, CONSULTING ENGINEERS

Morris H. Klegerman, P.E.
James E. Ure, P.E.

LA SALLE HYDRAULIC LABORATORY, LTD.

F. E. Parkinson
George Galina

GENERAL ELECTRIC COMPANY

Dr. Ralph R. Boericke
Dr. Carl Koch

U. S. ENVIRONMENTAL PROTECTION AGENCY

Richard Field, P.E., Project Officer, Chief, Storm & Combined
Sewer Section (Edison, New Jersey)

AMERICAN PUBLIC WORKS ASSOCIATION

Board of Directors

Herbert A. Goetsch, President
Ray W. Burgess, Vice President
Erwin F. Hensch, Immediate Past President
Robert D. Bugher, Executive Director

Jean V. Arpin
John T. Carroll
Donald S. Frady
Lambert C. Mims
James J. McDonough
Robert D. Obering
John J. Roark
James E. McCarty
Kenneth A. Meng
Frank R. Bowerman
Wesley E. Gilbertson
Rear Admiral A. R. Marschall

APWA RESEARCH FOUNDATION

Board of Trustees

Samuel S. Baxter, Chairman
Ross L. Clark, Vice Chairman
Robert D. Bugher, Secrtary-Treasurer
Richard H. Sullivan, General Manager

Fred J. Benson
John F. Collins
Jean L. DeSpain
Richard Fenton
W. C. Gribble
John A. Lambie
James E. McCarty
Marc C. Stragier

SECTION I

CONCLUSIONS, RECOMMENDATIONS AND OVERVIEW OF THE STUDIES

Conclusions

1. A helical flow device has been developed and demonstrated, as an expanded section of a combined sewer line, for the dual purpose of removing settleable suspended solids from combined sewer overflows, and to serve as an overflow spill weir regulator for the discharge of clarified effluent to receiving waters or to retention and/or treatment facilities.

2. The helical bend regulator can operate efficiently as a flow-through, nonmechanical channel bend device in removing settleable solids and, thereby, reducing the pollutional impact of periodic overflow incidents.

3. The solids removed from the combined sewer flows may tend to shoal in the deep invert section of the helical bend chamber during storm flow conditions.

4. Model tests showed that these deposits remain dormant during such high-flow periods and are then moved or self-scoured out of the invert by dry-weather flows and discharged, via a foul sewer outlet, to the interceptor sewer and downstream wastewater treatment works. Similar conditions should prevail in prototype helical bend installations but the scale representation of combined sewer solids is not confirmed and the self-scouring action experienced in the model studies must be demonstrated under prototype operations. (*Note:* A prototype unit in Nantwich, England has not experienced the buildup of solids during operation.)

5. Washing or flushing facilities, and regular maintenance procedures should be provided in prototype helical bend installations until the removal of solids deposits by dry-weather scouring action has been confirmed.

6. Uniformity of flow as it enters the helical bend section of the regulator-concentrator facility is of utmost importance to the successful operation of the secondary flow actions induced in the chamber.

7. A straight section of conduit, ahead of the helical bend section, is required to assure effective solids recovery rates. This straight section length should be five times the diameter of the inlet sewer (5D).

8. If no straight section is provided, the recovery rates for organic solids in the helical bend will be reduced approximately 10 percent below the efficiency attained with the 5D straight approach line.

9. Beyond this 5D straight approach length, greater lengths will have minimal effect on solids removal efficiencies. A 10D straight section will further improve removals by less than five percent.

10. Grit recoveries will not be greatly affected by changes in the length of the straight approach section.

11. The straight horizontal transition length from the inlet pipe diameter, out to the full helical bend channel width of three times the inlet diameter, should be at least 15 times the inlet diameter.

12. The transition section must be roofed or covered to provide the proper flow conditions for secondary motion and helical action in the bend section. The cover or roof should rise from the crown of the inlet pipe to the hydraulic gradient at the end of the transition section.

13. The drop through the structure can be confined to the slope of the incoming sewer; although greater slopes to encourage self-scouring should not present any problems.

14. The length of the bend is determined by the inlet diameter. A radius of 16D should be used.

15. A 60 degree segment is adequate to develop the full effects of the helical flow principle.

16. Most of the floatable solids entering the helical bend regulator will be retained in the chamber by the scum board or dip plate, located ahead of the overflow weir, during storm flow conditions. As the discharge rate decreases and the surface of the combined

flow in the helical chamber recedes, the floatables will drop with the flow level and be removed with the channel bottom deposits during dry-weather flow.

17. A design procedure has been developed for use in dimensioning the geometrical configuration of full-scale prototype applications having specific flow rates, solids characteristics, and percentages of dry-weather flows diverted to interceptor sewers and downstream treatment facilities. The design criteria are based on a maximum flow of three times dry-weather flow through the foul sewer outlet at the end of the bend section.

18. Mathematical techniques have been developed for computing the particle and liquid flowfields in open channel bends.

Recommendations

1. The hydraulic model studies and the computer-mathematical simulation of the helical bend combined sewer overflow regulator indicate that this *flash* method of solids removal, without use of mechanical appurtenances, can produce excellent efficiencies with reasonable size units in combined sewer systems. The results are so promising that they should be confirmed in a full-scale prototype installation at the earliest possible opportunity.

Such an installation in the field will provide confirmation of the pattern of solids deposition in the deeper channel portion of the helical bend, located along the inner circumference of the bend section, and of the ability of dry-weather flows in this restricted deep channel to self-scour the deposited solids into the foul sewer outlet.

The full-scale field prototype installation should be fully instrumented to record performance under actual combined sewer conditions. Facilities should be provided for sampling the stratified bed load of the inlet flow and the overflow by means of vertical arrays of sampling probes. The flow over the weir should be sampled at several locations to determine the distribution of solids lost with the overflow, as a function of position along the side weir length. A full regimen of laboratory control studies could be planned and instituted to explore the helical flow patterns created in the prototype unit under normal service conditions. Out of such a pilot prototype investigation will come operating experience that can assist in the application of this promising and economical device to meet the *2Q* challenge of effective regulator-overflow control – control of both quantity and quality of combined sewer discharges to receiving waters.

Overview

A study[1] conducted by the American Public Works Association (APWA) Research Foundation in 1969-70, Problems of Combined Sewer Facilities and Overflows, disclosed that combined sewer regulator-overflow devices on the American continent did little to improve the quality of liquid spills from these facilities into receiving waters. The environmental impact of these discharges into the nation's waters was characterized as a pollutional paradox in view of current concern over the secondary treatment and even higher degrees of purification of sewage and industrial processing wastewaters.

The findings of the 1969-70 investigation have catalyzed subsequent studies on how economical and efficient devices can be utilized to eliminate part of the suspended solids contained in admixed sewage storm flows in combined sewers prior to the wasting of major volumes into surface water sources. In short, the endeavors have been aimed at making such regulator-overflow facilities perform two functions: Control the flow rate of combined sewer overflows and improve the quality of such spill volumes.

A study[2] conducted by APWA, The Swirl Concentrator as a Combined Sewer Overflow Facility, described the development and demonstration of a nonmechanical swirl concentrator as an economical means of removing suspended solids from combined sewer overflow wastewaters.

To supplement the search for workable means of accomplishing the clarification of combined sewer overflows, and thereby

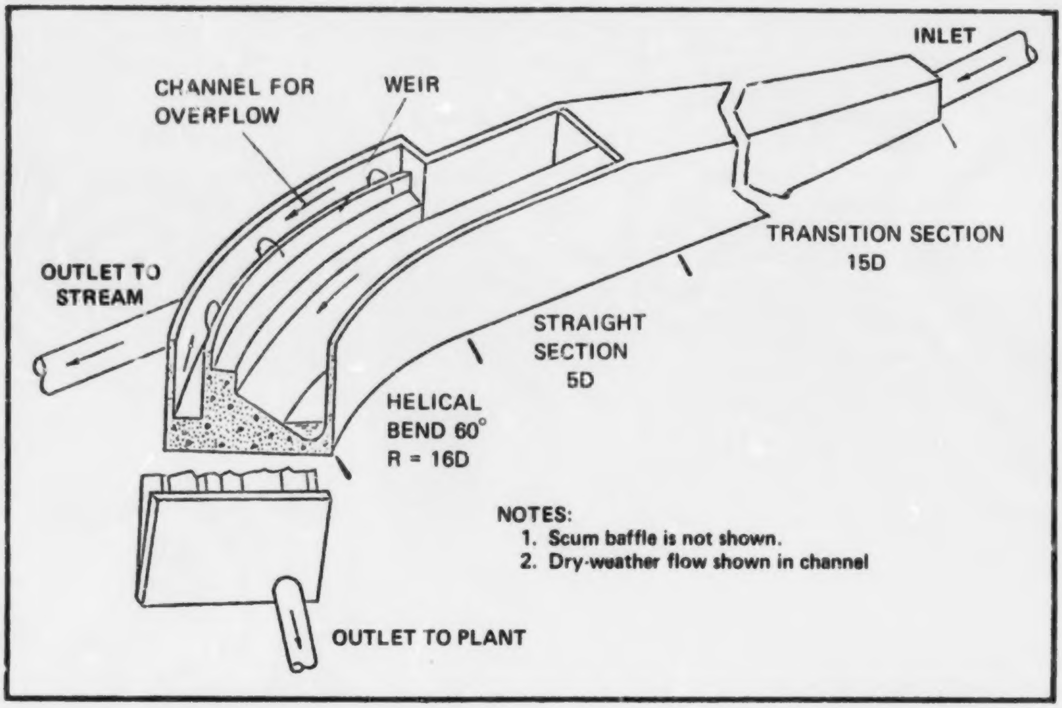

NOTES:
1. Scum baffle is not shown.
2. Dry-weather flow shown in channel

FIGURE 1 ISOMETRIC VIEW OF HELICAL BEND REGULATOR

reducing the pollution load imposed by such periodic discharges, the current study has investigated the feasibility of achieving the removal of solids from combined sewer flows by means of a helical bend incorporated into an expanded section of such a sewer system. This device would utilize the secondary flow patterns produced by helical hydraulic phenomena to deposit solids in the invert of a helical channel section, adjacent to the inner curve of the conduit, and to allow a clarified effluent to overflow a side spill weir for discharge to receiving waters or to retention and/or treatment facilities.

Figure 1. Isometric View of Helical Bend Regular, shows the important elements of the facility. The device may require only one mechanical part, a control on the outlet to allow a predetermined rate of flow to the interceptor sewer if this advanced type of positive control is desired.

Hydraulic model studies carried out at the LaSalle Hydraulic Laboratory at Montreal, Canada, and mathematical model-computer studies performed by the Re-entry and Environmental Systems Division of the General Electric Company at Philadelphia, Pennsylvania, have resulted in the development of a helical regulator-separator device. Searching investigations of the liquid and solids flow patterns through a helical bend section have been carried out, preceded by a roofed- or covered-transition section length 15 times the inlet sewer diameter, expanding the flow-through conduit to a diameter three times that of the inlet sewer followed by a straight-flow section ahead of the helical bend channel having a length of ten times the inlet pipe diameter.

The studies have demonstrated the efficacy of the helical bend principle in achieving a *flash* separation of solids from the combined sewer flow and the diversion of a *foul* flow of up to three times the dry-weather flow into the interceptor sewer and thence to downstream treatment facilities. Investigations have shown the ability of the helical separator to act as a nonmechanical overflow regulator by means of a side weir overflow arrangement along the outer radius of the treatment chamber.

The results of helical flow patterns for these purposes have been gratifying. They confirm and augment previous findings described by Dr. T. M. Prus-Chacinski in a thesis at the Imperial College of Science, London, England;[3] demonstrated in a prototype installation at Nantwich, England; and outlined in a consulting report to APWA by Dr. Prus-Chacinski as part of his advisory services in connection with the current study.

As a result of hydraulic and mathematical studies, basic design data have been evolved for use by designers in applying the helical regulator-separator to prototype installations in combined sewer systems.

SECTION II
THE STUDY

The study was designed to investigate the efficiency of pipe and channel bend configurations in separating suspended solids in combined sewer flows and diverting such concentrated solids to the fraction of the volume which is carried by the interceptor line to wastewater treatment facilities. The studies investigated the solids separation patterns induced by the helical motion established in the flow-through bend sections of pipe or channels, and the consequent clarification of the overflows from the helical device into receiving waters or into holding or treatment facilities for the overflow volumes.

The investigative procedures covered both hydraulic model configurations and results, and mathematical model evaluations.

Dr. T. M. Prus-Chacinski reported[4] at a 1967 Symposium on Storm Sewage Overflows sponsored by the Institution of Civil Engineers on the results of a study he had conducted utilizing secondary motions in a bend to separate solids from the moving flow of sewage. In recent years, Dr. Prus-Chasincki and the firm with whom he is associated, C. H. Dobbie and Partners, designed a combined sewer overflow regulator for the City of Nantwich, England. A hydraulic model study was conducted by the Mersey and Weaver River Authority. Financing of the construction was, in part, by the Construction Industry Research and Information Association.

At the initiation of this study, C. H. Dobbie and Partners were engaged to develop an initial design for the hydraulic model which would incorporate the tentative findings from the operation of the Nantwich unit and adapt the design to United States practices, i.e., to provide a maximum of three times dry-weather flow to downstream treatment facilities. Appendix C. Background and Preliminary Design, is the C. H. Dobbie and Partners report which established the essentially third generation configuration for the hydraulic and mathematical model tests.

The flow pattern phenomenon utilized in the helical bend principle involves liquid-solids separation which occurs when flow moves around a bend and creates secondary currents which tend to move the water surface toward the outside of the bend and to induce bottom current angles which move to the inside of the curve. This separation principle is well known in river sections where the deepest part of the channel is usually scoured on the outside of any bend and finer material is lifted by the bottom currents and deposited along the inside shoreline.

The hydraulic model developed for the present studies was intended to impose the opposite geometry from that experienced in a natural stream; the deepest section of the helical bend line was located at the inside circumference. The intent was to provide the deepest part of the bend cross section where the solids removed by the secondary flow would have opportunity to settle out and be swept by the bottom flow to the outlet end of the bend and thence to downstream wastewater treatment facilities.

Appendix C reviews the established facts about helical motion in single bends, the areas where uncertainty exists, and the basis for the initial design of the hydraulic model.

This study confirmed the findings outlined by Dr. Prus-Chacinski in a preliminary report to the American Public Works Research Foundation on the model of helical combined sewer overflow regulators. Selected points from Dr. Prus-Chacinski's report follow. They are of significance in the translation of the hydraulic and mathematical model findings into practical design guidelines. They are used to preface the design factors evolved by both the hydraulic and mathematical study personnel.

1. All bends investigated to date (1973) have not been longer than 180°.
2. It has been established that in such bends in rectangular channels prominent helical motion exists in the form of one helix, in which the direction of flow, about one-third of the depth near the bottom, is toward the inner wall; and in another, about two-thirds of the depth near the top is toward the outer wall.

3. The angle between the circumferential direction and the direction of the transverse flow is very much greater near the bed than near the surface; therefore, the resulting helix is assymetric and very much flattened toward the free surface.
4. In such a helix the strength of the helical motion in a rectangular channel is proportional to the angle of the direction of flow next to the bed.
5. Such a single helix changes the velocity distribution, both in vertical and in horizontal along the bend; around 60° to 80° of the bend the slow bed water is upturned to the top. There the velocity distribution is different than in a *normal* straight open channel: the maximum velocity occurs in the lower half of the depth.
6. Around the same region the pattern of helical flow changes (at least in a rectangular channel) and a second helix in the opposite direction starts to form at the outer wall. This second helix gradually grows towards the end of the bend 180° long.
7. Around the same region the area of maximum velocity across the channel (at least in a rectangular channel), which almost from the beginning of the bend is at the inner wall, shifts to the outer wall and remains there up to the end of a 180° long bend.
8. The maximum strength of the primary helix occurs at about 40° of the bend and decreases very slowly to the end of the 180° long bend.
9. The described pattern of the helical motion in a rectangular channel can exist only if the flow at the entry to the bend is completely free of any transverse currents. This is a fundamental requirement.
10. The strength of the helix is relatively insensitive to the velocity distribution across the channel at the entry to the channel (at least in a rectangular channel).
11. The strength of the initial helix is much more sensitive to the velocity distribution in the vertical at the entrance to the bend. The initial strength can be increased by artificially distorting the vertical velocity distribution at the entry to the bend in such a way that the velocity near the surface is increased.
12. The initial strength can be decreased by artificially depressing the maximum velocity in the vertical at the entry.
13. Such changes of the strength of the helical flow disappear around 60° to 80° of the bend; from there on, the motion returns to *normal* helical motion.
14. Introduction of an artificial helical flow at the entry to the bend can produce an infinite variety of patterns of helical motion. The strength of one helix can be slightly increased or decreased. Introduction of more than one helix at the entry to the bend can result in patterns of two or three helices. Such pattern persists for at least 45° along the length of the bend and probably for a greater length.
15. Helical flow similar in shape has been experimentally documented in the bends of rectangular channels with depth-to-width ratio from about 0.12 to about 1.0; triangular channel with the symmetrical apex and with the apex near to the outer wall; trapezoidal channels; parabolic channels; eliptical channels; semicircular channels; and rectangular channels with semicircular bottom. The strength of a primary single helix is probably the greatest in semicircular channels.

Figure 2, Helical Bend Regulator – Form 1, as investigated by Dr. Prus-Chacinski,[5] was presented at the 1967 Symposium. Figure 3, Helical Bend Regulator – Form 2, as investigated by the Mersey & Weaver River Authority is a photograph of the facility designed for Nantwich. Figure 4, Helical Bend Regulator – Form 3, as investigated by American Public Works Association, is the configuration chosen for the initial model tests. A review of these three figures reveals a change to simplicity of shape and an improved method of takeoff to the interceptor sewer to prevent the outlet from being plugged by rags and debris.

Starting with the configuration in Figure 4, concurrent hydraulic and mathematical model studies were conducted.

The basic structural features of significance in the helical bend model are: the inlet from the entrance sewer section to the device; the transition section from the inlet to the expanded cross section of the straight-run section ahead of the bend; the overflow side weir and scum board, or so-called dip plate; and the foul outlet for the concentrated solids removed in the secondary flow pattern, together with the means for controlling the amount of this underflow going to the treatment works.

The hydraulic model was constructed at the LaSalle Hydraulic Laboratory. Configuration changes and internal auxiliary flow control and effluent improvement modifications, as well as detailed studies of the helical flow patterns developed and the suspended solids removal efficiencies achieved, were studied. The report of the hydraulic model studies is presented as Appendix A to this report.

The mathematical model and computer simulation of the device was conducted by the General Electric Company. The report of the mathematical model study is presented as Appendix B to this report.

The ultimate purpose of both studies was to correlate and confirm findings by both hydraulic and mathematical means and to develop design criteria which will enable engineers to utilize the helical flow principle for solids removal from combined sewer flows and to properly regulate the overflow of clarified wastewater to receiving waters or points of retention and/or treatment. The design basis is presented in Section III.

Hydraulic Model Studies

The transition from the sewer line to the overall helical system was made of Plexiglas,® 20 diameters (20D) long to assure proper flow deceleration. This transition section was followed by a straight-flow Plexiglas section of 10D length to carry the flow to the start of the bend. It was built of Plexiglas, using a 2.44 m (8 ft) radius from the extension of the inlet pipe centerline. Since the model was developed to demonstrate the basic principles of the secondary motions created in the helical bend, the curvature was originally carried around through an angle of 120°. Side channels were provided on each side to accommodate the clear overflow discharge from either the inside or outside circumference of the bend. Control of either

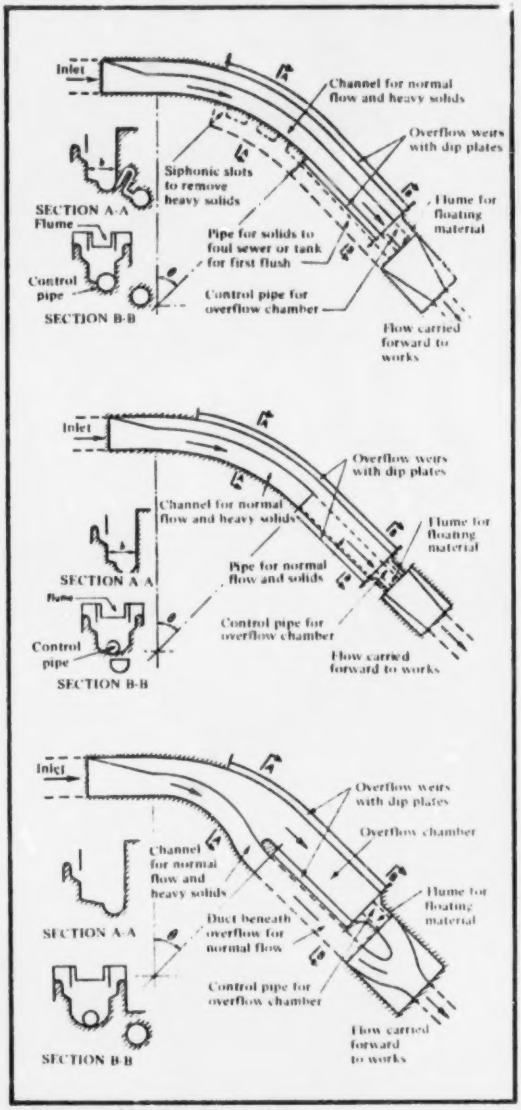
Inlet
Channel for normal flow and heavy solids
Overflow weirs with dip plates
Siphonic slots to remove heavy solids
SECTION A-A
Flume
Flume for floating material
Pipe for solids to foul sewer or tank for first flush
Control pipe
SECTION B-B
Control pipe for overflow chamber
Flow carried forward to works
Inlet
Overflow weirs with dip plates
Channel for normal flow and heavy solids
Flume for floating material
Pipe for normal flow and solids
SECTION A-A
Flume
Control pipe for overflow chamber
Control pipe
Flow carried forward to works
SECTION B-B
Inlet
Overflow weirs with dip plates
Overflow chamber
Channel for normal flow and heavy solids
Flume for floating material
Duct beneath overflow for normal flow
SECTION A-A
Control pipe for overflow chamber
Flow carried forward to works
SECTION B-B

Courtesy of Dr. Prus-Chacinski

FIGURE 2 HELICAL BEND REGULATOR, 1967
as presented in 1967 at the Symposium in London, England sponsored by the Institution of Civil Engineers

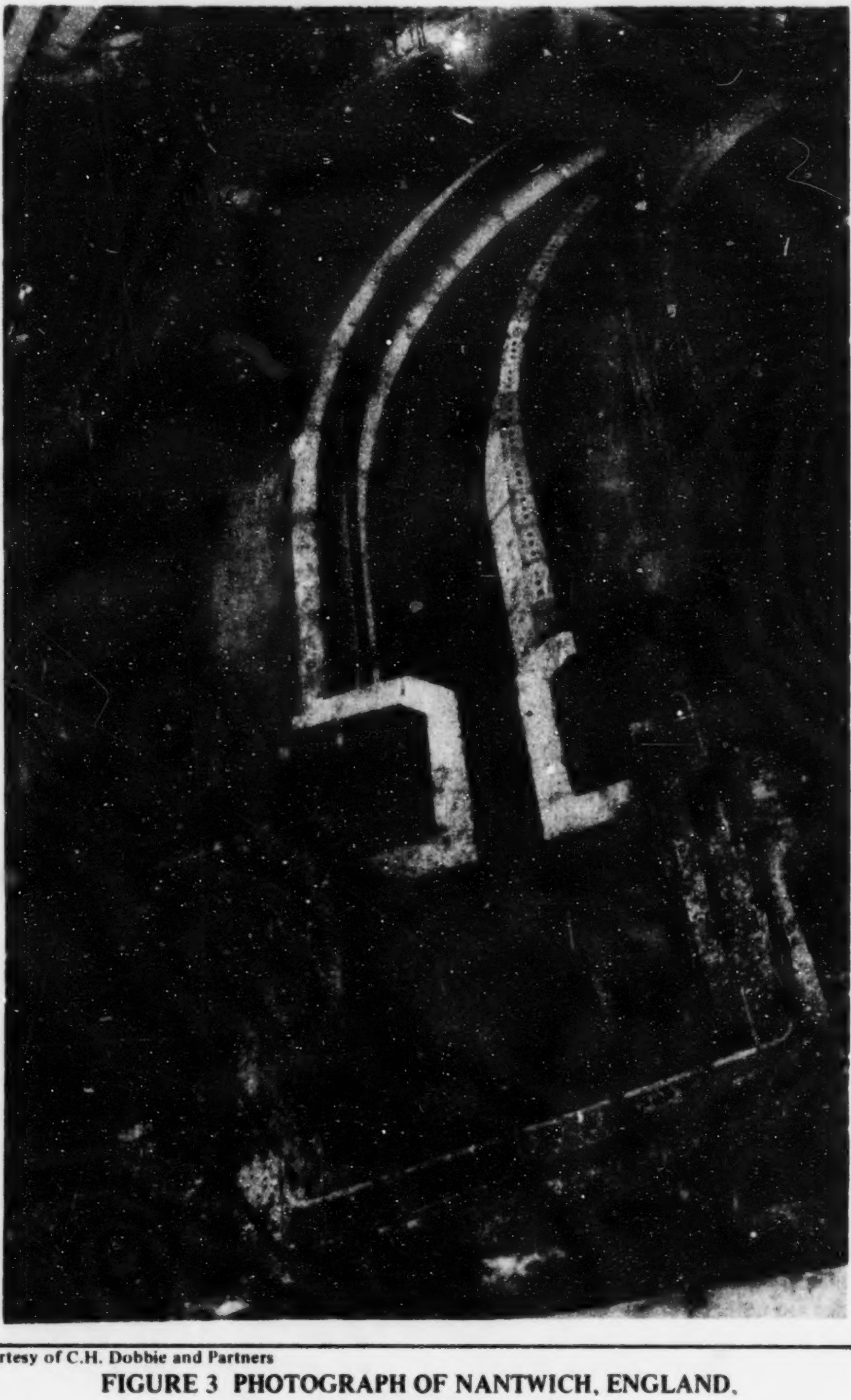

Courtesy of C.H. Dobbie and Partners

FIGURE 3 PHOTOGRAPH OF NANTWICH, ENGLAND, HELICAL BEND REGULATOR

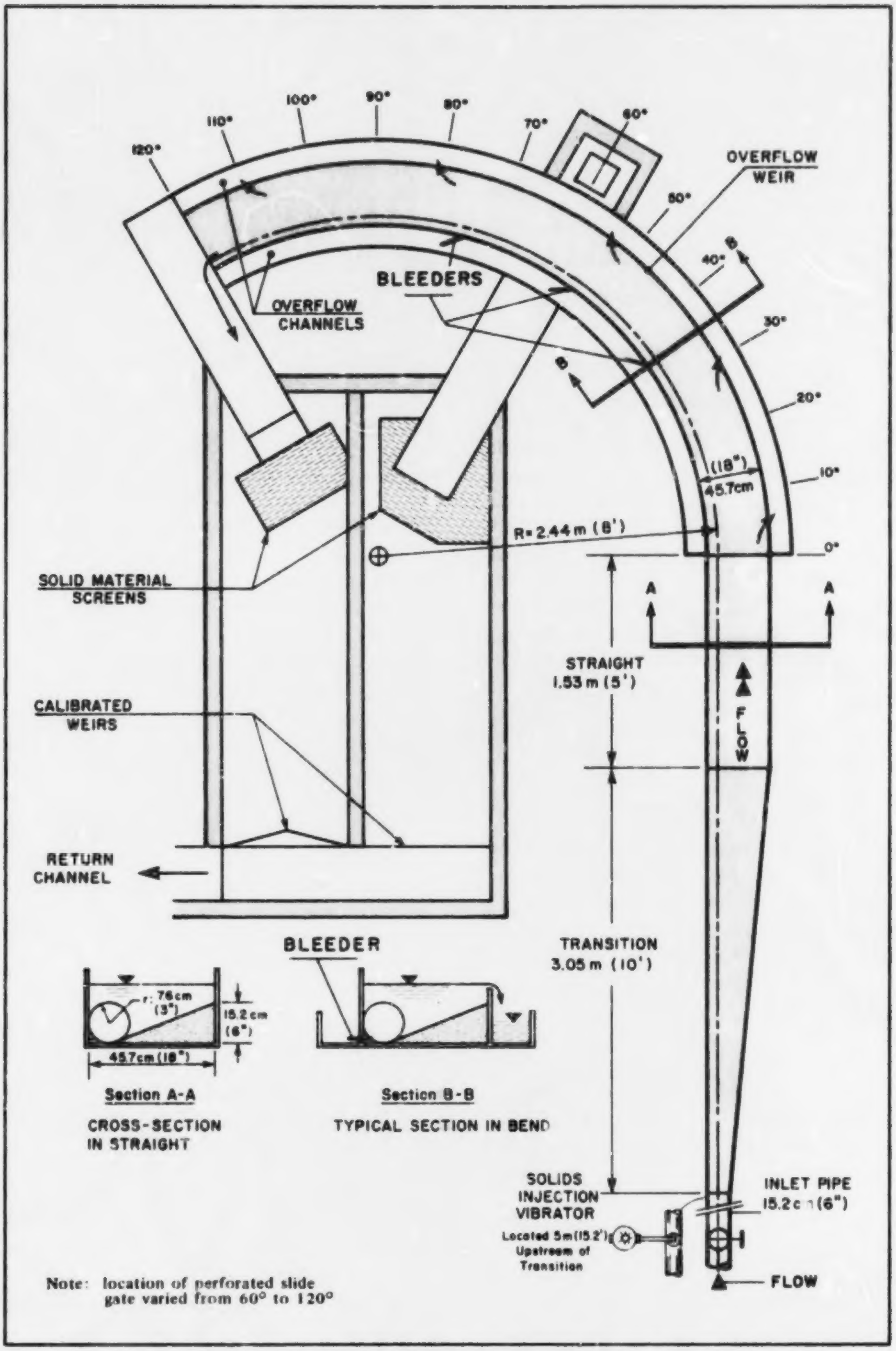

Note: location of perforated slide gate varied from 60° to 120°

FIGURE 4 HELICAL BEND REGULATOR – FORM 3 (Model Layout)

the entire flow through the bend, or just the small foul outflow was provided by a perforated slide gate at the 120° position.

The basic floor cross section inside the transition section, the straight section and the bend was constructed of polished cement mortar, as shown in Figure 4. The original layout could accommodate simple modifications of the Plexiglas overflow weirs for the purpose of changing their positions horizontally or their crest levels. Similar variations in scum board location and depth could be provided.

Unmeasured water flows entered the helical bend complex through the supply pipe which was fitted with a discharge control valve and equipment with which to inject predetermined amounts and types of solids whose removal characteristics and performance were to be studied. The overflow water was diverted to a calibrated Rehbock weir basin where water levels could be read and the rate of discharge determined. Similarly, the foul outflow from the bottom of the bend channel, containing the deposited solids, was diverted to a second basin for measurement over a small 90° V-notch weir. These control devices are shown in Figure 5, Discharge Measuring Weirs.

Injection of Process Black ink on the floor of the bend, applied with hand syringe, produced clearly defined traces of the bottom or floor flow angles which could be measured by means of a protractor. These trace tests demonstrated the presence of the anticipated helical secondary flow patterns.

Tests for the efficiency of solids separation in the helical flow pattern were performed in accordance with recognized standard methods. One liter of the selected model solids was introduced into the water supply via the supply line. This solids material entered the bend flow and was exposed to the separation process. Any solids that were swept over the overflow weir were captured on a screen in the measuring basin. The balance normally was retained as a deposit in the bend and recovered in the diversion basin when it was flushed from the bend section. Any solids contained in the foul outflow during the model run were also captured and retained in the collection chamber.

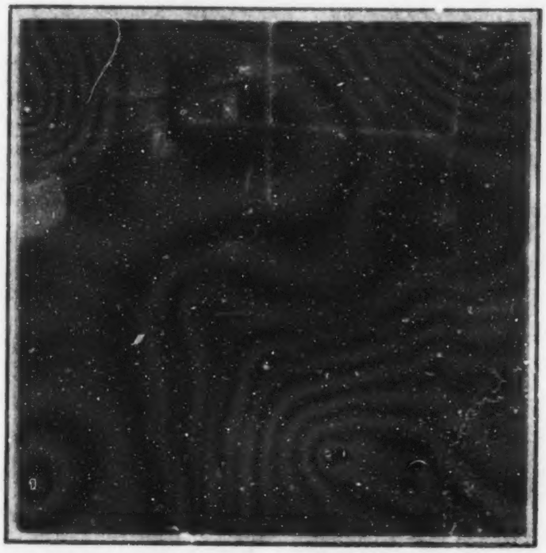

FIGURE 5 DISCHARGE MEASURING WEIRS

The volumes of the two fractions – the solids passing over the overflow weir and the solids contained in the foul outflow – were measured to determine if any material had been lost. The recovery rate, or efficiency of solids separation, was computed as the ratio of the solids retained in the bend compared with the original 1-liter input, expressed as a percentage.

The model scale selected for comparison with a rational prototype size was 1:6. The pertinent scale relations were:

Scale	1:6
Time	$1/\sqrt{6}$. = 1/2.45
Discharge	$1/6^{5/2}$ = 1/88

The prototype combined sewer overflow in the corresponding 91.5 cm (3 ft) sewer was computed at 0.85 m^3/sec (30 cfs) flowing full, which would correspond to 9.1 l/sec (0.339 cfs) in the model. To simplify operations in the model, a discharge of 10 l/sec (0.354 cfs) was used, giving a storm discharge of 0.88 m^3/sec (31.1 cfs). Selected discharges in the model were 10, 7.5, 5, and

2.5 l/sec (0.354, 0.265, 0.177 and 0.088 cfs), corresponding to 0.88, 0.66, 0.44 and 0.22 m^3/sec (31.1, 23.3, 15.55 and 7.78 cfs) in the prototype. Dry-weather flow (dwf) was defined as one percent of the storm flow, or on the model 0.1 l/sec(0.004 cfs), and in the prototype 8.81 l/sec (0.31 cfs). The basic decision was made that during storm flows, 3 dwf would be withdrawn continuously through the foul outlet at the end of the helical bend section – 26.4 l/sec (0.93 cfs).

As stated, the preliminary studies of secondary flow patterns and solids removal results were carried out with the original model, as shown in Figure 4. Subsequently, modifications were made in the bend configurations and internal ancillary structural details. In all, the LaSalle Hydraulic Laboratory report, Appendix A, covers 16 modifications and 59 test runs, involving various changes in the body of the bend and other variations in length of transition and straight-flow sections ahead of the bend structure.

Over and above the basic structural configurations of the helical bend composite provided for the studies, the LaSalle investigations placed great stress on the introduction of the proper solids materials into the inflow water to simulate in a prototype installation actual combined sewage.

SOLIDS SIMULATION

In defining the pollutant materials to be removed from the regulated overflows, two categories were considered: grit, with specific gravity of 2.65 and settleable organics with specific gravity of 1.2. Details of the simulation procedures are given below:

Grit

The prototype gradation of the grit material in sewage which is to be removed in the helical structure was chosen as shown in Figure 6, Prototype Gradation for Grit and Settleable Organic Material. The outside grain-size limits of 0.2 and 2.0 mm (No. 70 and No. 10 sieve) represent medium and fine sand as defined by the Unified Soil Classification System. The specific gravity of the grit was assumed as 2.65, and the straight-line grain-size distribution was selected as a representative average of grit-size data reported for existing raw sewage influent at treatment plants. Concentration was considered as being from 20 to 360 mg/l.

Particle sizes smaller than about 1 mm (No. 18 sieve) are known to remain suspended and transported in flowing water according to equations of the type reported by Meyer-Peter and Muller,[5] or H. A. Einstein.[6]

Between 1 mm and 0.2 mm (No. 18 and No. 70 sieve) the particles are in the transition zone between the above equations and the Stokes relation. Since the particles involved in both prototype and model extended into both ranges, across the transition zone, the above equations could not adequately describe the scale relations.

It was necessary, therefore, to use curves of particle settling velocities as shown in Figure 7, Settling Velocities for Solids in Still Water. For a given grit size with specific gravity 2.65 in prototype, the settling velocity was determined from Figure 7. Based on Froude's law of similitude, this was divided by the square root of the scale being considered to find the required model settling velocity. By referring to Figure 7 with this model settling velocity, the model particle sizes were found for the simulating materials – Gilsonite or Petrothene.

The physical relations used here can be expressed as follows:

Model scale = λ = L_p/L_m

where L_p and L_m are corresponding lengths in the prototype and the model respectively.

From Froude's Law, the velocity simulation is expressed by the equation:

$$\frac{V_p}{V_m} = \sqrt{\frac{L_p}{L_m}} = \sqrt{\lambda}$$

and

$$V_m = \frac{V_p}{\sqrt{\lambda}}$$

For example, for the scale ratio of prototype to model of 6:1, the settling velocity in the prototype should be divided by the square root of 6, or 2.45. From Figure 7, the settling velocity of prototype grit of

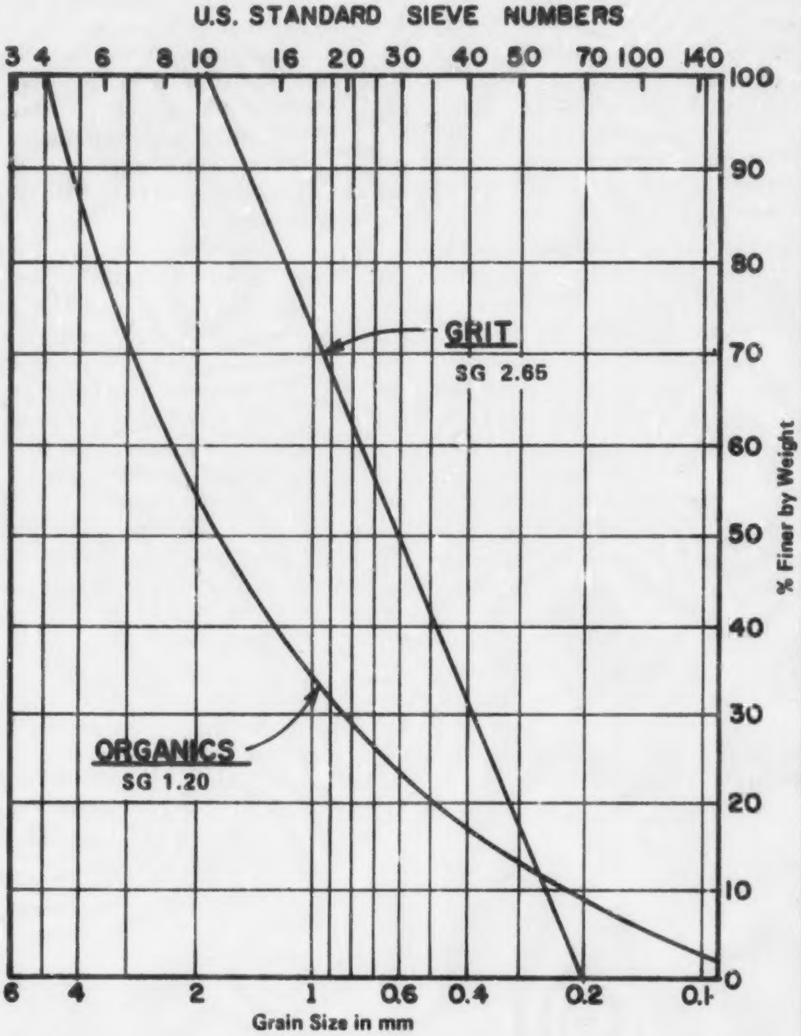

U.S. SIEVE SIZE	SIZE mm	% FINER BY WEIGHT	
		GRIT	ORGANICS
4	5.0	100	100
10	2.0	100	53
20	0.84	63	31
40	0.42	31	17
50	0.30	18	14
70	0.20	0	10

FIGURE 6 PROTOTYPE GRADATION FOR GRIT AND SETTLEABLE ORGANIC MATERIAL

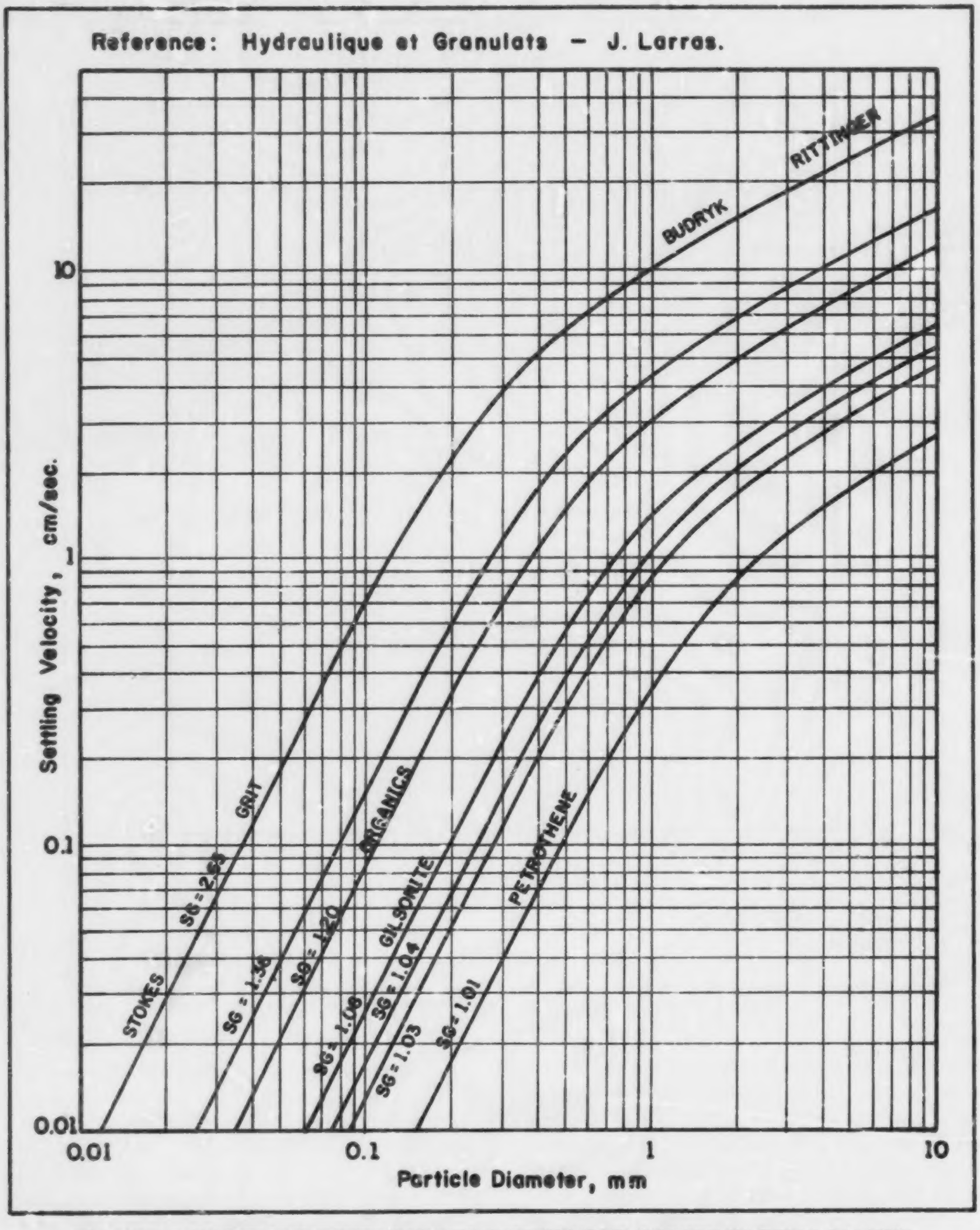
Reference: Hydraulique et Granulats – J. Larras.

FIGURE 7 PARTICLE SETTLING VELOCITIES FOR SOLIDS IN STILL WATER

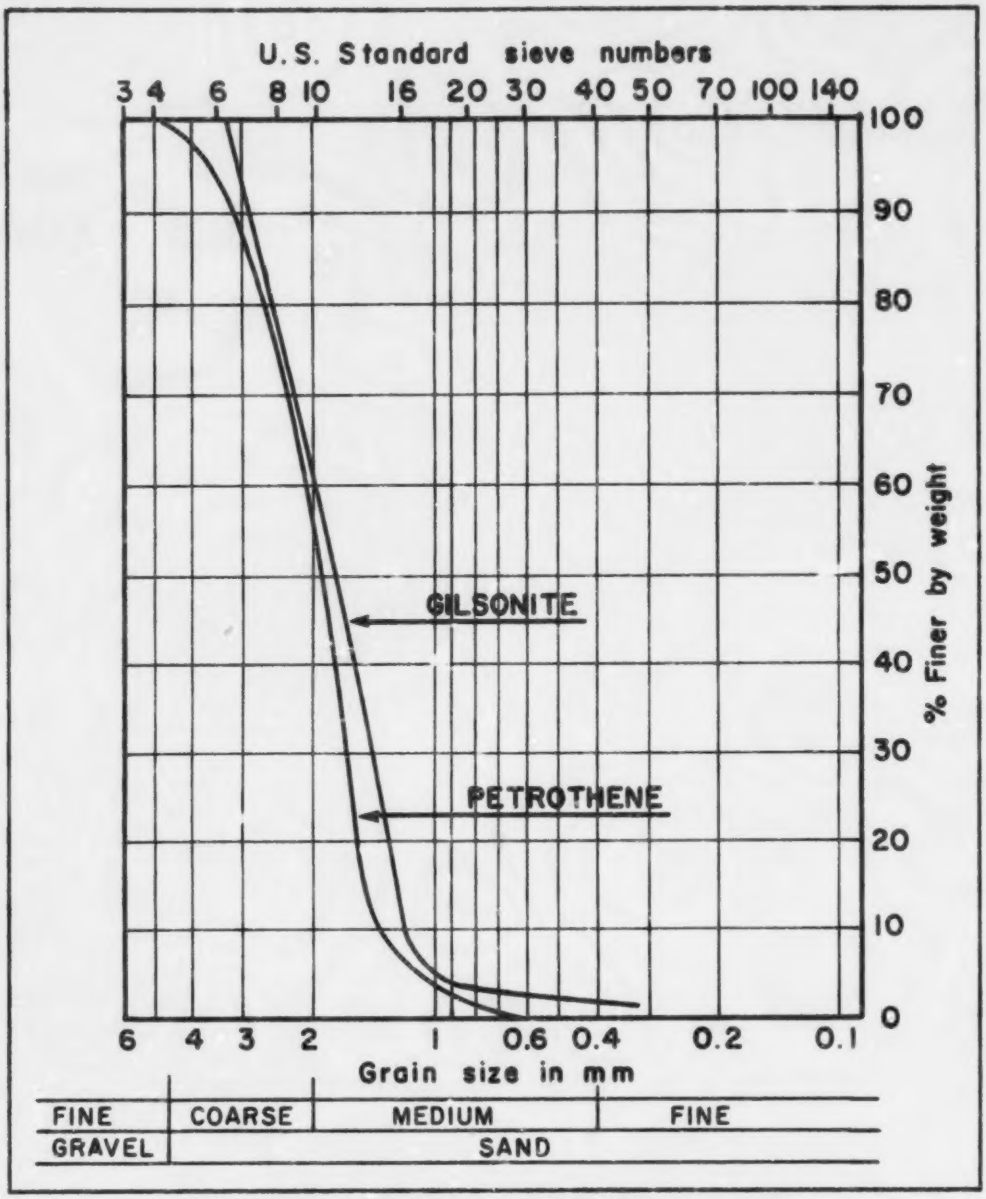

FIGURE 8 GRADATION CURVES FOR GILSONITE AND PETROTHENE USED IN MODEL

0.2 mm (70 mesh) size is 2.2 cm/sec (0.86 in./sec). The model settling velocity is then 0.90 cm/sec (0.35 in./sec). Thus, in the model, the grit of 0.2 mm size (70 mesh) can be simulated by 0.70 mm (0.27 in.) Gilsonite, or 2.1 mm (0.83 in.) Petrothene.

The Gilsonite and Petrothene available for test work in the laboratory had the grain size distributions shown in Figure 8, Gradation Curves for Gilsonite and Petrothene Used in Model. Practical limits represented on these curves were chosen between 0.5 and 3.0 mm (0.02 in. and 0.12 in.) (No. 35 and 6 sieves), and the corresponding prototype grit sizes simulated were calculated. The results are shown in

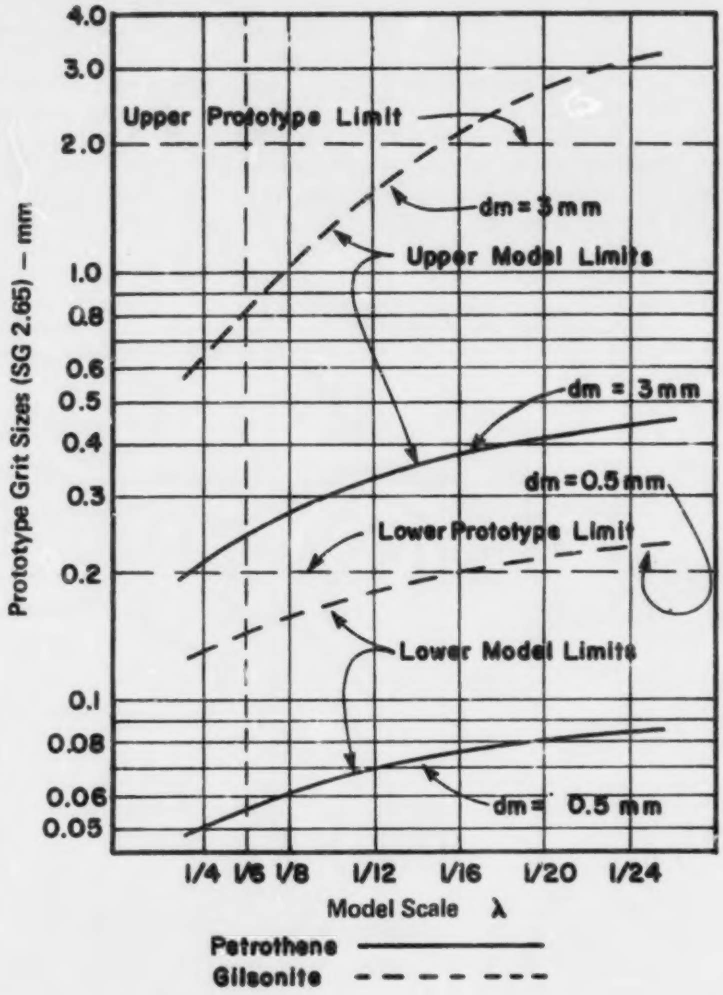

FIGURE 9 PROTOTYPE GRIT SIZES SIMULATED BY GILSONITE AND PETROTHENE IN MODEL

Figure 9, Prototype Grit Sizes Simulated by Gilsonite and Petrothene in Model.

This figure shows that for smaller scales, up to about 1/16, the Gilsonite did not cover the larger prototype particle sizes. However, it was reasoned that if the structure under study showed a particular recovery rate for these scales, the larger particles not simulated would have settled equally as well.

Conversely, the range covered by the Petrothene includes all of the Lower Prototype Limit, and drops down to much finer particles. In fact, as was demonstrated later, the Gilsonite settled out completely for all cases tried, so the Petrothene was used exclusively for the development tests, and all comparisons are for Petrothene recovery. This means that the figures quoted are a severe evaluation of the structure; all the grit in the defined range was removed, and the comparisons are for even finer particles.

Organics

The settleable organic material desired to be removed from the flow in the prototype was assumed to have a specific gravity of 1.2, and a grain-size distribution as shown in Figure 7. The same Froude model scale-up procedure was followed, and the limits simulated by the Gilsonite and Petrothene were calculated as shown in Figure 10, Prototype Settleable Organic Material Sizes Simulated by Gilsonite and Petrothene in Model.

The upper limits offered no difficulty; all the larger sizes were very easily covered by the Gilsonite. However, there remained a small section of the lower limit which was not covered by the Petrothene for scales smaller than about 1/10. This portion might be

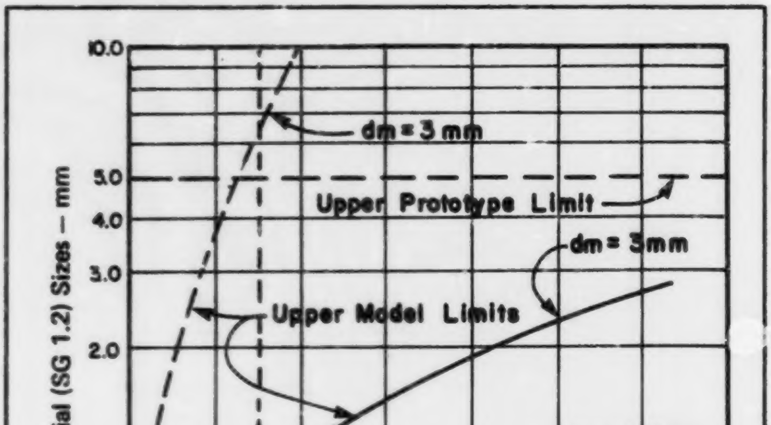

FIGURE 10 PROTOTYPE SETTLEABLE ORGANIC MATERIAL SIZES SIMULATED BY GILSONITE AND PETROTHENE IN MODEL

considered as lost but, at most, it actually represents only 10 percent of the prototype settleable organics at the smallest scales.

Floatables

Only brief tests were carried out to simulate floating pollutants which were assumed to have a specific gravity between 0.9 and 0.998, and a size range between 5 and 25 mm. Concentrations of 10 to 80 mg/l were assumed. In the model studies, uniformly sized polythene particles 4 mm in diameter and a specific gravity of 0.92 were used.

Mathematical Model Studies

The mathematical studies were carried out on a theoretical model, as shown in Figure 4. The mathematical model provided for the same general features as the hydraulic model, namely, a fixed inlet diameter, a transition section, a straight section, and a helical bend that comprised a 60° section. The configuration of the bend cross section provided a deeper area at the inner curve, a set overflow-weir and scum board for overflow purposes, and an overflow collection trough. Underflow from the separator was provided at the 60° location at the end of the bend.

The mathematical computer-simulation studies involved detailed numerical calculation of the liquid flowfield based on the equations of motion, together with appropriate boundary and initial conditions. The velocity field for the solid particles was approximated by superimposing the settling velocity on the calculated liquid velocity flowfield. The spatial variations in the particle concentration throughout the bend were then calculated numerically from the mass conservation equation with turbulent diffusion. Mathematical relations governing the scaling of the liquid flow and particle flow were evolved from the governing equations.

Of final significance was the mathematical development of comparisons of calculated mathematical model results with test data. This phase of the mathematical model-computer evaluation study compared the calculated flowfield with test data and correlated calculated concentration field findings with the results developed with the hydraulic model. The findings of the mathematical model studies were translatable into design techniques for the development of prototype installations of the helical bend as an overflow regulator and as a solids separator to improve the quality of overflow wastewaters from combined sewers.

SECTION III
DESIGN FACTORS FOR HELICAL BEND REGULATOR SEPARATOR FACILITIES

The hydraulic studies yielded data which can be utilized to develop full-scale design values for reasonable prototype dimension. The LaSalle Hydraulic Laboratory investigations were on prototype inlet sewer 0.915 m (3 ft) in diameter. The design discharge Q_D, was found by taking a nominal flood flow velocity in the range of 1.20 - 1.50 m/sec (4 tp 5 ft/sec). For the design discharge actually simulated in the test procedures, 0.88 m^3/sec (31.1 cfs), the flow velocity would be 1.35 m/sec (4.4 ft/sec).

Design Guidelines

The designer should use the following figures for designing the helical separator. These figures are:

Figure 11 Predicted Prototype Grit Recovery vs Design Flowrate Ratio
Figure 12 Predicted Prototype Settleable Organic Material Recovery vs Design Flowrate Ratio
Figure 13 Recommended Transition Profile
Figure 14 Effect of Transition Slope
Figure 15 Design Flowrate vs Inlet Diameter
Figure 16 Recommended Plan Layout
Figure 17 Water Level in Regulator Above Weir
Figure 18 Recommended Cross Sections

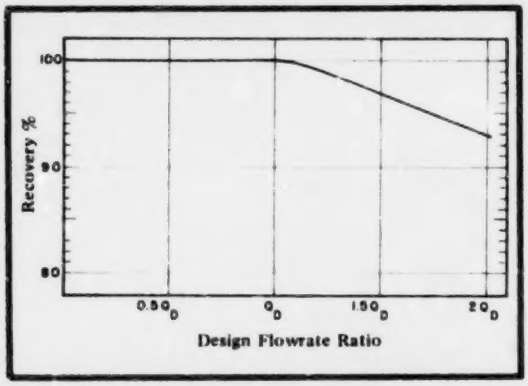

FIGURE 11 **PREDICTED PROTOTYPE GRIT RECOVERY VS DESIGN FLOWRATE RATIO**

The first step is to determine the design flowrate. This might be based on a storm flow expected to occur with a frequency of 5 or 10 years, or some other period, depending on the local design criteria. Usually larger flows than the selected design discharge may occur, depending on the capacity of the sewer system when surcharged. Figure 11 indicates that the grit recovery will decrease to 97 percent with a flow equal to 1.5 times the design flowrate, and to 93 percent with a flow equal to 2 times the design flowrate. Hence, the efficiency of grit removal is not greatly affected by flows up to twice the design flowrate.

Similarly, Figure 12 indicates the decrease in recovery of organic matter with increase in flow. Thus, for 1.5 times design flowrate, the efficiency decreases to about 87 percent; and for 2 times design flowrate, the efficiency decreases to about 75 percent.

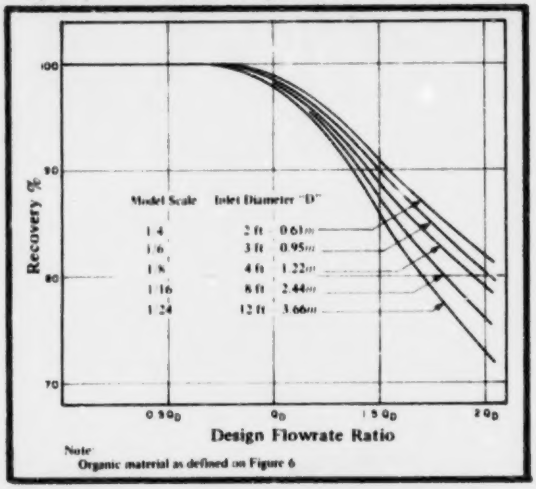

Note:
Organic material as defined on Figure 6

FIGURE 12 **PREDICTED PROTOTYPE SETTLEABLE ORGANIC MATERIAL RECOVERY VS DESIGN FLOWRATE RATIO**

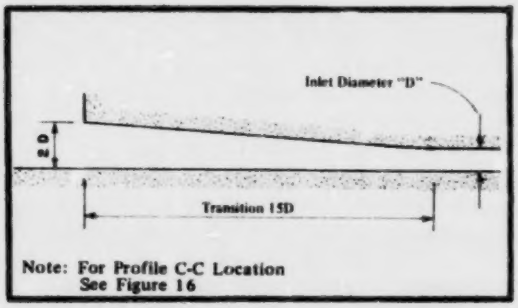

Note: For Profile C-C Location
See Figure 16

FIGURE 13 RECOMMENDED TRANSITION PROFILE

From the foregoing, it would appear that a considerable increase in flow above the design flowrate can occur without greatly affecting the operating efficiency of the helical separator.

Transition Slope

As shown in Figure 13, the recommended transition has a length of 15 D and a height of D at the inlet and 2 D at the outlet. In the laboratory model the invert of the transition was level. In practice this is not desirable because this would cause deposition of solids on the invert during periods of minimum flow. Therefore, the invert should have some slope. To prevent any surcharge at the inlet, the top of the transition should be kept level and the invert given a slope. The slope should be either the slope of the inlet, or the slope that will satisfy the hydraulic slope S in the Manning Equation, whichever is greater.

The resultant hydraulic conditions either with the invert level or the top level is shown in Figure 14, Effect of Transition Slope. The transition with the level top has the following

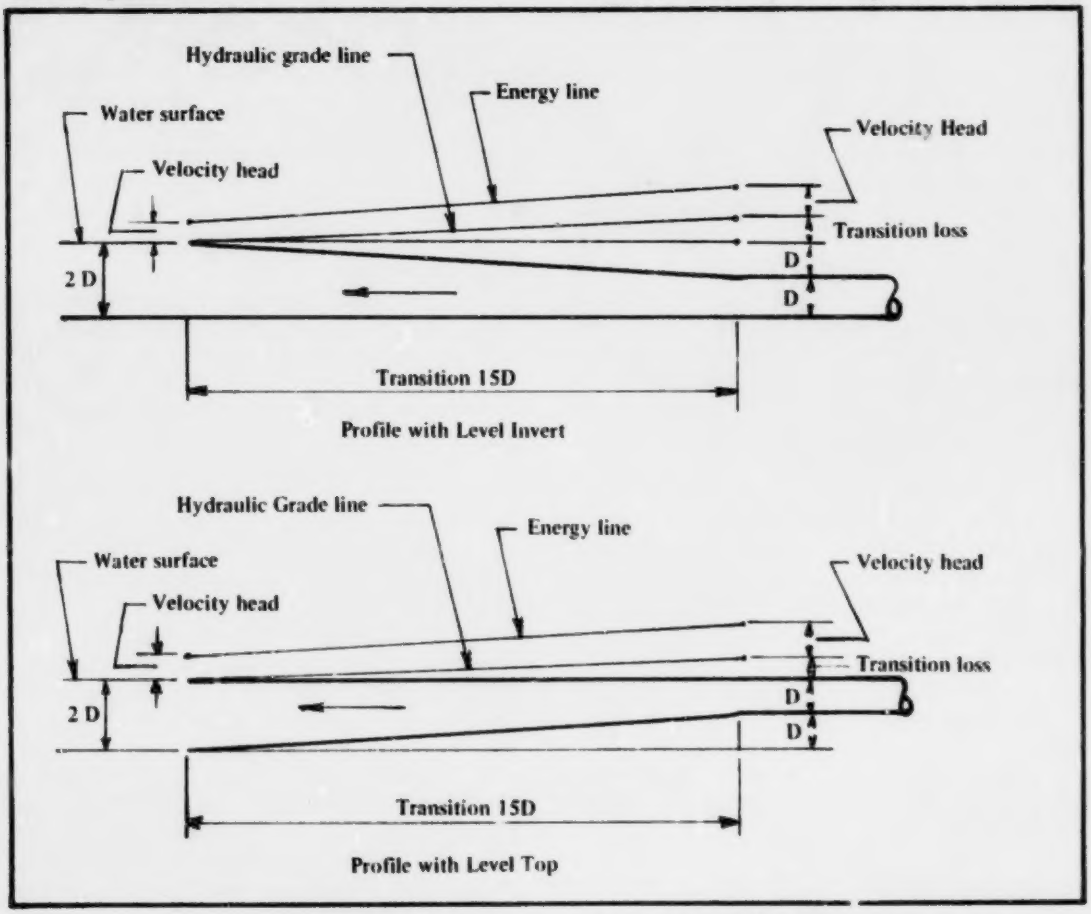

FIGURE 14 EFFECT OF TRANSITION SLOPE

advantages: (1) The sewer is not surcharged upstream of the transition except for loss of head in the transition, which may be minor; and (2) the slope will increase the velocity through the helical separator as the storm flow subsides which may aid in flushing deposits out of the helical section. The chief disadvantage of providing too great a slope in the transition is that the outlet pipe to the stream from the helical separator may be lowered so much that the extension of the existing sewer cannot be utilized for this purpose. Therefore, each situation must be evaluated before selecting the slope. Again as a minimum, the transition should have the same slope as the incoming sewer.

Transition Length

The transition length as given in Figure 13 is 15 D. The value of D is selected from Figure 15, Design Flowrate vs Inlet Diameter. Assume the designer selects a D of 1.83 m (6 ft) from Figure 15 as appropriate for the design flowrate. Then the recommended transition length is 27.4 m (90 ft). However, assume the existing sewer has a diameter of 1.52 m (5 ft) rather than 1.83 m (6 ft). The problem is how to effect the connection from the existing sewer to the transition. The most logical way would be to extend the transition to meet the existing sewer while reducing the area at the same rate as occurs in the transition. The area of the transition at the entrance would be 0.785 D^2 and at the exit 4.70 D^2. These areas are equivalent to squares with a side of 0.885 D at the entrance and of 2.16 D at the exit. Accordingly, the slope of the side of the transition would be equal to 1.28 D divided by 30 D, or 0.0426. This slope has an angle of 2 degrees 26 minutes. Thus, if the diameter of the existing sewer is 0.30 m (1 ft) smaller than the selected D, the transition should be extended by 3.5 m (11.6 ft).

It would also seem logical to reduce the length of the transition by a similar process if the area of the existing sewer is larger than the area of the transition inlet selected from the design charts.

Transition Inlet Size

All dimensions of the helical separator are related to D, the diameter of the transition inlet. After determining the design flowrate, the designer should select the inlet diameter, D, from Figure 15, which shows the simple scaled-up values according to the Froude Law, for the design discharge, Q_D, as well as 1.5 Q_D and 2 Q_D. These have been computed covering the likely range of applicable flood discharges and pipe sizes that will be encountered in any prototype installations.

Seldom will the value of D be that of a standard pipe size. Hence, the designer should select the nearest D corresponding to a standard pipe size. If the indicated D falls between two pipe sizes, the larger D will give a separator with greater efficiency than the smaller D. For instance, if the design flowrate is 2.83 m^3/sec (100 cfs), the indicated D will be 1.45 m (4.75 ft). The designer can select a D of 1.52 m (5 ft) which is equivalent to a design flowrate of 3.11 m^3/sec (110 cfs), or a D of 1.37 m (4.5 ft), equivalent to a design flowrate of 2.40 m^3/sec (85 cfs). If the latter capacity is chosen, the design flowrate will be 18 percent larger than the separator capacity. From Figure 11, the grit removal efficiency will be reduced to 99 percent of the total gritload. From Figure 12, the settleable organic removal will be reduced to about 96 percent.

If, in the example given above, the existing sewer should have a diameter equal to one of the possible D selections, then it would be logical to select the D which matches the existing sewer size. Otherwise, the transition should be extended as discussed previously.

The overall length of the helical separator is approximately 37 D including the transition and straight sections, as shown in Figure 16, Recommended Plan Layout. If a D of 1.37 m (4.5 ft), is selected, the length will be 50.9 m (167 ft), whereas if a D of 1.52 m (5 ft) is selected, the length will be 56.4 m (185 ft). A third possibility, assuming the existing sewer is 1.37 m (4.5 ft) and the D indicated by the chart is 1.4 m (4.75 ft), would be to base all dimensions on the indicated D and to extend the transition according to the method explained previously. In this case, the transition would be extended an amount equal to one-half the difference in diameters, divided by 0.0426 or 0.91 m (3 ft). The overall length in this case would be 37 times D plus 0.91 m (3 ft), or 5.45 m (179 ft).

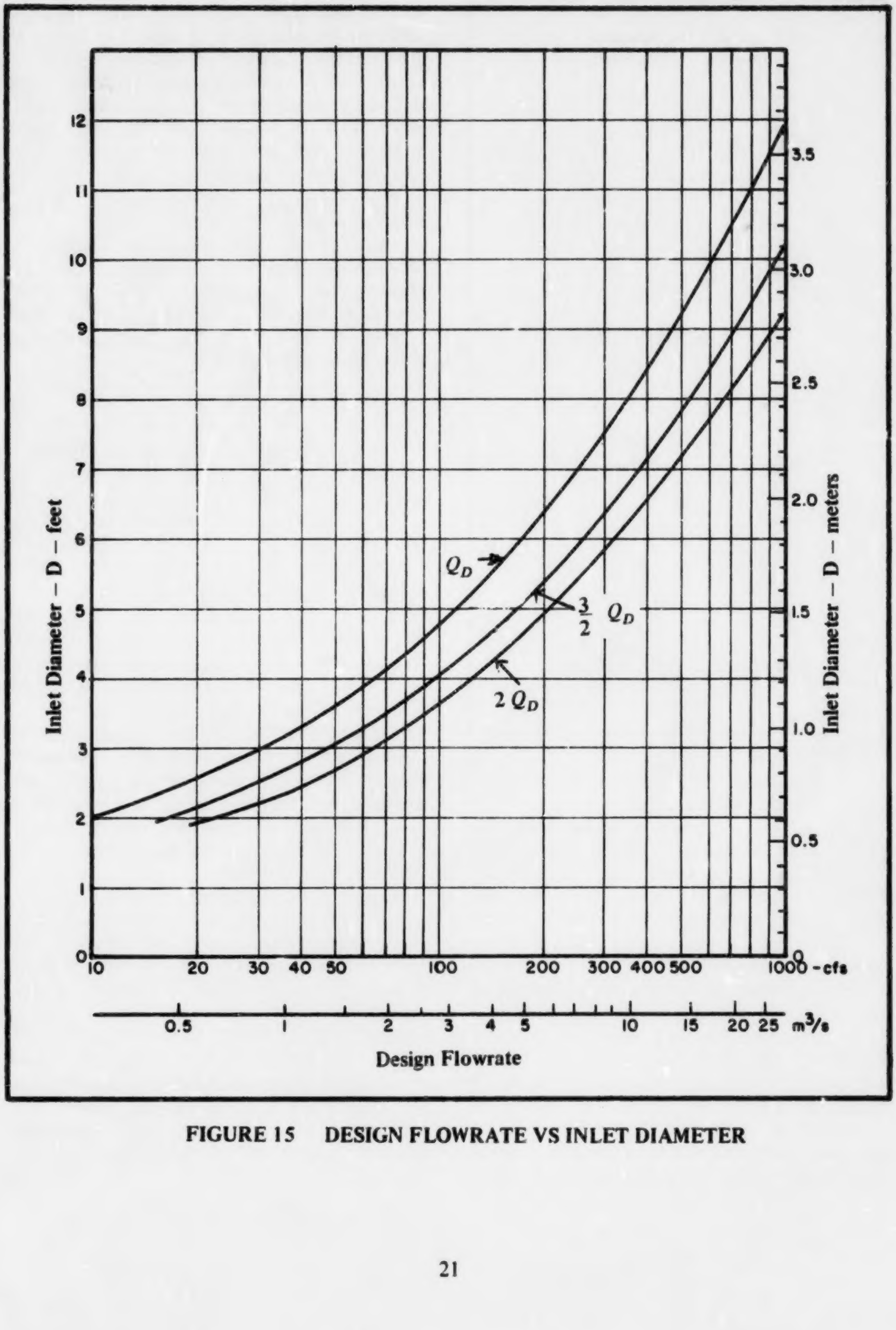

FIGURE 15 DESIGN FLOWRATE VS INLET DIAMETER

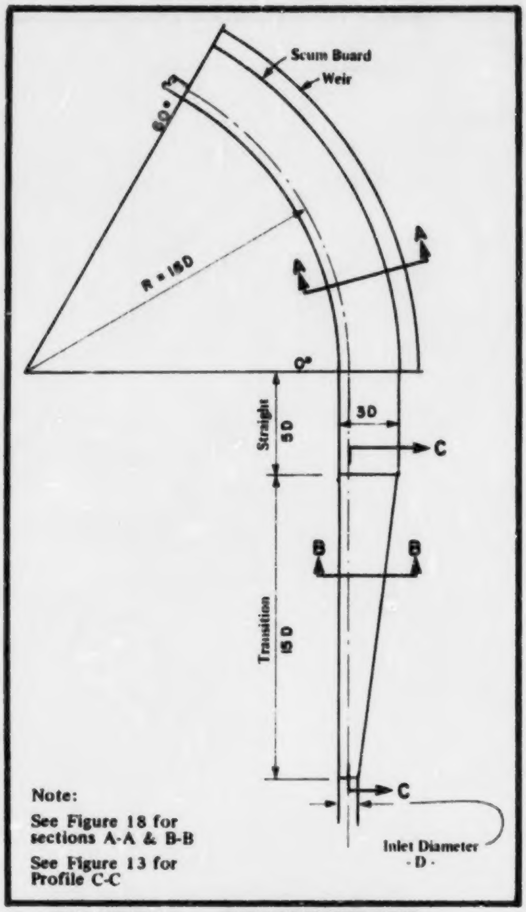

Note:
See Figure 18 for sections A-A & B-B
See Figure 13 for Profile C-C

FIGURE 16 RECOMMENDED PLAN LAYOUT

Thus, the designer is faced with the choice of three lengths – either 50.9 m (167 ft), 56.4 m (185 ft) or 54.5 m (179 ft). Obviously the largest helical separator will provide the most efficient operation.

Velocities in Transition

As a matter of interest the velocities at the inlet and outlet ends of the transition were computed for five values of D, from Figure 17. The D values selected were 0.91, 1.22, 1.52, 1.83 and 2.13 m (3,4,5,6, and 7 ft). The results are shown in Table 1, Velocities in Transitions. These data indicate an outlet velocity from the transition ranging from 0.22 m/sec (0.71 fps) to 0.36 m/sec (1.17 fps). This compares with the usual criteria of velocities between 0.23 m/sec (0.75 fps) and 0.38 m/sec (0.75 fps) and 0.38 m/sec (1.25 fps) in a rectangular grit channel with velocity control. In general, the outlet velocities are about one-sixth the inlet velocities. All velocities are based on the sections flowing full.

Channel Slope

In the laboratory model the channel of the helical separator was level. In practice the channel should be given enough slope to maintain a self-cleansing velocity of 0.61 m/sec (2.0 fps) with DWF (average dry-weather flow).

Assume the following:

D = 0.91 m (3.0 ft)
Design flowrate = 0.85 m^3/sec (30 cfs)
DWF = 1 percent of design flowrate
= 0.008 m^3/sec (0.3 cfs)
Peak DWF = 0.025 m^3/sec (0.9 cfs)

From a chart showing hydraulic properties of circular sections when the flowrate is one percent of the full section, the depth is seven percent of the full depth and the velocity is 31 percent of the velocity of the full section. The desired slope is that of a section when flowing full at a velocity of 0.61 m/sec (2.0 fps), divided by 0.31, or 1.98 m/sec (6.5 fps). From a nomograph of flow for Manning n = 0.013, the required slope of the channel for a diameter of 0.91 m (3.0 ft) is 0.48 percent. If the peak dry-weather flow is 3 times DWF the following data prevail:

When slope is 0.48%
Q = 0.025 m^3/sec (0.90 cfs)
d = 0.11 m (0.36 ft)
v = 0.58 m/sec (2.0 fps)

The foregoing assumes a circular section in the channel when flow is 1 percent and 3 percent of design flowrate. From a visual comparison of a large-scale section of channel with a circular section it is evident that flow conditions in a circular section will prevail for the depths of flow considered above. The foregoing indicates that peak dry-weather flows should cause no deposition in the channel.

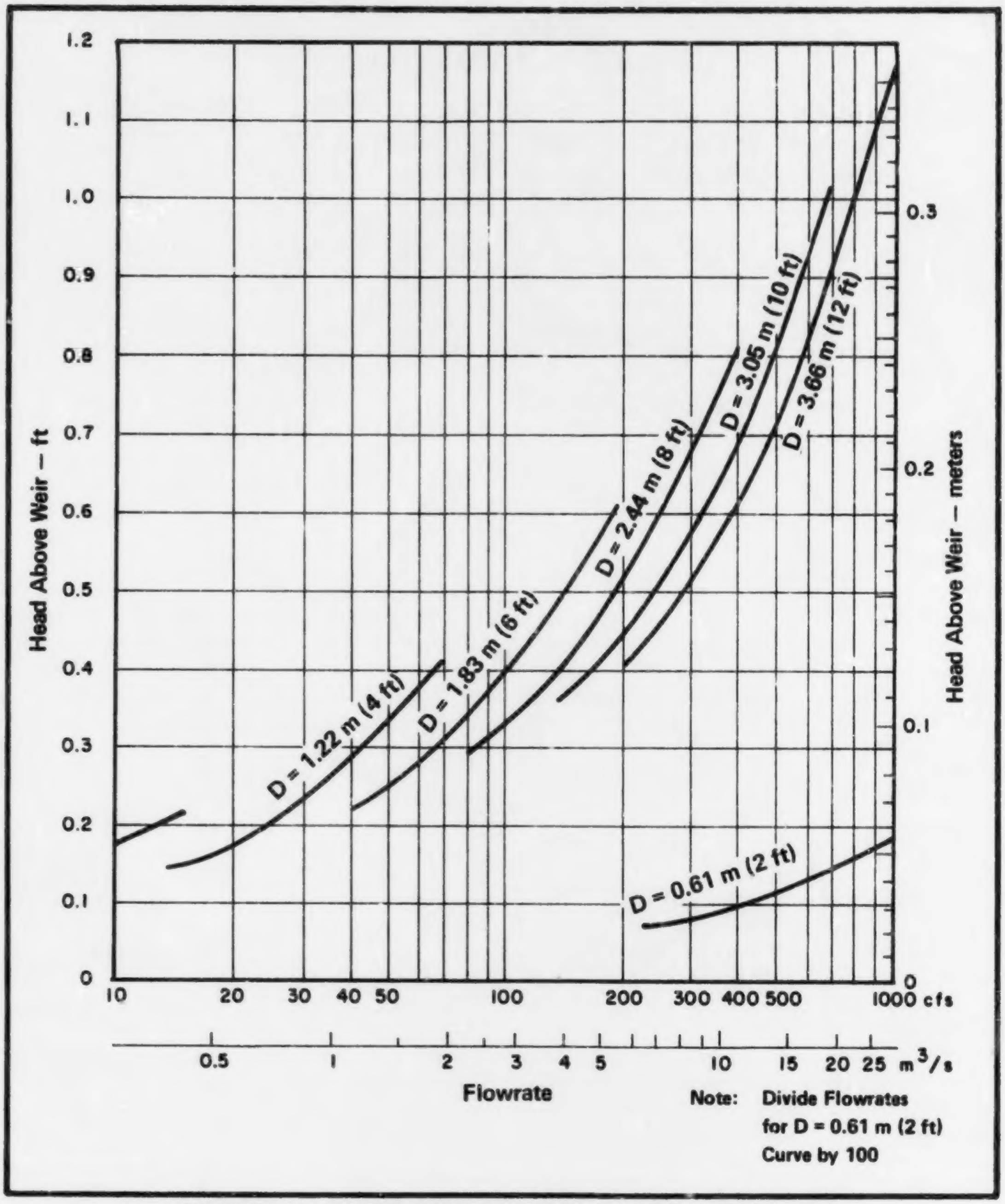

FIGURE 17 WATER LEVEL IN REGULATOR ABOVE WEIR

TABLE 1
VELOCITIES IN TRANSITIONS

Inlet Diameter	Design Discharge	Area		Velocity	
		Inlet	Outlet	Inlet	Outlet
0.91 m (3 ft)	0.85 m^3/s (30 cfs)	0.65 m^2 (7.0 sf)	3.93 m^2 (42.3 sf)	1.31 m/s (4.3 fps)	0.22 m/s (0.71 fps)
1.22 m (4 ft)	1.84 m^3/s (65 cfs)	1.17 m^2 (12.6 sf)	6.98 m^2 (75.2 sf)	1.58 m/s (5.2 fps)	0.26 m/s (0.86 fps)
1.52 m (5 ft)	3.11 m^3/s (110 cfs)	1.82 m^2 (19.6 sf)	10.9 m^2 (117 sf)	1.71 m/s (5.6 fps)	0.29 m/s (0.94 fps)
1.83 m (6 ft)	4.96 m^3/s (175 cfs)	2.63 m^2 (28.3 sf)	15.7 m^2 (169 sf)	1.89 m/s (6.2 fps)	0.30 m/s (1.0 fps)
2.13 m (7 ft)	7.65 m^3/s (270 cfs)	3.58 m^2 (38.5 sf)	21.4 m^2 (230 sf)	2.13 m/s (7.0 fps)	0.36 m/s (1.17 fps)

Note: Inlet Area = $0.785 D^2$
Outlet Area = $4.70 D^2$ when depth is 2D.

Weir Discharge

Previous research on side overflow weirs indicates that with a relatively high weir, as proposed in the helical separator, the usual weir discharge equations provide a reasonable basis of design. The usual equation is as follows:

$$Q = C L H^{3/2}$$

where

Q = flowrate in m^3/sec (cfs)
C = coefficient
L = length of weir in m (ft)
H = head on weir in m (ft)

The coefficient C varies depending on whether the weir is sharp crested or broad crested and depending on the head and width of the weir.

In the laboratory model the weir was made of Plexiglas and maintained in level position. The heads on the weir were measured at the 35 degree position. The heads on the weir for various values of D and flowrates are shown in Figure 17. Heads were obtained from this figure for various flowrates and the value of C was computed in the weir equation. The results indicated a range of C (based on use of U.S. customary units) from 3.3 to 3.7, with most values being 3.4 or 3.5. Such values are usually associated with sharp-crested weirs.

In practice a sharp-crested weir would be made of a steel or fiber glass plate. The only advantage of such a weir over a broad-crested weir is that it is easier to make adjustable. However, this is considered of minor importance.

Experience in Great Britain, where side overflow weirs have been used more widely than in the United States, favors the use of a weir with a semicircular shape. This shape seems preferable for the helical separator.

The coefficient of a broad-crested weir varies with the width of crest and head on the weir. For the widths and heads likely to occur in the helical separator the value of C (for U.S. customary units) may range from 2.8 to 3.3. The use of a C value of 3.0 (for U.S. customary units) for design purposes is suggested. An example follows:

Design flowrate	= 0.85 m^3/sec (30 cfs)
D	= 0.91 m (3.0 ft)
L (weir length)	= 18.83 D
	= 17.2m (56.5 ft)
Assume flow to plant	= 0.028 m^3/sec (1.0 cfs)
Q (over weir)	= 0.82 m^3/sec (29.0 cfs)
In English units Q	= $CLH^{3/2}$
If C = 3.0 then H	= 0.095m (0.32 ft)

The weir height is 1-5/6 D from Figure 18, Recommended Cross Sections. Therefore:

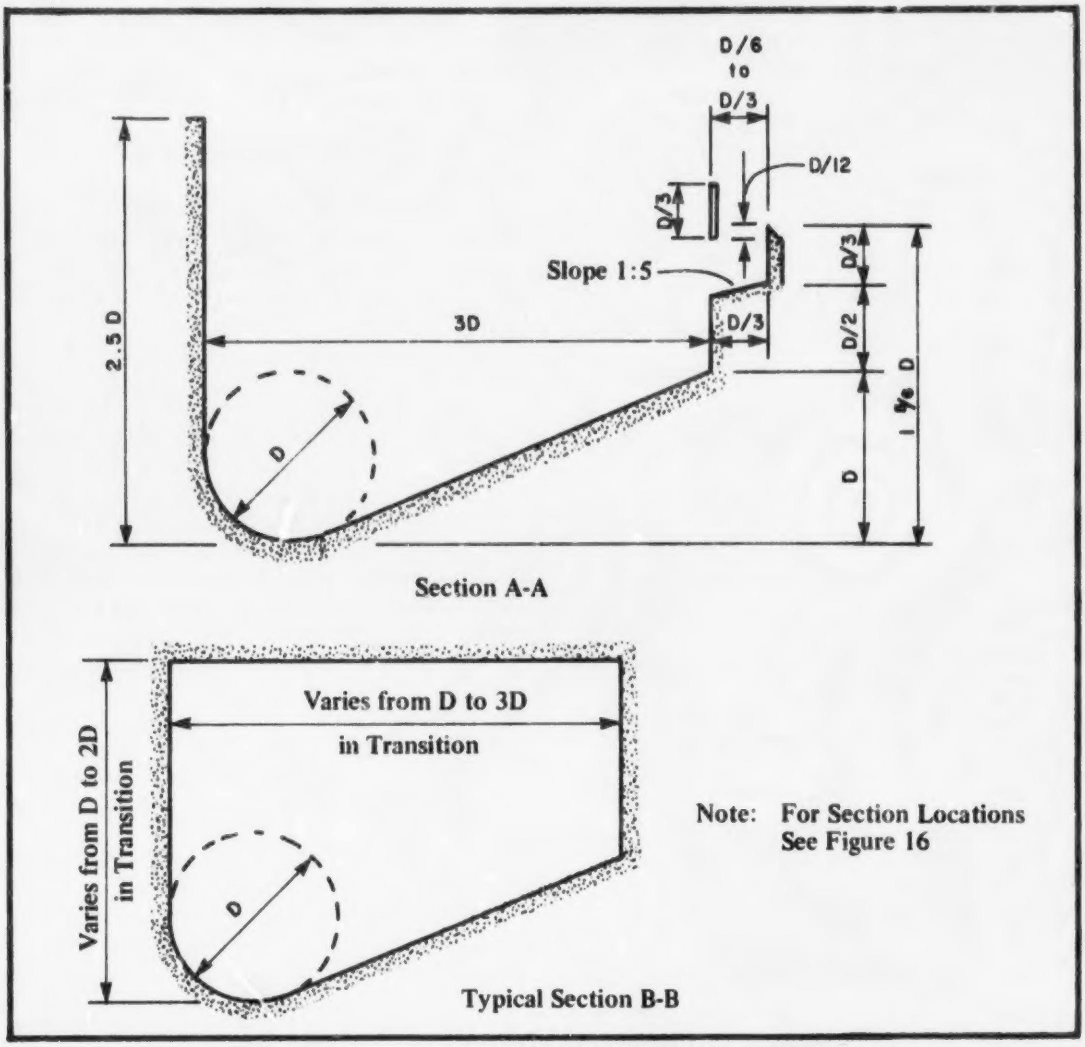

Section A-A

Typical Section B-B

Note: For Section Locations See Figure 16

FIGURE 18 RECOMMENDED CROSS SECTIONS

Weir height = 1.68 m (5.50 ft)
Head on weir = 0.095 m (0.32 ft)
Water depth = 1.77 m (5.81 ft)

However, to meet the laboratory demonstrated requirements that the transition be flowing full, the water depth should be 2D or 1.83 m (6.0 ft). Therefore, in this case the weir height should be a minimum of 1.73 m (5.68 ft) so that the transition outlet is flowing full when design flowrate occurs.

Outlet Control

Various methods of controlling the flow from combined sewer overflow regulators are discussed in an EPA report.[7] This report indicates that close control of the outlet flow requires the use of a sluice gate controlled by a float and actuated by either water power or an electric motor. On smaller structures where the use of such devices is not justified, one method of control is by use of a manually-operated gate. The intent is to only operate such gates to clear them of debris or to change the opening size.

The use of such gates may result in considerable variation in the flow diverted to the treatment plant. This may not be serious when this flow is only a small percentage of the total flow tributary to the plant. To indicate the possible range in flow, the following example is based on the use of a manually-operated gate on the outlet to the treatment plant. The minimum size gate used should be 0.20 m (0.67 ft) square but a gate with a minimum size of 0.30 m (1.0 ft) square is preferable.

Legend

A = Cross-sectional Area
D = Diameter
V = Velocity
d = Depth of flow
Q = Quantity of flowrate
b = Width of opening
C = Coefficient
DWF = Average dry-weather flow

$g = 9.81$ m/sec^2 (32.2 ft/sec^2)

Pertinent Data

DWF = 0.008 m^3/sec (0.30 cfs)
Peak DWF = 0.025 m^3/sec (0.90 cfs)

Try sluice gate 0.30 m (1.0 ft) square
Assume opening 0.10 m (0.33 ft) high
Then A = 0.03 m^2 (0.33 sf)

Determine depth upstream of gate when:
Q = 0.025 m^3/sec (0.90 cfs)
$Q = C A \sqrt{2gH}$
0.025 m^3/sec (0.9 cfs)
= 0.7 x 0.031 m^2 (0.33 sf) x 4.43 (8.03) x $\sqrt{H}$
H = 0.21 m (0.69 ft) on center line of orifice

Depth of flow is H, plus one-half height of orifice, or 0.26 m (0.86 ft). This is much greater than the normal depth of flow at the peak dry-weather flow of 0.11 m (0.36 ft) computed previously. Therefore, the velocity will be much less than the 0.58 m/sec (2.9 fps) computed previously and may cause deposition of grit at peak dry-weather flow.

Determine flow to the treatment plant when the water level is at weir crest.

Depth of flow in chamber is 1.83 m (6.0 ft)
Head on center of orifice is 1.77 m (5.83 ft)
$Q = C A \sqrt{2gh}$
= 0.7 x 0.03m^2 (0.33sf) x 4.43 (8.03)
1.33m (2.41 ft)
= 0.127 m^3/sec (4.46 cfs) = 15 DWF

Hence, the flow to the plant will exceed 15 DWF during periods of design discharge if there is no further restriction to flow downstream of the sluice gate. One way to restrict the flow is to design a sewer between the sluice gate manhole and the interceptor in such a way that it will convey the peak dry-weather flow without surcharge but will become surcharged when the flow exceeds the peak dry-weather flow. This procedure is described and illustrated by an example in an EPA report.[7]

Spillway Channel

The side channel in the helical section which conveys the overflow from the weir to the outlet sewer leading to the stream should be designed for the maximum flow expected to pass through the separator. The maximum flow will depend on the storm frequency for which the combined sewer is designed, as well as on the extent to which the combined sewer can be surcharged by storm flows greater than the design flow. It should also be assumed that the pipe outlet to the treatment plant is not in use either by design or by accident. On this basis it is possible for the maximum flow to exceed the design flowrate by 50 to 100 percent.

As an example, assume that the design flowrate is 0.85 m^3/sec (30 cfs) and the maximum flow is 1.27 m^3/sec (45 cfs). The side channel can be designed as a lateral spillway channel with the weir discharge spilling into it throughout its length. To aid in self-cleaning, it is desirable to set the downstream end of the channel above the invert of the outlet pipe and to provide a slope in the channel so that at low depths of flow the velocity will exceed 0.31 m/sec (1.0 fps).

The channel should be designed large enough so that the upstream water surface will not cause submergence of the weir.

The general equation for determining the depth of flow in a lateral spillway channel is the following:[8]

$$h_o = \sqrt{\frac{{h_c}^3}{h_1} + (h_1 - 1/3il)^2} - 2/3il$$

where

h_o = upstream water depth
h_c = critical depth
h_1 = downstream water depth when flow is submerged
i = slope of channel
l = length of channel
and

$$h_c^3 = \frac{Q^2}{gb} - 2$$

where
b = width of channel

The factors in the foregoing equation are depicted in Figure 19, Spillway Channel Profile. Actually, only 17.83/18.83, or 95 percent of the maximum flow discharges directly into the spillway channel. In the following example, however, it is assumed that all the maximum flow is conveyed by the channel.

Assume the following data:
Design flowrate = 0.85 m³/sec (30 cfs)
Q(side channel) = 1.27 m³/sec (45 cfs)
Outlet pipe diameter = 0.91 m (3.0 ft)
Weir height = 1.83 m (6.0 ft)
Then
Outlet velocity = 1.95 m/sec (6.4 fps)
Entrance loss = $\frac{1.5V^2}{2g}$ = 0.29 m (0.96 ft)
Elevation invert outlet pipe = 0.00 m (0.00 ft)
Elevation weir = 1.83 m (6.00 ft)
Elevation water at entrance = 1.21 m (3.96 ft)
Length of channel = length of weir, less outlet diameter = 16.3 m (53.5 ft)

Initial computation indicated that a channel 1.83 m (6.0 ft) deep and 0.31 m (1.0 ft) wide would cause submergence of the weir. For maintenance purposes a minimum width of channel of 0.61 m (2.0 ft) is considered desirable.

Preliminary computation with zero slope and the downstream end of the channel at elevation 0.0 indicated a water depth at the upstream end of the channel of 1.49 m (4.9 ft).

The effect of submergence on broad-crested weirs is surprisingly small. If necessary the fall in the water surface over the weir can be limited to 50 percent of the head on weir without affecting the discharge over the

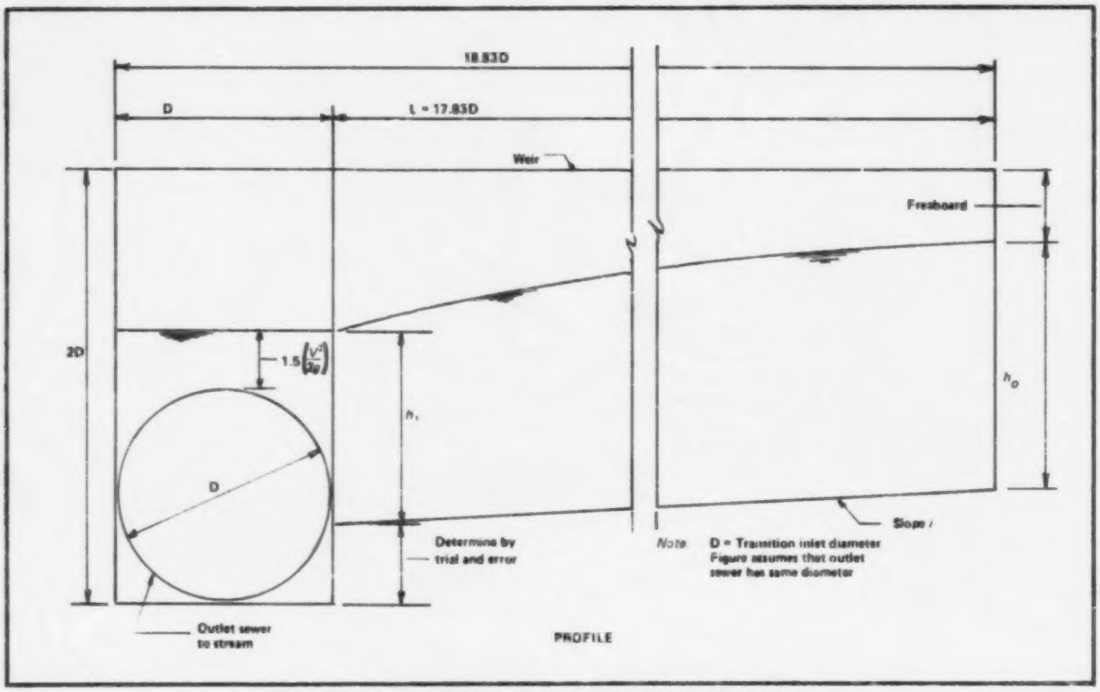
18.83D
D
L = 17.83D
Weir
Freeboard
2D
$1.5\left(\frac{V^2}{2g}\right)$
h_1
D
h_o
Slope i
Determine by trial and error
Note: D = Transition inlet diameter
Figure assumes that outlet sewer has same diameter
Outlet sewer to stream
PROFILE

FIGURE 19 SPILLWAY CHANNEL PROFILE

HELICAL BEND REGULATOR

Design Example

Straight Pipe

Assume pipe designed so that at DWF the velocity is about 2 fps

$D = 3.0$ ft $S = 0.44$ % $n = 0.013$

Q full = 45 cfs $v = 6.5$ fps

For Q design = 30 cfs

$\frac{Q_1}{Q_2} = \frac{30}{45} = 0.67$

$\frac{d_1}{d_2}$ = 0.6 from chart[1]

$d_1 = 0.6 \times 3.0 = 1.8$ ft

$\frac{v_1}{v_2}$ = 1.07 from chart[1]

$v_1 = 1.07 \times 6.5 = 7.0$ fps

For Q DWF = 0.3 cfs

$\frac{Q_1}{Q_2} = \frac{0.3}{45} = 0.007$

$\frac{d_1}{d_2} = 0.06$ $d_1 = 0.06 \times 3 = 0.18$ ft

$\frac{v_1}{v_2} = 0.29$ $v_1 = 0.29 \times 6.5 = 1.9$ fps

OK almost 2.0 fps

For Q3(Peak DWF) = 0.9 cfs

$\frac{Q_1}{Q_2} = \frac{0.9}{45} = 0.02$

$\frac{d_1}{d_2} = 0.1$ $d_1 = 0.1 \times 3 = 0.3$ ft

$\frac{v_1}{v_2} = 0.4$ $v_1 = 0.4 \times 6.5 = 2.6$ fps

Helical Bend Regulator, Design Example (continued)

Straight Pipe D = 3 ft

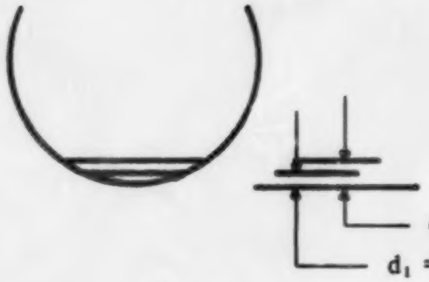

$d_1 = 0.3$ ft Q = 0.9 cfs

$d_1 = 0.18$ ft Q = 0.3 cfs

Helical Bend Regulator

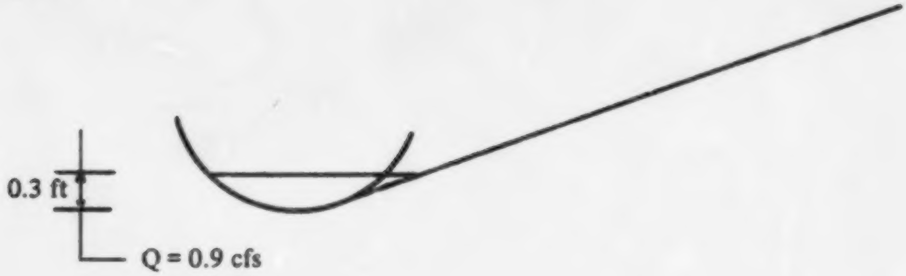

At 3 DWF the area will only be slightly larger in separator than in 3 ft diameter pipes. Assume velocity the same

v = 2.6 fps

Exit Pipe -- Assume 1.0 ft diameter

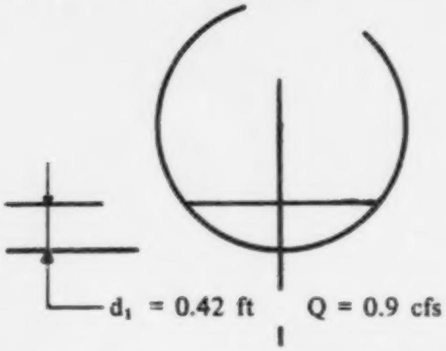

S = 0.44 %

Q = 2.4 cfs v = 3.0 fps

$$\frac{Q_1}{Q_2} = \frac{0.9}{2.4} = 6.37$$

$$\frac{d_1}{d_2} = 0.42 \qquad d_1 = 0.42 \text{ ft}$$

$$\frac{v_1}{v_2} = 0.92 \qquad v_1 = 0.92 \times 3 = 2.8 \text{ fps}$$

Lower invert of outlet pipe 0.12 ft below invert of separator so as not to raise water surface

Determine outlet design
when Q = 30 cfs
so that Q outlet = 0.9 cfs
Weir Length
Angle = 60° D = 3 ft

Helical Bend Regulator, Design Example (continued)

Weir Radius = $16D + 2.5D + D/3$

$= (16)(3) + (2.5)(3) + 1$

$= 56.5$ ft

Weir Length = $\frac{60}{360}\left(2\pi R\right) = \frac{2\pi}{6}\left(56.5\right)$

$= 59$ ft

Head on Weir Q per ft $= \frac{30}{59} = 0.51$ cfs

Use Rehbock K

$Q = KLH^{3/2} = 3.41\ (1)\ H^{3/2} = 0.51$

$H^{3/2} = 0.15$

$H = 0.28$ ft

Depth of Water

1-5/6 D $= \frac{11}{6}\ (3) = 5.50$ ft

Head on weir = $\underline{0.28}$

Total water depth = 5.78 ft

Assume short tube exit D = 1.0 ft

$A = \frac{\pi D^2}{4} = 0.785$ sf

$Q = CA\sqrt{2gH}$

$= (0.7)(0.785)\ (8.03)\sqrt{5.28}$

$= 10.1$ cfs

Too large

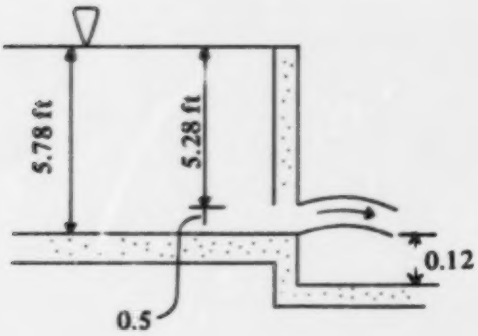

Outlet Design

Determine orifice area for

$Q = CA\ \sqrt{2gH}$

$0.9 = (0.7)\ (A) \quad 8.03\ \sqrt{5.28}$

$A = 6.9 \div 12.9 = 0.07$

$A = \frac{\pi D^2}{4}$

$D = \sqrt{\frac{0.07}{0.785}} = \sqrt{0.09} = 0.3$ ft

Helical Bend Regulator, Design Example (continued)

Orifice should be greater than 0.67 ft. If orifice is made this size so that only 0.9 cfs or 3DWF would pass when tank is full, then it is apparent that the tank would fill up whenever 3DWF occurs which might be the peak daily flow.

To prevent deposition of solids on the separator floor and to prevent cleaning the separator in dry weather periods, the separator and outlet should pass up to 3 DWF without raising levels in separator to weir levels.

Try throttle pipe on outlet

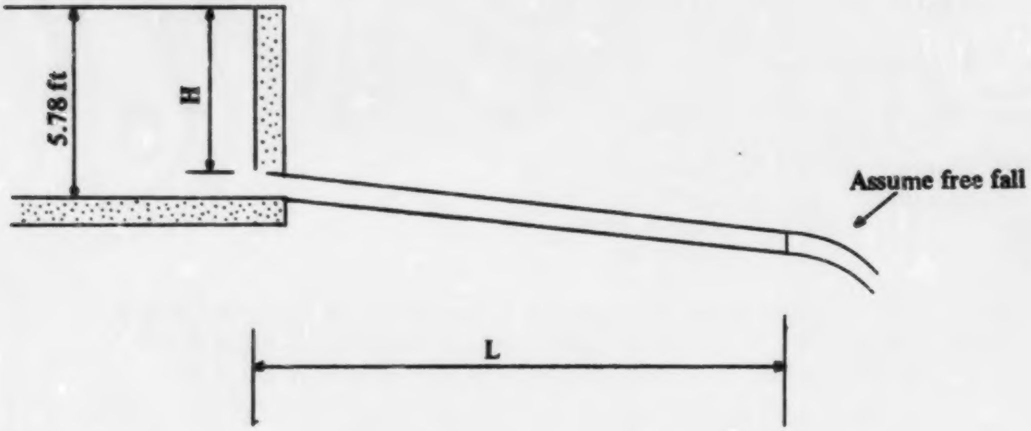

Outlet Design

Use 8-inch pipe as minimum
Use s = 0.4% as minimum
For n = 0.013 $Q = 0.75$ cfs $v = 2.2$ fps $\frac{v^2}{2g} = 0.08$ ft

For QDWF = 0.3 cfs
$\frac{Q_1}{Q_2} = \frac{0.3}{0.75} = 0.4$
If discharge ratio is 0.4, then depth is 44% and velocity 94%
$d = .44$ $D = 0.44 \times 0.67 = 0.3$ ft
$v = .94$ $V = 0.94 \times 2.2 = 2.1$ fps
Assume L = 100 ft $H = 5.78 - 0.67 = 5.11$ ft
For Q3DWF = 0.9 cfs
v = 2.5 fps $\frac{v^2}{2g} = 0.1$ $s = 0.5\%$

Entrance & exit loss	1.5 x 0.1 =	0.15
Slope hydraulic gradient	100 x 0.5% =	0.50
		0.65
Actual pipe slope		0.40
Water surface above top pipe		0.25
Water surface in tank		0.67
Depth water in tank		0.92 ft

Helical Bend Regulator, Design Example (continued)

Determine Q max when tank is full

Assume entrance and exit loss = 1.2 ft

Slope H.G = $\left(\frac{5.11 - 1.2}{100}\right)$ 100+0.4 = 4.3%

Q max = 1.6 cfs v = 7.2 fps $\frac{v^2}{2g}$ = 0.8

Thus with 8 in. throttle pipe 100 ft long the maximum Q will be 1.6 cfs or about 5 times DWF.

Try other lengths of pipe

L ft	5% HG	Q cfs	v fps	$\frac{v^2}{2g}$	Q DWF
200	2.45	1.8	5.4	0.5	6
300	1.9	1.6	4.7	0.4	5.3
400	1.45	1.4	4.0	0.3	4.7
600	1.2	1.3	3.8	0.2	4.3

A length of 400 ft should be the maximum for an 8 in. sewer. Therefore it is obvious that if the discharge is to be limited to 3 DWF some type mechanical device should be used to close the outlet opening as the water level rises in the separator.

Determine depth of water in tank with throttle pipe 400 ft long, when Q = 0.9 cfs

Required 5	= 0.5%	(See previous page)
400 x 0.5%	=	2.0 ft
Slope sewer 400 x 0.4%		1.6
		0.4 ft
Entrance & exit loss 1.5 $\frac{v^2}{2g}$		0.15
Head on top of pipe		0.55 ft
Diameter pipe		0.67
Depth of water in tank		1.22 ft

---

weir. As computed previously the head on the weir is 0.095 m (0.32 ft) and little elevation can be gained by assuming a submerged weir. Therefore design can be based on no submergence of weir. It is also desirable to locate the downstream end of the discharge channel above the outlet pipe invert to prevent deposition in the channel. Therefore the downstream end of the channel was set at elevation 0.30 m (1.0 ft) and the channel slope set at 0.005. The resultant freeboard of 0.18 m (0.6 ft) indicated that the channel could have been raised an additional 0.18 m (0.6 ft). The final data are as follows:

Elevation downstream invert of channel	0.3 m (1.0 ft)
Rise in channel	0.09 m (0.3 ft)
Elevation upstream invert of channel	0.40 m (1.3 ft)
h_0	1.25 m (4.1 ft)
Elevation upstream water surface	1.65 m (5.4 ft)
Elevation weir	1.83 m (6.0 ft)
Freeboard	0.18 m (0.6 ft)

In the foregoing example, it was assumed that the outlet pipe was located at the end of the channel. If the outlet pipe were located at the center of the side channel this would result in a lesser rise of the water surface in the spillway channel.

Typical Dimensions

For the purpose of comparing the helical separator with the swirl concentrator, three design flows were selected as follows: 1.42 m^3/sec (50 cfs), 2.83 m^3/sec (100 cfs), and 5.66 m^3/sec (200 cfs). The dimensions of the helical separator are based on Figures 15, 16, 18, and on Profile with Level Top, in Figure 14, Effect of Transition Slope. The resultant dimensions are tabulated in Table 2, Helical Bend Regulator Dimensions. The dimensions of the swirl concentrator are based on Figures 7, and 11 through 18, of Report EPA-670/s-74-039, Relationship Between Diameter and Height for the Design of a Swirl Concentrator as a Combined Sewer Overflow Regulator. (July 1974) The resultant dimensions are shown in Table 6, Swirl Concentrator Dimensions.

It should be noted that the helical separator sized in Table 2 will remove 100 percent of grit, whereas the swirl concentrator sized for the same discharge in Table 6 will remove only 90 percent of grit. This is because the published design charts for the swirl concentrator provide for 70, 80, and 90 percent recovery (or removal) of grit. Later in this section, under the heading "Comparison of Costs," a method is developed to indicate the possible cost of a swirl concentrator to remove 100 percent of grit.

TABLE 2
HELICAL BEND REGULATOR DIMENSIONS

Design Discharge	m^3/s	1.42	2.83	4.67
	(cfs)	(50)	(100)	(165)
Inlet Diameter	D - m	1.07	1.52	1.83
	(ft)	(3.5)	(5.0)	(6.0)
Transition Length	15D - m	16.0	22.9	27.4
	(ft)	(52.5)	(75.0)	(90.0)
Straight Section - Length	5D - m	5.33	7.62	9.14
	(ft)	(17.5)	(25.0)	(30.0)
Radius	16D - m	17.1	24.4	29.3
	(ft)	(56.0)	(80.0)	(96.0)
Width	3D - m	3.20	4.57	5.49
	(ft)	(10.5)	(15.0)	(18.0)
Minimum Wall Height	2.5D - m	2.67	3.81	4.57
	(ft)	(8.75)	(12.5)	(15.0)
Channel to Top Weir	$1\frac{5}{6}$D - m	1.95	2.77	3.35
	(ft)	(6.4)	(9.1)	(11.0)
Height End of Transition	2D - m	2.13	3.05	3.66
	(ft)	(7.0)	(10.0)	(12.0)
Scum Baffle Height	$\frac{D}{3}$ - m	0.36	0.52	0.61
	(ft)	(1.2)	(1.7)	(2.0)
Distance from Weir to Bottom of Baffle	$\frac{D}{12}$ - m	0.09	0.13	0.15
	(ft)	(0.3)	(0.4)	(0.5)
Weir Height	$\frac{D}{3}$ - m	0.36	0.52	0.61
	(ft)	(1.2)	(1.7)	(2.0)
Distance Wall to Weir:				
Max	$\frac{D}{3}$ - m	0.36	0.52	0.61
	(ft)	(1.2)	(1.7)	(2.0)
Min	$\frac{D}{6}$ - m	0.18	0.26	0.30
	(ft)	(0.6)	(0.85)	(1.0)

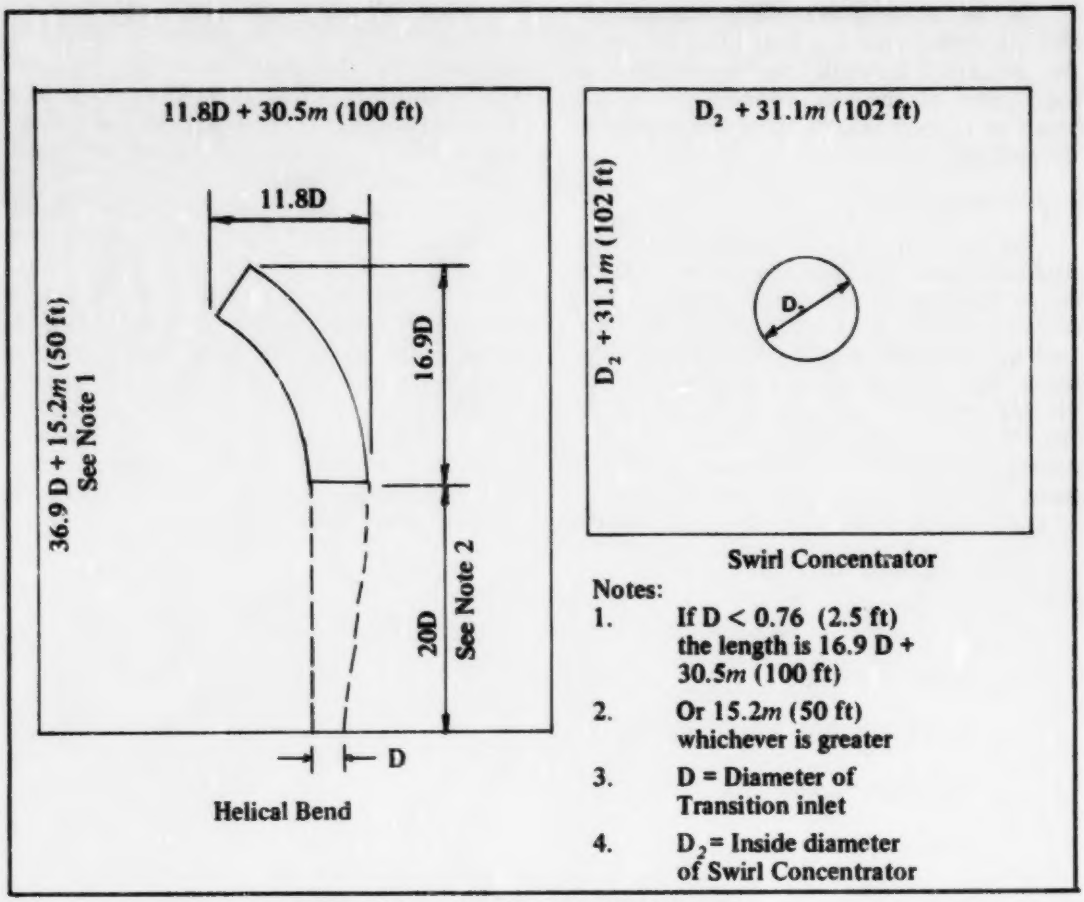

Notes:

1. If D < 0.76 (2.5 ft) the length is 16.9 D + 30.5m (100 ft)
2. Or 15.2m (50 ft) whichever is greater
3. D = Diameter of Transition inlet
4. D_2 = Inside diameter of Swirl Concentrator

FIGURE 20 SITE REQUIREMENTS

Site Requirements

The size of the buffer or protective zone required around the helical separator will depend to a large extent on the environment of the neighborhood. In any locality, a buffer zone at least 15.2 m (50 ft) wide would be desirable. Therefore, the site requirements given herein are based on a 15.2 m (50 ft) buffer zone around all open or above-ground parts of the facility. Because the transition is below the surface, no buffer zone is required for that part of the structure; however, it is assumed that all of the transition section is located on the site.

On the foregoing basis, the site requirements for both the helical separator and the swirl concentrator are shown in Figure 20, Site Requirements. The required lot dimensions and areas for three sizes of each facility are shown in Table 3, Site Dimensions and Areas for Helical Bend and Swirl Concentrator Regulators. As explained previously, the site dimensions are based on a helical separator to remove 100 percent of grit and a swirl concentrator to remove 90 percent of grit.

It is evident from Table 3 that the site requirements for the helical bend are greater than for the swirl concentrator and that the larger the design flow the greater the difference. For the design flows of 1.42 m^3/sec (50 cfs), 2.83 m^3/sec (100 cfs) and 5.66 m^3/sec (200 cfs), the helical bend requires a site 49 percent, 106 percent, and 137 percent greater, respectively, than the swirl concentrator.

TABLE 3
SITE DIMENSIONS AND AREAS FOR HELICAL BEND AND SWIRL CONCENTRATOR REGULATORS

	Swirl Concentrator	Helical Separator
Capacity	**1.42 m^3/s (50 cfs)**	
Site Size	**38.0 m x 38.0 m (124.5 ft x 124.5 ft)**	**43.0 m x 54.6 m (141 ft x 179 ft)**
Site Area	**1,440 m^2 (15,500 sf)**	**2,340 m^2 (25,200 sf)**
Relative Area	**1.00**	**1.63**
Capacity	**2.83 m^3/s (100 cfs)**	
Site Size	**40 m x 40 m (131.5 ft x 131.5 ft)**	**48.5 m x 71.5 m (159 ft x 234 ft)**
Site Area	**1,600 m^2 (17,300 sf)**	**3,460 m^2 (37,200 sf)**
Relative Area	**1.00**	**2.15**
Capacity	**4.67 m^3/s (165 cfs)**	
Site Size	**42 m x 42 m (138 ft x 138 ft)**	**52.0 m x 82.8 m (171 ft x 272 ft)**
Site Area	**1,770 m^2 (19,000 sf)**	**4,300 m^2 (46,500 sf)**
Relative Area	**1.00**	**2.45**

Comparison of Hydraulic Head Losses in Helical Bend and Swirl Concentrator Regulator

The available head at a specific site may be a critical factor in the choice of the specific type of combined sewer regulator to be used. The head loss must be considered for two conditions: (1) For periods of dry-weather flow, and (2) for periods of wet-weather flow. The available head during dry-weather flow will depend on the difference in elevation between the combined sewer and the interceptor that will convey the flow to the wastewater treatment plant. The available head during wet-weather flow will depend on the difference in elevation between the combined sewer and the water surface of the receiving stream. A further consideration in the latter case is whether the existing combined sewer is to be used to convey the overflow from the regulator to the receiving stream or to any holding or treatment facilities involved.

In periods of dry weather there will be open channel flow through the regulator, and hence the drop in invert and hydraulic gradient will be similar from the regulator inlet to the foul outlet. In wet-weather periods there may be a considerable difference between the drop in invert and the drop in hydraulic gradient from the regulator inlet to the clear outlet.

The usual practice is to design combined sewers to run full at design discharge, i.e., the hydraulic gradient is at the top of the pipe. In special cases, due to topography or for other reasons, it may be possible to design the sewer to be surcharged, i.e., the hydraulic gradient is above the top of the sewer. Both cases are considered below. To simplify the discussion, the slope of the channel in the regulator to maintain a dry-weather flow velocity that will prevent solids deposition has not been included in the required drop in the invert.

In the following comparisons, the head losses are given as a multiple of the inlet dimension: D, the inlet diameter of the helical separator; and D_1 the side of the square inlet of the swirl concentrator. To show that D and D_1 are approximately the same for the same discharge, their values for three discharges are given, as follows:

Design Discharge	m^3/sec	1.42	2.83	5.66
	(cfs)	(50)	(100)	(200)
D	m	1.07	1.52	1.98
	(ft)	(3.5)	(5.0)	(6.5)
D_1	m	0.90	1.52	1.83
	(ft)	(3.0)	(5.0)	(6.0)

First, consider the case where there is to be no surcharge on the inlet during design discharge.

In the helical separator the transition will have a level top as shown in Figure 14. The drop in the invert of the transition will be 1.0 D. Therefore, the drop in the invert from the inlet to the foul outlet will be 1.0 D (neglecting the slope of the channel through the regulator). The loss in the hydraulic gradient will also be 1. O D. The invert of the clear outlet will be at approximately the same elevation as the invert of the separator, as explained previously in the discussion of the weir overflow spillway channel. Therefore, the drop in the invert between the inlet and the clear outlet will also be 1.0 D. The loss in the hydraulic gradient may be the same as the drop in the invert or it may be slightly different depending on outlet design.

The dimensions of the swirl concentrator as a Combined Sewer Overflow Regulator are given in Figure 11, General Design Details, of Report EPA-670/2-74-039, Previously cited. The general construction details are shown in Figures 12, 13, and 14 of EPA Report R2-72-008, titled "The Swirl Concentrator as a Combined Sewer Overflow Regulator Facility." (Sept. 1972)

If there is to be no surcharge on the inlet sewer, the crown must be at a distance above the invert of the chamber equal to H_1 (the height of weir above the chamber invert), plus the head on the weir. The drop in the invert of the sewer will be this distance less D_1, the dimension of the inlet. The foul outlet is located below the chamber bottom. Assuming a foul outlet diameter of 0.31 m (1.0 ft) and concrete cover over the outlet to the same amount, the distance from the chamber invert to the outlet invert is 0.61 m (2 ft).

Excluding the channel slope through the concentrator, the drop in the invert from the inlet to the foul outlet is, therefore, 0.8 D_1 to 1.5 D_1, plus 0.6 m (2.0 ft). The foul outlet pipe diameter may exceed 0.31 m (1.0 ft) diameter for larger flows, thus increasing the total drop somewhat. The hydraulic gradient will have a similar drop.

The clear outlet is also located below the chamber floor and, if a 0.31 m (1.0 ft) concrete cover is provided over the outlet, the vertical distance from the chamber invert to the invert of the clear outlet will be 1.0 D_1, plus 0.31 m (1.0 ft). Combining this with the entrance drop of 0.8 D_1 to 1.5 D_1, will result in a total drop in the invert from the inlet to the clear outlet of 1.8 D_1 to 2.5 D_1, plus 0.31 m (1.0 ft). The drop in the hydraulic gradient in this case will be different. The circular weir is set a distance equal to the head on the weir below the top of the inlet sewer. If there is no submergence of the weir then the loss in the hydraulic gradient will be equal to this head. Trial computations indicate the head on the weir is about 0.2 D_1. Allowing for friction losses in the outlet pipe and some freeboard downstream of the weir, the drop in hydraulic gradient is about 0.4 D_1.

When the inlet sewer is surcharged different hydraulic conditions will exist in the helical separator. If the inlet is surcharged an amount equal to D, the transition invert will be level, as shown in Figure 14. The drop in the invert from the inlet to the foul outlet will be zero (neglecting the channel slope through the separator). The drop in hydraulic gradient will also be zero. Likewise, the drop in the invert from the inlet to the clear outlet will be zero. However, the loss in hydraulic gradient for this case will be 1.0 D.

In the case of the swirl concentrator, if a surcharge of D_1 is permitted then the crown of the sewer can be set a distance of D_1 below the water surface of the chamber. The drop from the chamber invert to the foul outlet will be 0.61 m (2.0 ft), as previously computed. Therefore, the drop in the invert from the inlet to the foul outlet will be 0 to 0.5 D_1, plus 0.61 m (2.0 ft). The drop in

TABLE 4
TYPICAL HEAD LOSSES IN HELICAL BEND AND SWIRL CONCENTRATOR REGULATORS

	Helical Separator	Swirl Concentrator
Dry Weather Flow – Drop in Invert		
Helical Separator		
Transition invert level	None	
Transition roof level	1.0 D	
Swirl Concentrator		1.08 D to 1.33 D
Wet Weather Flow		
Helical Separator		
Transition invert level		
Hydraulic grade	1.0 D	
Drop in invert	None	
Transition roof level		
Hydraulic grade	1.0 D	
Drop in invert	1.0 D	
Swirl Concentrator		
Hydraulic grade		0.58 D
Drop in invert		2.1 D

Note: Friction losses not included in above Table.

hydraulic gradient will be the same. The drop from the chamber invert to the clear outlet invert will be 1.0 D_1, plus 0.31 m (1.0 ft), as before. Therefore, the total drop from the inlet invert to the clear outlet invert will be 1.0 D_1 to 1.5 D_1 plus 0.31 m (1.0 ft). The drop in hydraulic gradient will be about 0.4 D_1 as computed previously.

The data relative to the foregoing discussion are shown in Table 4, Typical Head Losses in Helical Bend and Swirl Concentrator Regulators.

From the Table, it is apparent that the drop in the invert is always greater in the swirl concentrator than in the helical separator. When the inlet sewer is not surcharged, the drop to the foul outlet is only slightly greater but the drop to the clear outlet is about twice as great. When the inlet sewer is surcharged an amount equal to D or D_1, the drop in the invert is zero in the helical separator, compared to the minimum drop of 0.61 m (2.0 ft) to the foul outlet and of 1.0 D_1, plus 0.31 m (1.0 ft) to the clear outlet in the swirl concentrator. For dry-weather flows, the drop in hydraulic gradient is similar to the drop in the invert. For wet-weather flows, the drop in hydraulic gradient from the inlet to the clear outlet in the swirl concentrator is about one-half that for the helical separator.

Construction Details

Means of access must be provided to the curved section of the separator for maintenance purposes, including possible washing down after each storm event. The provision of a superstructure over this section is desirable for safety and esthetic reasons, and for confining possible odors. The type of superstructure used will depend on the character of the locality. As a minimum and for purposes of this report, the walls are assumed to be of concrete block and the roof of precast concrete units. For roof spans exceeding about 8.5 m (28 ft), it will be necessary to provide structural steel framing.

A cross section of the helical separator with a superstructure is shown in Figure 21, Typical Cross Section, Helical Bend Regulator. In this Figure, for cost estimating

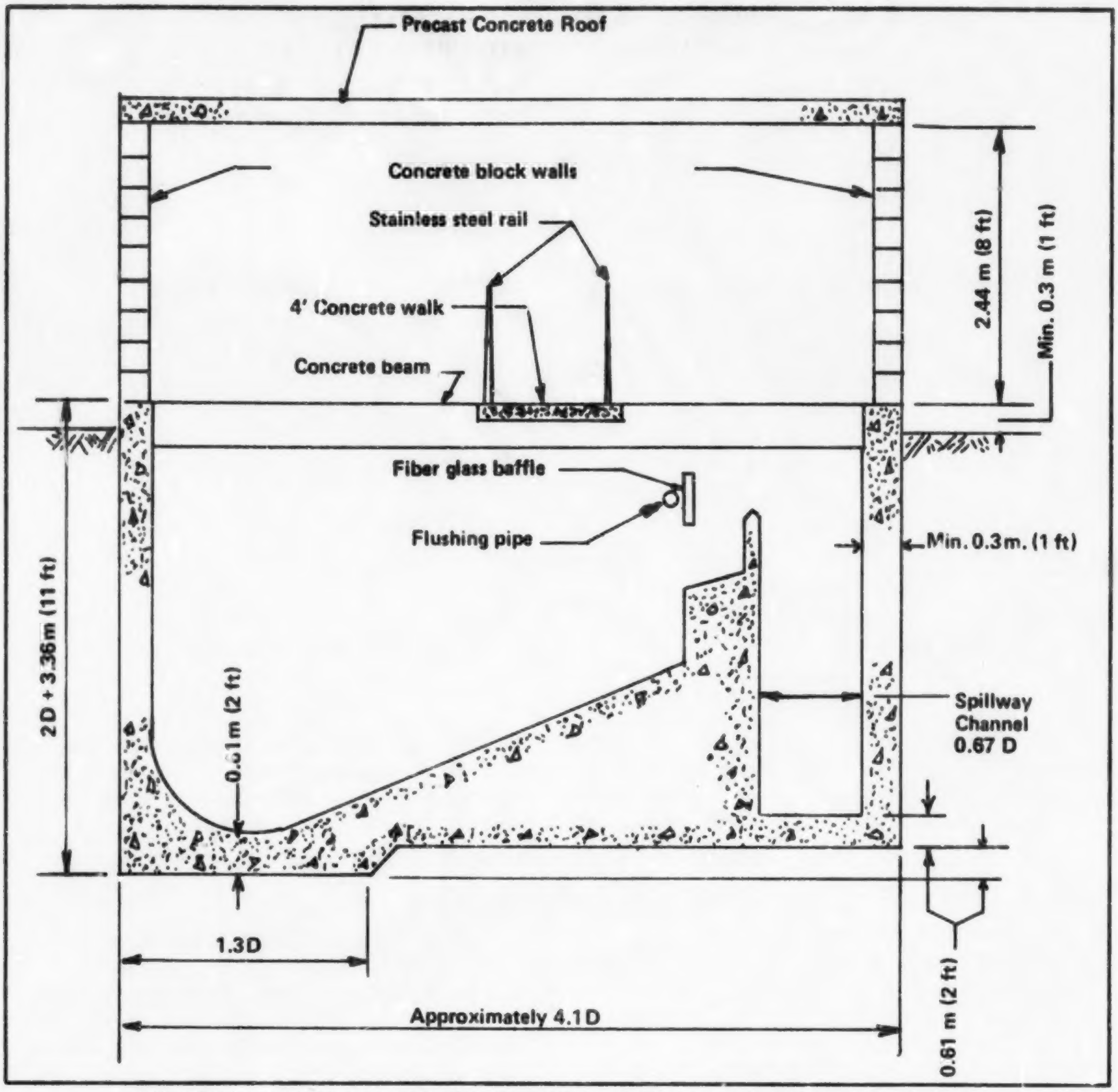

FIGURE 21 TYPICAL CROSS SECTION – HELICAL BEND REGULATOR

purposes the width of structure is indicated as 4.1 D and the width of spillway channel as 0.67 D. For any specific case the width and elevation of the spillway channel may vary from that shown in Figure 21, Typical Cross-Sectional Helical Separator, as explained previously.

The hydraulic conditions require that the transition section be provided with a roof. These conditions do not apply to the straight section, having a length of 5 D, preceding the curved section. It is not apparent from the model studies that this section will require the same maintenance as the curved section. Accordingly, there appears to be no need to make this section accessible.

For purposes of this report it has been assumed that the straight section will have walls 2.5 D high and will be provided with a concrete roof at that elevation.

Other construction details considered necessary or desirable are as follows:

a. Provide concrete walls with a minimum thickness of 0.3 m (1 ft), extending above grade a minimum height of 0.3 m (1 ft).
b. Provide a concrete walk 1.2 m (4.0 ft) wide.
c. Provide a stainless steel railing on each side of the walk.
d. Provide a fiberglass scum baffle hung from the beams or supported from the weir.
e. Provide a flushing water pipe on the channel side of the scum baffle and hung from the beams. Connect this line to the public supply with a backflow device, if this is permitted by local code. If this is not permissible, provide a storage tank to store overflow from the weir and a submersible pump to use for washing down. The usual criteria of 3.1 l/s (50 gpm) at 28,120 N/m^2 (40 psi) for flushing purposes at treatment plants should be applicable to the helical separator facility. Hose connections should also be provided in case the stream from the wash water pipe is not effective.
f. Provide concrete block walls with a height of 2.4 m (8.0 ft).
g. Provide a precast concrete roof.
h. Provide adequate electric lights.
i. Provide roof ventilators.
j. Provide doors at both ends of the structure for ventilation and access.

Cost estimates of the helical separator were made for two purposes: (1) to indicate the probable construction cost of the facility; and (2) to compare its costs with that of the swirl concentrator used as a combined sewer regulator.

The cost estimates are considered to be reasonable engineers' estimates. However, during periods of economic inflation, it is not unusual for contractors' bids to materially exceed engineers' estimates.

In making a choice between the helical separator and the swirl concentrator, it is possible that other factors related to the specific site of the facility may be of greater importance than the difference in construction costs.

Quantity Basis

The estimated quantities are based on the following:

a. The transition will be constructed with a drop in the invert equal to D as shown in Figure 14, so that the sewer upstream of the transition will not be surcharged.
b. The straight section preceding the curved section will have walls 2.5 D high and concrete roof.
c. The superstructure over the curved section will be as shown in Figure 21.
d. The width of the curved section is assumed to be 4.1 D; the width of the spillway channel is assumed to be 0.67 D.
e. The cover on the sewer at the transition inlet will be 2.44 m (8.0 ft).
f. The ground is level and the subsurface is earth with no groundwater problems.
g. All concrete walls will have a minimum thickness of 0.3 m (1.0 ft), except the weir.
h. Sheet piling will be required about 0.6 m (2.0 ft) outside the structure.
i. Transverse concrete beams will be required at 4.5 m (15 ft) intervals with the cross section 0.45 m (1.5 ft) square.
j. The continuous concrete walk will be 1.22 m (4.0 ft) wide and 0.20 m (0.67 ft) thick.

Cost of Helical Separator

The costs are based on the following:

a. The Engineering News-Record Construction Cost Index average for the United States is 2,100
b. Unit prices are as follows:

Steel Sheer Piling	\$ 86/m^2	\$ 8/sf
Excavation	\$ 16/m^3	\$ 12/cy
Reinforced Concrete	\$326/m^3	\$250/cy
Concrete Block Walls	\$107/m^2	\$ 10/sf
Roof	\$150/m^2	\$ 14/sf

c. Miscellaneous costs are assumed to be 25 percent of the foregoing items and to include a manual sluice gate and manhole, handrail, flushing water facilities, scum baffle, electrical work, roof ventilators and doors.
d. The estimated cost of the bypass sewer during construction is based on providing a sewer of the same diameter as a transition inlet around the proposed separator, plus an allowance for temporary connections at each end.
e. Contingent and engineering costs will be 25 percent of the foregoing items.

The resultant costs are shown in Table 5, Construction Cost of Helical Bend Regulators.

Cost of Swirl Concentrator

Typical dimensions for three sizes of the swirl concentrator are given in Table 6, Swirl Concentrator Dimensions, based on Figures 7 and 11 of Report EPA-670/2-74-039. The cost estimates are based on these dimensions and on the construction details shown in Figures 12, 13, and 14 of Report EPA-R2-72-008.

TABLE 5
CONSTRUCTION COST OF HELICAL BEND REGULATOR

Capacity 1.42 m^3/s (50 cfs)

ITEM	QUANTITY		AMOUNT
Sheet Piling	420 m^2	(4,550 sf)	$ 36,150
Excavation	950 m^3	(1,240 cy)	15,200
Reinforced Concrete	250 m^3	(330 cy)	81,500
Concrete Block Walls	114 m^2	(1,230 sf)	12,200
Roof	85 m^2	(910 sf)	12,750
		Sub Total	$157,800
Miscellaneous Costs		25%±	39,450
Bypass Sewer			20,000
		Sub Total	$217,250
Contingent & Engineering Costs			54,000
		Total	$271,250

Capacity 2.83 m^3/s (100 cfs)

ITEM	QUANTITY		AMOUNT
Sheet Piling	710 m^2	(7,700 sf)	$ 61,050
Excavation	2,200 m^3	(2,800 cy)	35,200
Reinforced Concrete	475 m^3	(620 cy)	154,850
Concrete Block Walls	160 m^2	(1,740 sf)	17,150
Roof	170 m^2	(1,800 sf)	25,500
		Sub Total	$293,700
Miscellaneous Costs		25%±	73,300
Bypass Sewer			39,000
		Sub Total	$406,000
Contingent & Engineering Costs		25%±	102,000
		Total	$508,000

Capacity 4.67 m^3/s (165 cfs)

ITEM	QUANTITY		AMOUNT
Sheet Piling	950 m^2	(10,200 sf)	$ 81,700
Excavation	3,200 m^3	(4,180 cy)	51,100
Reinforced Concrete	679 m^3	(888 cy)	221,350
Concrete Block Walls	200 m^2	(2,130 sf)	21,400
Roof	250 m^2	(2,700 sf)	37,500
		Sub Total	$413,150
Miscellaneous Costs		25%±	103,850
Bypass Sewer			56,000
		Sub Total	$573,000
Contingent & Engineering Costs		25%±	143,000
		Total	$716,000

TABLE 6
SWIRL CONCENTRATOR DIMENSIONS

Design Discharge	m^3/3	1.42	2.83	4.67
	(cfs)	(50)	(100)	(165)
Diameter of Chamber	D_2 m	6.85	9.0	11.0
	(ft)	(22.5)	(29.5)	(36.0)
Diameter at Inlet	D_1 m	1.15	1.50	1.83
	(ft)	(3.75)	(4.92)	(6.00)
Height No. 1				
1-5/6 D + 2.74 m	m	4.55	5.18	5.79
(i-5/6 D 2 2.74 m	(ft)	(14.9)	(17.0)	(19.0)
Height No. 2				
Floor to Weir d_1	m	1.71	2.26	2.74
	(ft)	(5.6)	(7.4)	(9.0)
Head on Weir for 150%	m	0.27	0.40	0.55
Design Discharge	(ft)	(0.9)	(1.3)	(1.8)
Clearance to Walk	m	0.30	0.30	0.30
	(ft)	(1.0)	(1.0)	(1.0)
Headroom	m	2.44	2.44	2.44
	(ft)	(8.0)	(8.0)	(8.0)
Total	m	4.72	5.40	6.03
	(ft)	(15.5)	(17.7)	(19.8)
Use for Height	m	4.72	5.40	6.03
	(ft)	(15.5)	(17.7)	(19.8)

Note: Height is from invert to underside of roof.

The height of the structure from the invert of the chamber to the underside of the roof is based on the following criteria:

Criteria 1: The clearance between the top of the walk and the water surface is 0.31 m (1.0 ft) when the discharge is 150 percent of design discharge and the foul outlet is not functioning. The head on the weir is determined from Figure 11, Head Discharge Curve for Circular Weir, in Report EPA-R2-72-008. It is assumed that the emergency weir starts overflowing when inflow to the chamber reaches the maximum design discharge for the facility.

Criteria 2: The headroom above the walk is 2.44 m (8.0 ft). The depth of the structure below the ground surface was based on the following criteria:

Criteria 3: The cover on the crown of the sewer is 2.44 m (8.0 ft).

Criteria 4: To prevent surcharge on the inlet sewer, the crown of the inlet sewer shall be the same elevation as the water surface at design discharge.

As shown in Table 6, the depth below the ground surface, based on Criteria 3 and 4, is less than the interior height, based on Criteria 1 and 2; therefore, the height is adequate to provide a structure with a roof above the ground surface. If the roof slab is assumed to be 0.25 m (0.83 ft) thick, then the top of roof is about 0.61 m (2 ft) above the ground surface, as shown in Table 6.

Additional assumptions for estimation purposes are as follows:

a. The walls are 0.30 m (1.0 ft) thick.
b. The roof is of poured concrete, about 0.25 m (0.83 ft) thick, with two beams 0.92 m (3.0 ft) by 0.46 m (1.5 ft).
c. The bottom concrete slab is 0.61 m (2.0 ft) thick.
d. The concrete walk is 1.22 m (4.0 ft) wide and supported on concrete beams.
e. The superstructure is 3.96 m (13.0 ft) long by 1.52 m (5.0 ft) wide, by 2.44 m (8.0 ft) high.

The unit prices used were the same as those used for the helical separator.

The miscellaneous cost is taken as 25 percent and is intended to include stairs, handrail, scum baffle, circular weir, flushing water system and pipes, a manual sluice gate and manhole, electrical work, ventilating work and doors.

The cost of the bypass pipe is assumed to be 50 percent of the bypass pipe for the helical separator.

Contingent and engineering costs are taken as 25 percent of the foregoing.

The costs of the three selected sizes of swirl concentrators, designed for 90 percent removal of grit, are shown in Table 7, Construction Cost – Swirl Concentrator.

Comparison of Costs

The estimated costs are shown graphically in Figure 22, Estimated Construction Costs – Helical Bend and Swirl Concentrator Regulator. As explained previously, although the two structures are sized for the same

TABLE 7
CONSTRUCTION COST – SWIRL CONCENTRATOR

Capacity 1.42 m^3/s (50 cfs)

Item	Quantity	Amount
Sheet Piling	200 m^2 (2,160 sf)	$ 17,200
Excavation	460 m^3 (600 cy)	7,360
Reinforced Concrete	98 m^3 (128 cy)	31,948
Concrete Block Walls	27 m^2 290 sf)	2,889
Roof	6 m^2 (65 sf)	900
Outlet Pipes		1,300
Downshaft and Plate		2,000
	Sub Total	$ 63,597
Miscellaneous Costs	25%±	15,403
Bypass Sewer		10,000
	Sub Total	$ 89,000
Contingent & Engineering Costs 25%±		22,000
	Total	$111,000

Capacity 2.83 m^3/s (100 cfs)

Item	Quantity	Amount
Sheet Piling	290 m^2 (3,120 sf)	$ 24,940
Excavation	900 m^3 (1,180 cy)	14,400
Reinforced Concrete	156 m^3 (204 cy)	50,856
Concrete Block Walls	27 m^2 (290 sf)	2,889
Roof	6 m^2 (65 sf)	900
Outlet Pipes		3,000
Downshaft and Plate		3,000
	Sub Total	$ 99,985
Miscellaneous Costs	25%±	24,515
Bypass Sewer		19,500
	Sub Total	$144,000
Contingent and Engineering Costs 25%±		36,000
	Total	$180,000

Capacity 4.67 m^3/s (165 cfs)

Item	Quantity	Amount
Sheet Piling	375 m^2 (4,030 sf)	$ 32,250
Excavation	1,360 m^3 (1,780 cy)	21,760
Reinforced Concrete	216 m^3 (282 cy)	70,416
Concrete Block Walls	27 m^2 (290 sf)	2,889
Roof	6 m^2 (65 sf)	900
Outlet Pipes		4,000
Downshaft and Plate		5,000
	Sub Total	$137,215
Miscellaneous Costs	25%±	34,785
Bypass Sewer		28,000
	Sub Total	$200,000
Contingent & Engineering Costs	25%±	50,000
	Total	$250,000

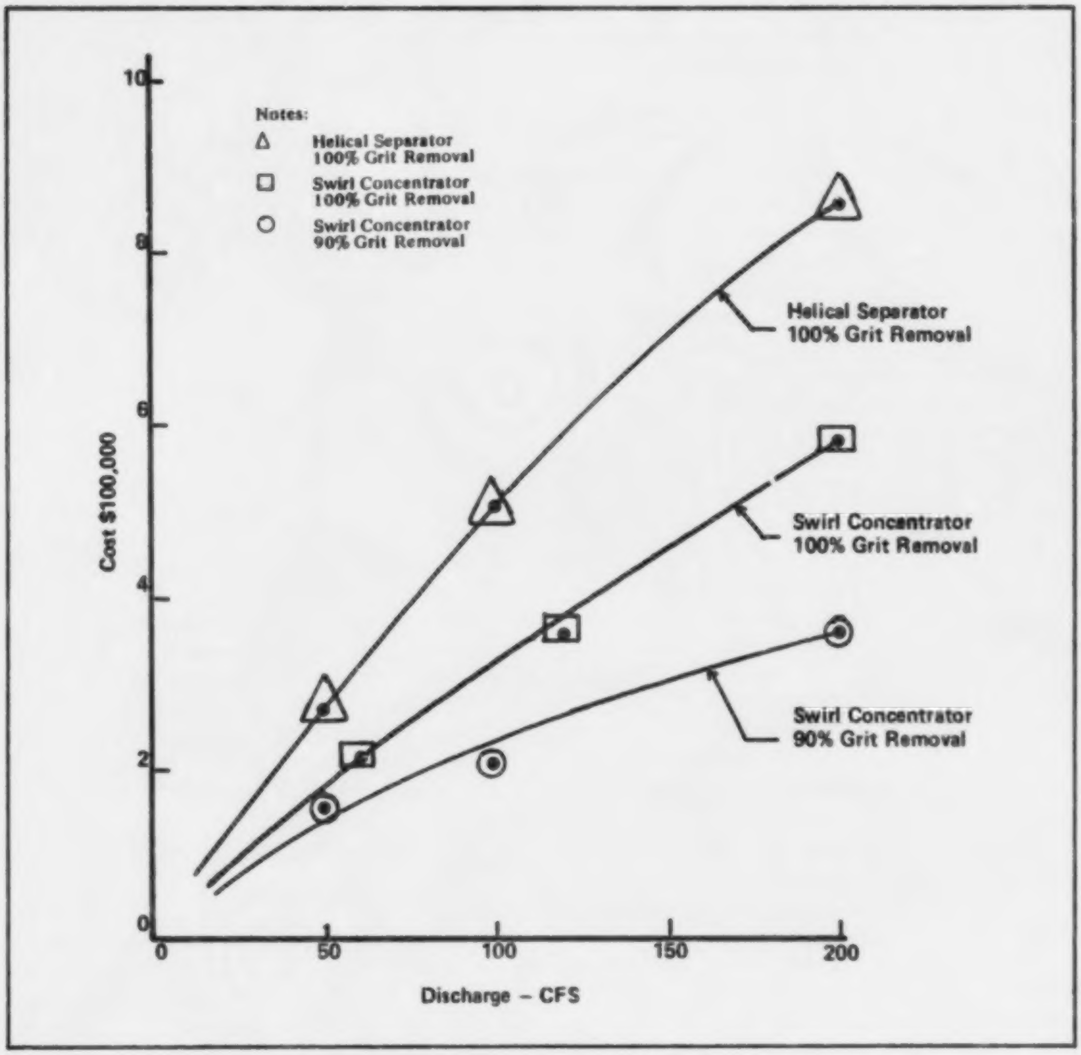

FIGURE 22 ESTIMATED CONSTRUCTION COSTS – HELICAL BEND AND SWIRL CONCENTRATOR REGULATOR

discharge, the helical separator will remove 100 percent of the grit compared to 90 percent for the swirl concentrator. The use of 90 percent removal is based on Report EPA-670/2-74-039, dated July, 1974, in which design curves are presented for 90, 80, and 70 percent recovery (or removal) of grit. An earlier report on the swirl concentrator, Report EPA-R2-72-008 of September, 1972, includes Figure 22, Separation Efficiency Curve, in Appendix I thereof. This curve indicates that a swirl concentrator designed for 90 percent removal of grit will remove 100 percent of grit when the discharge is 60 percent of the design discharge. Therefore, to remove 100 percent of the grit the structure should be sized for a discharge equal to 167 percent of the design discharge. Using this method, the costs of swirl concentrators to remove 100 percent of grit were estimated and the results shown in Figure 22.

The summary of all the estimated costs is shown in Table 8, Comparison of Construction Costs – Helical Bend and Swirl

TABLE 8
COMPARISON OF CONSTRUCTION COSTS – HELICAL BEND AND SWIRL CONCENTRATOR REGULATORS

Capacity	Swirl Concentrator	Helical Separator
1.42 m^3/s (50 cfs)	$111,000	$271,000
2.83 m^3/s (100 cfs)	180,000	508,000
4.67 m^3/s (165 cfs)	250,000	716,000

Note: Land costs not included.

Concentrator Regulators. The results indicate that, for the sizes used in the Table, the helical separator will cost 1.7 to 2.5 times as much as a swirl concentrator designed for 90 percent grit recovery and 1.5 to 1.6 times as much as one designed for 100 percent grit recovery.

Alternate Design – Solids Removal Efficiency

Further design techniques and the rationale based on mathematical data were evolved as a result of the model studies carried out by the General Electric Company. The procedure for designing a helical flow separator for a given discharge flowrate and specific suspended material is as follows:

Step 1: Characterize the settling properties of the suspended solids. A study[9] (see reference section) has emphasized the variability of the settling properties at different geographical locations. Once the cumulative distribution of settling velocities has been determined from column settling tests, the distribution should be broken down into 10 or more fractions, and the performance calculations outlined below should be repeated for each settling velocity fraction. Thus, assume that 10 percent of the material settles at a velocity lower than w_2 etc. The performance for each settling velocity is then determined and the overall recovery efficiency is computed as the weighted average of the recovery for the individual fractions.

Step 2: Determine a scale factor, S, as the ratio

$$S = \frac{Q_D}{Q_1}^{2/5}$$

in which Q_D is the design discharge rate and Q_1 is a selected flowrate within the range of the laboratory experiments 0 to 0.85m^3/sec (0-31.1 cfs). Selecting Q_1 near the lower end of the range will give better recovery efficiencies, but will also require a larger unit. The selection of Q_1 can be iterated, as described in the subsequent step.

Step 3: Determine a rough estimate of the prototype performance by calculating first an equivalent settling velocity w_e from

$$w_e = \frac{w_{.5}}{\sqrt{s}}$$

where $w_{.5}$ is the median (50%) settling velocity from the cumulative distribution determined in Step 1. The initial estimate of efficiency can then be found by entering Figure 23, Predicted Separation Efficiency Versus Settling Velocity at Several Flowrates, with settling velocity w_e, and interpolating for the recovery efficiency at the selected flowrate Q_1. If this estimated efficiency is lower than about 80 percent, it is probably desirable to select a lower value of Q_1 (to provide a larger unit), and repeat steps 2 and 3. Conversely, if the estimated efficiency is greater than 95 percent, a smaller unit will probably suffice, and a larger Q_1 can be selected.

Step 4: A refined estimate of the recovery efficiency can be obtained by calculating an equivalent settling velocity for each settling velocity fraction w_i of step 1.

$$w_{e_i} = \frac{w_i}{\sqrt{s}}$$

The recovery efficiency for each of these fractions is then determined from Figure 23 as in Step 3. The overall recovery efficiency is the weighted average of the results for each individual fraction.

Step 5: The inlet diameter, D, should then be

$$D = 0.95\ s\ (\mathrm{ft})$$

or

$$D = 3\ S\ (\mathrm{meters})$$

The inlet dimensions are given in terms of D as described in the preceding paragraphs.

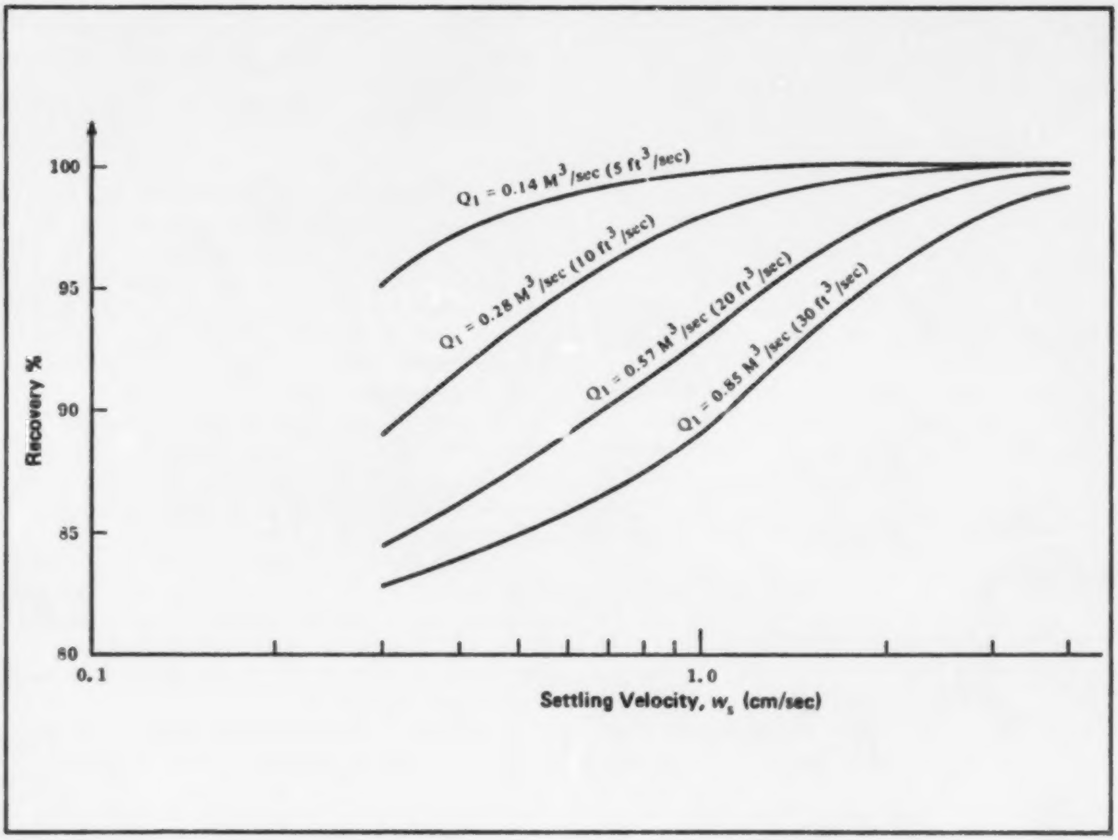

FIGURE 23 PREDICTED SEPARATION EFFICIENCY VERSUS SETTLING VELOCITY AT SEVERAL FLOWRATES

SECTION IV
IMPLEMENTATION

Use of the helical bend combined sewer overflow regulator should be considered where there is a requirement to improve the quality of the combined sewer overflow, or where there is insufficient hydraulic head to allow construction of a swirl concentrator. Table 4 indicated the typical hydraulic head losses in both the helical bend and swirl concentrator regulators. The helical bend regulator, because of its length, can be expected to have a higher construction cost than the swirl concentrator. Removal of floatable solids should be of the same order.

An important difference in the operation of the two units, however, is that the solids removed from the overflow by the helical bend regulator may be expected to be released to the interceptor sewer at the end of the storm – the *first flush* will be at the end of the storm. This characteristic may result in less shock loading and more efficient operation at the treatment facility.

The helical bend regulator is essentially linear and, thus, construction should be possible within existing street rights-of-way. The essential features of the device are as follows:

Inlet: The inlet is the collector sewer of any shape.

Transition Section: The helical bend can curve to the right or left, depending on the direction of flow in the interceptor sewer or the available right-of-way. The transition section flares from the inlet to a width of 3D in a distance of 15D. The section also deepens to a depth of 2.0D. The section is covered to facilitate the development of uniform flow conditions.

Straight Section: A 5D straight section with the same configuration as the remainder of the structure is required to fully control the flow and eliminate cross currents.

Bend: A 60 degree bend of a radius is selected on the basis of the design used. The floor of the bend should be smooth.

Weir: A side-spill, curved weir along the outside of the bend is used to draw off the clarified overflow.

Scumboard: A scumboard is set 1/6D to 1/3D in from the weir, with a minimum submergence depth, to trap floatables.

Outlet: The outlet should be sized to allow 4.5 to 5 times the dry-weather flow to pass without activating the regulation characteristics. This will allow passage of peak dry-weather flows. However, maximum flow to the wastewater treatment plant during storm events is limited to 1 to 3 times its dry-weather flow. Thus, a mechanical gate controlled by the flow in the interceptor is desirable. The outlet should be either 30.4 cm (12 in.) or of a size capable of being cleaned very easily in order that rags and other debris will not clog the opening.

The helical bend regulator can be constructed of concrete or any other appropriate material. Ordinarily, it will be desirable to construct the regulator within a chamber in order that maintenance may be readily performed.

Normal requirements for such chambers, such as ventilation, lighting, safe access and other features must be provided.

SECTION V
Glossary of Pertinent Terms
Helical Bend Report

Combined Sewer – A pipe or conduit which collects and transports sanitary sewage, with its component commercial and industrial wastes and inflow and infiltration during dry-weather conditions, and which, in addition, serves as the collector and conveyor of stormwater runoff flows from streets and other sources during precipitation and thaw periods; thus, a pipe or conduit which handles all of these wastewaters in a single or "combined" facility

Dip Plate – A vertical plate or baffle which is partially immersed in flowing liquid in a manner that will prevent the discharge of surface or floating materials over an outlet weir; in the helical bend studies, a baffle plate placed near the overflow weir, at a predetermined distance therefrom and with a predetermined depth of "dip" or immersion, to prevent the overflow of floating solids with the clarified effluent

DWF (Dry-Weather Flow) – The flow through the helical bend during periods when no stormwater runoff is collected and transported by the combined sewer which discharges through the helical bend section

Equation of Motion – A mathematical equation which expresses the hydraulic patterns of flow occurring in any vessel, chamber, conduit or other appurtenant structure in which fluid flow is occurring

Foul Sewer – The sewer connected to the foul outlet of the helical bend, through which the solids slurry deposited in the bottom of the helical section is discharged to a downstream wastewater treatment facility or to any other predetermined point of disposal

Floatables – The lighter-than-water solids, including congealed floating materials which rise to the surface of the wastewater flowing through the helical bend regulator, and which must be intercepted and prevented from discharging with the clarified effluent flowing over the outlet weir; the material retained by a dip plate or scum board

Floor Flow Angle – The angular pattern of the flow of wastewater and solids as it traverses the bottom or floor of the helical bend separator as part of the helix form of liquid movement through the device; in this study, the floor flow angles were disclosed by the pattern of movement along the bend floor of Process Black ink injected at appropriate points along the floor.

Gilsonite® – Synthetic solid material utilized in the helical bend studies to simulate the grit particles which will be contained in combined sewer flows to be handled in prototype units in actual field practice; material having a specific gravity of 1.06 and a size range of 0.5 to 3 mm

Grit – Heavier and larger-sized solids contained in stormwater flows in combined sewers, or in dry-weather flows, which because of their size and specific gravity settle in a helical bend separator more readily than organic materials contained in the flow; material having a specific gravity of 2.65, more or less, and an effective size of 0.2 mm.

Helical Bend – A physical configuration of a pipe or open channel which results in a bend or radius through which a liquid flow occurs in a manner that produces helical, or secondary flow phenomena, inducing the rapid separation of solids from the liquid and the deposition of the solids along the inner diameter of the radius; in the study, the total helical bend assembly consisted of a transition section, a straight section, and the bend section

Helical Flow – The pattern of liquid flow induced by the helical bend, characterized by a helical configuration, or secondary motion, created in the liquid flow

Hydraulic Head Loss – The lowering of the hydraulic flow line through a pipeline, device, chamber or other facility, due to dynamic conditions which produce friction, turbulence or other conditions that are translated into loss of pressure, or head, or free water gradient surface level

Mass Flux – The rate of flow of the total body of liquid and solids flowing through any device or facility, such as a helical bend; the flow energy in the total fluid body in the device or facility; a measure of the strength of a field of force in a given area, such as in any part of a helical bend section, in the case of the study reported herein

Organic Solids – Solids of a non-grit or light-weight nature, contained in a sewer flow, which are subject to decomposition and consequent oxygen-consumption in receiving waters into which stormwater overflows from combined sewers discharge, and which impose pollutional oxygen-demand loadings on such water resources; the function of a helical flow regulator is to control the volume of overflow wastewaters and to remove grit and organic solids from the effluent.

Petrothene® – A synthetic plastic material which has a specific gravity of 1.01 and was used in the helical separator studies to simulate the lighter organic materials contained in combined wastes handled by prototype helical bend regulators in actual field practice

Prototype – A full-scale replica of the laboratory test model (in this case, of the helical bend model), designed in scaled-up proportion to the test model, for use in actual field installations; the study provided design criteria for the dimensioning of various sizes of full-scale installations to handle predetermined volumes of combined sewer flows

Recovery – The percentage of solids introduced into the helical bend separator-regulator with the combined wastewater flow that will settle in the bend chamber and be drawn off from the bottom via the foul outlet and the foul sewer; the measure of the efficiency of the helical bend device in clarifying the overflow effluent and thereby reducing the pollutional effect of the overflow incidents on receiving waters

Regulator – Any device in a combined sewer system which regulates or controls the amount of concentrated wastewater diverted to interceptor sewers and downstream treatment facilities and, consequently, the amounts of effluent discharged to receiving waters, or holding or treatment facilities

Scum Board – A vertical plate or baffle which is partially immersed in the flow liquid and partially above the flow line, in order to capture and retain floating scum solids and prevent their discharge over an overflow weir with the clarified effluent; in this study, a scum board and a dip plate have similar functions

Solids Simulation – The use of test solids in the model, of a weight and size which simulate, in scale-down, the composition and character of solids materials in actual combined sewer flows to be handled in prototype devices – in this case, in prototype helical bend systems in combined sewer lines

Straight Section – The part of the helical bend structure which precedes the bend section and delivers the flow uniformly and without velocity interferences into the helical section; in the studies of the helical bend principle, it was determined that the straight section having a length of five times the diameter of the sewer pipe will be required for effective solids recovery in the helical bend system

Spillway Channel – The channel or conduit which receives the overflow effluent from the helical bend weir section and delivers it to a pipe or conduit leading to receiving waters, or facilities for the retention and/or treatment of the clarified wastewater discharge

Swirl Concentrator – A cylindrical chamber in which hydraulic flows experience swirl-type liquid flow patterns that induce relatively rapid separation of solids from the flow, and, thereby, produce a clarified effluent which is discharged from the chamber, freed from solids which are collected in the bottom of the swirl chamber and discharged via a foul sewer outlet; in this study, the helical separator was intended to perform the same general function as a swirl concentrator used as a combined sewer regulator

Transition Section – That portion of the helical bend composite which carries the combined sewer flow from the entering sewer pipe section and delivers it to the straight section and thence to the bend section; the transition section in the studies had a length of at least fifteen times the inlet sewer diameter and expanded the flow cross section to three times the inlet diameter

WWF (Wet-Weather Flow) – The flow in the combined sewer during periods of precipitation or thaw runoff, composed of the dry-weather flow plus the storm runoff volume

The following are registered trademarks:

Gilsonite
Petrothene
Perspex
Plexiglas

SECTION VI
REFERENCES

1. *Problems of Combined Sewer Overflow* FWPCA – WP-20-11, December, 1967.

2. *Swirl Concentrator as a Combined Sewer Overflow Regulator Facility*, EPA – R2-72-008, September 1972. PB-214 687.

3. *The Secondary Flow in a Meandering Channel*, by T.M. Prus-Chacinski, Unpublished, PhD Thesis, University of London, 1955.

4. *Secondary Motion Applied to Storm Sewage Overflows*, by T.M. Prus-Chacinski and J. W. Wielogorski, Symposium on Storm Sewage Overflows, Institute of Civil Engineers, London, 1967.

5. *Formulas for Bed-Load Transport* by E. Meyer-Peter and R. Muller, Proceedings IAHR Second Meeting, Stockholm, 1948.

6. *The Bed-Load Function for Sediment Transportation in Open Channel Flows* by H. A. Einstein, U.S. Department of Agriculture, Technical Bulletin No. 1026, September 1950.

7. *Combined Sewer Regulation and Management – Manual of Practice*, FWQA – 11022 DMUO, July 1970.

8. *Water Supply and Waste Water Disposal*, by G. M. Fair and J. C. Geyer – John Wiley & Sons, Inc., New York, 1954.

9. *Physical and Settling Characteristics of Particulates in Storm and Sanitary Wastewaters*, by Robert J. Dalrymple, Stephen L. Hodd, and David C. Morin, EPA-670/2-75-011, April 1975.

APPENDIX A
HYDRAULIC MODEL STUDY

This report covers the hydraulic studies of the helical bend application to the separation of solids from combined sewer flows as carried out at the LaSalle Hydraulic Laboratory, Montreal, Quebec, Canada.

The most complete investigation of the helical bend principle, as applied to the current investigation, was carried out by Dr. T. M. Prus-Chacinski, as reported in his 1955 thesis at Imperial College of Science, London, titled *The Secondary Flow in a Meandering Channel.*[2] He augmented his 1955 thesis with further studies as a Partner of C. H. Dobbie and Partners, Consulting Engineers, London, at the University of Surrey and the Mersey River Authority Hydraulic Laboratory in Warrington, near Liverpool. These studies led to the construction of a prototype at Nantwich, Cheshire, England, for research on behalf of the Construction Industry Research and Information Association.

As flow proceeds around a bend, secondary currents develop, with the upper volume tending to move toward the outside, while the bottom current angle is directed toward the inside of the bend. Actual trace studies made of this secondary motion show that it describes a spiral or helical pattern. This phenomenon is well known in rivers where the deepest section of the channel is usually scoured on the outside of any bends, and the fine sand has been buoyed up by the bottom currents and deposited at the inside.

In the present study of the bend principles, the object was to impose just the opposite geometry from that of a natural stream – i.e., to have the deepest point at the inside of the bend. In this manner, the pollutants would be carried by the helical flow down into the deepest section where they would have optimum opportunity to settle out. Furthermore, the flow velocities in the study were to be controlled in the transition and straight sections so the solids would begin to concentrate in the lower stratum of the flow. The combined effect of these two phenomena would be to settle the solids out of the liquid flow, and to concentrate them in the deepest section of the chamber, where they could be delivered, via a foul sewer, to the treatment plant. The major part of the liquid flow would then be clarified and could be discharged over a weir for discharge to the receiving stream, or to subsequent holding or treatment processes.

Starting with a basic structure layout established by Dr. Prus-Chacinski, the object of the study was to evaluate the effects of changes in width, depth, length of approach channels, and discharge and conduit configurations on solids separating efficiency.

The inlet pipe to the model was selected as a 15.2 cm (6 in.) diameter P.V.C. pipe. Based on the agreed geometric proportions to start the study, this first dimension established the model layout as shown on Figure 4 of the foregoing report, Helical Bend Regulator–Separator, Form 3 (Model Layout), and as depicted in Figure 24, Downstream View of Model, and Figure 25, Upstream View of Model.

Unmeasured water flows were delivered through the supply pipe, which was fitted with a discharge control valve and solids injection equipment, shown in Figure 26, Solids Injection Vibrator. The original structure began at the entrance to the transition section; this was made of Plexiglas® and was 20 diameters (20D) long to ensure adequate flow deceleration. Following this, a straight length of 10 D, also constructed of Plexiglas, carried the flow to the start of the bend.

The bend itself was built of Plexiglas, using a 2.44-m (8 ft) radius from the extension of the inlet pipe centerline. Since the model was intended to demonstrate the basic principles of the secondary motions being studied, the bend was carried around through an angle of 120°. Side channels were provided on each side to accommodate the clear overflow spill from either the inside or the outside of the bend. Control of either the whole flow or just the small foul outflow was provided by a perforated slide gate at the 120° position.

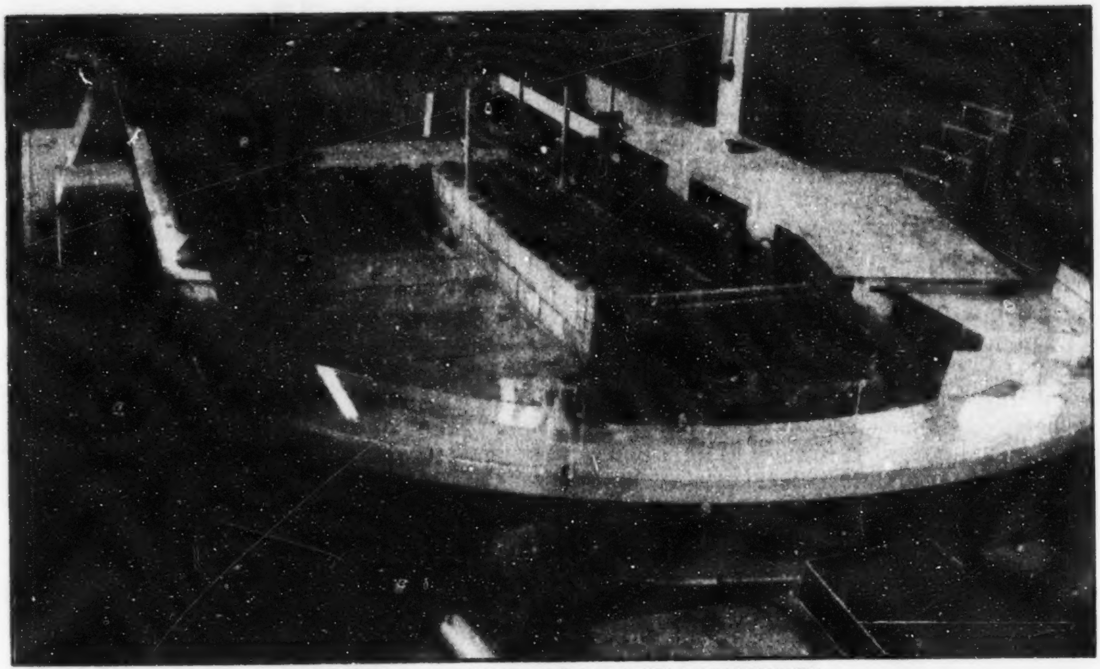

FIGURE 24 DOWNSTREAM VIEW OF MODEL

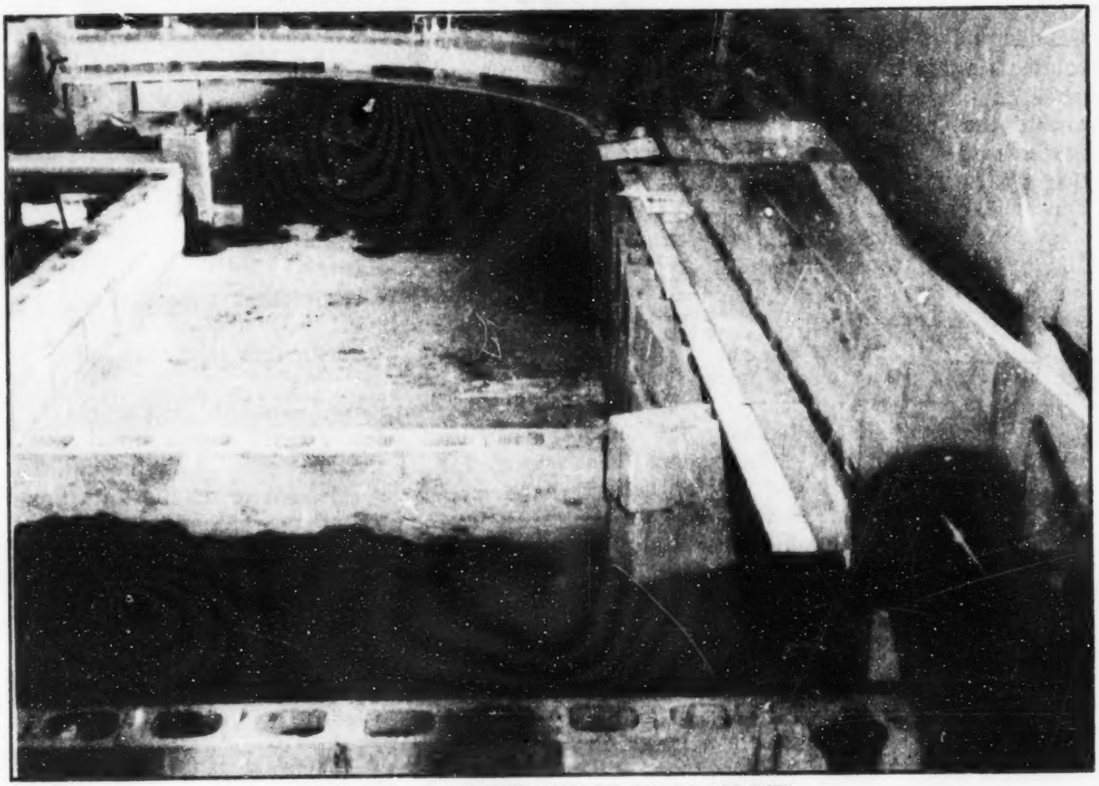

FIGURE 25 UPSTREAM VIEW OF MODEL

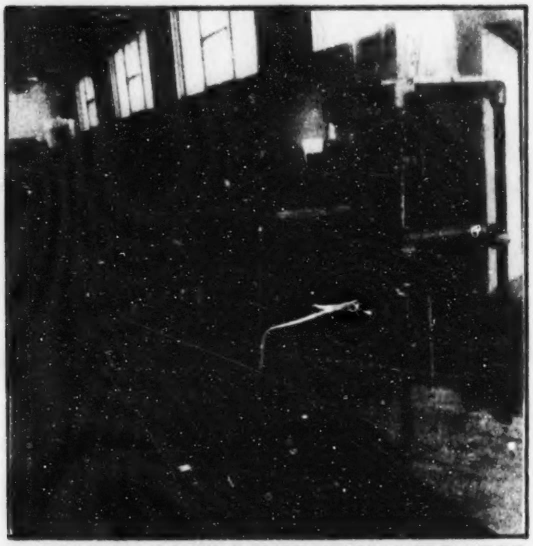

FIGURE 26 SOLIDS INJECTION VIBRATOR

The basic floor cross section inside the transition, straight sections, and the bend was made of polished cement mortar, as shown in Figure 4 of the foregoing report. Simple modifications to the Plexiglas overflow weirs could be made to either change their positions horizontally or their levels.

Flow spilling over the side weir was directed to a calibrated Rehbock weir basin, where the water levels could be read and the discharge determined. Similarly, the foul outflow was taken to a second basin for measurement over a small 90° V-notch weir, as was shown in Figure 5, Discharge Measuring Weirs.

Injections of Process Black ink were introduced on the floor of the bend. They created clearly defined trace patterns which could be read with a protractor to measure the angle of the flow along the floor.

Tests involving solids recovery were performed, using a standard procedure. One liter of the selected model solids was injected at a predetermined rate into the supply pipe. The material entered the structure in the flow, and was subjected to the helical separation process. Any of the solids that went over the weir were caught on a screen in the measuring basin. The rest normally remained as a deposit in the bend, and were recaptured after the test by means of a screen.

The volumes of the two fractions were measured to determine that no material had been lost. The recovery rate, or efficiency, was then computed as the ratio if the solids retained in the bend with respect to the original 1-liter input, expressed as a percentage.

The model scale selected for comparisons to a reasonable prototype was 1/6. The pertinent scale relations are:

Scale = 1/6
Time = $1/\sqrt{6} = 1/2.45$
Discharge = $1/6^{5/2} = 1/88$

The prototype storm discharge with the pipe flowing full in the corresponding prototype 91.5-cm (3-ft) sewer was computed as 0.85 m^3/sec (30 cfs) which would correspond to 9.6 l/sec (0.339 cfs). In fact, to simplify operations on the model, a discharge of 10 l/sec (0.354 cfs) was used, giving a storm discharge of 0.88 m^3/sec (31.1 cfs).

Dry-weather flow (dwf) was defined as being one percent of the storm flow, or on the model 0.1 l/sec (0.004 cfs), and in the prototype 8.8 l/sec (0.31 cfs) through the foul outlet, to the interceptor sewer and the treatment works.

The methods used for solids simulation were presented in Section II.

The first tests were carried out with the model as shown on Figure 4, and overflow spill over the full 120° bend, for discharges of 5, 10, 15 and 20 l/sec (0.177, 0.354, 0.531 and 0.708 cfs, respectively). The helical motion was found to be very well defined. Measurements were made of the floor flow angles at the 35° position for straight-through flow, i.e., no spill over the weir, as shown on Figure 27, Top and Bed Flow Angles. The method for determining the angular flow along the floor of the helical bend is shown in Figure 28, Floor Flow Angles Measuring Equipment.

The resulting angles were treated, following Dr. Prus-Chacinski's equation, in the form:

$$\text{Tan}\ \alpha_0 = C_1 \ W/r_c/R_n{}^{1/4}$$

where:

α_0 = floor angle
C_1 = coefficient
W = wetted perimeter
r_c = central radius of bend
R_n = Reynolds number

and plotted on a partial copy of Figure 28 from his thesis, and included here as Figure

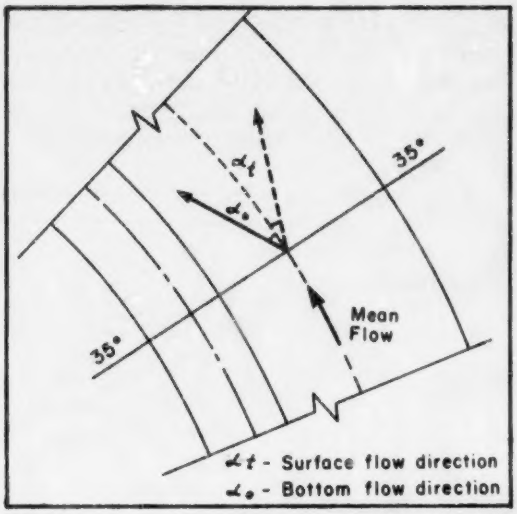
α_t
α_o
35°
35°
Mean Flow
α_t - Surface flow direction
α_o - Bottom flow direction

FIGURE 27 TOP AND BED FLOW ANGLES

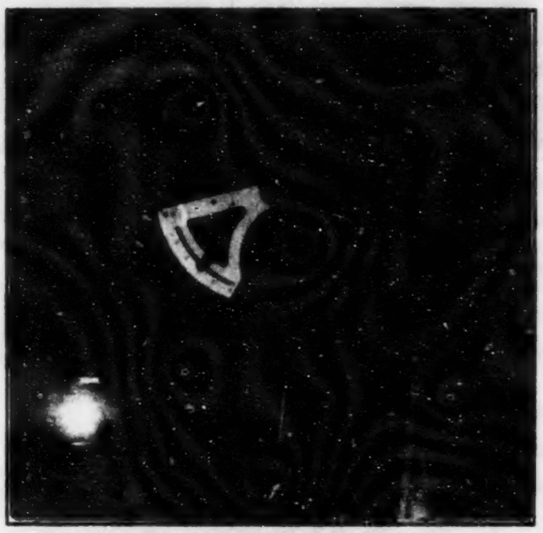

FIGURE 28 FLOOR FLOW ANGLE MEASURING EQUIPMENT

29, Bed Angle Relationships for Straight-Through Flow. The preliminary test points fell just below Dr. Prus-Chacinski's work for rectangular and semi-circular channels, but they were fairly close to those for triangular channels with the deepest point at the outside of the bend.

The fact that the points were lower than the Prus-Chacinski findings would normally indicate that the flow angle on the floor was less, from which it would be deduced that the helical action was weaker. However, observation in the model indicated just the opposite. Although the angle was perhaps lower, the helical flow was very strong, and the angular flow was acting over the full width of the floor. Brief tests with shredded Petrothene ® showed the model to be very efficient in concentrating the settleables toward the inner wall of the bend.

Further tests were performed, using various discharges up to 20 l/sec (0.708 cfs), first with spill over the full 120° bend. At this maximum discharge, deposits containing about 70 percent of the injected material appeared in the 60° to 70° range. A temporary wall was placed at the 60° position and Petrothene® was introduced again. About 60 percent of the material was deposited between the 30° and 50 ° points. From these first results, it appeared that careful attention should be paid to moving the solids through the structure to the foul outlet during a storm so as to prevent a build-up of so large a deposit that the dry-weather flow might be unable to move it out of the helical bend section.

Scale Selection and Discharges

As a result of the preliminary tests described above, the most likely acceptable discharge range had been defined in the model, so a firm scale was selected for further testing. This was taken as 1/6, meaning that the prototype inflow pipe would be 91.5-cm (3 ft) diameter. The selected discharges in the model were 10, 7.5, 5, and 2.5 l/sec, (0.354, 0.265, 0.177 and 0.088 cfs), corresponding to 0.88, 0.66, 0.44, and 0.22 m^3/sec (31.1, 23.3, 15.55 and 7.78 cfs) in the prototype.

The dry-weather flow (dwf) was specified as being one percent of the storm flow, or 8.8 l/sec (0.31 cfs) in the prototype. This would normally flow through the structure at a shallow depth along the invert, and discharge through the foul outlet to the treatment plant. It was further decided that during any storm event, three times the dry-weather flow (3 dwf) would be discharged through the foul outlet – i.e., 26.4 l/sec (0.93 cfs).

A series of rapid modifications were made in the model and tested in an attempt to determine the importance of the geometric

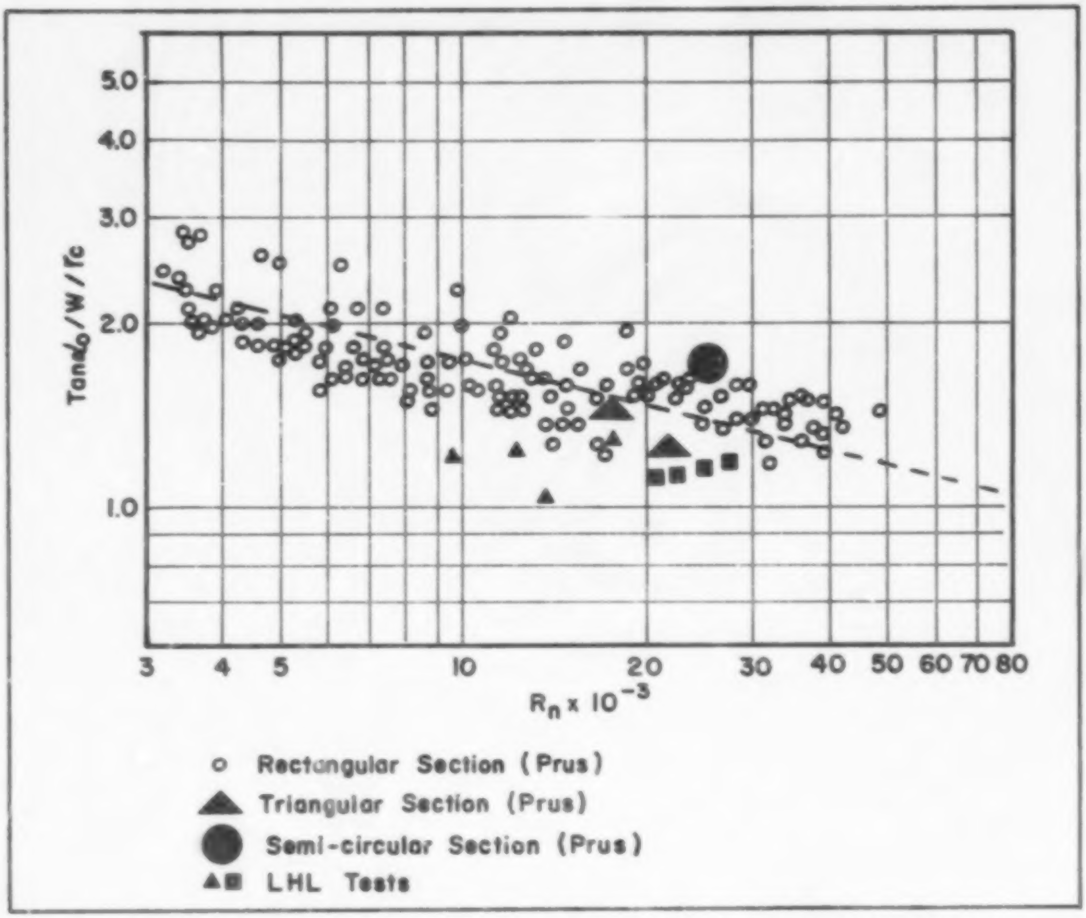

FIGURE 29 BED ANGLE RELATIONSHIPS FOR STRAIGHT-THROUGH FLOW

variables. All four discharges were run for a few tests, but it quickly became evident that only the 0.88 m^3/sec (31.1 cfs) should be used for comparisons, or at times, the 0.66 m^3/sec (23.3 cfs). Petrothene was used as the settleable material for most tests, with only one or two check runs using Gilsonite.

Data given in Table 9, Recovery Results – Modifications 1-8, show the recovery results for the first series of modifications tested. All cases shown are for the 0.88 m^3/sec (31.1 cfs) overflow discharge and 26.4 l/sec (0.93 cfs) foul outflow, with Petrothene used as the test material. All values are for prototype dimensions.

From the outset it was obvious that the long transition and straight sections formed a very efficient settling chamber. With Modifications 1 and 2, it was noted that all the Petrothene was deposited on the floor in the bend, so changes were made in an effort to cause the material to flow through to the foul outlet. This pattern seemed difficult to achieve with a short bend, so the full 120° length was tested. (Test 9) with the bleeder at 55°.

The recovery efficiency was reduced so much that this approach was given no further consideration. The bleeder was a small-diameter discharge pipe located as shown in Figure 30, Modification 6 – Tests 23-29.

The taper in Modification 4 induced much stronger helical motion, to such a degree as to cause an upflow and to carry more material up over the weir. The change is

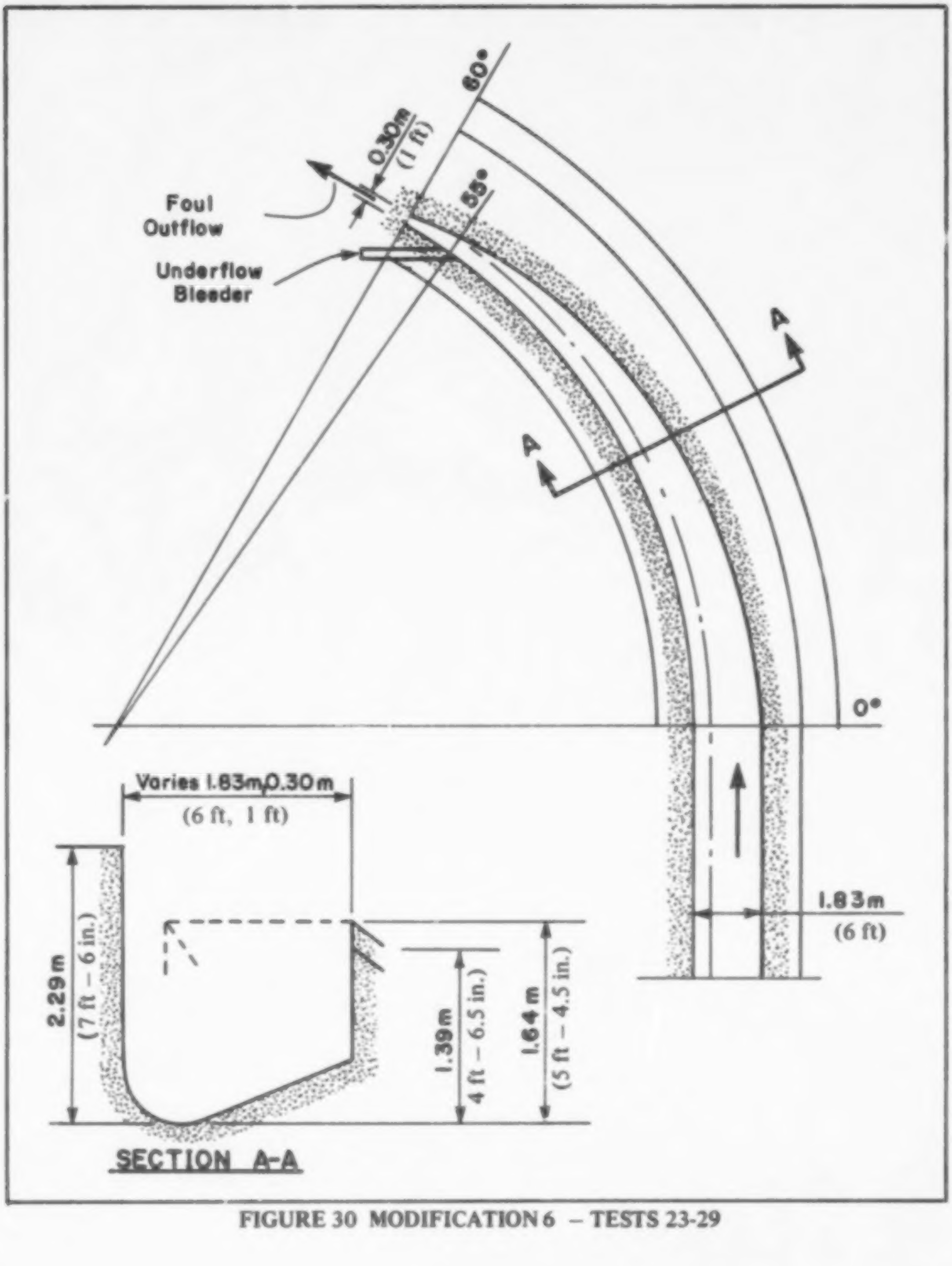

FIGURE 30 MODIFICATION 6 – TESTS 23-29

TABLE 9

RECOVERY RESULTS – MODIFICATIONS 1-8

Modification Number	Ref. Fig.	Test No.	Bend Length	Weir Length	Weir Height m. ft.	Recovery %
1	9	1	60°	60°	1.64 (5.38)	100
2	9	4	50°	50°	1.64 (5.38)	85
3	9	7	40°	40°	1.64 (5.38)	82
Orig.	1	9	120°	120°	1.64 (5.38)	50 (through bleeder at 55°)
4	10	13	60°	10°-50°	1.26 (4.13)	90
		16	60°	10°-50°	1.64 (5.38)	90
5	11	17	60°	60°	1.64 (5.38)	75
		20	60°	15°-60°	1.64 (5.38)	60
		22	60°	60°	1.33 (4.38)	60
6	12	23	60°	60°	1.33 (4.38)	65
		28	60°	60°	1.64 (5.38)	70 (through bleeder at 55°)
7	13	30	50°	50°	1.64 (5.38)	85
8	14	32	60°	60°	1.64 (5.38)	85
		34	60°	60°	1.39 (4.55)	83

shown in Figure 31, Modification 4 – Tapered Outlet. In spite of this increased secondary flow, the Petrothene recovered was still all on the floor of the bend, most of it ahead of the 35° position. Weir height and length changes did not have much apparent effect.

Modification 5 was the first attempt to enter the bend at a higher velocity so the Petrothene would be carried through to the foul outlet. The layout is shown in Figure 32, Modification 5 – Narrow Inlet, 2D Wide; and Figure 33, Modification 5 – Tapered Bend. The recovery rates dropped slightly, but the bottom deposits had moved along to the 35° to 55° position. The outstanding feature of this layout was the surface eddy which formed at the end of the helical bend near the 60° position. At times it entrained material from the bottom, causing it to upsurge to the surface and to be carried over the overflow weir.

Narrowing the end of the bend in Modification 6 did not result in carrying the material any further toward the foul outlet. Test 28, with the bleeder at 55° operating, produced a slight improvement.

Shortening the bend to 50° in Modification 7 gave encouraging results, with an increased recovery. Modification 8 was tested as a means of having a simpler, parallel-sided bend. Recoveries were good, but no improvement over the tapered format was evident.

Although slightly less Petrothene was recovered in a 1.83 m-wide (6 ft) channel (2 D) than the 2.745 m (9 ft) channel (3 D), it was investigated to see if there was any merit in achieving a narrower structure. (Gravity and dynamics of motion provide removal, not the structure). The channel was finally reduced to a 1.372 m (4 ft - 6 in.) width (1.5 D), to check on the minimum reasonable dimensions. This configuration is shown in Figure 34, Minimum Width Inlet, 1.5 D Wide; and Figure 35, Narrowest Bend, 1.5 D Wide.

Tests were carried out for the 0.88 m^3/sec (31.1 cfs) and 0.66 m^3/sec (23.3 cfs), cases in each instance For both total discharges, the foul discharge was maintained constant at 26.4 l/sec (0.93 cfs), or 3 dwf. Results of these tests are given in Table 10,

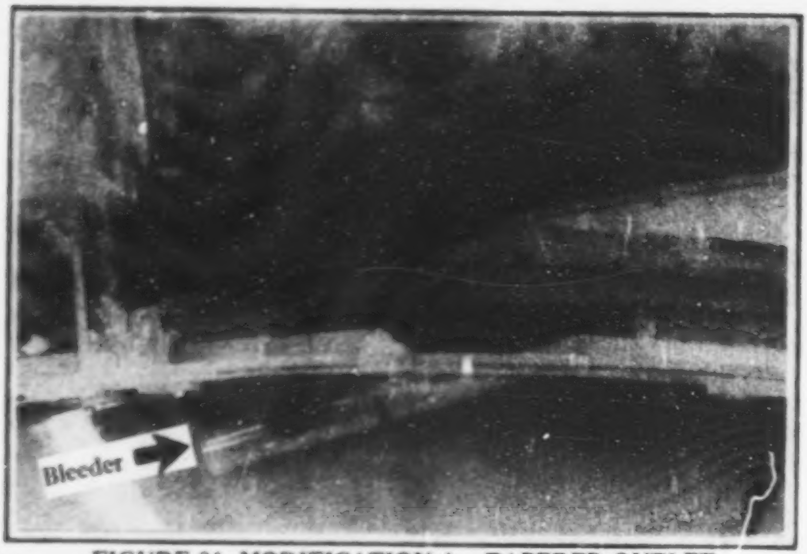

FIGURE 31 MODIFICATION 4 – TAPERED OUTLET

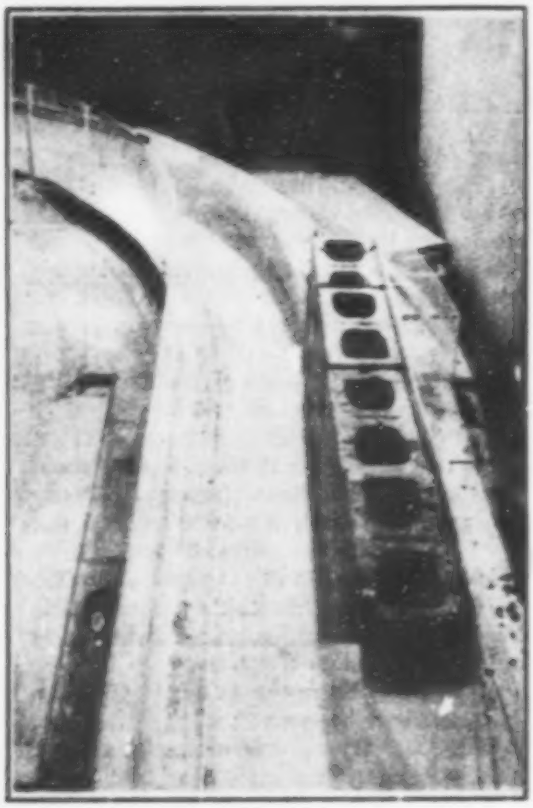

FIGURE 32 MODIFICATION 5 –
NARROW INLET 2D WIDE

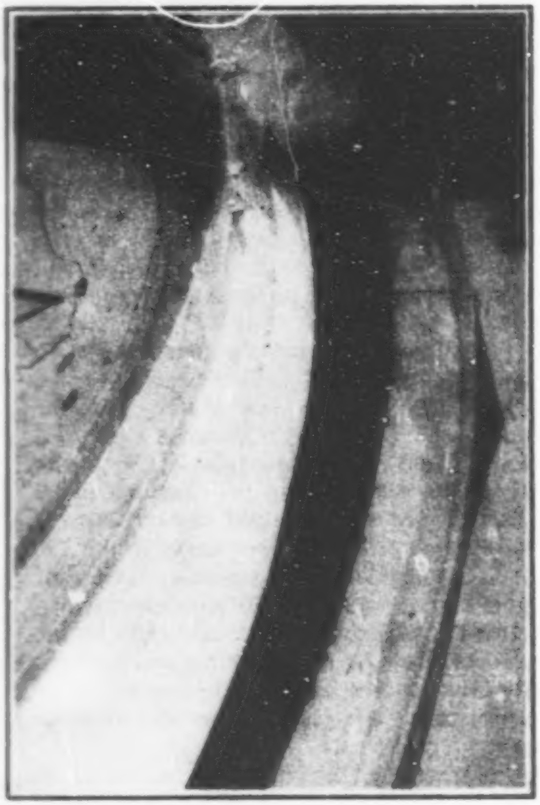

FIGURE 33 MODIFICATION 5 –
TAPERED BEND

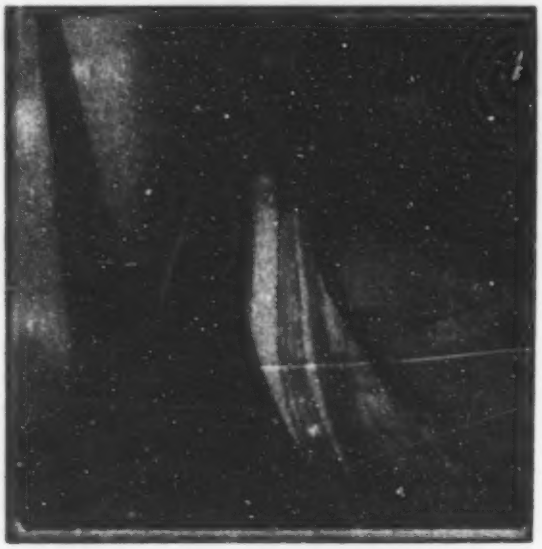

FIGURE 34 MINIMUM WIDTH INLET, 1.5D WIDE

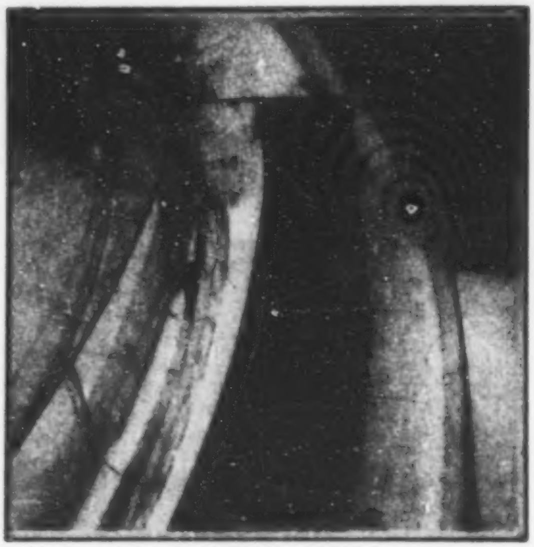

FIGURE 35 NARROWEST BEND, 1.5D WIDE

Recovery Results, Modifications 9, 10, 12, 14-18.

Figure 36 , Modification 9 – Tests 38-39, shows that the bend was shortened to 50°. The object was to attempt to eliminate the deposition of material on the sloping floor between 45° and the end of the bend. In Test 32, this deposit was considerable. Test 38 was only partially successful in eliminating the material.

A truncation was made at the end of the channel in Modification 10, as shown in Figure 37, Modificiation 10 – Tests 40-41. This, too, was insufficient to prevent the deposit. It did, however, slightly reduce the back-eddy in the end zone.

Figure 38, Modification 12 – Tests 46-47, shows that a Z-shaped partition was provided to allow flow over 60° of the weir, with the foul outlet placed at 50°. This offset arrangement aggravated the back-eddy to the extent that all material reaching beyond 45° was uplifted and carried over the weir immediately without any chance of settling.

At this stage, the first tests of shortening the inlet transition were tried, as shown in

TABLE 10

RECOVERY RESULTS – MODIFICATIONS 9, 10, 12, 14-18

Modification Number	Ref. Fig.	Test No.	Bend Length	Channel Width		Recovery	%
				m	ft.	Q=0.85 l/sec (30 cfs)	Q=0.64 l/sec (22.5 cfs)
9	15	38	50°	183	(6)	87	100
10	16	40	50°	183	(6)	88	100
12	17	46	60°	183	(6)	82	96
14	18	53	60°	183	(6)	65	77
15	18	55	60°	183	(6)	63	89
16	19	57	60°	1.372	(4.5)	65	85
17	21	59	60°	1.372	(4.5)	-	85
18	21	60	60°	1.372	(4.5)	-	70

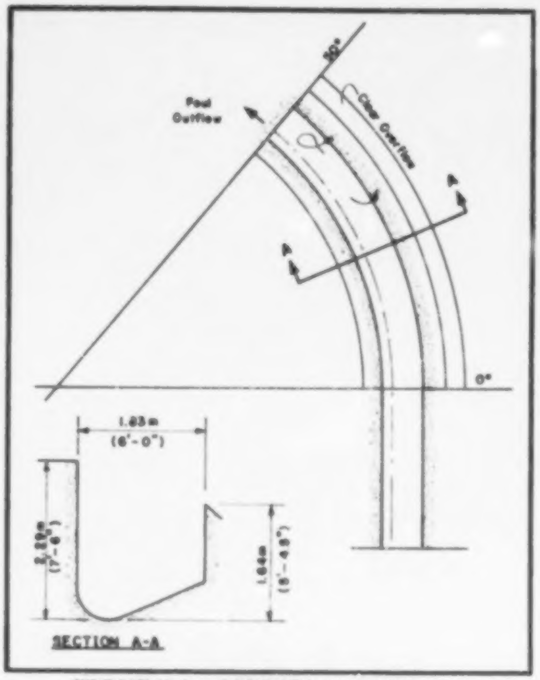

FIGURE 36 MODIFICATION 9 – TESTS 38-39

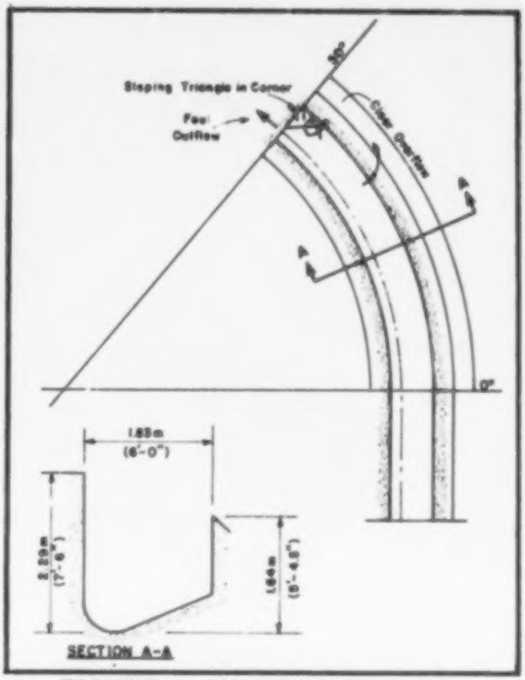

FIGURE 37 MODIFICATION 10 – TESTS 40-41

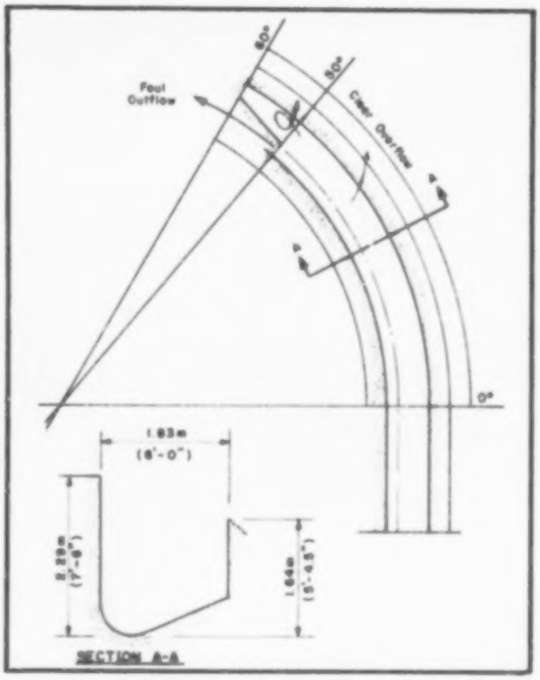

FIGURE 38 MODIFICATION 12 – TESTS 46-47

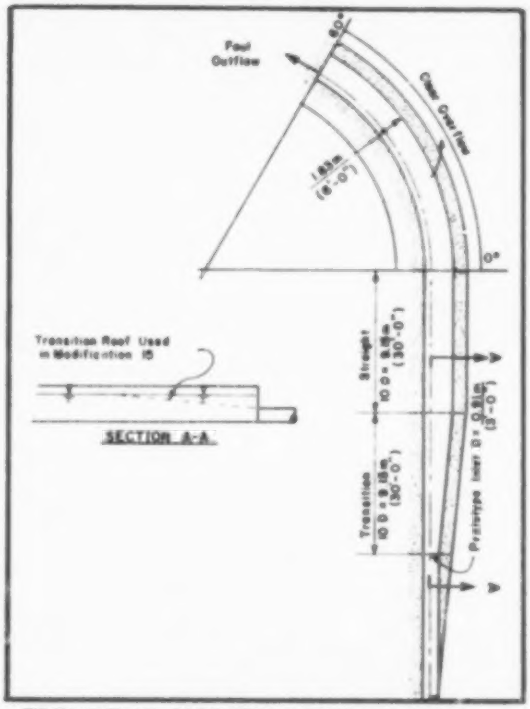
60°
Foul Outflow
Clear Overflow
1.83m (6'-0")
0°
Transition Roof Used in Modification 15
SECTION A-A
Straight 10 D = 9.15m (30'-0")
Transition 10 D = 9.15m (30'-0")
Prototype Inlet D = 0.91m (3'-0")
A
A

FIGURE 39 MODIFICATIONS 14 & 15 – TESTS 53-55

Figure 39, Modification 14 and 15 – Tests 53-55. This reduced the transition to 10D, or 9.15m (30 ft) prototype. There was no roof in Modification 14 to guide the flow, as shown on Figure 39. Test 53 showed a sharp drop in recovery – i.e., 65 percent as compared to 85 percent in Test 32. In the model, it was visually evident that the flow entering the transition did not expand efficiently, so that at the 0° position entry to the bend, considerable turbulence and lack of flow uniformity across the section were experienced.

A sloping roof was placed in the transition for Modification 15. This change was still insufficient to guide the flow, and too much irregularity remained at the 0° position. It can be concluded that with the asymmetrical entrance, 10 D is an insufficient length for expansion from the 0.915 m-diameter (3 ft) inlet pipe, D, to the 1.83 m (6 ft) channel, 2 D wide.

At this stage, it was decided that there would be insufficient economical justification for providing a narrower channel. Once the excavation is made for a particular structure, the cost difference between a channel 2 D and 3 D wide would be minimal. This reasoning led to resumption of studies of a wider section.

However, before reverting to a wider section, a few brief tests were carried out with the section narrowed down even further to 1.5 D, or 1.372 m (4.5 ft) prototype. The same shortened inlet was retained, and flow at the 0° position appeared to be fairly evenly distributed. Of course, the flow rate was much faster than in the preceding tests. The recovery rates of 65 percent for 0.88 m³/sec (31.1 cfs) and 85 percent for 0.66 m³/sec (23.3 cfs) seemed to conform well when compared with the wider channels, as shown on Figure 40, Petrothene Recovery in Model as Function of Bend Channel Width.

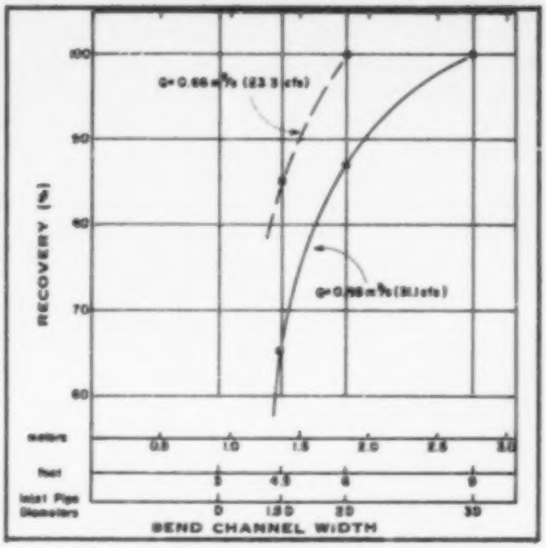

FIGURE 40 PETROTHENE RECOVERY IN MODEL AS FUNCTION OF BEND CHANNEL WIDTH

Even with this narrowed channel, most of the material recovered was in the form of deposits on the bend floor. Two minor changes were investigated in an effort to move this material along to the foul outlet. The first was a series of corner blocks 15.2 cm (6 in.) high and 22.95 cm (9 in.), projecting out from the side wall, as shown in Figure 41, Modifications 17 and 18 – Tests 60-61. Only the 0.66 m³/sec (23.3 cfs) case was tested; it

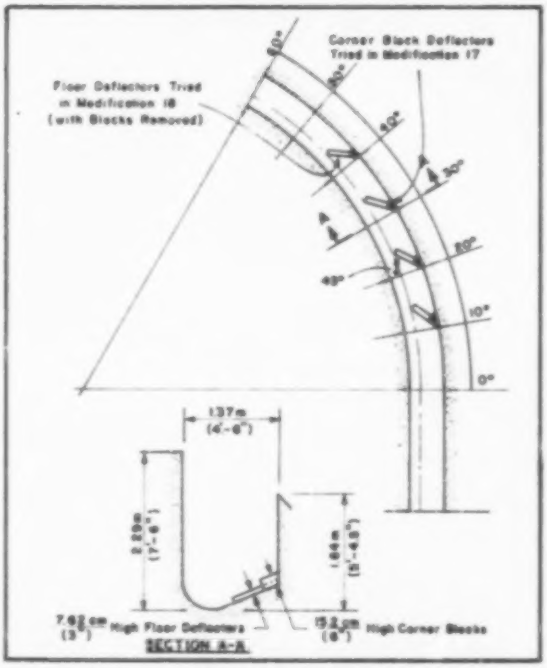

Corner Block Deflectors Tried in Modification 17
Floor Deflectors Tried in Modification 18 (with Blocks Removed)
60°
50°
40°
30°
20°
10°
0°
A
A
45°
1.37m (4'-6")
2.29m (7'-6")
1.64m (5'-4.5")
7.62 cm (3") High Floor Deflectors
15.2 cm (6") High Corner Blocks
SECTION A-A

FIGURE 41 MODIFICATIONS 17 & 18 – TESTS 60-61

gave an 85-percent recovery. This represented practically no change from the configuration without the corner blocks. Next, the blocks were removed, and a series of floor baffles 7.62 cm (3 in.) high were installed, as shown in Figure 41.

These baffles generated so strong a secondary current, that the Petrothene deposits, were re-suspended and carried over the weir. The recoveries dropped to 50 percent and 70 percent.

The preceding studies resulted in resumption of interest in the bend with the full 3 D or 2.745-m (9 ft) width originally built in the model. The studies showed that this bend, 60° long, when supplied through the original inlet configuration shown on Figure 42, Inlet Configurations Tested, recovered 100 percent of the Petrothene for a 0.88-m ^{3}/sec (31.1 cfs) discharge. Therefore, tests were undertaken to see how much the inlet length could be reduced and still retain an acceptable rate of recovery. No scum boards were used in these tests.

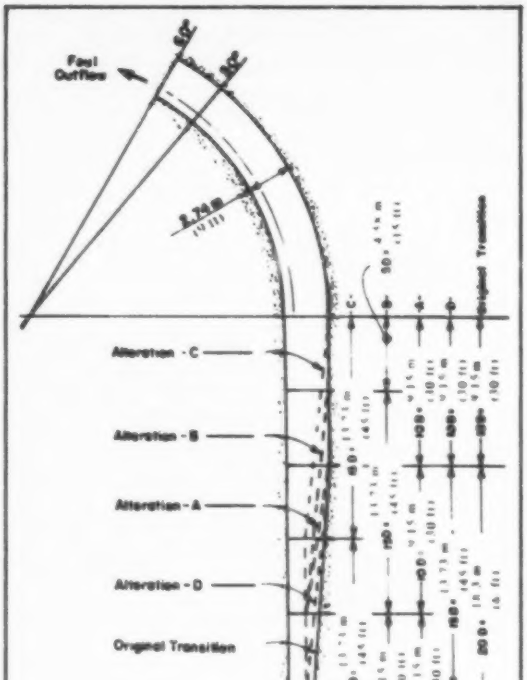

FIGURE 42 – INLET CONFIGURATIONS TESTED

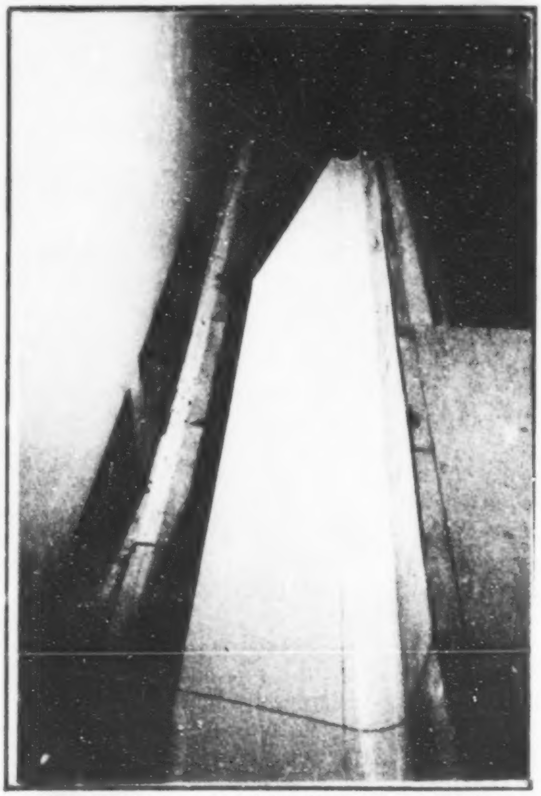

FIGURE 43 TRANSITION 10D LONG

As shown on Figure 42. Alteration A consisted of advancing the 0.915 m-diameter (3 ft) inlet pipe 9.15 m (30 ft), providing the transition out to the 2.745-m (9 ft) width in 9.15 m (30 ft), or 10 D, and retaining a 9.15 m (30 ft) straight section as depicted in Figure 43, Transition 10 D Long. It was evident that the flow jet did not expand well in this short transition and significant turbulence entered the bend, disturbing the helical secondary flow. Recoveries for 0.66 m^3/sec (23.3 cfs), and 0.88 m^3/sec (31.1 cfs), respectively, were 95 percent and 89 percent, as shown on Figure 44, Petrothene Recovery in 60° Bend for Various Inlet Configurations.

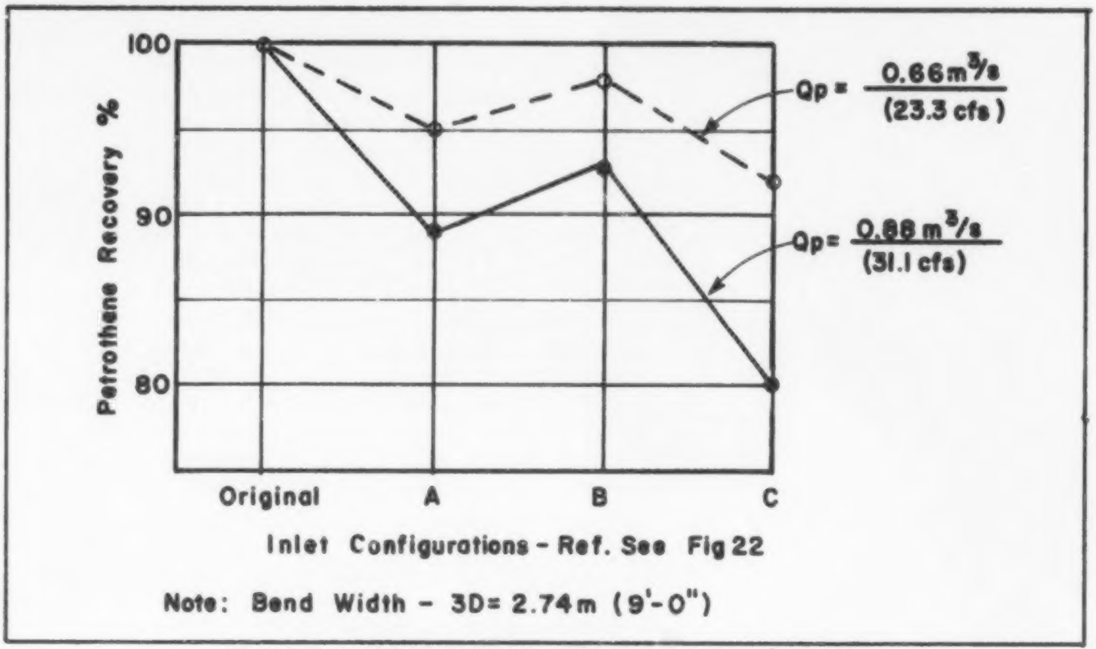

FIGURE 44 PETROTHENE RECOVERY IN 60° BEND FOR VARIOUS INLET CONFIGURATIONS

Alteration B, Figure 42, provided the start of the transition from the same point, but it expanded over 13.73 m (45 ft) or 15 D to reach the 2.745-m (9 ft) width. This is shown in Figure 45, Transition 15 D Long. Just 4.58 m (15 ft) of straight line remained ahead of the bend. Flow through this configuration was much improved; it expanded smoothly to fill the cross section effectively before entering the bend. As shown in Figure 44, the recoveries for the 0.66 m³/sec (23.3 cfs) and 0.88 m³/sec (31.1 cfs) discharges rose to 98 percent and 93 percent, respectively. Compared with the original long transition and straight sections, the flow ebtering the bend now was slightly more turbulent, but helical motion was still generated.

Since the transition in Alteration B appeared to be operating well, it was moved forward so it reached its full width just at the bend entrance. This was Alteration C, shown in Figure 42. The turbulence entering the bend was too strong in this case; Figure 44 shows the drop in recoveries.

The obvious recommendation was to retain Alteration B, and this was used for the following tests with scum boards. The reasoning for this choice was based on the fact that it resulted in only a seven percent drop in recovery from the original case, with a structure that is 9.15 m (30 ft) shorter. Implicit in this configuration is the requirement for a transition 15 D long to provide satisfactory deceleration of the flow while expanding to the 3 D channel width in the straight section. A flat sloping roof covers the transition, starting at the height D and rising to 2 D over the 15 D length.

As shown on the cross section in Figure 46, Scum Board Locations Tested, the scum board was tested at four different depths of immersion and at three distances out from the weir lip. For each of these locations, the Petrothene recovery was determined for the 0.88-m³/sec (31.3 cfs) discharge, with both the 50° and 60° bends. Figure 47, Petrothene Recovery in 50° Bend for Various Scum Board Locations, and Figure 48, Petrothene Recovery in 60° Bend for Various Scum Board Locations, show the test results.

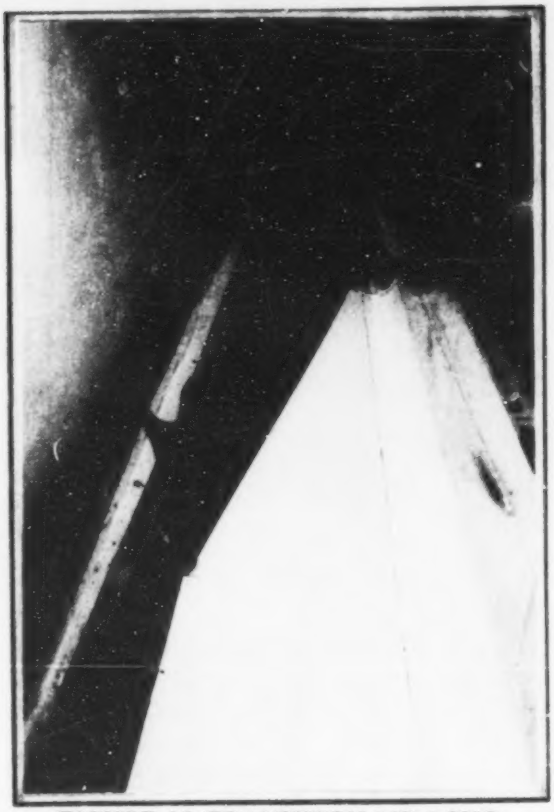

FIGURE 45 TRANSITION 15D LONG

It was immediately evident that the deepest scum board locations, 45.8 cm (18 in.), or D/2, below the weir lip, seriously disturbed the helical flow. Figure 49, Floor Flow Angles with Scum Board D/2 Deep, shows the bottom flow pattern. The recoveries fell off sharply, as well, and brief tests with Process Black ink showed that the floor angles were severely modified, even rising toward the weir at some points.

There was some improvement when the scum board immersion was reduced to 30.4 cm (1 ft) below the lip, particularly for the 60° bend length.

When the Scum board was just 15.2 cm (6 in.) below the lip, the recoveries rose significantly. In the 50° bend length, it reached about 84 percent, whereas, for the free overflow case – i.e., with no scum board – the recovery was 87 percent, the optimum in these tests. Figure 50, Floor Flow Angles With Scum Board D/6 Deep, shows the effect of deep immersion.

In the 60° bend length, recoveries with the scum board reached 85 percent, but the free overflow performance was 93 percent, leaving a wider gap in performance. On this basis, the scum board was raised to just 7.6 cm (3 in.) below the lip. However, instead of

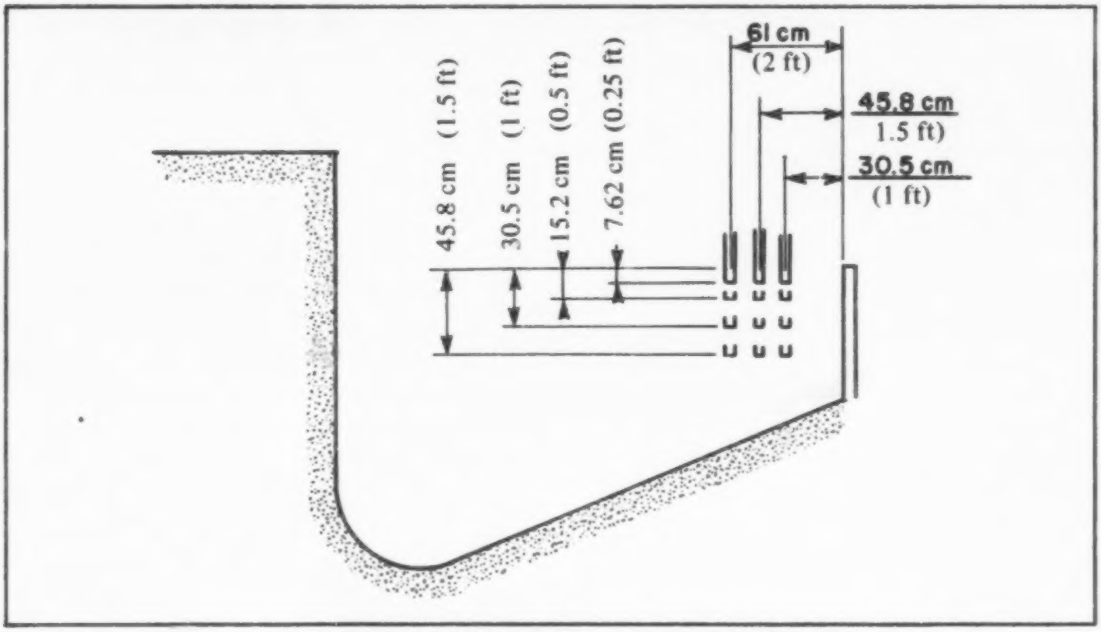

FIGURE 46 SCUM BOARD LOCATIONS TESTED

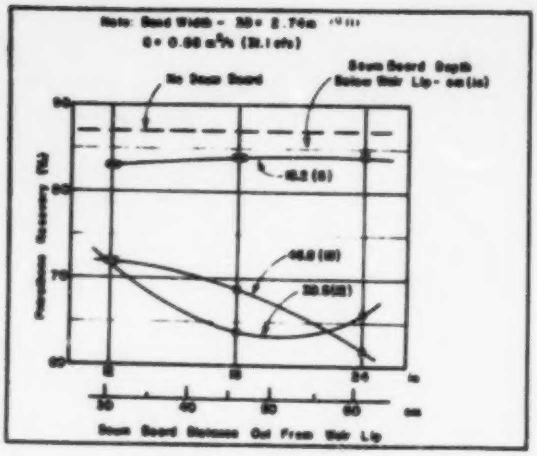

FIGURE 47 PETROTHENE RECOVERY IN 50° BEND FOR VARIOUS SCUM BOARD LOCATIONS

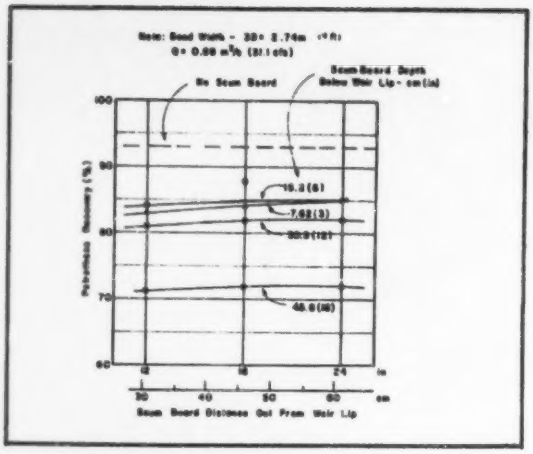

FIGURE 48 PETROTHENE RECOVERY IN 60° BEND FOR VARIOUS SCUM BOARD LOCATIONS

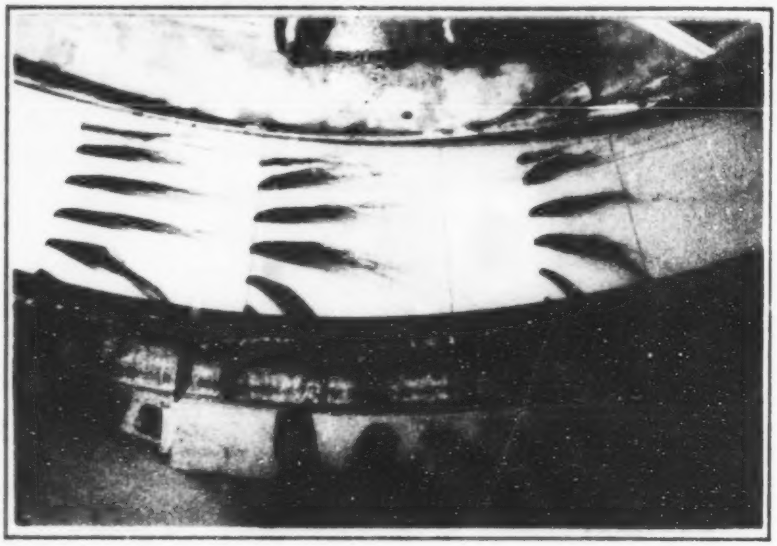

FIGURE 49 FLOOR FLOW ANGLES WITH SCUM BOARD D/2 DEEP

a recovery increase, a slight decrease was experienced.

The margin which remained between the recoveries for the no-scum board configuration and the shallowest scum board cases shown for the 60° bend in Figure 48 was from 93 percent down to 85 percent. This seemed too high a price to pay for adding the scum board. Observations on the model indicated that placing the scum board out in front of the weir, right in the main flow through the bend, caused significant disturbance. Also, previous work had shown that the 50° bend with scum board could not exceed 85 percent recovery, whereas the 60° bend showed the possibility of reaching better than 90 percent efficiency. Therefore, the 60° length was retained for further development.

Brief intermediate tests with the weir set back from the bend channel limit, and the scum board on the limit, led to the offset weir arrangement shown in Figure 51, Cross Section of Offset Weir in Bend. Weir details are shown in Figure 52, 60°Bend With Offset

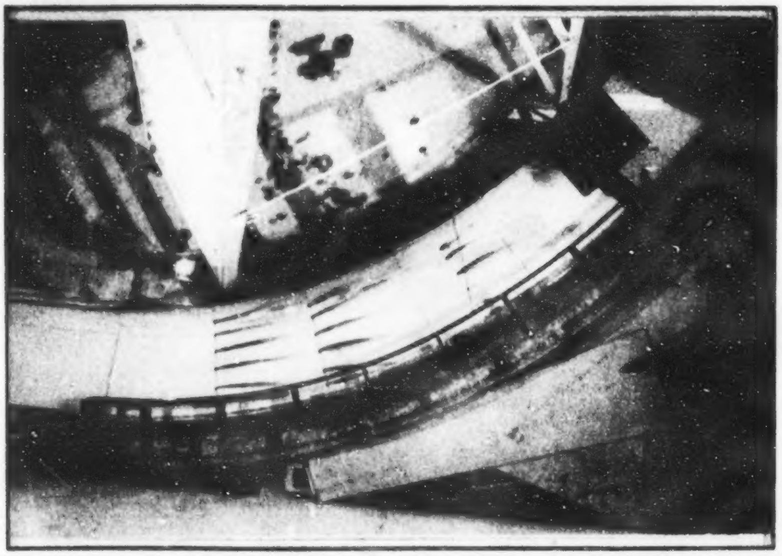

FIGURE 50 FLOOR FLOW ANGLES WITH SCUM BOARD D/6 DEEP

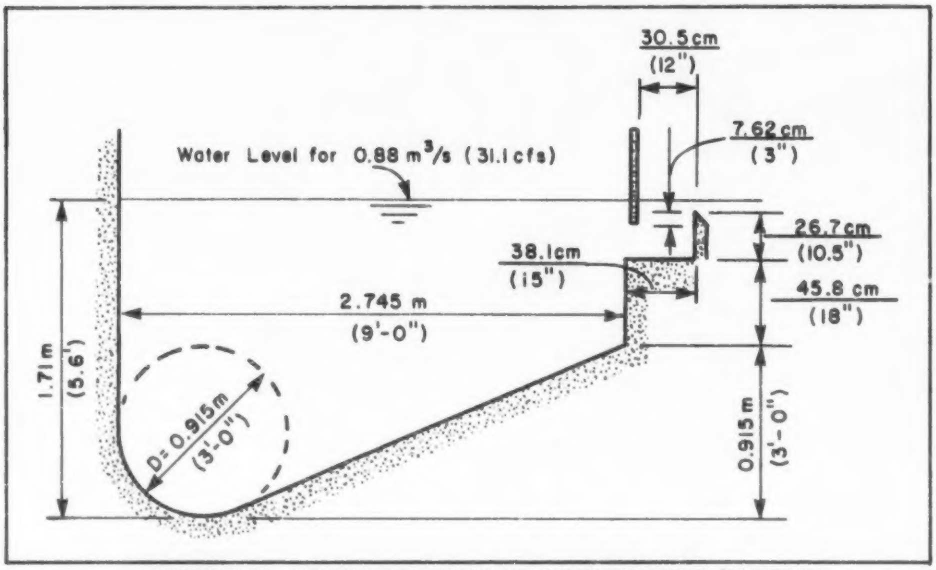

FIGURE 51 CROSS SECTION OF OFFSET WEIR IN BEND

Weir; Figure 53, Upstream View of Scum Board on Offset Weir; in Figure 54, Downstream View of Bend and Offset Weir; and in Figure 55, Scum Board on Offset Weir.

Tests run with this cross section and a 60° bend showed that the scum board did not adversely affect the recovery rates. At this stage, therefore, a series of tests was carried out using various inlet configurations.

Earlier studies had shown that the transition length had to be 15 D to give adequate flow deceleration. This form was retained, and it was tested for a discharge of 0.88 m^3/sec (31.1 cfs), first with no straight section, as shown in Alteration C in Figure 42, then with straight sections 5D and 10D long (Alterations B and D on Figure 42). The corresponding Petrothene recovery rates are

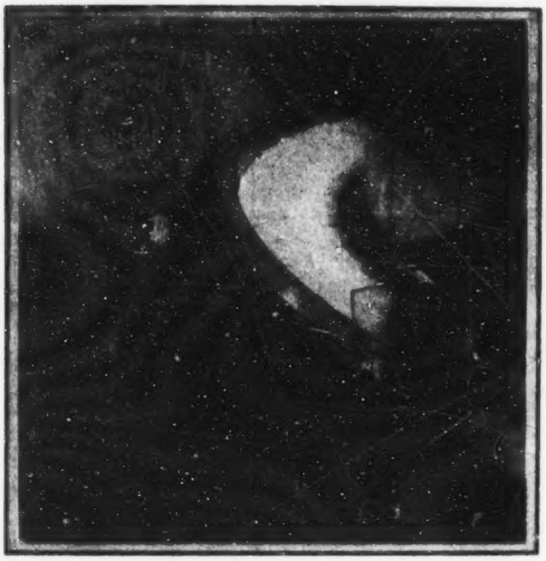

FIGURE 52 60° BEND WITH OFFSET WEIR

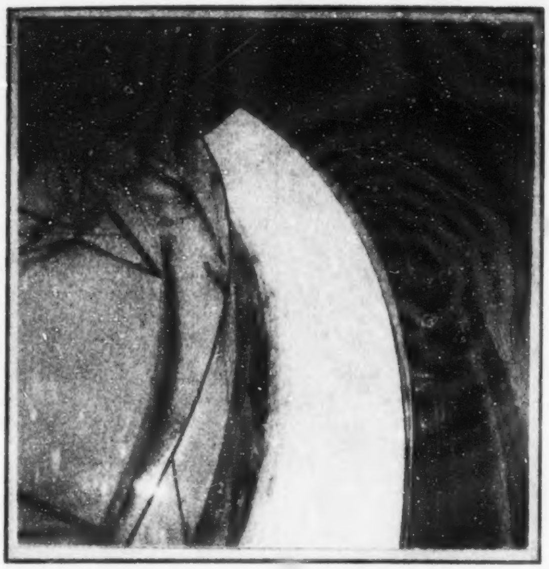

FIGURE 54 DOWNSTREAM VIEW OF BEND AND OFFSET WEIR

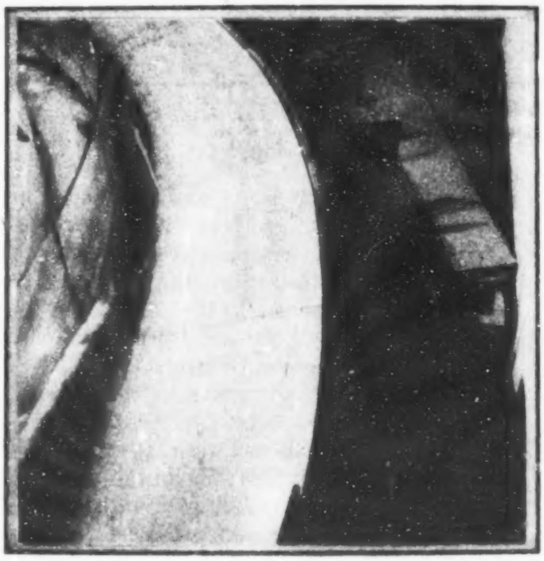

FIGURE 53 UPSTREAM VIEW OF SCUM BOARD ON OFFSET WEIR

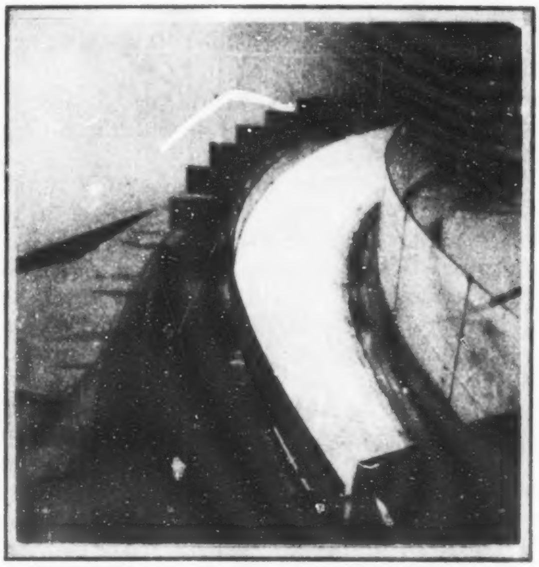

FIGURE 55 SCUM BOARD ON OFFSET WEIR

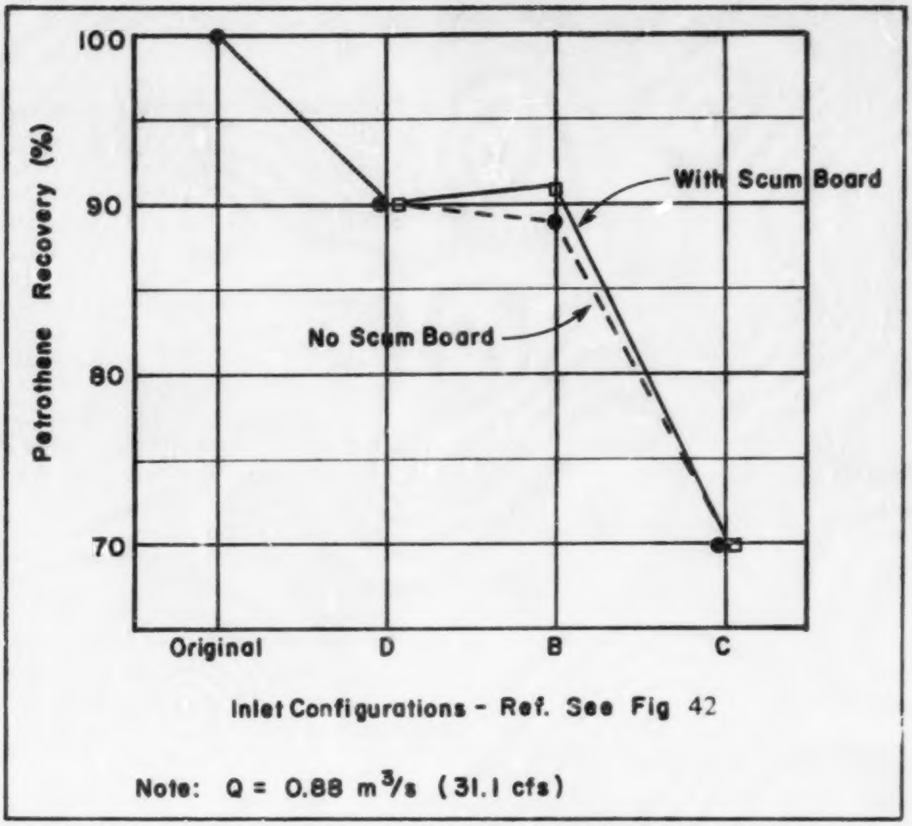

FIGURE 56 PETROTHENE RECOVERY IN 60° BEND WITH OFFSET WEIR AND VARIOUS INLET CONFIGURATIONS

shown in Figure 56, Petrothene Recovery in 60° Bend with Offset Weir and Various Inlet Configurations.

It is evident that a straight section is essential for proper operation of the helical separator. The fact that Alteration B, with the scum board, gave a higher recovery than Alteration D should not be accorded too much significance. The differences here are within the order of accuracy of the model tests.

With this offset weir arrangement, the scum board did not introduce any undesirable disturbances when compared to the free overflow weir. On the basis of these results, the cross section shown in Figure 52 was retained as the recommended configuration, along with the inlet designated Alteration B in Figure 42.

Floatables entering the structure gradually decelerated around the bend and gathered in a gentle eddy rotating counter-clockwise between the 45° and 60° locations. After the storm flow subsided, the floatables receded with the surface of the water and were discharged through the foul outlet with the dry-weather flow.

At this stage the model operating characteristics had been sufficiently defined to establish a determination governing the discharge relations. The maximum discharge used during testing, as described in the section on Scale Selection and Discharges, was defined as the Design Discharge, Q_D. On the model, Q_D was 10 l/sec (0.354 cfs); in the prototype it was six times larger, as considered in this report – 0.88 m^3/sec (31.1 cfs).

Having determined the optimum configuration of the basic cross section shown

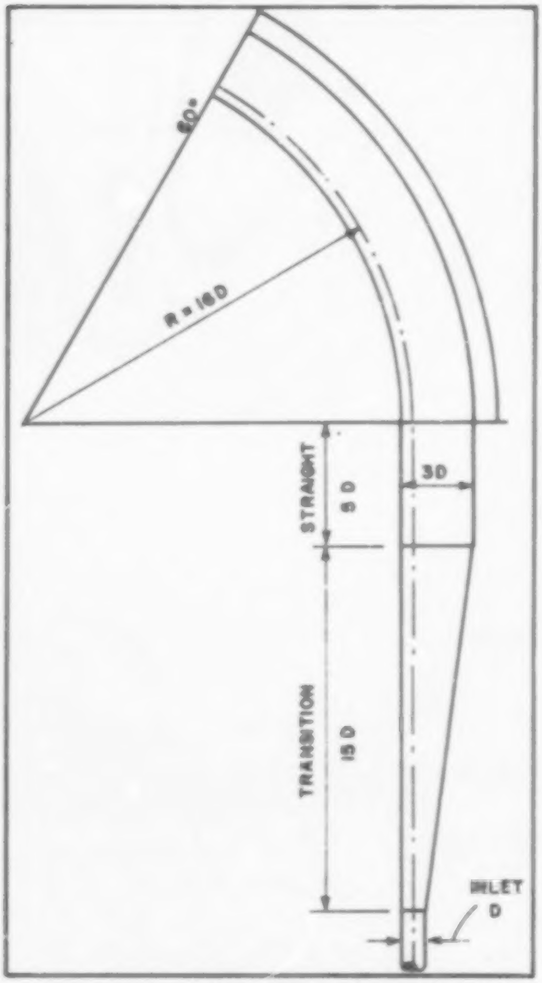

FIGURE 57 PROVING TESTS LAYOUT

on Figure 52, the plan dimensions in Figure 57, Proving Tests Layout, were related for detailed testing over the range of discharges in the model. Both Gilsonite and Petrothene were used in these tests and the results are shown on Figure 58, Soiids Recovery in Model.

In predicting the prototype recoveries expected with grit, reference was made to Figure 9 showing the sizes simulated by the Gilsonite and Petrothene materials used in the model. It appeared that over practically the whole range of scales, the Gilsonite represented the grit satisfactorily. Figure 11, Predicted Grit Recovery for All Scales, was then prepared, using the Gilsonite recovery rate appearing in Figure 58.

Using Gilsonite to simulate prototype organic material in the model as shown on Figure 10 covered the major portion of larger particle sizes. The upper portion appearing in Figure 10 for each given scale was multiplied by the Gilsonite recovery rates from Figure 58 for Q_D, 1.5 Q_D and 2 Q_D, and taken as the prototype recovery for the particle sizes in that zone.

The particle sizes lying below the dm = 0.5 mm line for Gilsonite in Figure 10 were assumed to be entirely represented by the Petrothene. Similarly, this portion for each scale was multiplied by the Petrothene recovery rates from Figure 61 for Q_D, 1.5 Q_D, and 2 Q_D, and taken as the prototype recovery for the lower zone.

These two prototype recoveries simulated by Gilsonite and Petrothene in the model were added together and presented on Figure 12, Predicted Prototype Settleable Organic Material Recovery.

It is, therefore, possible to find the predicted recovery rates for grit and organic materials as defined in Figure 6, for any scale of prototype structure by using Figure 11, and Figure 59, Velocity Contours on 0° Cross Section.

It was found during the development testing that the solids materials recovered were normally in the form of deposits on the floor of the bend. Only traces, normally less than two percent, were carried through the foul outlet during the storm flow incidents. For most tests, the Petrothene and Gilsonite were deposited or shoaled in the bend between the 15° and 60° locations. A fair proportion of the Gilsonite settled to the floor in the straight section, but it was subsequently moved into the bend.

As the discharge was reduced in the model, as it returned to dry-weather flow, most of the depostis were scoured out and discharged through the foul outlet. However, it is possible that this self-scouring phenomenon during dry-weather flow in the model simualtion may not take place in any prototype installation, so provision should be made in design for some form of wash-down facility or for some other form of regular maintenance.

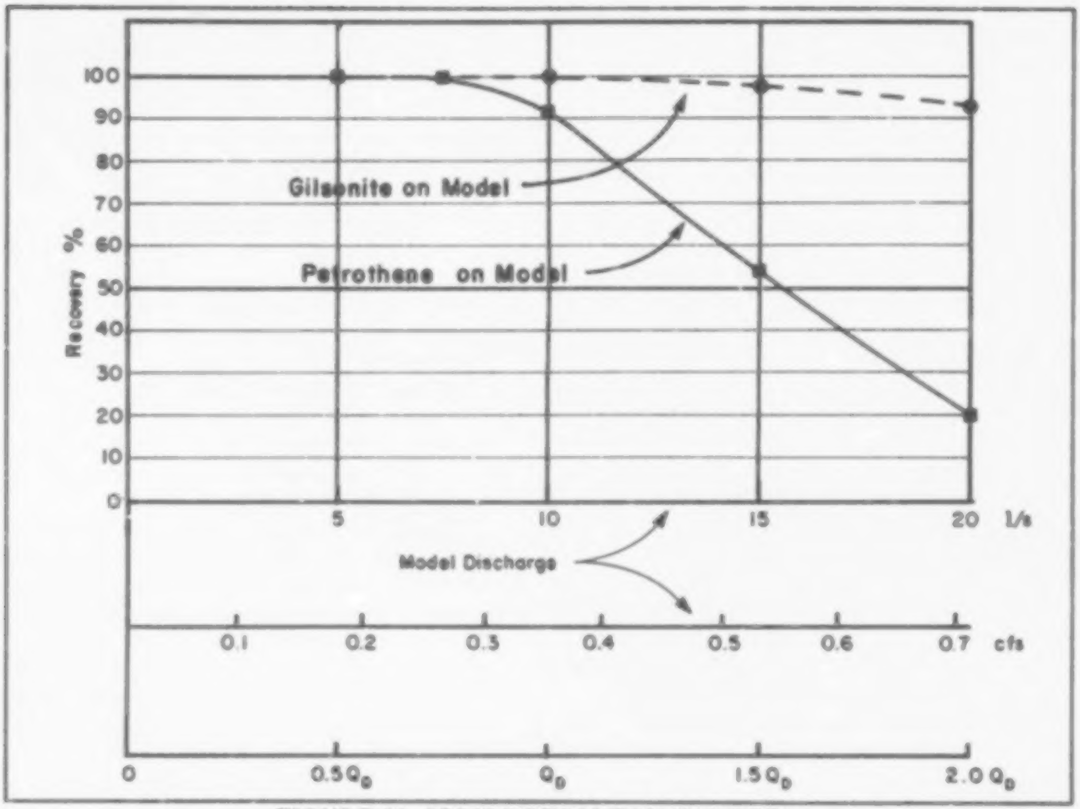

FIGURE 58 SOLIDS RECOVERY IN MODEL

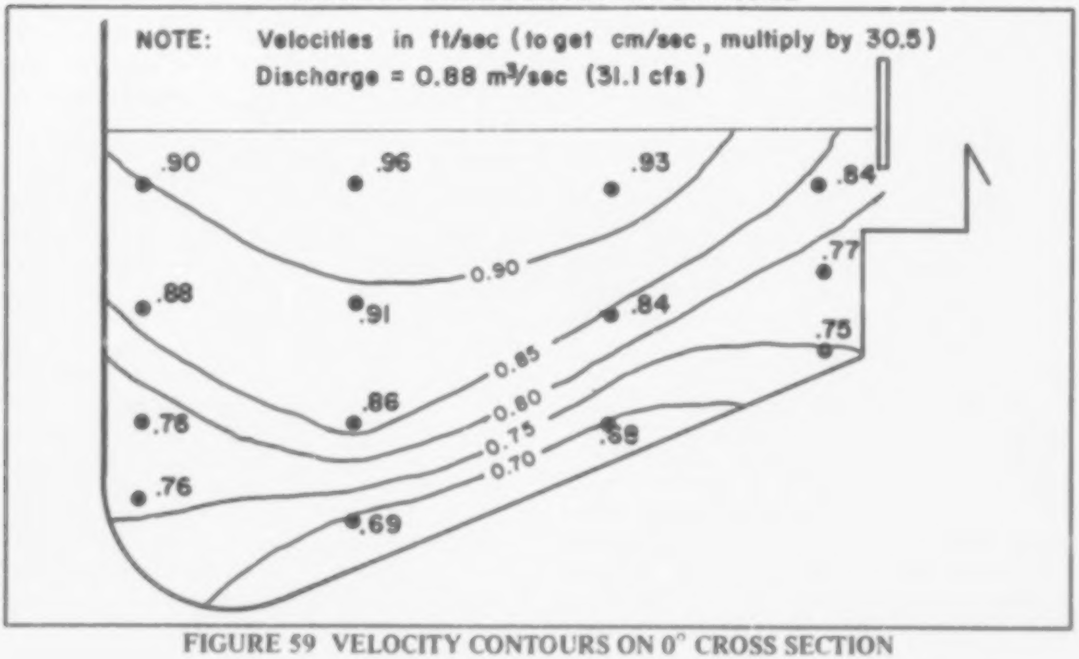

FIGURE 59 VELOCITY CONTOURS ON 0° CROSS SECTION

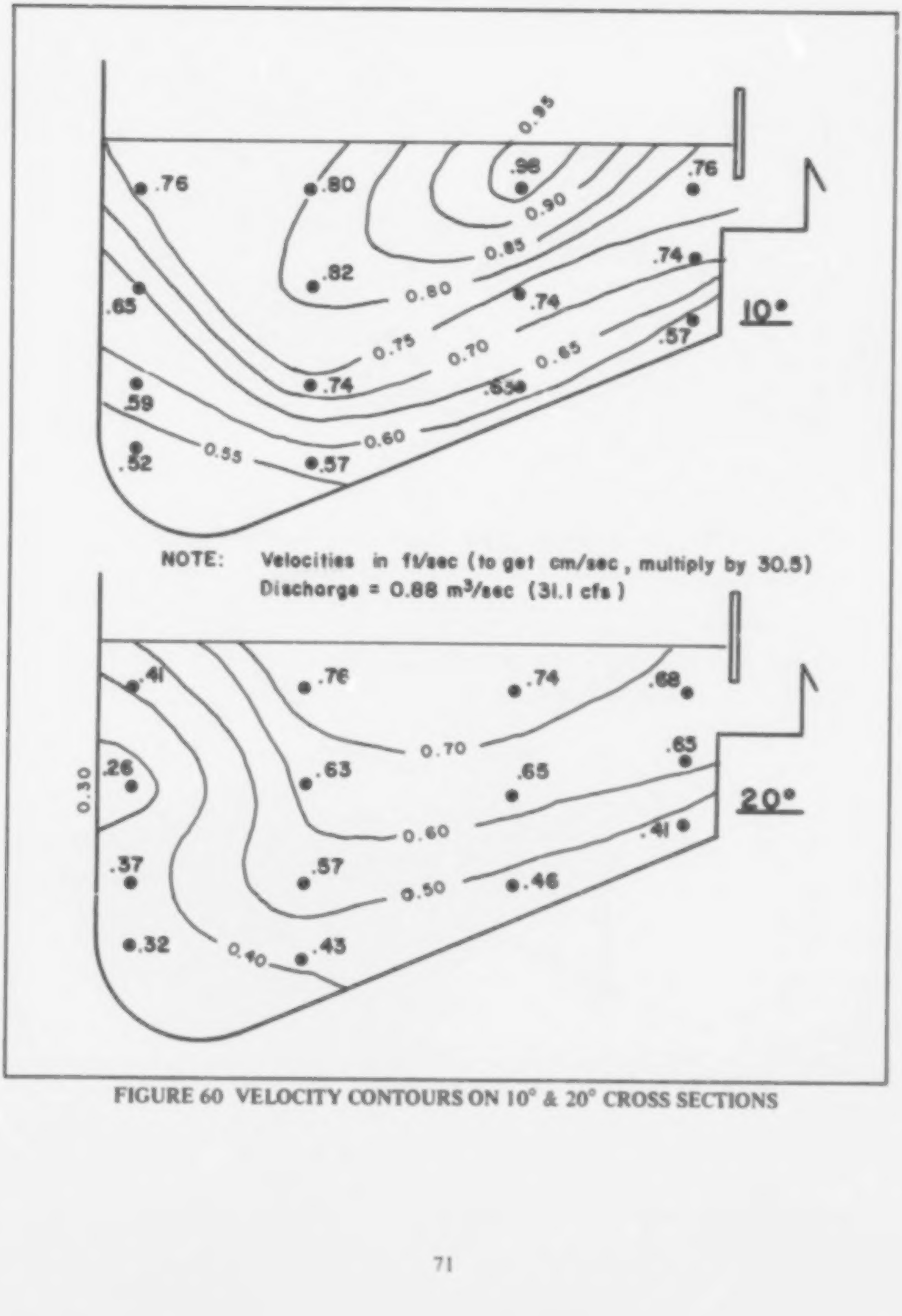

NOTE: Velocities in ft/sec (to get cm/sec, multiply by 30.5)
Discharge = 0.88 m³/sec (31.1 cfs)

FIGURE 60 VELOCITY CONTOURS ON 10° & 20° CROSS SECTIONS

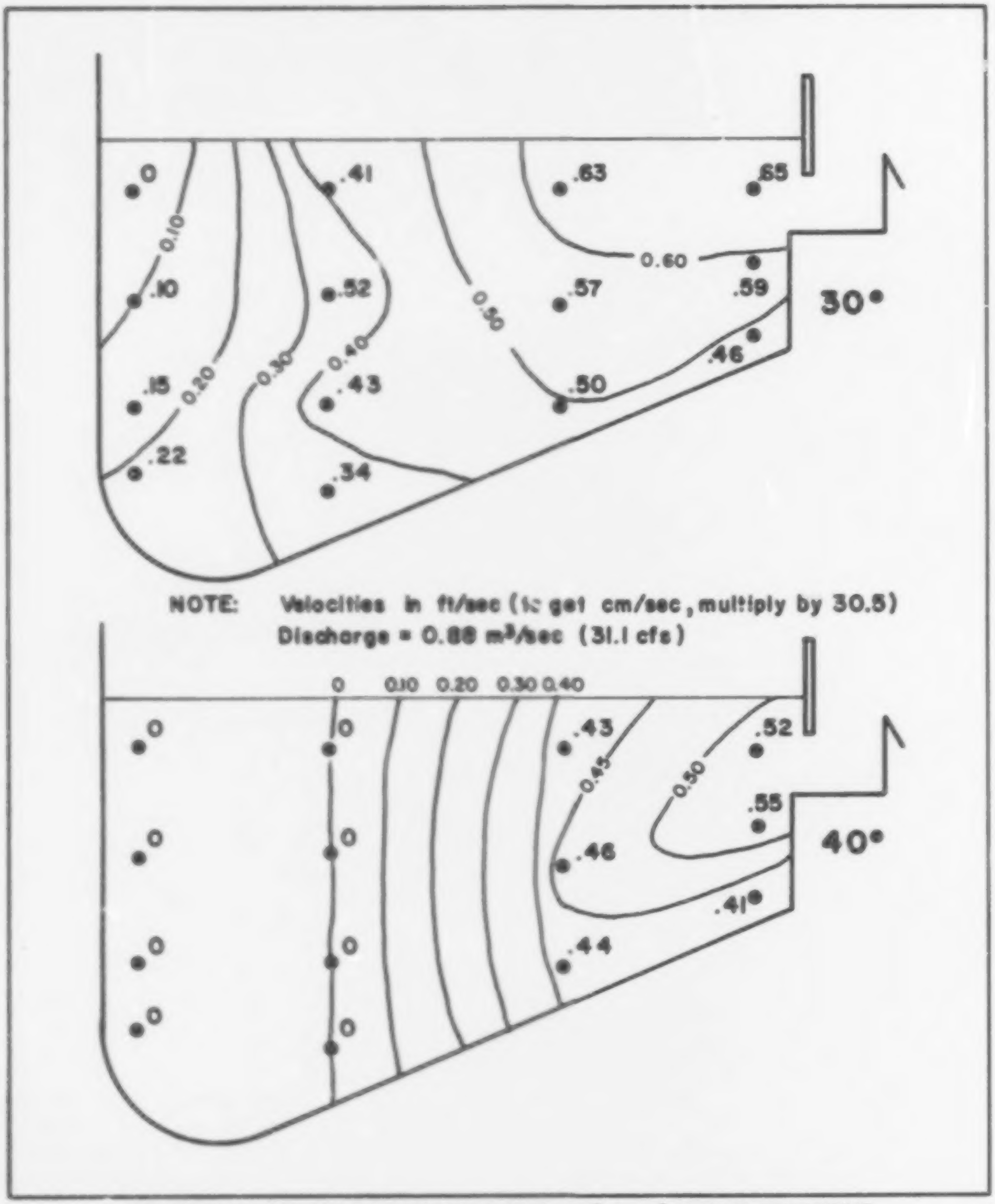

NOTE: Velocities in ft/sec (to get cm/sec, multiply by 30.5)
Discharge = 0.88 m³/sec (31.1 cfs)

FIGURE 61 VELOCITY CONTOURS ON 30° & 40° CROSS SECTIONS

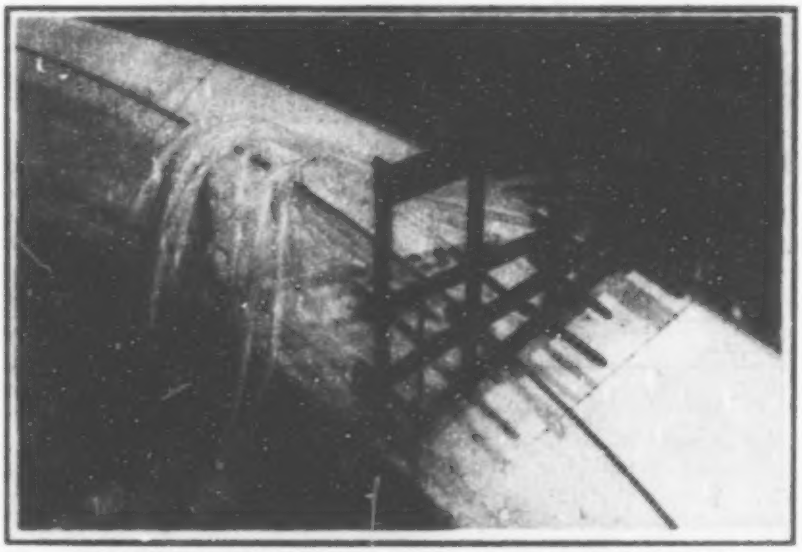

FIGURE 62 SOLIDS CONCENTRATION SAMPLING JIG

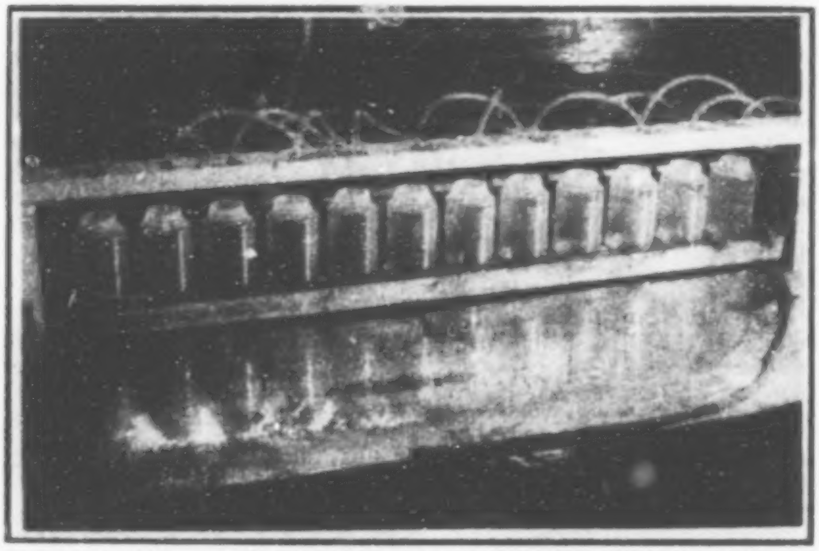

FIGURE 63 SIMULTANEOUS FILLING OF SOLIDS SAMPLING BOTTLES

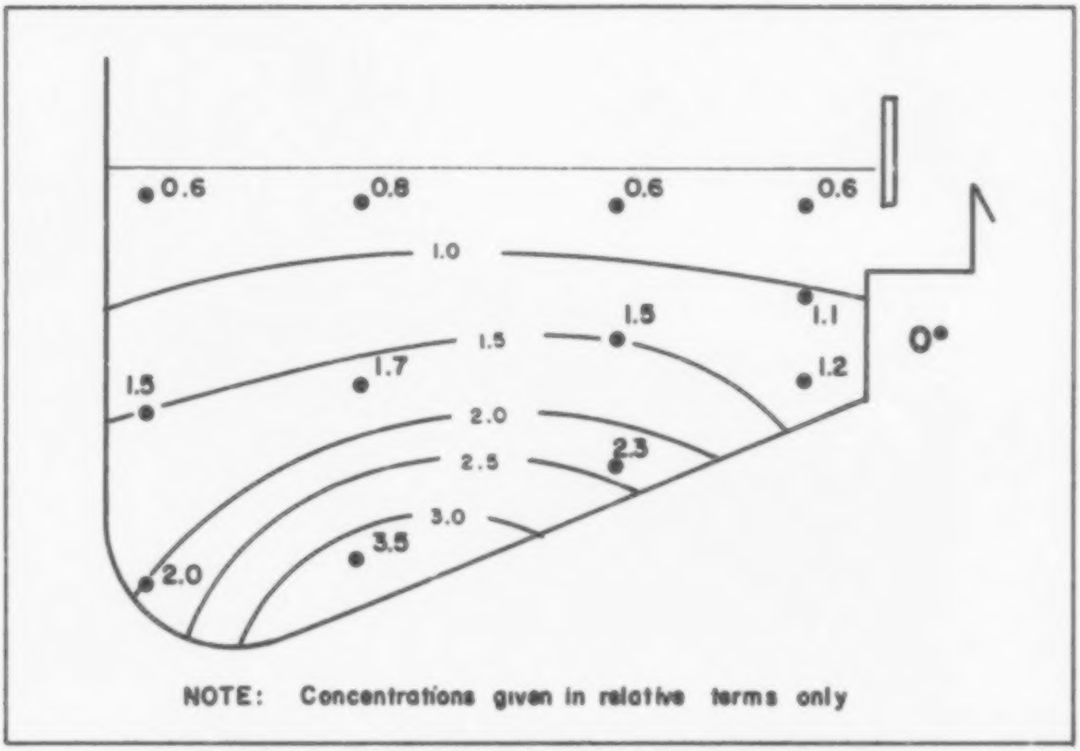

NOTE: Concentrations given in relative terms only

FIGURE 64 SUSPENDED SOLIDS CONCENTRATIONS ON 0° CROSS SECTION

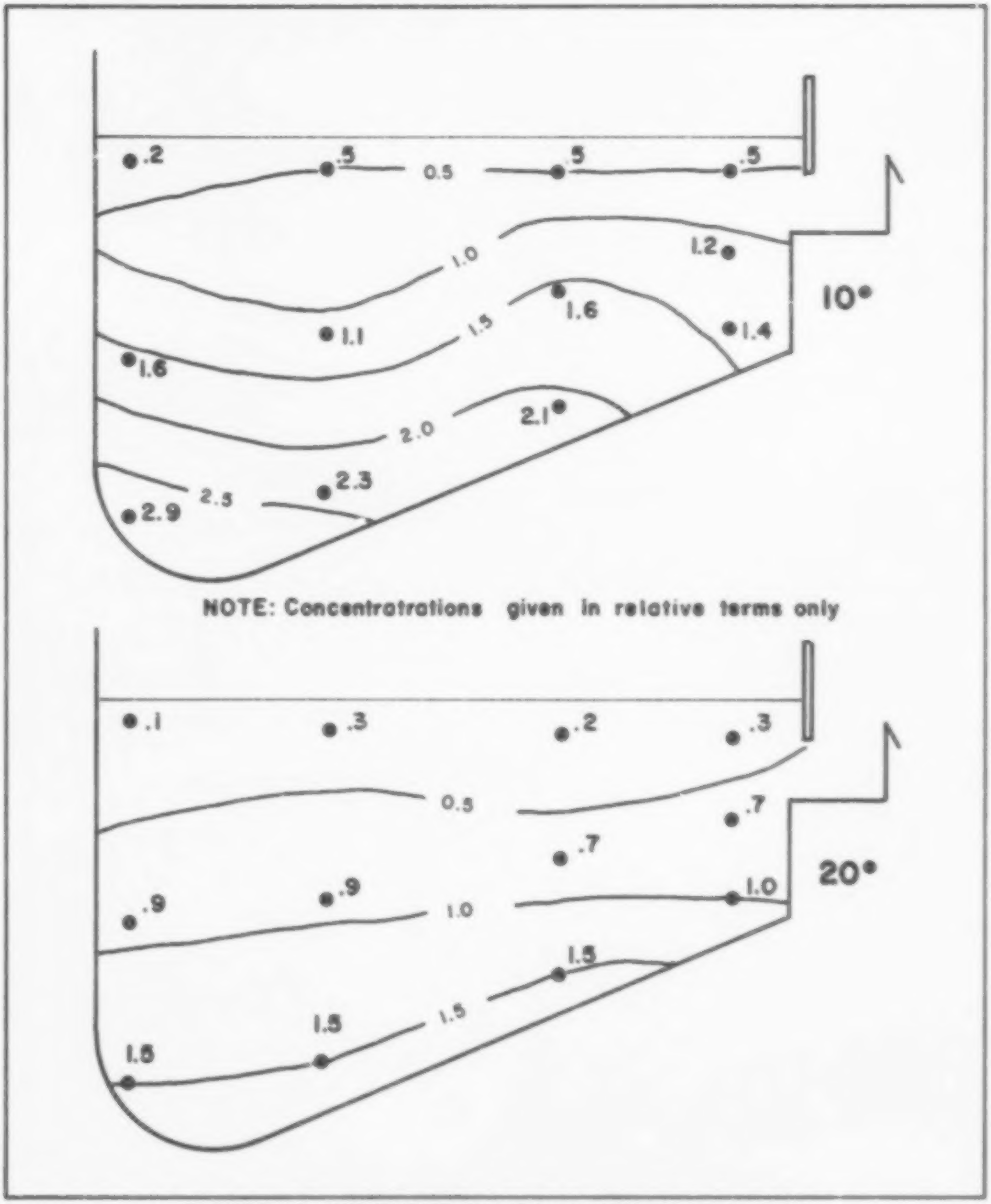

NOTE: Concentratrations given in relative terms only

FIGURE 65 SUSPENDED SOLIDS CONCENTRATIONS ON 10° & 20° CROSS SECTIONS

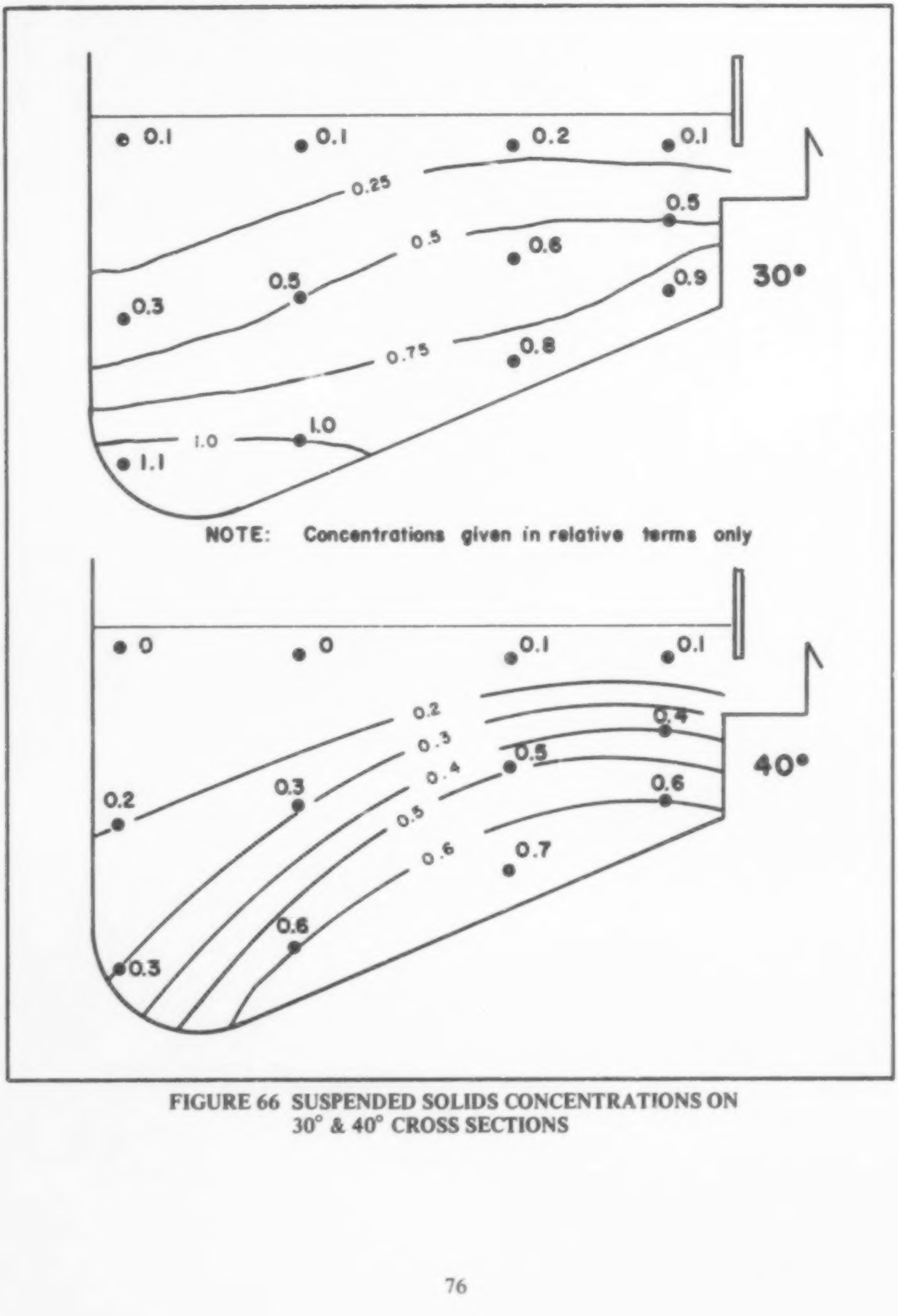

NOTE: Concentrations given in relative terms only

FIGURE 66 SUSPENDED SOLIDS CONCENTRATIONS ON 30° & 40° CROSS SECTIONS

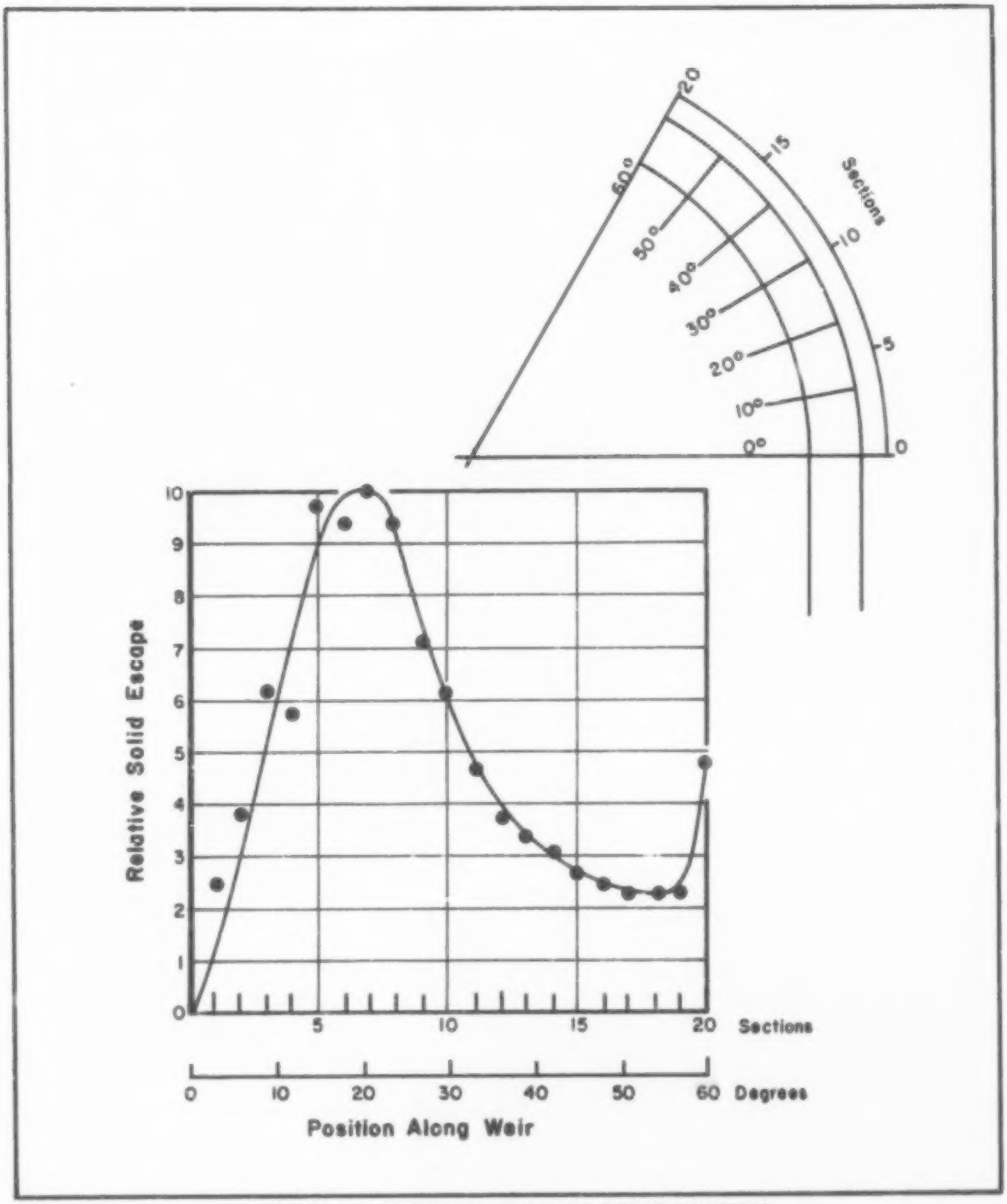

FIGURE 67 DISTRIBUTION OF SOLIDS WHICH ESCAPE OVER THE WEIR

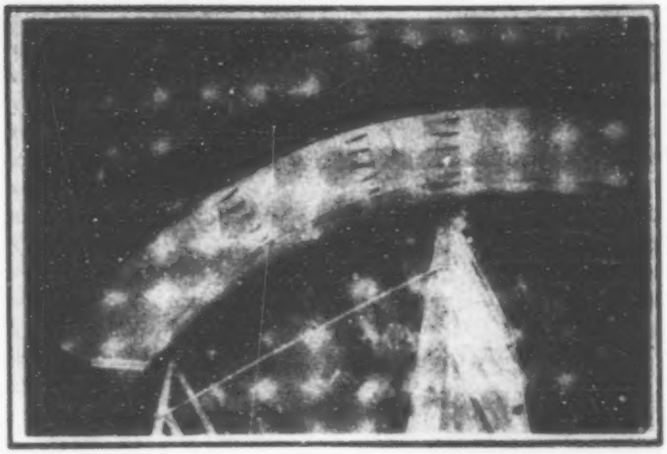

Floor flow angles for 120° bend with no overflow

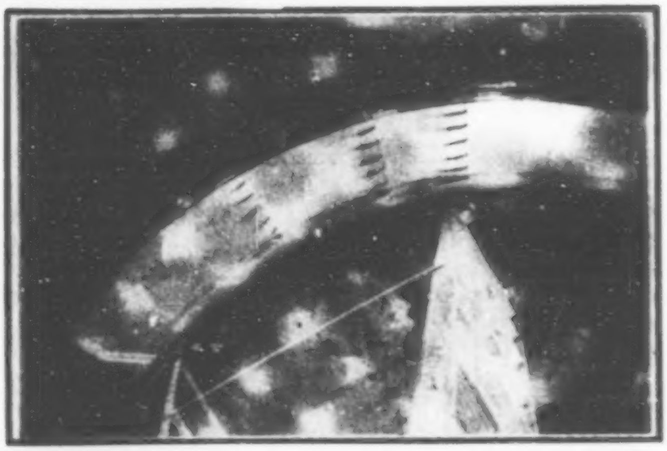

Floor flow angles for 60° bend, free overflow by offset weir

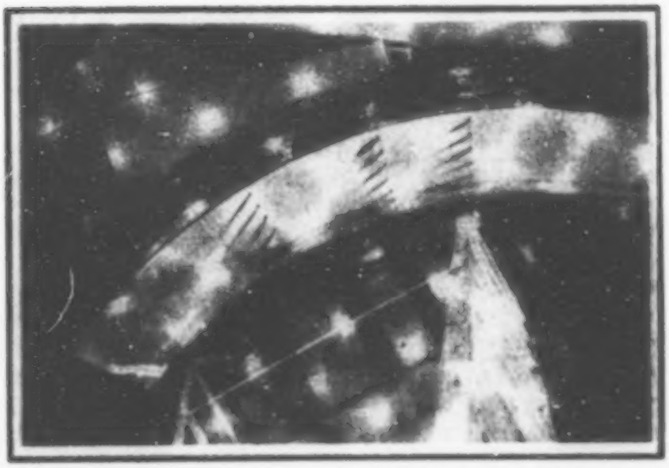

Floor flow angles for 60° bend with scum board on offset weir

FIGURE 68 FLOOR FLOW ANGLES

Another approach would be to provide sufficient slope from the inlet to the foul outlet of the structure to induce all deposited solids to be scoured out and flushed away with the dry-weather flow. The model invert had no slope in any of the tests.

Testing the Performance of the Recommended Layout

Utilizing the model forms shown in Figures 51 and 57, final proving tests were carried out to define the structure's flow characteristics, to serve as guidance for the work being carried out on the mathematical model.

First, the tangential flow velocities in the bend were measured with a midget propellor current meter for the discharge of 0.88 m^3/sec (31.1 cfs). Readings were taken at 14 points on each of the cross sections, at the 0°, 10°, 20°, and 40° positions. The prototype velocities found were plotted at the corresponding points, and contours of even velocity values were drawn as shown on Figures 59, 60, and 61, Velocity Contours on 0°; on 10° and 20°; and on 30° and 40° Cross Sections.

The same cross section locations were used for installing a special suspended solids sampling device, as depicted in Figure 62, Solids Concentration Sampling Jig. Twelve 6.4-mm (1/4 in.) I.D. Plexiglas sampling tubes were fixed on a frame, directed upstream to intercept the flow. A flexible tygon tube ran from each sampling tube to a wooden stand, under which 1-liter sampling bottles could be introduced, as shown in Figure 63, Simultaneous Filling of Solids Sampling Bottles.

With the model subjected to clear water only, each of the tubes was primed and they were all adjusted to provide the same discharge. Petrothene injection was begun by means of the vibrator, and as soon as the cloud of suspended material reached an equilibrium state at the cross section being tested, the bottles were slipped under the 12 tygon tube discharges. This system provided simultaneous samples of the suspended solids in the flow at all 12 points.

Results of these tests are shown in Figures 64, 65, and 66, Suspended Solids Concentration Contours on 0°; on 10° and 20°; and on 30° and 40° Cross Sections.

The length of the overflow weir in its offset position was 302 cm (118.8 in.). A catch screen was fitted outside the weir and divided into 19 sections, each 15.2 cm (6 in.) long, with the twentieth being just 12.2 cm (4.8 in.) long. The standard Petrothene injection procedure was followed, and the particles escaping over the weir were caught in the corresponding sections on the screen. The corresponding fractions in each section were measured and plotted as shown on Figure 67, Distribution of Solids Which Escape Over Weir.

Using the special Process Black ink, the floor flow angles (α_o on Figure 68) were measured at six points across the cross sections at 10°, 20° and 35°, for each of three separate layouts:

1. 120° bend with straight through flow
2. 60° bend with offset weir, but no scum board
3. 60° bend with offset weir and scum board.

The averages of these readings were computed and plotted in Figure 69, Comparative Average Floor Angles for Recommended Layout. The floor flow phenomena are shown in Figure 68, Floor Flow Angles for 120° Bend With No Overflow; for 60° Bend, Free Overflow by Offset Weir; and for 60° Bend With Scum Board on Offset Weir. The average of floor angles is plotted in Figure 69, Comparative Average Floor Angles for Recommended Layout.

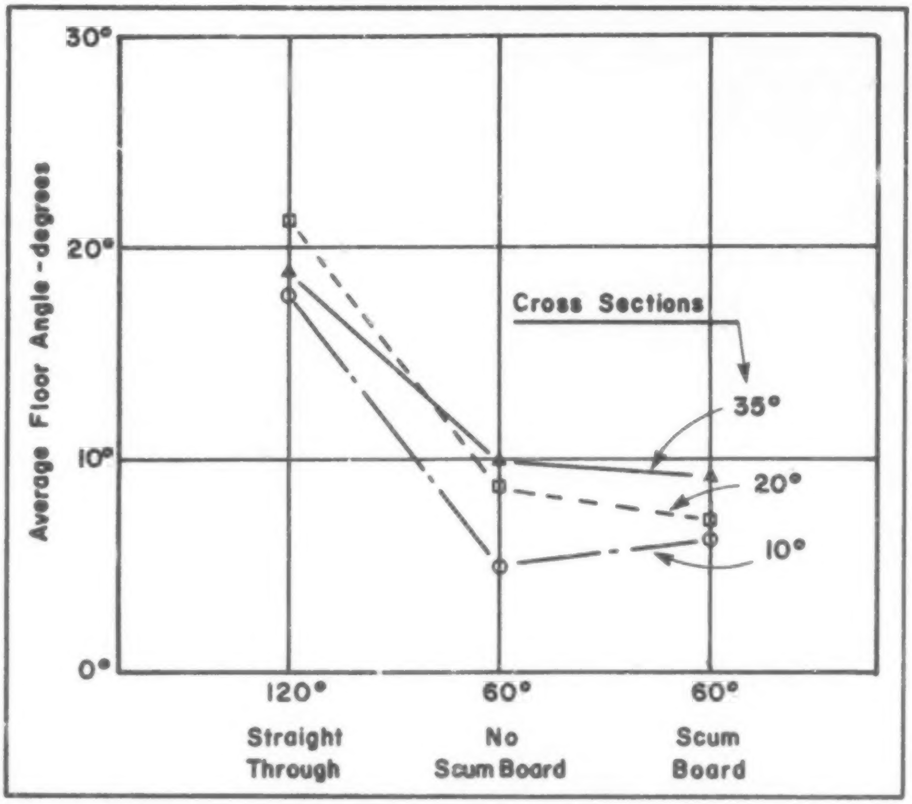

FIGURE 69 COMPARATIVE AVERAGE FLOOR ANGLES FOR RECOMMENDED LAYOUT

APPENDIX B

MATHEMATICAL MODEL STUDY

This report describes the development of a mathematical model and computer simulation of an open channel bend with a side overflow weir for the separation of grit and organic solids from combined sewer overflows. A companion hydraulic laboratory investigation was conducted by LaSalle Hydraulic Laboratory of Montreal.

The general features of the helical bend device are illusrated in Figure 4, Helical Bend Regulator – Form 3 (Model Layout) in Section II. The dimensions shown are for a prototype designed for a nominal peak flow of 0.85 m^3/sec, (30 cfs). The flow from the circular inlet sewer passes through a straight, rectangular transition section designed to spread the flow uniformly across the larger cross section of the device.

The flow then proceeds through a 60° bend, with cross section as shown in Figure 4. The clean overflow is withdrawn via a side weir located along the outside of the bend, while the concentrated solids are withdrawn via a foul sewer orifice in the end plate at the 60° position. Downstream control is used to limit the amount of flow discharged to the wastewater treatment plant to three times the dry-weather flow, or 0.025 m^3/sec, (0.9 cfs), for the nominal prototype design. The remainder of the inlet flow is discharged to receiving waters over the side weir, or to any holding or treatment facility which is intended to handle the overflow liquid.

The usefulness of this device for separating grit and organic solids from combined sewer overflows is enhanced by the secondary flow patterns which develop in the bend. These secondary flows form a clockwise spiral or helical flow pattern, in the direction of flow. The helical flow tends to sweep the bedload to the inside of the bend, so that relatively clearer liquid is discharged over the side weir. These secondary flow patterns have been studied extensively by many investigators, most notably by Dr. T. M. Prus-Chacinski,[1] who served as consultant on the present study. His report, Appendix C, contains an extensive bibliography of the previous work in this field.

The application of open channel bends to separation of solids from storm and combined sewer overflows has also been studied experimentally by Dr. Prus Chacinski,[2,3] and a prototype device shown in Figure 3 in the foregoing report, Photograph of Nantwich, England, Helical Bend Regulator, has been constructed by C. H. Dobbie and Partners, Consulting Engineers, under a research contract from the Construction Industry Research and Information Association, London. The objective of the present study has been to refine and extend this previous work in accordance with American conditions and practices.

LIQUID FLOW CALCULATION

The secondary flow which develops in a curved channel is of definite significance in determining the separation performance of the helical bend separator. The helical flow pattern tends to sweep the bedload to the inside of the bend, thereby reducing the amount of solids which pass over the weir, with the clarified combined sewer flow.

The helical secondary flow is induced by the vertical velocity profile at the entrance to the bend. An element of fluid near the center of the channel experiences an outward centrifugal force proportional to v^2/r, where v is the longitudinal velocity and r is the radius. This centrifugal force tends to raise the surface level at the outer radius of the bend, and lower it at the inside of the bend. Near the center of the channel, the centrifugal force is, therefore, balanced by internal pressure gradients caused by the slope of the water surface. However, near the bottom where the longitudinal velocity is lower, the pressure gradient overbalances the smaller centrifugal force, and the fluid near the bottom is accelerated toward the inside face of the bend. Conversely, at the surface where the longitudinal velocity is greatest, the centrifugal forces overbalance the pressure gradient so that water at the surface is accelerated toward the outside of the bend.

This results in a basic clockwise spiral flow pattern. For large angle bends, the redistribution of fluid by the secondary motions can lead to situations where the longitudinal velocity no longer increases monotonically from the bottom to the surface. Under these conditions, multiple helices may develop. However, even under these conditions, the acceleration of the fluid is controlled by the local balance of the centrifugal force (v^2/r) and the pressure gradient caused by the slope of the surface.

The important point in the preceding discusssion is that the secondary motion is essentially an inviscid flow phenomenon. The action of viscosity is important in establishing the vertical velocity profile in the flowing liquid at the entrance to the bend. However, given the initial vertical variations in velocity, the development of the helical secondary flow depends upon the balance of the centrifugal and pressure gradient terms in the equations of motion. The complex flow in the channel bend can, therefore, be adequately described without including viscous terms in the equations of motion.

This approach was adopted by Fox and Ball[4] in their computer model for the secondary flow in bends with no side weir. The present formulation represents an extension of this work to include discharge over a side weir, a more general channel cross section, and calculation of the resulting particulate concentration field and separation efficiency.

Equations of Motion

The basic equations for steady state flow of an incompressible fluid are the momentum and continuity equations:

$$\text{Momentum} \qquad \nabla \cdot (\nabla \vec{V}) + \frac{1}{\rho} \nabla p = 0 \qquad (1)$$

$$\text{Continuity} \qquad \nabla \cdot \vec{V} = 0, \qquad (2)$$

where $\vec{V}$ = velocity vector
ρ = fluid density
p = pressure

Consider first a curved rectangular channel. Any point in the channel can be located by the cylindrical coordinates (r, θ, z) as shown in Figure 70, Cylindrical Coordinate System.

Corresponding respectively to the coordinates (r, θ, ζ) are the velocity components (u, v, w), also shown in Figure 70. The general momentum and continuity equations (1) and (2) may be written in cylindrical coordinates:

$$\text{Momentum} \quad u\frac{\partial u}{\partial r} + \frac{v}{r}\frac{\partial u}{\partial \theta} - \frac{v^2}{r} + w\frac{\partial u}{\partial z} + g\frac{\partial \zeta}{\partial r} = 0 \qquad (3)$$

$$u\frac{\partial v}{\partial r} + \frac{v}{r}\frac{\partial v}{\partial \theta} + \frac{uv}{r} + w\frac{\partial v}{\partial z} + \frac{g}{r}\frac{\partial \zeta}{\partial r} = 0 \qquad (4)$$

$$\text{Continuity} \quad \frac{\partial u}{\partial r} + \frac{u}{r} + \frac{1}{r}\frac{\partial v}{\partial \theta} + \frac{\partial w}{\partial z} = 0 \qquad (5)$$

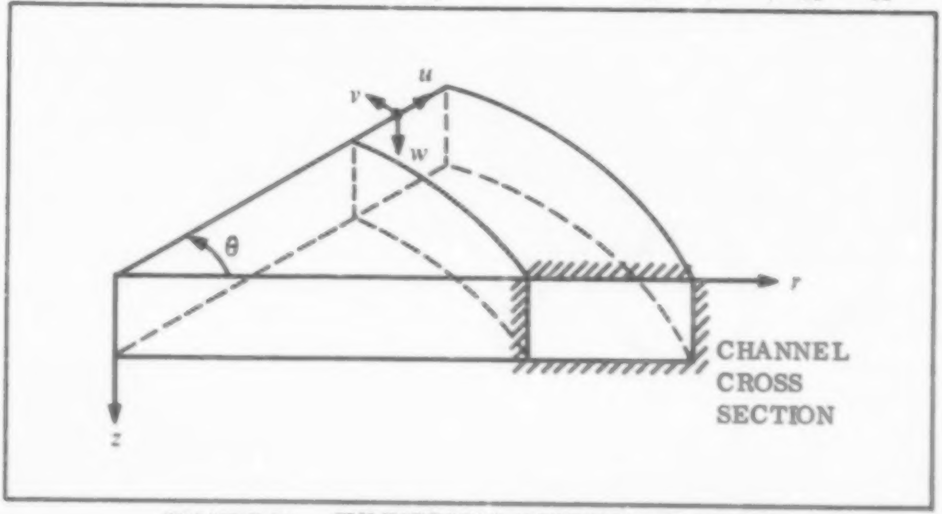

FIGURE 70 CYLINDRICAL COORDINATE SYSTEM

Here, the original pressure gradient terms have been replaced with derivatives of ζ, which represents slight variations in the fluid surface elevations. $\partial\zeta/\partial r$ is a positive quantity resulting from the fact that centrifugal force causes the surface elevation at the outside of the channel to be slightly higher than the elevation at the inside of the channel. The pressure gradient term of $g\partial\zeta/\partial r$ balances the radial acceleration v^2/r. The factor $\partial\zeta/\partial\theta$ is also positive due to the slight rise in surface elevation caused by the channel blockage. This factor has the effect of slowing the fluid (decreasing average v) as the channel blockage is approached.

For computational purposes, equations (3), (4), and (5) are rewritten as follows:

$$\frac{\partial u}{\partial \theta} = -\frac{r}{v}\left[u\frac{\partial u}{\partial r} - \frac{v^2}{r} + \frac{w\partial u}{\partial z} + g\,\frac{\partial \zeta}{\partial r}\right] \quad (6)$$

$$\frac{\partial v}{\partial \theta} = -\frac{r}{v}\left[u\frac{\partial v}{\partial r} + \frac{uv}{r} + w\frac{\partial v}{\partial z} + \frac{g}{r}\frac{\partial \zeta}{\partial \theta}\right] \quad (7)$$

$$w = -\int_{0}^{z}\left[\frac{\partial u}{\partial r} + \frac{u}{r} + \frac{1}{r}\frac{\partial v}{\partial \theta}\right] dz \quad (8)$$

A simplified summary of the computational procedure is as follows: At an angle Θ, suppose that at discrete points in r and ζ, values are known for $u(r,\theta,\zeta)$, $v(r,\theta,\zeta)$, and $w(r,\theta,\zeta)$. The quantities on the right hand sides of (6) and (7) can be calculated, and values for $\partial u(r,\theta,\zeta)/\theta$ and $\partial v(R,\theta,\zeta/\partial\theta$ follow. Then, u and v can be projected through an incremental angle $\Delta\theta$ to the $\theta + \Delta\theta$ plane:

$$u(r, \theta + \Delta\theta, z) = u(r, \theta, z) + (\partial u/\partial\theta)\Delta\theta \quad (9)$$

$$v(r, \theta + \Delta\theta, z) - v(r\theta, z) + (\partial v/\partial\theta)\,\Delta\theta \quad (10)$$

These new values in the $\theta + \Delta\theta$ plane are then applied to Equation (8) from which $w(r, \theta + \Delta\zeta)$ follows. With this the cycle is completed.

Radial Surface Slope

The terms on the right hand sides of equations (6), (7), and (8) can all be evaluated knowing u, v, and w in a given θ plane, but the terms $\partial\zeta/\partial r$ and $\partial\zeta/\partial\theta$ are not as obvious as the rest. Figure 71, Definition of Surface Shape in Channel Cross Section, shows a channel cross section, still represented by a rectangle, with an enlarged surface slope component.

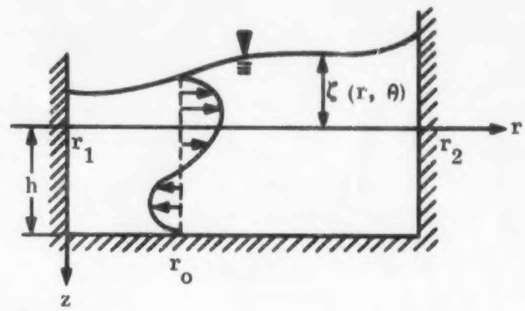

FIGURE 71 DEFINITION OF SURFACE SHAPE IN CHANNEL CROSS SECTION

Define $q(r, \theta)$ to be the lateral discharge across a line of constant radius r:

$$q(r,\theta) = \int_{-\zeta}^{h} u(r,\theta,z)\, dz \quad (11)$$

Velocity components $u(r_o, \theta, z)$ are illustrated in Figure 71. It is realistic to assume that the rate of lateral discharge does not vary with angle θ, so $\partial\theta = 0$, or

$$\frac{\partial q}{\partial \theta} = \left[\int_{-\zeta}^{h}\left(\frac{\partial u}{\partial \theta}\right) dz + \frac{\partial \zeta}{\partial \theta}\cdot u(r,\theta,-\zeta)\right] = 0 \quad (12)$$

The Slope $\partial\zeta/\partial\theta$ is very small, so

$$\frac{\partial q}{\partial \theta} \cong \int_{-\zeta}^{h}\left(\frac{\partial u}{\partial \theta}\right) dz = 0 \quad (13)$$

However, $(\partial u/\partial\theta)$ is known from Equation (6), so,

$$\int_{-\zeta}^{h}\left[-\frac{ru}{v}\frac{\partial u}{\partial r}+v-\frac{rw}{v}\frac{\partial u}{\partial z}-\frac{rg}{v}\frac{\partial\zeta}{\partial r}\right]dz=0, \tag{14}$$

from which

$$g\frac{\partial\zeta}{\partial r}=\frac{\frac{1}{r}\int_{-\zeta}^{h}\left[v-\frac{ru}{v}\frac{\partial u}{\partial r}+v-\frac{rw}{v}\frac{\partial u}{\partial z}\right]dz}{\int_{-\zeta}^{h}\left(\frac{1}{v}\,dz\right)} \tag{15}$$

All of the terms on the right hand side of this expression follow directly from the knowledge of u, v, and w, so the resulting $g\partial\zeta/\partial r$ may be substituted into Equation (6). This technique for obtaining the radial surface slope, $\partial\zeta/\partial r$, was developed by Fox and Ball.[4]

Longitudinal Surface Slope

The fluid flow solution is treated computationally as an initial value problem, so only initial conditions at the upstream end of the base are needed. However, in making this simplification, there is no way that the fluid can *feel* the presence of the dam at the downstream end of the channel, so a mechanism is needed to slow the average longitudinal velocity as it proceeds around the channel arc. The first possibility investigated involved artificially increasing the surface $\zeta(r,\theta)$ with increasing angle θ. The integral of the surface slope, $\zeta_1(r,\theta)$, can be found from $(\partial\zeta/\partial r)$ in Equation (15):

$$\zeta_1(r,\theta)=\int_{r_1}^{r}\left(\frac{\partial\zeta(r,\theta)}{\partial r}\,dr\right) \tag{16}$$

where r_1 is the inner radius of the channel bend. The average surface height is then:

$$\bar{\zeta}_1(\theta)=\frac{1}{r_2-r_1}\int_{r_1}^{r_2}\zeta_1(r,\theta)\,dr, \tag{17}$$

where r_2 is the outer radius of the bend.

The resulting surface elevation, $\zeta(r,\theta)$, has a zero average value:

$$\zeta(r,\theta)=\zeta_1(r,\theta)-\bar{\zeta}_1(\theta) \tag{18}$$

To this zero mean surface, an average value, increasing with angle θ, was added. The result was the desired slowing of the average longitudinal flow, but at angles greater than 40° local backflows developed. These backflows are not unrealistic, but are incompatible with the formulation of the initial value problem.

An alternative means for slowing the longitudinal flow is to slightly decrease the average longitudinal velocity at each incremental angle θ at which the velocities are computed. $\zeta(r,\theta)$ in Equation (18) is still computed to evaluate $\partial\zeta/\partial\theta$ which is needed in Equation (8). If the inflow rate is Q_o, and the foul flow withdrawal rate is Q_s, then a flow rate equal to $(Q_o - Q_s)$ must flow over the weir. Assuming a uniform discharge rate over the weir over the arc length θ_m, the discharge over the weir per radian is $(Q_o - Q_s)/\theta_m$. So, at any angle $0\leq\theta\leq\theta_m$, the flow rate in the channel must be:

$$Q_L(\theta)=Q_o-\frac{(Q_o-Q_s)}{\theta_m}\theta \tag{19}$$

However, if at any angle θ, $v_1(r,\theta,\zeta)$ the velocity is calculated from Equation (10), the channel flow rate would be computed to be:

$$Q_{L_1}(\theta)=\int_{r_1}^{r_2}\int_{0}^{h(r)}v_1(r,\theta,z)\,dz\,dr \tag{20}$$

The desired slowing effect will take place if $v_1(r,\theta,z)$ at each point is multiplied by $(Q_c(\theta)/Q_{c_1}(\theta))$. This will always be a positive constant, very nearly equal to unity. Calculated in this way, negative values of v (backflow) will not develop:

$$v(r,\theta,\zeta)=\frac{v_1(r,\theta,z)\left[Q_o-\frac{(Q_o-Q_s)}{\theta_m}\theta\right]}{\int_{r_1}^{r_2}\int_{0}^{h(r)}v_1(r,\theta,z)\,dz\,dr} \tag{21}$$

This approximation, therefore, allows treatment of the flow as an initial value problem, while still partially accounting for the variation in longitudinal velocity, v, which arises from the secondary fluid motion (u, w).

Coordinate Transformation

For computational purposes, it is convenient to deal with a rectangular array of points in each θ plane. If the channel cross section were rectangular, Equations (6), (7), (8), and (15) could be used directly. The channel cross section is, however, approximately a trapezoid so a transformation is used to map the trapezoidal cross section into a rectangular computational space.

In Figure 72(a), Coordinate Transformation, if at both $r = r_1$, and $r = r_2$, the vertical sides are divided into the same number of equally spaced intervals, the intervals at $r = r_1$ will obviously be greater than at $r = r_2$. But in Figure 73(b), the intervals at $R = R1$ and $R = R2$ will be equal. The transformation $(r, \theta, \zeta) \rightarrow (R, \Theta, \zeta)$ transforms the trapezoid into a rectangle. To accomplish this transformation, define

$$Z = z/h(r) \qquad R = r \qquad \Theta = \theta$$

$$0 < Z < 1 \qquad R1 < R < R2 \qquad 0 < \theta < \theta_m ,$$

where

$$h(r) = h_1 + \frac{h_2 - h_1}{r_2 - r_1} (r - r_1), \tag{22}$$

or

$$h(r) = h_a + h_b \cdot r, \tag{23}$$

where

$$h_a = h_1 - r_1 \frac{h_2 - h_1}{r_2 - r_1}, \tag{24}$$

and

$$h_b = \frac{h_2 - h_1}{r_2 - r_1} \tag{25}$$

The derivatives in the (r, θ, z) system are related to those of the (R, Θ, Z) system as follows:

$$\frac{\partial}{\partial r} = R_r \frac{\partial}{\partial R} + Z_r \frac{\partial}{\partial Z} + \Theta_r \frac{\partial}{\partial \theta} = \frac{\partial}{\partial R} - Z_r \frac{\partial}{\partial Z} \tag{26}$$

$$\frac{\partial}{\partial \theta} = R_\theta \frac{\partial}{\partial R} + Z_\theta \frac{\partial}{\partial Z} + \Theta_\theta \frac{\partial}{\partial \theta} = \frac{\partial}{\partial \Theta} \tag{27}$$

$$\frac{\partial}{\partial z} = R_z \frac{\partial}{\partial R} + Z_z \frac{\partial}{\partial Z} + \Theta_z \frac{\partial}{\partial \theta} = Z_z \frac{\partial}{\partial Z} \tag{28}$$

Where $R_r = \partial R / \partial r$, $Z_r = \partial Z / \partial r$, etc.

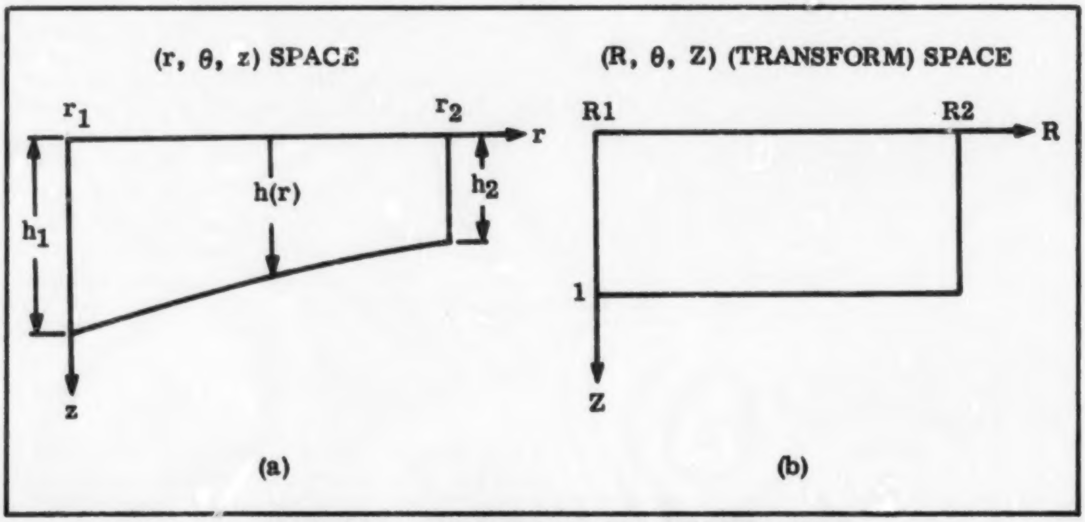

FIGURE 72 COORDINATE TRANSFORMATION

From the definition of the transformation:

$$Z_r = \frac{h_b Z}{h(r)} \quad \text{and} \quad Z_z = \frac{1}{h(r)} \tag{29}$$

To summarize:

$$R = r$$

$$\frac{\partial}{\partial r} = \frac{\partial}{\partial R} - \frac{h_b Z}{h(r)} \frac{\partial}{\partial Z}$$

$$Z = z/h(r)$$

$$\frac{\partial}{\partial z} = \frac{1}{h(r)} \frac{\partial}{\partial Z}$$

$$\Theta = \theta \qquad \frac{\partial}{\partial \theta} = \frac{\partial}{\partial \Theta}$$

Simplified Transformed Equations

When the transformed partial derivatives in equations (26), (27), and (28) are applied to Equations (6), (7), (8), and (15), the results are as follows:

$$\frac{\partial u}{\partial \Theta} = \frac{-R}{v} \left[u\left(\frac{\partial u}{\partial R} - \frac{h_b Z}{h(r)} \frac{\partial u}{\partial Z}\right) - \frac{v^2}{R} + \frac{w}{h(r)} \frac{\partial u}{\partial Z} + g \frac{\partial \zeta}{\partial R} \right] \tag{30}$$

$$\frac{\partial v}{\partial \Theta} = \frac{-R}{v} \left[u\left(\frac{\partial v}{\partial R} - \frac{h_b Z}{h(r)} \frac{\partial v}{\partial Z}\right) + \frac{uv}{R} + \frac{w}{h(r)} \frac{\partial v}{\partial z} + \frac{g}{R} \frac{\partial \zeta}{\partial \Theta} \right] \tag{31}$$

$$w = \int_1^Z \left[\frac{\partial u}{\partial R} - \frac{h_b Z}{h(r)} \frac{\partial u}{\partial Z} + \frac{u}{R} + \frac{1}{R} \frac{\partial v}{\partial \Theta} \right] h(r)\, dZ \tag{32}$$

$$g \frac{\partial \zeta}{\partial R} = \left\{ \frac{1}{R} \int_0^1 \left[v - \frac{Ru}{v}\left(\frac{\partial u}{\partial R} - \frac{h_b Z}{h(r)} \frac{\partial u}{\partial Z} \right) - \frac{Rw}{v h(r)} \frac{\partial u}{\partial Z} \right] h(r)\, dZ \right\} \Big/ \int_0^1 \left(\frac{1}{v}\right) h(r)\, dZ \tag{33}$$

By referring to Figure 72(a) and noting that in Equation (23) h_b is the bottom slope, the velocities u and w are related approximately as follows:

$$\frac{-w}{u} \cong h_b\, Z \tag{34}$$

This shows that in any Θ plane, near the bottom ($Z = 1$), the flow is parallel to the bottom, and near the top ($Z = 0$), the vertical velocity component approaches zero. When this simplification is applied to Equations (30), (31), and (33), the following equations result in the form which is used for computation:

$$\frac{\partial u}{\partial \Theta} = \frac{-R}{v} \left[u \frac{\partial u}{\partial R} - \frac{v^2}{R} + g \frac{\partial \zeta}{\partial R} \right] \tag{35}$$

$$\frac{\partial v}{\partial \Theta} = \frac{-R}{v} \left[u \frac{\partial v}{\partial R} + \frac{uv}{R} + \frac{g}{R} \frac{\partial \zeta}{\partial \Theta} \right] \tag{36}$$

$$w = \int_1^Z \left[\frac{\partial u}{\partial R} - \frac{h_b Z}{h(r)} \frac{\partial u}{\partial Z} + \frac{u}{R} + \frac{1}{R} \frac{\partial v}{\partial \Theta} \right] h(r)\, dZ \tag{37}$$

$$g \frac{\partial \zeta}{\partial R} = \frac{\frac{1}{R} \int_0^1 \left[v - \frac{Ru}{v} \frac{\partial u}{\partial R} \right] h(R)\, dZ}{\int_0^1 \left(\frac{1}{v}\right) h(r)\, dZ} \tag{38}$$

The channel cross section is described by the radii r_1 and r_2, height of sides $H1$ and $H2$, and overflow height and position $B2$ and $B1$ as shown in Figure 73, Mathematical Representation of a Channel Cross Section. If Q^o is the inflow rate, and Q^s the foul flow withdrawal flow rate, the fluid will flow over the weir with a height ZO, given by the standard weir formula:

$$ZO = \left[\frac{Q_0 - Q_s}{3.33(r2)(\Theta_m)} \right]^{2/3}, \tag{39}$$

where Θ_m is the arc length of the flow chamber. The coordinate system shown in Figure 73 has its origin at the inner radius and at the surface of the fluid. Along the vertical surfaces, there is no radial flow except at the overflow outlet, hence:

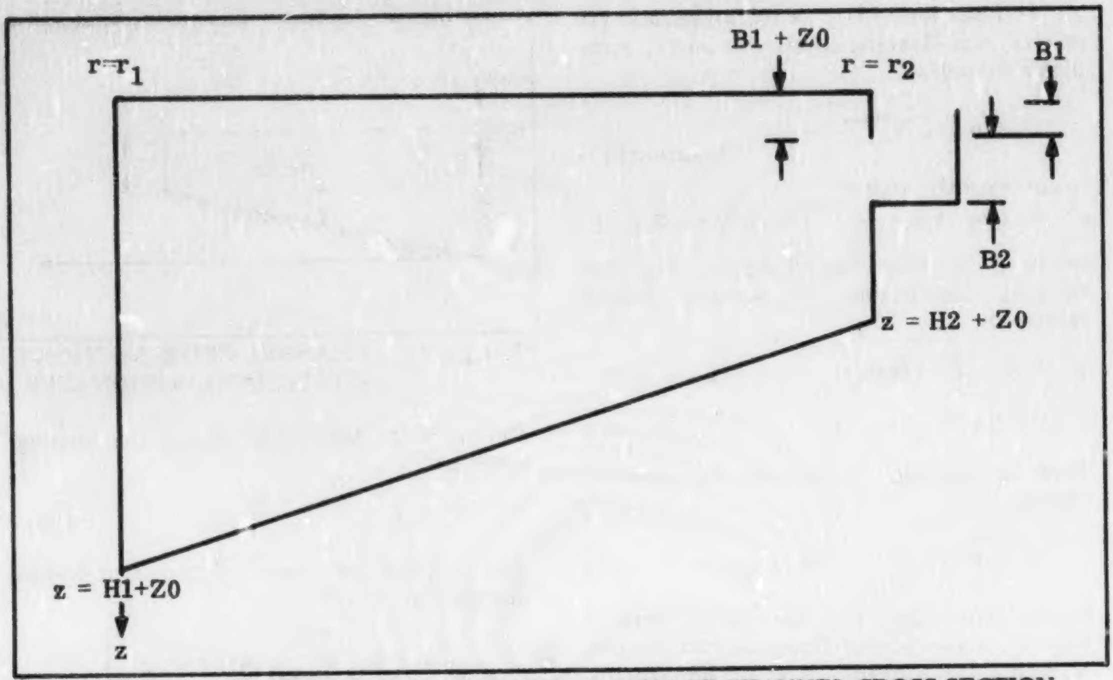

FIGURE 73 MATHEMATICAL REPRESENTATION OF CHANNEL CROSS SECTION

$$u(r,\theta,z) = 0 \quad \left\{ \begin{array}{l} r = r_1 \\ r = r_2, \text{ except outlet} \end{array} \right\} \tag{40}$$

The outlet has a height $B2$ and length $r_2\Theta_m$, so the radial flow rate at the overflow outlet is as follows:

$$u(r,\theta,z) = \frac{Q_0 - Q_s}{r_2\Theta_m}$$

$$\left\{ \begin{array}{l} r = r_2 \text{ and} \\ (B1 + Z0) \leqslant z \leqslant (B1 + B2 + Z0) \end{array} \right\} \tag{41}$$

Finally, along the bottom, the flow is tangent to the bottom:

$$w(r,\theta,z) = -u(r,\theta,z) \left(\frac{h_1 - h_2}{r_2 - r_1} \right)$$

$$z = Z_0 + h_b r + h_a \tag{42}$$

or

$$w(r,\theta,z) = h_b \, u(r,\theta,z)$$

Flow Field Initial Conditions

To start the computation, initial values for the velocity components u, v, and w are required at the entrance to the bend. The initial values for the longitudinal component, v, are derived first.

Initial Values for Longitudinal Velocity, v

Consider a wide rectangular channel. At large distances from the vertical walls, the velocity distribution perpendicular to the (x,y) plane is a function only of the height, y, above the channel bottom. The velocity is given by the Prandtl-von Karman universal velocity-distribution law[5].

$$v = \frac{1}{k} \sqrt{\frac{\tau_o}{\rho}} \ln (y/y_o), \tag{43}$$

where:

τ_o = bottom shear stress
ρ = density
k = von Karman constant
y_o = length related to the roughness height.

The term $\sqrt{\tau_o/\rho}$ is the friction velocity, V_f, which is given by:

$$V_f = \sqrt{f/8} \; \bar{V} \tag{44}$$

where f is the Darcy friction factor from the Manning equation

$$f = \frac{0.453 \, gn^2}{H^{1/3}} \tag{45}$$

In Equation (45), g is the acceleration of gravity, n is Manning coefficient and H is the hydraulic radius.

If $C = \frac{1}{k} \sqrt{\tau_o / \rho}$, Equation (43)

is equivalently written:

$$v = C \ln (y/y_o) = C \, [\ln (y/h) + \ln (h/y_o)] ,$$

where h is the channel depth. For this velocity distribution the average channel velocity is:

$$\overline{V} = C \int_0^1 [\ln (y/h) + \ln (h/y_o)] \, d(y/h)$$

$$= C [\ln (h/y_o) - 1 .] \tag{46}$$

Then an equivalent expression for equation (44) is:

$$v = \overline{V} + C (1 + \ln (y/h)) \tag{47}$$

In this expression, $\overline{V}$ is the average channel velocity, a function of flow rate and channel cross-sectional area only. The second term is a perturbation term which predicts slower moving fluid near the bottom and faster flow near the surface.

Now suppose that the channel is not *wide*, so that the effects of the vertical walls are felt. A functional form analogous to Equation (43), taking into account bottom and both walls is as follows:

$$v = C \ln \left[\left(\frac{y}{y_o}\right) \left(\frac{x}{y_o}\right) \left(\frac{a-x}{y_o}\right) \right]$$

in which a is the width of the channel.

Again, expressing the velocity in average and perturbation terms, the result is analogous to Equation (47):

$$v = \overline{V} + C \left[3 + \ln \left[(y/h) \, (x/a) \, \left(\frac{a-x}{a}\right) \right] \right]. \tag{49}$$

Finally, consider the channel cross section shown on Figure 74, Channel Cross Section in Cartesian Coordinates, in a Cartesian reference frame.

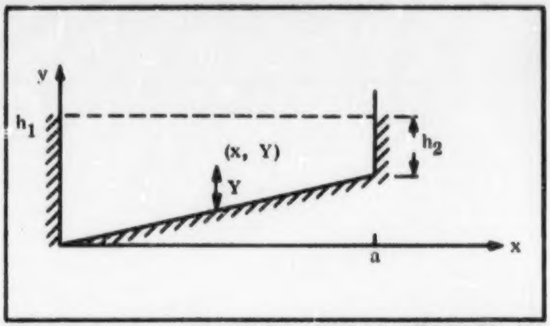

FIGURE 74 CHANNEL CROSS SECTION IN CARTESIAN COORDINATES

Define Y as the height above the sloping bottom:

$$Y = y - \left(\frac{h_1 - h_2}{a}\right) x \tag{50}$$

The appropriate form of the Prandtl-von Karman law is as follows:

$$v = C \ln \left[\left(\frac{Y}{y_o}\right) \left(\frac{x}{y_o}\right) \left(\frac{a-x}{y_o}\right) \right] \tag{51}$$

Again, in terms of average velocity, it can be shown that this velocity distribution can be written:

$$v(x,y) = \overline{V} + C \left\{ \ln \left[\left(\frac{Y}{h_1}\right) \left(\frac{x}{a}\right) \left(\frac{a-x}{a}\right) \right] + \tfrac{1}{2} + \left(\frac{4h_1 + 2h_2}{h_1 + h_2}\right) + \frac{h_2^2}{h_1^2 - h_2^2} \ln \left(\frac{h_2}{h_1}\right) \right\} \tag{52}$$

where the average velocity, $\overline{V}$, is obtained by dividing the total flow by the cross-sectional area:

$$\overline{V} = \frac{Q}{\tfrac{1}{2}(h_1 + h_2) a} \tag{53}$$

This result, in an (x,y) plane, is easily transformed into the r, z plane defined in Figure 72(a) by using the following:

$$r = r_1 + x$$
$$z = h_1 - y$$
$$a = r_2 - r_1 \tag{54}$$

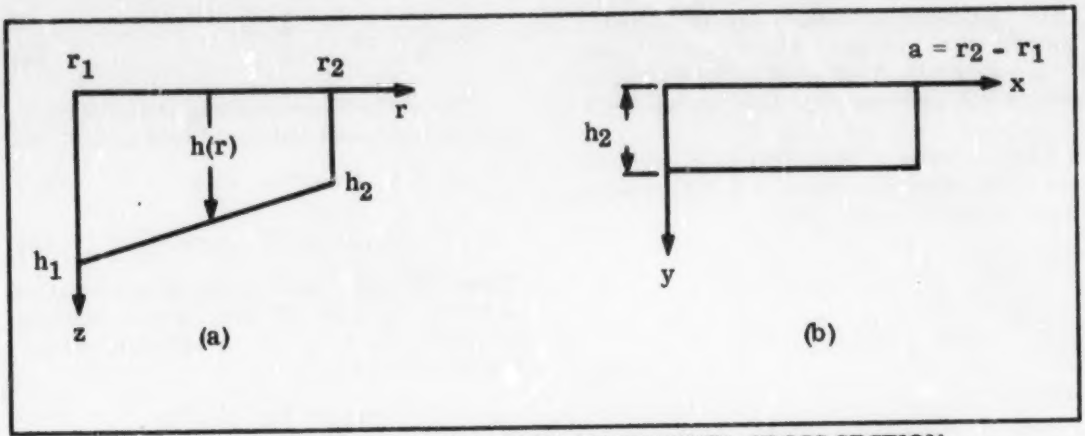

FIGURE 75 TRANSFORMATION OF CHANNEL CROSS SECTION TO RECTANGULAR REGION

Initial Values for the Cross-Flow Velocities *u* and *w*

The initial values for the cross-flow velocities describe the flow from the interior of the channel over the weir at the entrance to the bend, before the customary helical flow pattern develops.

The *u* and *w* velocity components lie in the $\Theta = 0$ plane, and are, respectively, in the radial (r) and vertical (z) directions. Figure 75(a), Transformation of Channel Cross Section to Rectangular Region, shows the channel cross section, while Figure 75(b) shows a transformed cross section.

The ultimate goal is a velocity field in Figure 75(a), where flow is parallel to both the top ($z = 0$) and the bottom ($z = h(r)$), and no flow crosses the sides ($r = r_1$ and $r = r_2$) except for a point sink at $r = r_2$, and $z = 0$, which represents the flow over the weir. Several steps are required to reach this point:

(a) In Figure 75(b) a potential flow field solution is derived which crosses and is perpendicular to x = 0 at a uniform rate on $0 \leq y \leq h_2$. All flow is removed at a sink at $x = a, y = 0$.

(b) The field is rotated through a variable angle so that in Figure 75(a) flow is parallel to the sloping bottom, at $\zeta = h(r)$, while remaining parallel to the horizontal surface at $z = 0$.

(c) Velocity components are then scaled such that they exponentially approach zero as $r \rightarrow r_1$, showing the actual situation where no flow crosses this wall.

Returning to the first step, the problem is to derive a two-dimensional potential flow solution in the transformed coordinate system shown in Figure 75(b). A stream function, ψ is introduced such that the velocities,

$$u_1 = \frac{\partial \psi}{\partial y}, \quad w_1 = -\frac{\partial \psi}{\partial x} \tag{55}$$

automatically satisfy the two-dimensional continuity equation:

$$\frac{\partial u_1}{\partial x} + \frac{\partial w_1}{\partial y} = 0 \tag{56}$$

For potential flow, the stream function is the solution of the following:

$$\nabla^2 \psi = 0 \tag{57}$$

along with the boundary conditions:

$$y = 0 \qquad \psi = 0 \qquad 0 < x < a \tag{58}$$

$$x = 0 \qquad \psi = U_o y \qquad 0 \leq y \leq h_2 \tag{59}$$

$$y = h_2 \qquad \psi = U_o h_2 \qquad 0 \leq x \leq a \tag{60}$$

$$x = a \qquad \psi = U_o h_2 \qquad 0 < y \leq h_2 \tag{61}$$

where

$$U_o h_2 = \frac{(Q_o - Q_s)}{r_2 \theta_m} \quad \text{(discharge/unit length).} \tag{62}$$

These boundary conditions are such that a uniform flow crosses between $y = 0$ and $y = h_2$ at $x = 0$. A point sink is located at $x = a$, $y = 0$, while no other flow crosses $y = 0$, $y = h_2$, and $x = a$.

The solution of Equation (57), with the above boundary conditions at points interior to the boundary, is given by:

$$\psi = U_0 y + \sum_{n=1}^{\infty} C_n \sin\left(\frac{n\pi y}{h_2}\right) \sinh\left(\frac{n\pi x}{h_2}\right) \qquad (63)$$

where

$$C_n = \frac{2U_0 h_2}{n\pi \sinh\left(\frac{n\pi a}{h_2}\right)} \qquad (64)$$

In practice, an infinite series cannot be completely evaluated, so Equation (63) includes all terms up to the point where:

$$\left| \frac{2U_0\, h_2 \sinh(n\pi x/h_2)}{n\pi \sinh(n\pi a/h_2)} \right| < 0.01\, \psi \qquad (65)$$

Now, suppose that the velocity components u, and w, are rotated by a variable angle so that u_1 is parallel to the channel top and bottom, as shown in Figure 76, Rotation of Velocity Components.

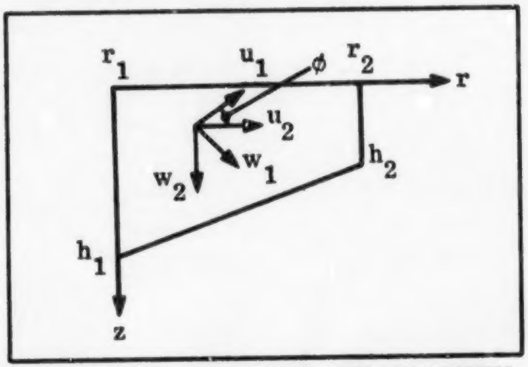

FIGURE 77 ROTATION OF VELOCITY COMPONENTS

The angle ϕ is chosen so that there is enough rotation to make u_1 parallel to the bottom at $z = h(r)$, while there is no rotation at $z = 0$:

$$\phi = \frac{z}{h(r)} \tan^{-1} \frac{h_1 - h_2}{r_2 - r_1} \qquad (66)$$

Then the corresponding velocities (u_2, w_2) in the cylindrical coordinate system are:

$$u_2 = u_1 \cos\phi + w_1 \sin\phi \qquad (67)$$

$$w_2 = -u_1 \sin\phi + w_1 \cos\phi \qquad (68)$$

These velocities must next be scaled by a factor F, so that the same lateral discharge exists for any value of r, despite the variable bottom depth $h(r)$:

$$u_3 = F \cdot u_2 \qquad w_3 = F \cdot w_2, \qquad (69)$$

where the scale factor, F, is chosen so that

$$\int_0^{h(r)} F \cdot [u_2 \cos\phi - w_2 \sin\phi]\, dz = \int_0^{h_2} u_1\, dy \qquad (70)$$

But

$$u_2 \cos\phi - w_2 \sin\phi = u_1 \qquad (71)$$

so

$$\int_0^{h(r)} F \cdot u_1\, dz = \int_0^{h_2} u_1\, dy \qquad (72)$$

Using the transform $z = (h(r)/h_2)\, y$, it follows that:

$$F = h_2/h(r), \qquad (73)$$

so,

$$u_3 = \frac{h_2}{h(r)} (-u_1 \cos\phi + w_1 \sin\phi) \qquad (74)$$

$$w_3 = \frac{h_2}{h(r)} (-u_1 \sin\phi + w_1 \cos\phi) \qquad (75)$$

Finally, the desired initial cross-flow velocities u and w are respectively u_3 and w_3, exponentially scaled such that u and w approach zero at $r = r_1$:

$$u = \frac{h_2}{h(r)} e^{\frac{(r - r_2)}{Kr}} [u_1 \cos\phi + w_1 \sin\phi] \qquad (76)$$

$$w = \frac{h_2}{h(r)} e^{\frac{(r - r_2)}{Kr}} [-u_1 \sin\phi + w_1 \cos\phi] \qquad (77)$$

At $r = r_2$, the scale factor is unity. An experimentally determined acceptable value for the constant is $Kr = 1.5$.

These approximate initial values for u and w describe the flow in the cross-flow (r, z) plane at $\Theta = 0$, which arises because the flow upstream of $\Theta = 0$ has already adjusted to the presence of the weir. This flow generally proceeds from the inside toward the outside of the bend, and upward from the bottom. The exact values of the velocities are not critical, because the flow will re-adjust itself as the computation proceeds downstream.

Numerical Method for Liquid Flow

The transformed space shown in Figure 72(b) is divided into a rectangular grid as shown in Figure 77, Computational Grid in Transformed Space. Grid points are spaced by a distance ΔR radially, and ΔZ vertically. Figure 77 is a plane in R and Z. A complete flow field solution includes a number of these planes separated by angular increments of $\Delta\Theta$.

The cross-flow velocities, $u(R,\Theta,Z)$ and $v(R,\Theta,Z)$, are calculated from Equations (35) and (36) by use of a predictor-corrector scheme. In both stages of this two-stage process, the right hand sides of these equations must be evaluated.

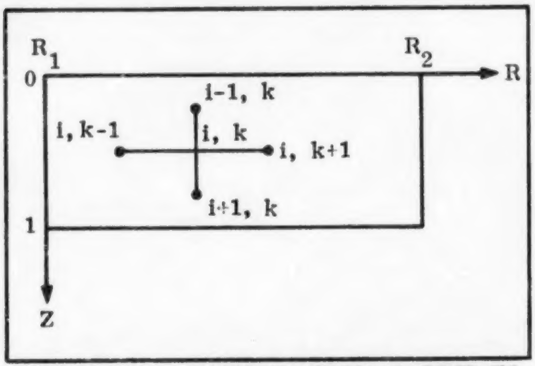

FIGURE 77 COMPUTATIONAL GRID IN TRANSFORMED SPACE

The longitudinal surface slope $\partial\zeta/\partial\Theta$ is evaluated in both stages as a backward difference:

$$\frac{\partial\zeta}{\partial\theta} = \frac{\zeta(R.\theta) - \zeta(R.\theta - \Delta\theta)}{\Delta\theta} \tag{78}$$

The evaluation of $\partial\zeta/\partial R$ is the same in both stages and is discussed in a subsequent paragraph. Both $u(R,\Theta,Z))$ and $v(R,\Theta, Z)$ are calculated by the predictor-corrector process, so it is sufficient to discuss only $u(R,\Theta,Z)$.

During the predictor stage, a predicted value $u(R,\Theta,Z)$ is found from:

$$\widetilde{u}(R, \theta + \Delta\theta, Z) = u(R,\theta,Z) + \Delta\theta \cdot \frac{\partial u}{\partial\theta} \tag{79}$$

Where $\partial u/\partial o$ is evaluated from Equation (35) in which the terms $\partial u/\partial R$ is found as a backward difference for $R < 0.5(R1+R2)$:

$$\frac{\partial u}{\partial r} = \frac{u(R,\theta,Z) - u(R - \Delta R,\theta,Z)}{\Delta R} \tag{80}$$

and a forward difference for $R > 0.5(R1 + R2)$:

$$\frac{\partial u}{\partial R} = \frac{u(R + \Delta R,\theta,Z) - u(R,\theta,Z)}{\Delta R} \tag{81}$$

The new $u(R,\Theta,Z)$ is then the average of the predicted $\widetilde{u}(R,\Theta + \Delta\Theta, Z)$ and a correction term:

$$u(R,\theta + \Delta\theta,Z) = \frac{1}{2}\left\{\widetilde{u}(R,\theta + \Delta\theta,Z) + u(R,\theta,Z) + \Delta\theta \cdot \partial\widetilde{u}/\partial\theta\right\} \tag{82}$$

Here, $\partial\widetilde{u}/\partial\Theta$ is evaluated using the predicted $\widetilde{u}$ and $\widetilde{v}$, and the backward and forward differences are reversed, so that $\partial\widetilde{u}/\partial r$ is a forward difference for $R < \frac{1}{2}(R1 + R2)$, and a backward difference for $R > \frac{1}{2}(R1 + R2)$. Both $w(R,Z)$ and $\partial\zeta/\partial R$ in Equations (37) and (38) must be calculated after each predictor-corrector cycle, and both contain the form:

$$\int_{Z1}^{Z2} f(Z)\,dZ \tag{83}$$

This integral is approximated by the trapezoidal rule:

$$\int_{Z1}^{Z2} f(Z)\,dZ \cong \sum_{I=I1}^{I2-1} \frac{1}{2}\left[f(I \cdot \Delta Z) + f(I + 1, \Delta Z)\right]\Delta Z, \tag{84}$$

where

$$Z1 = I1 \cdot \Delta Z \qquad Z2 = \cdot \Delta Z$$

Within the integrand of Equation (37), $\partial v/\partial \Theta$ is evaluated as a backward difference:

$$\frac{\partial v}{\partial \theta} = \frac{v(R,\theta,Z) - v(R,\theta - \Delta\theta,Z)}{\Delta\theta} \tag{85}$$

and the terms $\partial u/\partial R$ and $\partial u/\partial Z$ are evaluated as centered differences.

$$\frac{\partial u}{\partial r} = \frac{u(R + \Delta R,\theta,Z) - u(R - \Delta R,\theta,Z)}{2\Delta R} \tag{86}$$

$$\frac{\partial u}{\partial Z} = \frac{u(R,\theta,Z + \Delta Z) - u(R,\theta,Z - \Delta Z)}{2\Delta Z} \tag{87}$$

Liquid Flow Summary

The equations basic to fluid flow, the momentum and continuity equations, are presented as Equations (1) and (2). These equations are transformed to an equivalent set, Equations (3), (4) and (5), in cylindrical coordinates to represent the curvature of the channel. They are then expressed in Equations (6), (7), and (8) in a form from which the velocities (u,v,w), corresponding to coordinates (r,θ,z) can be calculated for a channel of rectangular cross section.

A surface height, $\zeta(r,\theta)$, is introduced to represent the fact that the fluid surface is not horizontal, but rises radially to counteract centrifugal force. Equation (15) provides the surface slope, $\partial\zeta/\partial r$, needed to calculate the radial velocity u. Then $\zeta(r,\theta)$ follows in Equation (8) as the integral of $(\partial\zeta/\partial r)$ over r.

Since the problem is formulated as an initial value problem, the channel blockage cannot be felt. Longitudinal velocity scaling in Equation (21) provides the necessary average velocity reduction. A coordinate transformation is made to account for the non-rectangular channel cross section. The simplified transformed equations needed to solve for (u, v, w) appear in Equations (35) to (38).

Boundary conditions define the channel walls, bottom, fluid surface, and overflow. An initial longitudinal velocity profile, $v(R,Z)$, is derived, based on the Prandtl-von Karman universal-velocity-distribution law. An initial velocity field for u and w in the plane of the channel cross section is developed to represent flow toward the overflow as a point sink.

Figure 78, Fluid Flow Solution Summary, summarizes the computational procedure, and shows the equations used in each step.

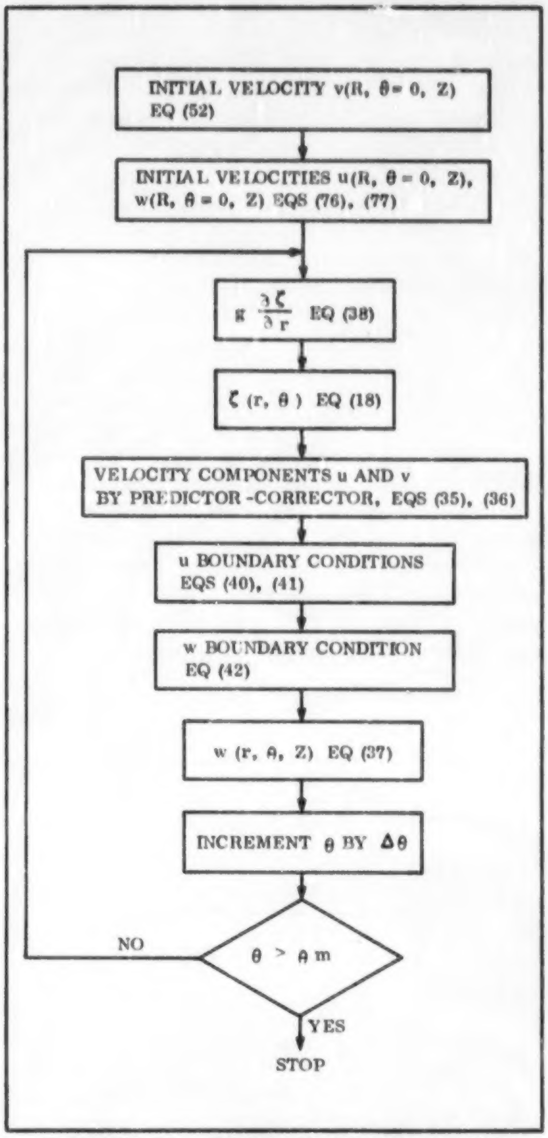
INITIAL VELOCITY v(R, θ = 0, Z) EQ (52)
INITIAL VELOCITIES u(R, θ = 0, Z), w(R, θ = 0, Z) EQS (76), (77)
g ∂ζ/∂r EQ (38)
ζ (r, θ) EQ (18)
VELOCITY COMPONENTS u AND v BY PREDICTOR-CORRECTOR, EQS (35), (36)
u BOUNDARY CONDITIONS EQS (40), (41)
w BOUNDARY CONDITION EQ (42)
w (r, θ, Z) EQ (37)
INCREMENT θ BY Δθ
NO
θ > θm
YES
STOP

FIGURE 78 FLUID FLOW SOLUTION SUMMARY

Particle Flow Calculation

The calculation of the particle flow field is carried out, based on the assumption that the particle number density is low so that particle interaction can be neglected. The individual particle velocities at each grid point can be accurately represented by superimposing the particle settling velocity on the calculated liquid velocities. The local concentration of the particle cloud is then calculated from the continuum continuity equation. These calculations are performed for a discrete particle size class, and are repeated for various settling velocities in order to represent the mixture of particle sizes to be encountered in practice.

Particle Flow Equation

The solution of the particle flow problem is carried out as an initial value problem, made possible by the assumption that there is no diffusion in the longitudinal (Θ) direction, and that no back-flow (negative ν velocities), occurs. Written in conservation form, the following equation describes the steady-state particle concentration (C) distribution:

$$\frac{\partial C}{\partial t} = -\nabla \cdot (V_p C) + \nabla \cdot (\epsilon \nabla C) = 0 \qquad (88)$$

$\vec{V}_p$ is the particle velocity vector comprised of the components $(u_p, \nu_p w_p)$. While u_p and ν_p are those calculated in the fluid flow problem, w_p is the sum of the component w from that solution, plus the particle settling velocity, w_s. Written in cylindrical coordinates the equivalent equation is:

$$\frac{1}{r}\frac{\partial(ruC)}{\partial r} + \frac{1}{r}\frac{\partial(\nu C)}{\partial \theta} + \frac{\partial(w_p C)}{\partial z} = \epsilon\left[\frac{1}{r}\frac{\partial}{\partial r}\left(r\frac{\partial C}{\partial r}\right) + \frac{1}{r^2}\frac{\partial^2 C}{\partial \theta^2} + \frac{\partial^2 C}{\partial z^2}\right] \qquad (89)$$

The eddy diffusivity has been assumed to be constant. The assumption of no longitudinal diffusion is equivalent to assuming that $(r^2)\ \partial^2 C/\partial\theta^2$ is small with respect to the other terms, and may be set to zero. Having done this, and re-arranging the factors, the equation becomes:

$$\frac{\partial}{\partial \theta}(\nu C) = -\left[\frac{\partial(ruC)}{\partial r} + r\frac{\partial(w_p C)}{\partial \zeta}\right] + \epsilon\left[\frac{\partial}{\partial r}\left(r\frac{\partial C}{\partial r}\right) + r\frac{\partial^2 C}{\partial z^2}\right] \qquad (90)$$

The numerical solution basically follows the same pattern as the solution for the liquid flow. The right hand side of Equation (90) is evaluated at grid points in a given θ plane; then,

$$(\nu C)_{r,\theta+\Delta\theta,z} = (\nu C_{r,\theta,z} + \Delta\theta\left(\frac{\partial(\nu C)}{\partial \theta}\right)_{r,\theta,z}, \qquad (91)$$

and

$$C(r,\theta+\theta,z) = \frac{(\nu C)r,\theta+\Delta\theta,z}{\nu(r,\theta+\Delta\theta,z)} \qquad (92)$$

Transformed Equation

As is the case for the fluid flow solution, the numerical solution of the concentration equation is made easier by a coordinate transformation. The transformation is repeated here:

$$R = r \qquad \frac{\partial}{\partial r} = \frac{\partial}{\partial R} + Z_r\frac{\partial}{\partial Z} \qquad (93)$$

$$\Theta = \theta \qquad \frac{\partial}{\partial \theta} = \frac{\partial}{\partial \Theta} \qquad (94)$$

$$Z = \frac{z}{h(r)} \qquad \frac{\partial}{\partial z} = Z_z\frac{\partial}{\partial Z}\,. \qquad (95)$$

where

$$Z_r = \frac{-Zh_b}{h(r)} \qquad (96)$$

and

$$Z_z = \frac{1}{h(r)} \qquad (97)$$

Applying this transformation to Equation (90):

$$\frac{\partial(\nu C)}{\partial \theta} = -\left[\frac{\partial(RUC)}{\partial R} + Z_r\frac{\partial(RUC)}{\partial Z} + RZ_z\frac{\partial(wC)}{\partial Z}\right] + \epsilon\left[\frac{\partial}{\partial R}\left(R\frac{\partial C}{\partial R}\right) + \frac{\partial}{\partial R}\left(RZ_r\frac{\partial C}{\partial Z}\right) + Z_r R\frac{\partial^2 C}{\partial Z\partial R}\right.$$

$$+ Z_r R \frac{\partial}{\partial Z} \left(Z_r \frac{\partial C}{\partial Z} \right)$$

$$+ R \left(Z_z \frac{\partial}{\partial Z} \left(Z_z \frac{\partial C}{\partial Z} \right) \right) \Bigg] \quad (98)$$

Boundary Conditions For Particle Flow

The boundary conditions for the particle concentration field, (Equation 88), require specification of the particle flux vector $\vec{F}$ defined as:

$$\vec{F} = \vec{V}_p C - \epsilon \nabla C \quad (99)$$

If $\vec{n}$ denotes the unit inward normal to one of the bounding surfaces, then the particle flux normal to this boundary is:

$$F_n = \vec{n} \cdot \vec{F} = C\vec{V}_p \cdot \vec{n} - \epsilon \frac{\partial C}{\partial n} \quad (100)$$

Along the vertical walls (except at the overflow), the particle flux, normal to the wall must be zero. Since the velocity normal to the wall is zero, $\vec{V}_p . \vec{n} = o$, for these surfaces, so that Equation (100) reduces to:

$$\frac{\partial C}{\partial n} = 0 \text{ (for vertical surfaces).} \quad (101)$$

Through the open surface of the channel there is also no particle flux. However, along this free surface, the vertical velocity of the liquid, w, is zero, but the particle velocity is the settling velocity, w_s. The rate at which particles settle from the surface must, therefore, balance the flux of particles toward the surface by diffusion, or, from Equation (100):

$$Cw_s - \epsilon \frac{\partial C}{\partial z} = 0 \quad \text{(open surface)} \quad (102)$$

Along the bottom, it is possible to specify either of two boundary conditions. The particle flux through the bottom can be assumed to be zero $(\vec{F} \cdot \vec{n} = 0)$ in which case all of the bed load remains in suspension Alternatively, particles reaching the bottom can be assumed to settle into a thin, highly concentrated sediment layer external to the computational mesh. The first boundary condition – all bed load remains in suspension – is probably somewhat closer to reality and has been used in the present model. However, some deposition of sediment is known to occur and, by neglecting this, the model will tend to under-predict the removal efficiency. To correct for this tendency, the eddy viscosity has been empirically calibrated against laboratory data, as will be described to reproduce the correct removal efficiency at the design flow rate.

Initial Concentration Distribution

An analytical derivation of the concentration in the $\Theta = 0$ plane is not as straightforward as the initial velocity calculation. The actual particle concentrations which exist at the entrance to the bend are influenced by the design of the entrance section. It was originally thought that the vertical variations in concentration could be obtained from the analytical solution for sediment transport in a straight open channel. However, the laboratory measurements revealed significant lateral concentration variations which could not be modeled with this approach. For this reason, the initial concentration distribution is based on measured data at 12 points in the channel cross section. Initial concentrations at each computational grid point are calculated as a linear two-dimensional interpolation of the four measured values surrounding each grid point. For grid points not surrounded by four data points, the interpolation becomes an extrapolation.

Numerical Method for Particle Flow

The numerical solution for $C(R,\Theta,Z)$ proceeds ahead in angle Θ, according to Equations (91) and (92). These require that the right hand side of Equation (98) be evaluated at grid points in R and Z at each Θ step. The points *(o)* at which C is calculated lie midway between the points *(x)* at which u, v, and w are calculated in the *(R,Z)* plane. Figure 79, Location of Computational Grid Points for Concentration Field Calculations, shows the arrangement.

The boundary conditions for the particle flow are built into the numerical procedure by specifying the appropriate particle fluxes to be zero at the solid surfaces and along the open top.

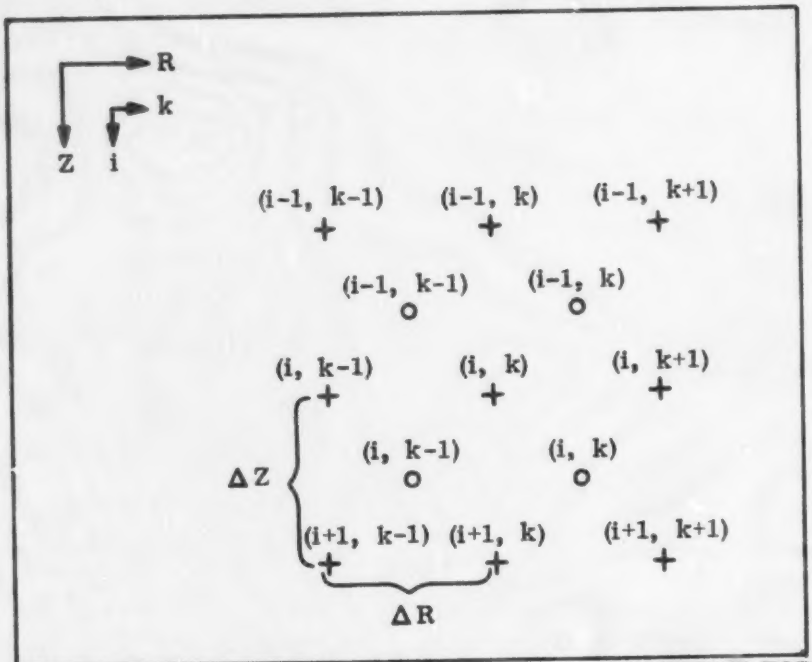

FIGURE 79 LOCATION OF COMPUTATIONAL GRID POINTS FOR FOR CONCENTRATION FIELD CALCULATION

The numerical calculation of each of the eight terms in Equation (98) is described below. In the first partial derivatives in the first three terms, care is taken so that mass flux is conserved.

Term 1

$$\frac{\partial(RuC)}{\partial R} = \frac{(\mathrm{Ru})_p\, C_p - (Ru)_m\, C_m}{\Delta R} \qquad (103)$$

where

$$(Ru)_p = \tfrac{1}{2} R_{k+1}\,(u_{i,k+1} + u_{i+1,k+1})$$
$$(Ru)_m = \tfrac{1}{2} R_k\,(u_{i,k} + u_{i+1,k})\ ,$$

and

$$C_p = C_{i,k}\ \mathit{for}\ (Ru)_p \geqslant 0$$
$$C_p = C_{i,k+1}\ \mathit{for}\ (Ru)_p < 0$$

$$C_m = C_{i,k-1}\ \mathit{for}\ (Ru)_m > 0$$
$$C_m = C_{i,k}\ \mathit{for}\ (Ru)_m \leqslant 0$$

R(k) and *Z(i)*, which will appear later, are evaluated at the points *(x)*.

Term 2

$$Z_r\,\frac{\partial(RuC)}{\partial Z} = \frac{(Z_r Ru_p)\,C_p - (Z_r Ru)_m\,C_m}{\Delta Z}$$
$$(Z_r Ru)_p = \frac{1}{8}\left[(Z_r)_{i,k} + (Z_r)_{i+1,k}\right](R_k + R_{k+1})\,(U_{i+1,k} + U_{i+1,k+1}) \qquad (104)$$

where

$$(Z_r Ru)_m = \frac{1}{8}\left[(Z_r)_{i,k} + (Z_r)_{i-1,k}\right](R_k + R_{k+1})\,(U_{i,k} + U_{i,k+1})\ ,$$

and

$$C_p = C_{i,k}\ \text{for}\ (Z_r Ru)_p \geqslant 0$$

$$C_p = C_{i+1,k}\ \text{for}\ (Z_r Ru)_p < 0$$

$$C_m = C_{i-1,k}\ \text{for}\ (Z_r Ru)_m > 0$$

$$C_m = C_{i,k}\ \text{for}\ (Z_r Ru)_m \leqslant 0\ .$$

$Z_r\ (i,k)$ and $Z_z(k)$ in the following expression are evaluated at the points (o).

Term 3

$$RZ_z \frac{\partial(wC)}{\partial z} = \frac{1}{2}(R_k + R_{k+1})\,(Z_z)_k \left[\frac{w_p C_p - w_m C_m}{\Delta Z}\right] \tag{105}$$

where

$$w_p = \frac{1}{2}(w_{i+1\,k} + w_{i+1,\,k+1})$$

$$w_m = \frac{1}{2}(w_{i,\,k} + w_{i,\,k+1}) \quad ,$$

and

$$C_p = C_{i,\,k} \text{ for } w_p > 0$$
$$C_p = C_{i+1,\,k} \text{ for } w_p < 0$$

$$C_m = C_{i-1,\,k} \text{ for } w_m > 0$$
$$C_m = C_{i,\,k} \text{ for } w_m < 0$$

The diffusion terms, 4 through 8, all span two increments in ΔR or ΔZ as written in the expressions to follow. However, when the points (0) are adjacent to the channel boundaries, only single spans in ΔR or ΔZ may be possible, in which case one-sided differences are used.

Term 4

$$\frac{\partial}{\partial R}\left(R\frac{\partial C}{\partial R}\right)$$
$$= \left[R_{k+1}\,(C_{i,\,k+1} - C_{i,\,k})\,/\Delta R - R_k\,(C_{i,k} - C_{i,k-1})\,/\Delta R\right]/\Delta R \tag{106}$$

Term 5

$$\frac{\partial}{\partial R}\left(RZ_r\frac{\partial C}{\partial Z}\right)$$
$$= \Big[(R_{k+1} + \tfrac{1}{2}\Delta R)\,(Z_r)_{i;k+1}\,(C_{i+1,\,k+1} - C_{i-1,\,k+1})\,/\,2\Delta z - (R_{k-1} + \tfrac{1}{2}\Delta R)\,(Z_r)_{i,\,k-1}\,(C_{i+1,\,k-1} - C_{i-1,\,k-1})\,/2\Delta Z\Big]/2\Delta R \tag{107}$$

Term 6

$$Z_r R\frac{\partial^2 C}{\partial Z\partial R} = \frac{1}{2}(Z_r)_{i,\,k}(R_k + R_{k+1})\,/\,2\Delta Z \Big[(C_{i+1,\,k+1} - C_{i-1,\,k+1})\,/2\Delta Z - (C_{i+1,\,k-1} - C_{i-1,\,k-1})\,/2\Delta Z\Big]/2\Delta R \tag{108}$$

Term 7

By substitution for Z_r,

$$Z_r R\frac{\partial}{\partial Z}\left[Z_r\frac{\partial C}{\partial Z}\right] = \frac{RZh_b^2}{h^2(r)}\frac{\partial}{\partial Z}\left[Z\frac{\partial C}{\partial Z}\right] \tag{109}$$

$$= \frac{(R_k + R_{k+1})\,(Z_i + Z_{i+1})h_b^2}{(h(R_k) + h\,(R_{k+1}))^2}\Big[Z_{i+1}(C_{i+1,k} - C_{i,k})\,/\Delta Z - Z_i\,(C_{i,k} - C_{i-1,k})\,/\,\Delta Z\Big]\,/\Delta Z \tag{110}$$

Term 8

Again, by substituting for Zz,

$$RZ_z\frac{\partial}{\partial Z}\left(Z_z\frac{\partial C}{\partial Z}\right) = \frac{R}{h^2(R)}\frac{\partial^2 C}{\partial Z^2}$$

$$= \frac{2(R_k + R_{k+1})}{(h(R_k) + h(R_{k+1}))^2}\left[\frac{C_{i+1,k} - C_{i,k}}{\Delta Z} - \frac{C_{i,k} - C_{i-1,k}}{\Delta z}\right]/\Delta z. \tag{111}$$

Finally, when integrating $C(R,\Theta,Z)$ ahead in Θ by use of equations (91) and (92), the velocity term, ν, is evaluated as the average of the four points surrounding each concentration mesh point.

Particle Flux Calculations

The particle flux crossing the $\Theta = 0$ plane is the integral of the product of concentration and longitudinal velocity over the cross section:

$$CQ_o = \int_{r_1}^{r_2} \int_{o}^{h(r)} v(r,\theta=o,z)\, dz\, dr$$

$$C(r,\theta = o,\zeta)\, dz\, dr \qquad (112)$$

The flux over the weir is a function of the radial velocity and concentration at that point. The flux between angles Θ_1 and Θ_2 is:

$$(CQ_w)_\theta \int_{\theta_o}^{\theta} \int_{B1+Zo}^{B1+B2+Zo} u(r_2,\theta,z)\, C(r_2,\theta,z) r_2\, dz\, d\theta .$$

Then, the total flux over the weir is:

$$(CQ_w)_{total} = (CQ_w)_{\theta=\theta_m} \qquad (114)$$

The removal efficiency is, then, the ratio of the material which did not pass over the weir to the input flux.

$$E = \frac{CQ_o - (CQ_w)_{total}}{CQ_o} \qquad (115)$$

Particle Flow Summary

The particle flow solution is treated as an initial value problem, starting with interpolated experimental data in the $\Theta = 0$ plane. After each $\Delta\Theta$ increment where velocity components u, v, and w are calculated, the concentration is calculated at points on a (r,z) plane grid. Equation (88) is the basic relation describing the concentration field. It is solved numerically in conservation form for the product (vC) at each angle θ; then, by dividing by v, the concentration C results. Equations (90) to (92) describe this process. In order to account for the non-rectangular channel cross section, a transformed equation for $\partial (vC)/\partial\theta$ is given in Equation (98).

The numerical solution method is a conservative upwind differencing scheme.

The numerical calculation of the individual terms of Equation (98) is described in Equations (103) to (111).

Finally, the particle flux calculations needed to determine efficiency are presented in Equations (112) to (115) Figure 80, Particle Flow Solution Summary, shows the overall flow and concentration calculation procedure. Figure 78 portrays details of the flow calculation.

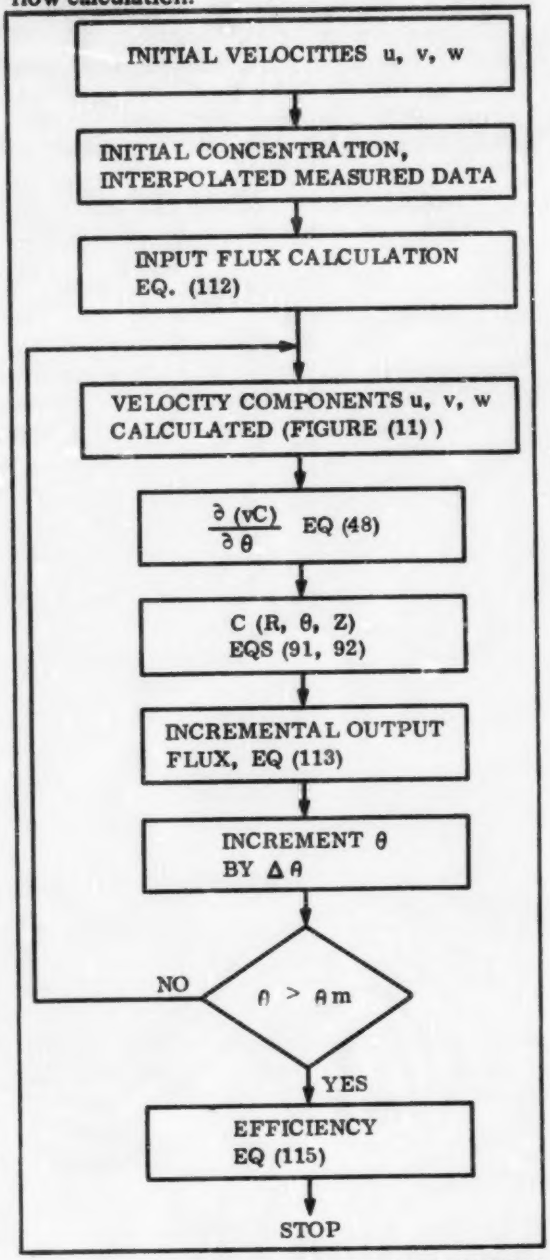
INITIAL VELOCITIES u, v, w
INITIAL CONCENTRATION, INTERPOLATED MEASURED DATA
INPUT FLUX CALCULATION EQ. (112)
VELOCITY COMPONENTS u, v, w CALCULATED (FIGURE (11))
∂ (vC) / ∂ θ EQ (48)
C (R, θ, Z) EQS (91, 92)
INCREMENTAL OUTPUT FLUX, EQ (113)
INCREMENT θ BY Δ θ
NO
θ > θm
YES
EFFICIENCY EQ (115)
STOP

FIGURE 80 PARTICLE FLOW SOLUTION SUMMARY

]

Approximate Solution for One-Dimensional Flow

In a uniform, wide rectangular channel, the suspended sediment tends to stratify, with a higher concentration occurring near the bottom, and lower concentration at the surface. The degree of stratification is influenced by the particle settling velocity and the turbulence in the channel. The classic analysis of bed-load stratification was published by Dobbins[6] in 1944. Dobbins studied a simplified version of Equation (88) in Cartesian coordinates in which the longitudinal velocity, v, was assumed to be constant, and u and w for the liquid were taken as zero. As in the present study, the longitudinal diffusion was neglected in comparison to vertical diffusion, and the particle velocity was approximated by superimposing the settling velocity, w_s, on the liquid flow. In the rectangular coordinate system shown in Figure 74 the simplified equation becomes:

$$\frac{\partial C}{\partial t} = \dot{V}\frac{\partial C}{\partial X} = \epsilon\frac{\partial^2 C}{\partial y^2} + w_s\frac{\partial C}{\partial y} \tag{116}$$

Because the longitudinal velocity, $\bar{V}$, is assumed constant, Equation (116) can be considered as a time-dependent problem in which the time, t, is the liquid flow time

$$t = \frac{x}{\bar{V}} \tag{117}$$

Dobbins obtained analytic solutions to Equation (116) for the boundary condition of no particle flux through the open surface at $y = h$. Expressed mathematically, this boundary condition is

$$\left(\frac{\partial C}{\partial y}\right)_{y=h} = \left(\frac{-w_s}{\epsilon}C\right)_{y=h}, \tag{118}$$

in analogy with Equation (102). At the channel bottom, Dobbins considered the boundary condition:

$$\left(\frac{\partial C}{\partial y}\right)_{y=o} = \frac{-w_s}{\epsilon}\ A, \tag{119}$$

in which A is an arbitrary constant representing the asymptotic bottom concentration at $t \to \infty$. For $A = 0$, the asymptotic concentration is zero, indicating that all of the material has settled out of suspension. The initial concentration distribution was assumed to be of the exponential form:

$$C(y,o) = C_o e^{-by}\ . \tag{120}$$

For the special case $B = 0$, Equation (120) corresponds to an initially uniform concentration. For this problem, Dobbins obtained the analytical solution:

$$C(y,t) = Ae^{\frac{-w_s y}{\epsilon}} + e^{\frac{-w_s y}{2\epsilon}} \sum_{n=1}^{\infty} C_n e^{-\left(\alpha_n^2 \epsilon + \frac{w_s^2}{4\epsilon}\right)t} \left[\cos\alpha_n y + \frac{w_s}{2\epsilon\alpha_n}\sin\alpha_n y\right], \tag{121}$$

where the constants, C_n, are evaluated from

$$C_n = \frac{2\alpha_n^2}{\left(\alpha_n^2 + \frac{w_s^2}{4\epsilon^2}\right)h + \frac{w_s}{\epsilon}} \left\{\frac{C_o\left[B + \left(\frac{w_s}{\epsilon} - B\right) e\left(\frac{w_s}{\epsilon} - B\right)h\ H_n\right]}{\left(\frac{w_s}{2\epsilon} - B\right)^2 + \alpha_n^2} - \frac{A\frac{w_s}{\epsilon}}{\left(\alpha_n^2 + \frac{w_s^2}{4\epsilon^2}\right)}\right\} \tag{122}$$

in which

$$H_n = \cos\alpha_n h + \frac{w_s}{2\epsilon\,\alpha_n}\sin\alpha_n h\ . \tag{123}$$

The values of α_n are obtained as the solution to the transcendental equation:

$$2\cot\alpha_n h = \frac{h\alpha_n}{\left(\frac{w_s h}{2\epsilon}\right)} - \frac{\left(\frac{w_s h}{2\epsilon}\right)}{\alpha_n h} \tag{124}$$

For the boundary conditions studied by Dobbins, it is necessary to specify the asymptotic bottom concentration, A. In practice, unless complete clearing of the flow is anticipated (so that $A = 0$), it is difficult to know what an appropriate value for A might be. Consequently, Dobbins' solution was rederived for the bottom boundary condition of zero mass flux through the bottom, or:

$$\left.\frac{\partial C}{\partial y}\right|_{y=0} = \left[-\frac{w_s}{\epsilon} C\right]_{y=0} \qquad (125)$$

in analogy with Equation (102). This boundary condition corresponds to that used in the numerical model, and assumes that the entire bedload remains in suspension. Under this condition, it can be shown that the solution to Equation (116) is:

$$C(y,t) = Ae^{\frac{-w_s y}{\epsilon}} + e^{\frac{-w_s y}{2\epsilon}} \sum_{n=1}^{\infty} C_n e^{-\left(\alpha_n^2 + \frac{w_s^2}{4\epsilon^2}\right)\epsilon t} \left[\cos \alpha_n y - \frac{w_s}{2\epsilon\alpha_n} \sin \alpha_n y\right], \qquad (126)$$

where

$$A = \frac{c_o\, w_s}{\epsilon B} \frac{\left(1 - e^{-Bh}\right)}{\left(1 - e^{-\frac{w_s h}{\epsilon}}\right)} \qquad (127)$$

$$\alpha_n = \frac{n\pi}{h} \qquad (128)$$

and

$$C_n = \frac{2C_o\left(\frac{w_s}{\epsilon} - B\right)\left(\frac{1}{h}\right)\left[(-1)^n e^{\left(\frac{w_s}{2\epsilon} - B\right)} - 1\right]}{\left[1 + \left(\frac{w_s}{2\epsilon\alpha_n}\right)^2\right]\left[\left(\frac{w_s}{2\epsilon} - B\right)^2 + \alpha_n^2\right]} \qquad (129)$$

This new solution is closely analogous, but somewhat simpler than that of Dobbins. Furthermore, the value of the previously unknown constant A, is now determined from the requirement that the longitudinal mass flux remain unchanged – i.e., all bed load remains in suspension. Although these solutions correspond to much simpler geometry than the helical flow separator, several useful insights into the more complicated problem can be obtained from a study of their analytical form. For example, in both Equations (122) and (126), the asymptotic vertical concentration distribution is shown to be a negative exponential:

$$C(y,\ t\to\infty) = A\ exp\ (-\, w_s\, y/\epsilon), \qquad (130)$$

which depends on the scale height "a" defined by

$$a = \epsilon/w_s. \qquad (131)$$

Thus, sediments with large settling velocities, w_s, will have small scale heights, corresponding to a very rapid decay in concentration with distance above the bottom. Furthermore, for a given settling velocity, the scale height is directly proportional to the eddy viscosity due to turbulence, ϵ. Thus, as the turbulence level is increased, the vertical concentration distribution tends to become more uniform, with less stratification. In the discussion by Camp(7) of Dobbins' paper, the eddy viscosity was evaluated as the vertical averaged value corresponding to the universal logarithmic velocity distribution as discussed in Equation (43). The resulting expression for ϵ is:

$$\epsilon = \frac{k}{6}\, h\, \bar{v} \sqrt{\frac{f}{8}}. \qquad (132)$$

where h is the channel depth, V is the average velocity, and f is the Darcy friction factor.

This useful result has been retained in the present analysis. The eddy viscosity increases directly with the average velocity. Since the recovery efficiency of the helical flow separator depends on the degree of bedload stratification, Equations (130) and (132) indicate the desirability of reducing the average velocity as much as possible by using a large channel cross section.

It was originally thought that the asymptotic vertical concentration distribution given by Equation (130) could be used directly to model the initial distribution at the entrance to the bend, by appropriate correlation of the scale height, "a". However, as noted, the laboratory results showed significant lateral variations which could not be accounted for with this approach. Additional useful insights can be obtained by studying the relationship between time and distance given by Equation (117). For a channel with a side weir, the average longitudinal velocity decreases in the downstream direction, due to loss of fluid over the weir. For uniform lateral discharge, the average velocity is given by:

$$\bar{V} = \frac{dx}{dt} = \frac{Q_o - Q_w \quad (x/L)}{A} \qquad (133)$$

in which Q_o is the flow rate at the start of the side weir, Q_w is the total flow over a weir of length L, and A is the cross-sectional area of the channel. Equation (133) can be integrated to give the following relation between distance and time:

$$t = \frac{-LA}{Q_w} \; ln \left[\frac{Q_o - Q_w \, (x/L)}{Q_o}\right]. \qquad (134)$$

Since the degree of stratification (and hence separator performance) which can develop within the separator depends on time (as shown in Equation 121 or 126), Equation (134) indicates that better performance can be achieved with longer retention times, τ, defined in the conventional manner:

$$\tau = \frac{vol}{Q} = \frac{LA}{Q_w}. \qquad (135)$$

By combining this result with the analytical form appearing in Equations (121) and (126), it can be concluded that a significant non-dimensional parameter, ϕ, affecting the separator performance is:

$$\phi = \frac{w_s^2 \tau}{\epsilon} \qquad (136)$$

where w_s is the settling velocity, τ is the retention time defined by Equation (135), and ϵ is the eddy viscosity. To increase separator efficiency, ϕ should be made as large as possible, which implies large retention times, τ, and small longitudinal velocities, to reduce ϵ. Furthermore, since the concentration decays exponentially with distance from the bottom, and the clear flow is withdrawn from the surface, it appears desirable to achieve a given retention time with a narrow, deep section, as opposed to a shallow, wide one. This conclusion strictly applies only to a straight channel. In the proposed curved channel, the induced secondary flows act to reduce the concentration of particulates in the overflow. The development of these secondary flows would be suppressed with a deep, narrow channel section.

Scaling of the Liquid Flow

The development of the secondary flow in the bend depends primarily on the distribution of the approach velocity at the entrance of the bend. If it can be shown that the non-dimensionalized inlet velocity profile is the same in both the model and the prototype, then maintaining the same Froude number,

$$F = \frac{V^2}{Lg}, \qquad (137)$$

in the model and the prototype will ensure that the flow patterns will be the same throughout the bend.

It was shown that the entrance velocities for the non-rectangular cross section can be represented by:

$$\frac{v}{V} = 1 + \left(\frac{C}{V}\right) \left\{ ln \left(\frac{x}{a} \cdot \frac{(a-x)}{a} \cdot \frac{y}{h_1}\right) + 1/2 + \left(\frac{4h_1 + 2h_2}{h_1 + h_2}\right) + \frac{h_2^2}{h_1^2 - h_2^2} \; ln \left(\frac{h_2}{h_1}\right) \right\}, \qquad (138)$$

where "a" is the width of the separator, h_1 and h_2 are the depths at the inner and outer walls, and Y is the distance from the bottom. This formula applies to both the prototype and the model and, since all terms inside the brackets are non-dimensional, each of these terms will be identical if the model and prototype are geometrically similar. Consequently, the same non-dimensional values of velocity (v/V) will result for both model and prototype if the term C/V is the same for model and prototype.

The constant C is given by:

$$C = 1/k \;\; V_f, \qquad (139)$$

where k is von Karman's constant, and V_f is the friction velocity

$$V_f = \sqrt{f/8}\ \bar{V}, \tag{140}$$

and where f is the Darcy friction factor. Therefore, the ratio of $C/\bar{V}$ will be the same in model and prototype if:

$$(\sqrt{f}\,)_m = (\sqrt{f}\,)_p. \tag{141}$$

The friction factor, f, can be determined from the Manning Equation:

$$f = \frac{0.453\, g\, n^2}{H^{1/3}}, \tag{142}$$

in which g is the acceleration of gravity (ft^2/sec) n is the Manning coefficient (sec ft$^{-1/3}$) and H is the hydraulic radius. Typical values of n are 0.009 for the model and 0.012 for the concrete prototype. Thus the ratio of friction factors is:

$$\frac{f_m}{f_p} = \left(\frac{n_m}{n_p}\right)^2 \left(\frac{H_p}{H_m}\right)^{1/3} \tag{143}$$

For a length scale of 1:6:

$$\frac{f_m}{f_p} = \left(\frac{0.009}{0.012}\right)^2 (6)^{1/3} = 1.025,$$

and so the ratio of C/V in model and prototype will be:

$$\frac{(C/\bar{V})_m}{(C/\bar{V})_p} = \sqrt{\frac{f_m}{f_p}} = 1.013,$$

which is very close to unity.

It can, thus, be seen that the lower model velocities are offset by its smoother surface, so that to a very close approximation the non-dimensional entrance velocities, $v/\bar{V}$ will be the same as for the prototype.

The entire flow in the bend will then be reproduced by maintaining the Froude number constant between model and prototype. Thus, if the prototype dimensions are S times larger than the model, the following relationship follow from Equation (137):

$$L_p = S\, L_m \tag{144}$$

$$V_p = \sqrt{\frac{L_p}{L_m}}\ V_m = \sqrt{S}\ V_m \tag{145}$$

$$Q_p = \frac{L_p^2\, V_p}{L_m^2\, V_m}\ Q_m = S^{5/2}\, Q_m \tag{146}$$

Scaling of the Particle Flow

Equation (89) for the particle concentration field applies to both the model and the prototype. If the equation is non-dimensionalized by dividing the concentration by the inlet concentration, C_o, dividing all lengths by the width of the channel, "a", and dividing all velocities by the average entrance velocity, $\bar{V}$, there results:

$$\frac{1}{\tilde{r}}\frac{\partial}{\partial \tilde{r}}(\tilde{r}\,\tilde{u}\,\tilde{c}) + \frac{1}{\tilde{r}}\frac{\partial}{\partial \theta}(\tilde{v}\,\tilde{c}) + \frac{\partial}{\partial z}(\tilde{w}_p\,\tilde{c})$$
$$= \left(\frac{\epsilon \bar{V}}{a^2}\right)\left[\frac{1}{\tilde{r}}\frac{\partial}{\partial \tilde{r}}\left(\tilde{r}\frac{\partial \tilde{c}}{\partial r}\right) + \frac{1}{\tilde{r}^2}\frac{\partial^2 \tilde{c}}{\partial \theta^2} + \frac{\partial^2 \tilde{c}}{\partial \tilde{z}^2}\right], \tag{147}$$

in which the tilde ($\tilde{}$) denotes a non-dimensional variable. This equation will be identical for the model and the prototype if the non-dimensional eddy diffusivities are the same:

$$\left(\frac{\epsilon \bar{V}}{a^2}\right)_m = \left(\frac{\epsilon \bar{V}}{a^2}\right)_p \tag{148}$$

The equation used to represent the eddy diffusivity is Equation (132):

$$\epsilon = \frac{k}{6}\ \bar{h}\ \bar{V}\ \sqrt{f/8},$$

where $\bar{h}$ is the mean depth. Equation (148), then, requires that:

$$\left(\frac{k}{6}\ \frac{\bar{h}\ \bar{V}^2}{a^2}\ \sqrt{f/8}\right)_m$$
$$= \left(\frac{k}{6}\ \frac{\bar{h}\ \bar{V}^2}{a^2}\ \sqrt{\frac{f}{8}}\right)_p \tag{149}$$

As was shown previously, $f_m \cong f_p$, and since the velocities and dimensions are related by Froude number scaling (Equations 144-146),

$$\bar{h}_p = s\, \bar{h}_m$$
$$a^2{}_p = s^2\, a^2{}_m$$
$$\bar{V}^2{}_p = s\, \bar{V}^2{}_m,$$

so that the equality in Equation (149) is preserved.

As a consequence, Froude number scale relationships between the model and prototype will ensure duplication of the non-dimensional concentration fields and, therefore, the recovery efficiency. The Froude scale relationship, $V_p = \sqrt{S}\ V_m$, applies to all velocities, including the particle settling velocity. Thus, to represent a given class of prototype particles in the laboratory model, the laboratory material must have a settling velocity of $S^{-1/2}$ times the prototype value, where S is the length scale.

Comparison of Mathematical Model Results with Test Data

Figures 81-83, Comparison of Measured and Predicted Velocity Profiles at 0°, 20°, and 40° respectively, show comparisons of calculated and measured longitudinal, *(v)*, velocities in cross sections at the indicated angular positions. The test data were obtained by LaSalle Hydraulic Laboratory in a companion study, as part of this project. The velocities shown are in ft/sec, prototype scale.

In Figure 81, the calculated velocity contours are in good agreement with the laboratory data. The predicted velocities at this position were calculated from Equation (52) applied to the prototype, for 0.85 m^3/sec (30 cfs) inlet flow, with a Manning coefficient n = 0.012 in Equation (45). As was shown, the non-dimensional velocity profile, (v/V), will be very nearly identical for both the model and the prototype, hence all calculation has been performed at prototype scale.

Figure 82 shows significant shifts in the longitudinal velocity at the 20° position. Due to the secondary fluid motion, low energy boundary layer fluid from the bottom is swept up to the surface at the inner radius of the bend, resulting in a low velocity region there. This is clearly seen in the laboratory data, but is not reproduced in the computer simulation. This deficiency in the computational technique was also noted in the results of Fox and Ball,[4] and is a result of incorrectly modeling the convective acceleration term $w\partial v/\partial z$ in Equation (34). In the work of Fox and Ball this term was neglected altogether. In the present model, the ratio of w and u was assumed to be of the form given Equation (34), which is correct along the bottom and the surface, but does not properly account for the upflow which occurs at the inner radius of the bend. An attempt was made to resolve the discrepancy by retaining all of the terms shown in Equation (31). However, with the additional terms, the computational technique became unstable.

In Figure 83, the laboratory data shows a separated (reverse) flow region near the inner bend. This is evidenced by the zero velocities in Figure 83(a). Dye studies reveal very small negative velocities in this region. The reverse flow region is the consequence of the low energy fluid being more rapidly decelerated than the faster moving fluid. The original technique used for calculating the longitudinal surface slope did result in the appearance of a reverse flow region in the computer simulation. However, the predicted reverse flow occurred further downstream because the calculated longitudinal velocities near the inner bend were greater than in the model, due to the $w\partial v/\partial \zeta$ term discussed above, and thus, took longer to decelerate.

In any event, the reverse flow region is incompatible with the initial value problem formulation and had to be eliminated in order to proceed. The resulting discrepancies in the longitudinal velocity field are not particularly important in computing the concentraion field. The differences in the longitudinal velocity do result in further errors in the cross-flow velocities u and w, which are potentially more critical. However, the principal effect of the reverse flow region is to raise the longitudinal velocity near the outer radius of the bend and to cause an eddy to appear just upstream of the baffle at 60°. This eddy causes a sudden uplift in the material discharged over the weir near the end of the bend, but the effect is very local.

Figure 84, Comparisons of Measured and Predicted Flow Angles on Bottom Along Channel Centerline, shows a comparison of the measured and predicted flow angles along the bottom centerline of the bed, with and without flow over the weir. To obtain the

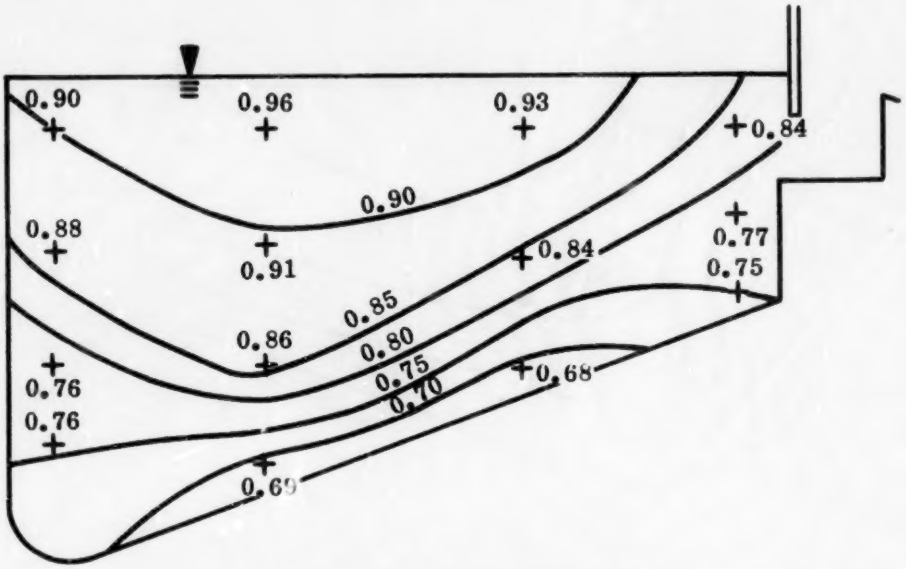

(a) Measured Velocities

NOTE: Velocities are relative

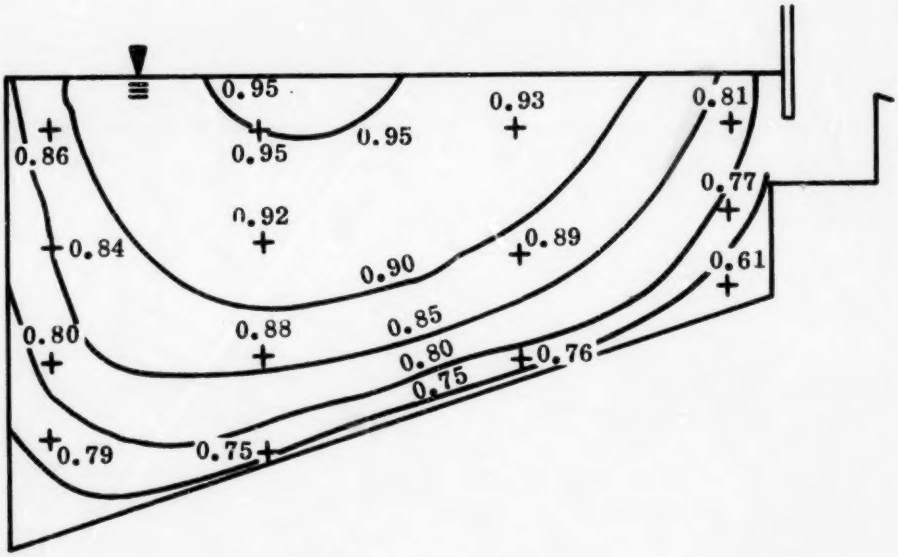

(b) Predicted Velocities

FIGURE 81 COMPARISON OF MEASURED AND PREDICTED VELOCITY PROFILES AT 0°

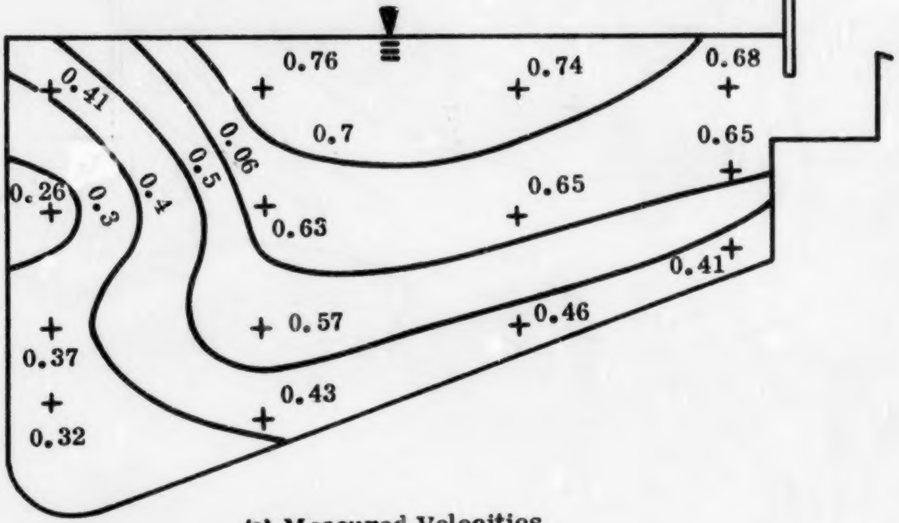

(a) Measured Velocities

NOTE: Velocities are relative

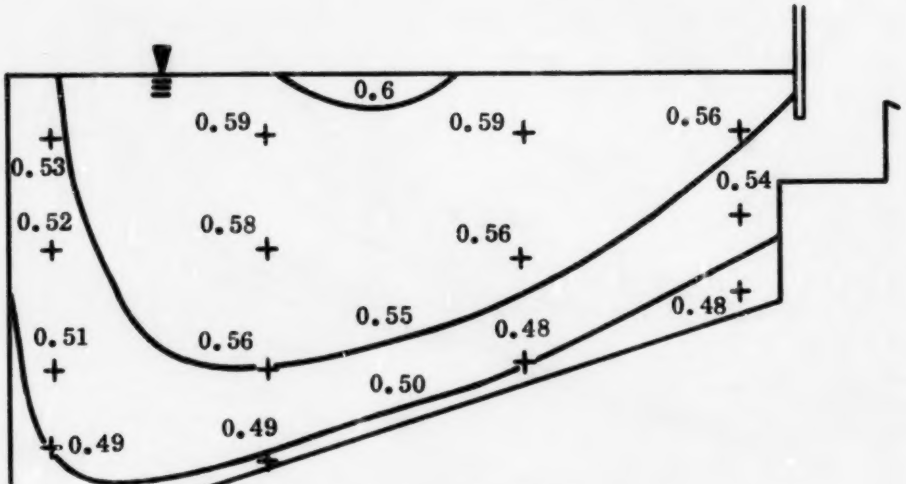

(b) Predicted Velocities

FIGURE 82 COMPARISON OF MEASURED AND PREDICTED VELOCITY PROFILES AT 20°

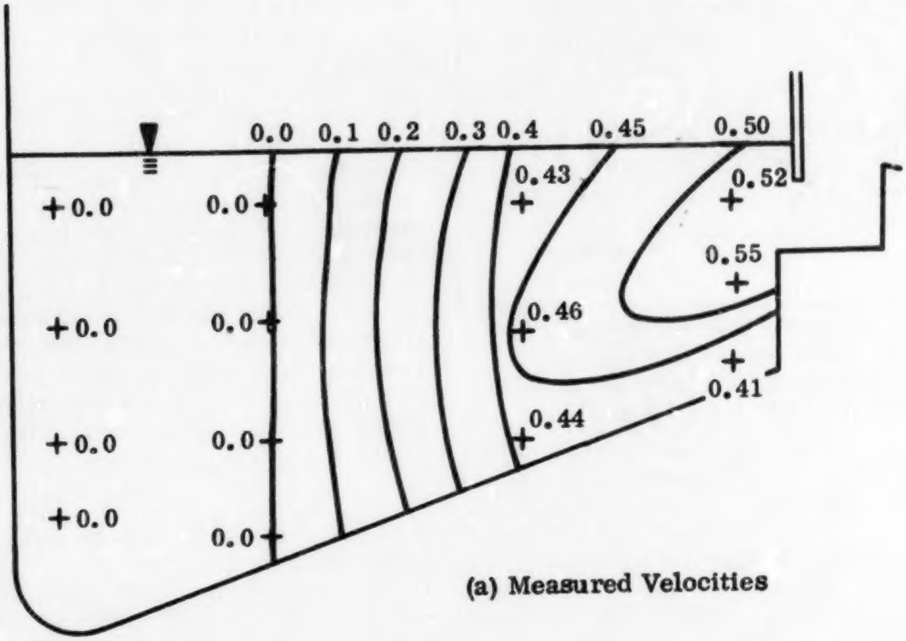

(a) Measured Velocities

NOTE: Velocities are relative

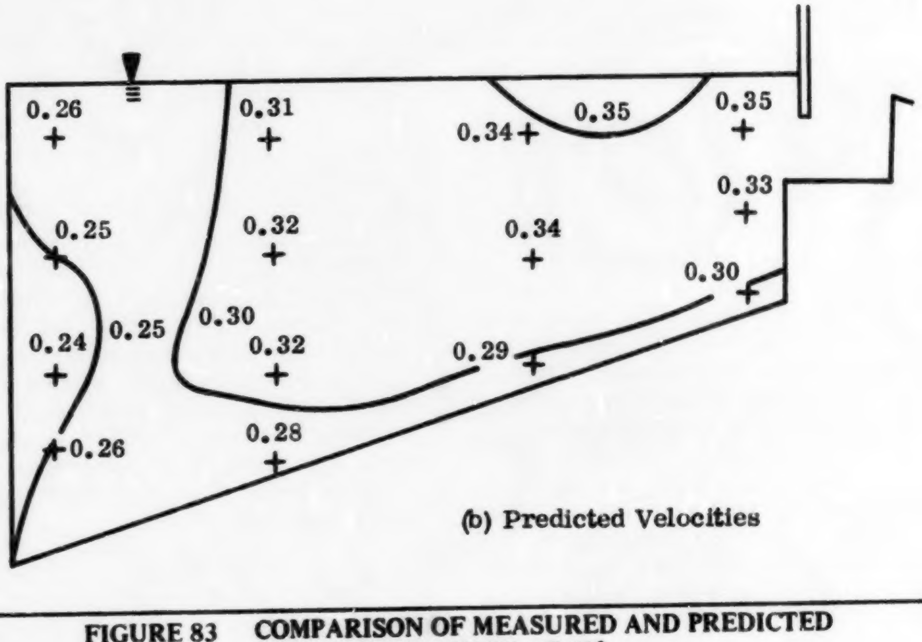

(b) Predicted Velocities

FIGURE 83 COMPARISON OF MEASURED AND PREDICTED VELOCITY PROFILES AT 40°

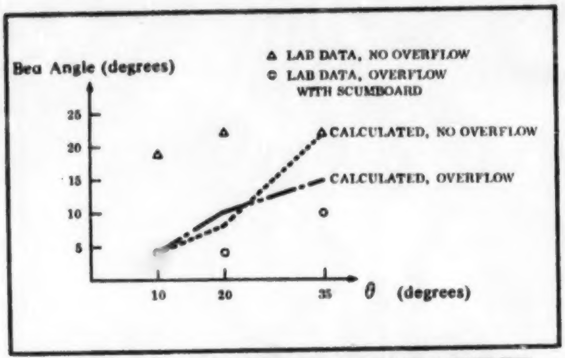

FIGURE 84 COMPARISON OF MEASURED AND PREDICTED FLOW ANGLES ON BOTTOM ALONG CHANNEL CENTERLINE

laboratory results with no overflow, the partition at 60° was removed so the flow proceeded uninterrrupted for a full 120°. With no overflow, the laboratory data indicate a bed flow angle near 22° along most of the bed, with 18° bed flow angle at the 10° position. This implies a very rapid initial growth in the bed flow angle. In contrast, the computer simulation indicates a continuous growth in bed flow angle, reaching 22° only at the 35° position. In this respect the present results are in agreement with those of Fox and Ball.[4] They showed a similar steady growth in bed angle in substantial agreement with their test data, although their work was for a flat bed.

The measurement of the bed flow angles is performed by using Process Black ink, placed along a radius at a given angular position. The fluid shear along the bottom causes threads of ink to extend downstream from the inked line, and the angle of these threads with respect to the ⊖ direction are measured with a protractor. The technique is accurate only to (±3°), but the differences in in the no overflow results shown in Figure 84 are too large to be explained as measurement inaccuracies. The very rapid initial growth in bed angle in the laboratory model is puzzling. There is no obvious reason why the laboratory and mathematical models should not be in better agreement in this respect.

The results for the bed angle in the presence of overflow are in much better agreement. For this case, the laboratory results indicate a slowly growing bed angle. The computer simulation matches the laboratory results at the 10° position and then somewhat overpredicts the growth in bed angle. However, the differences are less than 5°. Both the laboratory model and the computer simulation indicate substantially smaller bed flow angles in the presence of the discharge over the weir. This indicates that the helical secondary flow is largely destroyed by the weir and scum board. The reason for this is that the side weir at the outer bend effectively controls the water level there and prevents the development of a large radial surface slope. The smaller radial surface slope produces a smaller helical motion with smaller bed flow angles, as observed.

Comparison of Calculated Concentration Field with Laboratory Data

It was originally anticipated that the simple straight channel theory could be applied to the inlet transition section to obtain the initial concentration field at the 0° position. However, the laboratory data revealed significant lateral variations in concentration which could not be adequately accounted for with the simplified theory. Consequently, the initial conditions for the mathematical model were obtained by interpolating the measured concentration data at the 0° position, shown in Figure 85, Measured Values of Relative Petrothene Concentration at 0°. The measured concentrations are only applicable for shredded Petrothene at the nominal design discharge of 0.85 m³/sec, (30 cfs). At higher flow rates or lower settling velocities, the concentration distribution will be more uniform in the vertical direction. Conversely, at lower flows and higher settling rates, the bed load will be more stratified. To account for these differences, a correction was applied to the laboratory data, based on the theory.

The steady state vertical concentration distribution is of the form:

$$\frac{C}{C_0} = e^{\frac{-(w_s y)}{\epsilon}}, \qquad (150)$$

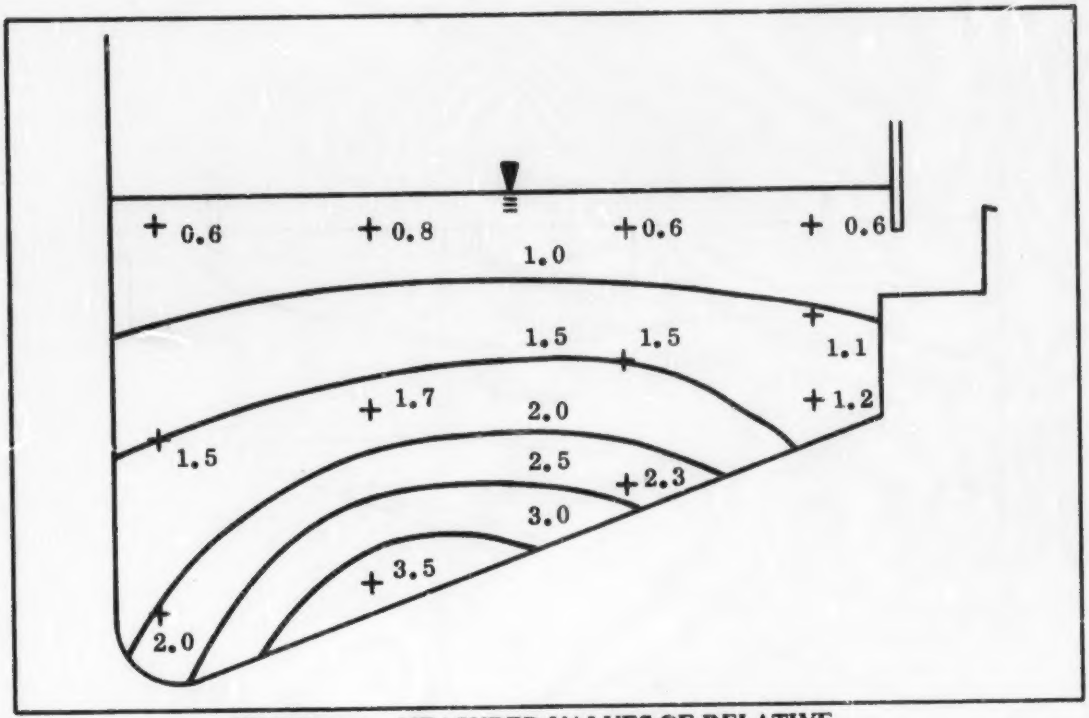

FIGURE 85 MEASURED VALUES OF RELATIVE PETROTHENE CONCENTRATION AT 0°

where y is the distance above the channel bottom, w_s is the settling velocity, and ϵ is the eddy diffusivity. Consequently, at flow rates or eddy viscosities, and settling velocities other than the nominal ones applying to the laboratory measurements (ws_o, and ϵ_o), the initial concentration data were taken as:

$$C(r,z) = C_0\,(r,z)\; e^{-\left[\frac{w_s}{\epsilon} - \frac{w_{s_o}}{\epsilon}\right] \bar{h}\,(1 - z/h_{(r)})} \quad , \qquad (151)$$

where $C_0\,(r,z)$ is the measured concentration field and h is the average depth. It is readily apparent that if $w_s/\epsilon = s_o/\epsilon_o$, no alteration results, whereas for a larger settling velocity or smaller flow rate, the concentration near the surface, $z = 0$, will be reduced, giving a more stratified distribution. Conversely, at lower settling velocities or higher flow rates, the concentrations near the surface are increased, giving a more uniform distribution.

Figures 86 and 87, Comparison of Measured Values of Relative Petrothene Concentration at 20° and at 40°, show the measured and predicted concentration fields for the nominal case of shredded Petrothene (prototype settling velocity of 1.22 cm/sec (0.04 ft/sec) at the design discharge of 0.85m^3/sec, (30 cfs). Figure 86 shows the comparison at the 20° position. The measured and predicted results are similar, having essentially horizontal isopleths, but the calculated results indicate a more highly stratified bed load. The very high predicted concentrations along the floor of the unit are the result of assuming that the entire bed load remains in suspension, where the laboratory measurements do not reflect the sediment on the bottom. These differences can be neglected. However, the calculated results also indicate very low concentration near the surface, whereas the laboratory results show significant amounts of material there. This discrepancy is caused by the large spread in

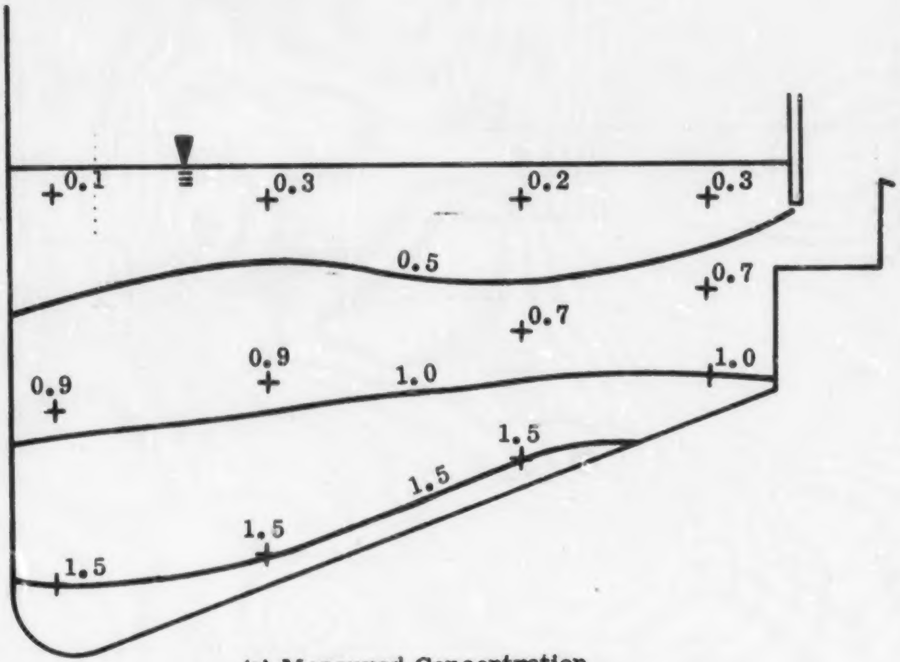

(a) Measured Concentration

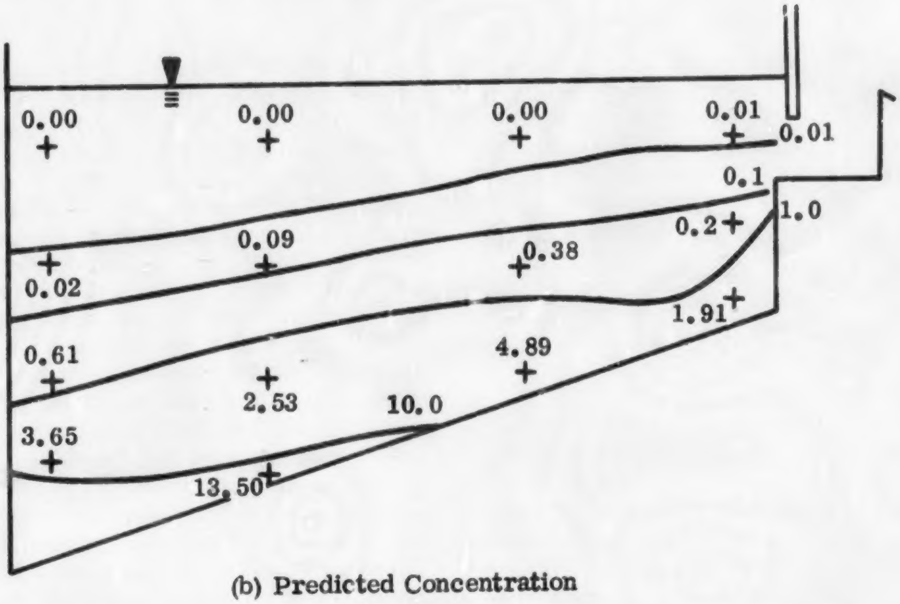

(b) Predicted Concentration

FIGURE 86 COMPARISON OF MEASURED VALUES OF RELATIVE PETROTHENE CONCENTRATION AT 20°

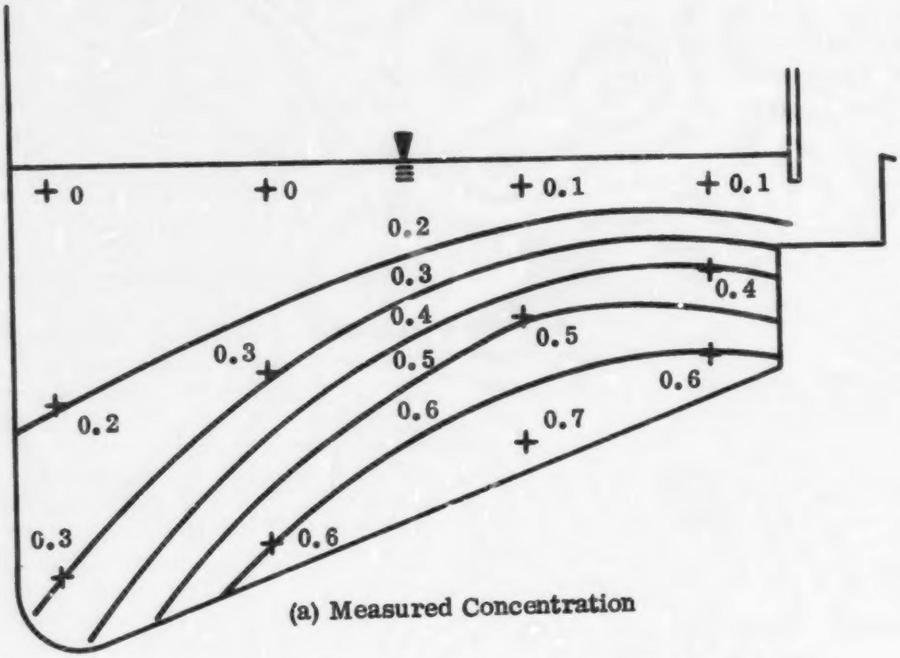

(a) Measured Concentration

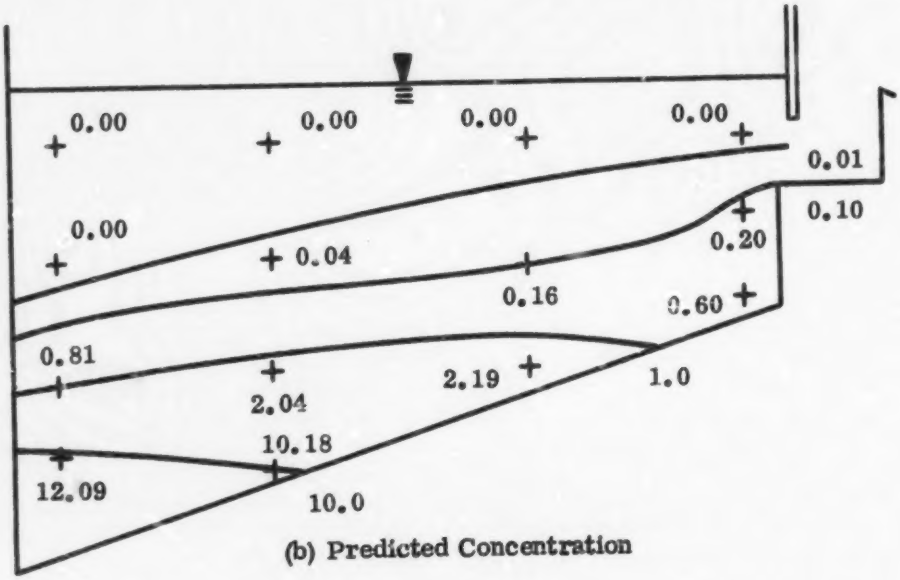

(b) Predicted Concentration

FIGURE 87 COMPARISON OF MEASURED VALUES OF RELATIVE PETROTHENE CONCENTRATION AT 40°

the settling velocities of the Petrothene. The simulation results were obtained for a single settling velocity applicable to the mid-range of the Petrothene size distribution. The laboratory results indicate that a significant fraction of the slower settling particles remains near the surface.

Figure 87 shows a similar comparison at the 40° position. Both the laboratory and the simulation results indicate very little material at the surface, although the laboratory results still indicate a less stratified bed load, due to the distribution of settling velocities. The most important comparison between the laboratory results and the computer simulation is the relative rate at which material is discharged over the weir. Figure 88, Mass Flux Over Weir as a Function of Angular Position, shows the percent of the original particles lost over the weir in each of twenty 3° angular segments. Figure 89, Cumulative Mass Flux over Weir as a Function of Angular Position, shows the cumulative percentage lost over the weir as a function of angular position. The mathematical model was calibrated to give the correct total percentage material lost – 9 percent – for this nominal case by adjusting the eddy diffusivity constant, k, in Equation (132). The selected value was 1.5, compared to a theoretical value of 0.4.

Figure 88 shows that in the laboratory model, the rate of material passing over the weir is initially low, but increases rapidly to a maximum at the 18° angular position. Thereafter, the rate of material loss decreases slowly. The initial transient rise in the laboratory results is not duplicated in the computer simulation, which indicates, instead, a rapid continuous decrease from a maximum at the 0° position. This significant difference in behavior is a consequence of incorrectly modeling the lateral flow over the weir. In the computer simulation, the lateral weir flow is assumed to be fully developed by the 0° position, and is accounted for by the initial distribution of the cross-flow velocities, u and w. As the flow enters the bend, the net lateral discharge, q, at each angular station is unchanged from the initial distribution, as a consequence of assuming $\partial q/\partial \Theta = 0$ in Equation (12). In fact, the laboratory results in Figure 88 indicate that the lateral discharge is not fully developed until near the 19° position.

The development of the lateral discharges is controlled by the weir which reduces the surface level at the outer bend radius, and thereby accelerates the fluid laterally toward the weir. Because of its inertia, a finite time is required for the lateral discharge to fully develop across the cross section, in contrast to the instantaneous flow adjustment assumed in the computer simulation. The reduction in surface elevation at the outer bend also inhibits the initial development of the helical motion.

As a consequence, the bed flow angle initially grows at a lower rate than indicated by the computer simulation, as shown previously in Figure 84. Several attempts were made in the computer studies to resolve these differences in flow behavior by properly simulating the development of the lateral discharge, $q(r,\Theta)$, along the channel. To do this, the lateral surface slope must be computed directly, instead of relying on Equation (38) which is derived on the incorrect assumption that $\partial q/\partial \Theta = 0$. In principle, the lateral surface slope, $\partial \zeta/\partial r$ is given by the ratio of the u and w velocity components at the surface:

$$\frac{\partial \zeta}{\partial r} = -\left(\frac{u}{w}\right)_{z=0} \qquad (152)$$

However, attempts to use this formulation resulted in an unstable calculation. It was concluded that proper calculation of the surface slope is incompatible with the initial value problem formulation. This is to be expected, because in subcritical flow, disturbances can propagate upstream. Such flows are, therefore, not properly posed initial value problems. To calculate the development of the lateral discharge would, therefore, require changing the entire formulation of the problem. In principle, this could be accomplished by using a relaxation technique. However, the fully three-dimensional character of the flow would entail use of a two-component stream function, and impractical increases in computer storage and run time. Instead, the present model formulation was retained, and the eddy

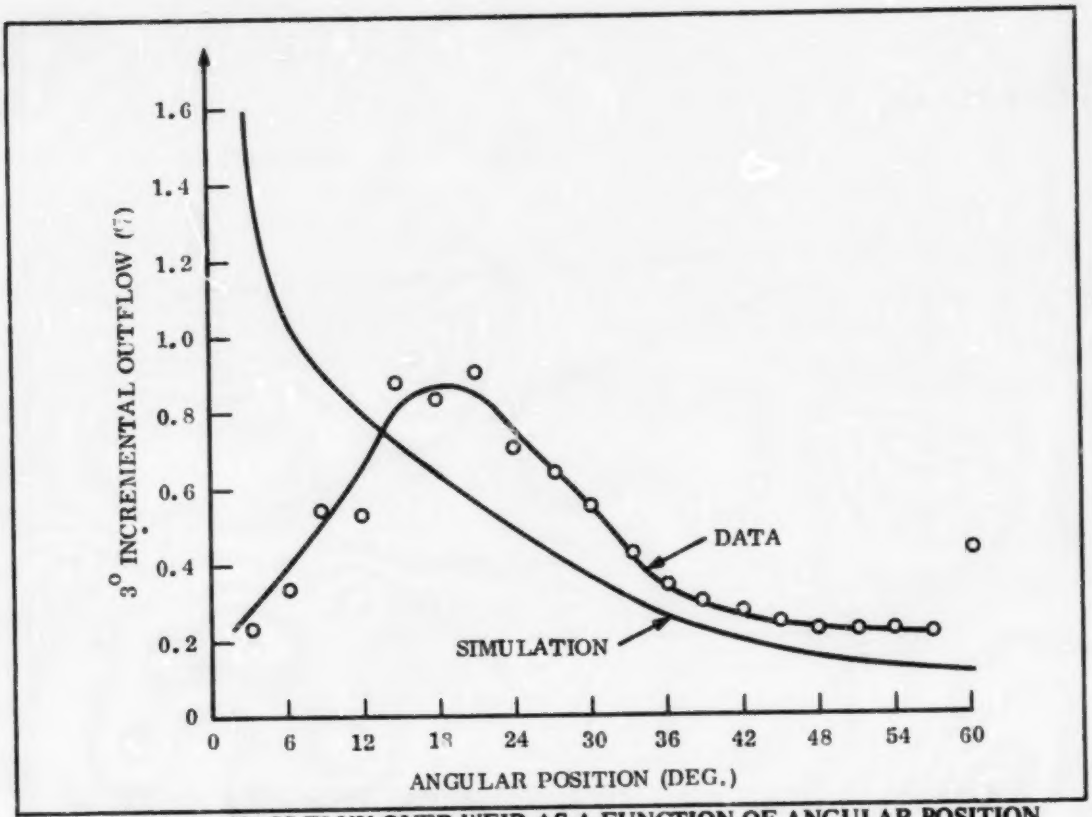

FIGURE 88 MASS FLUX OVER WEIR AS A FUNCTION OF ANGULAR POSITION

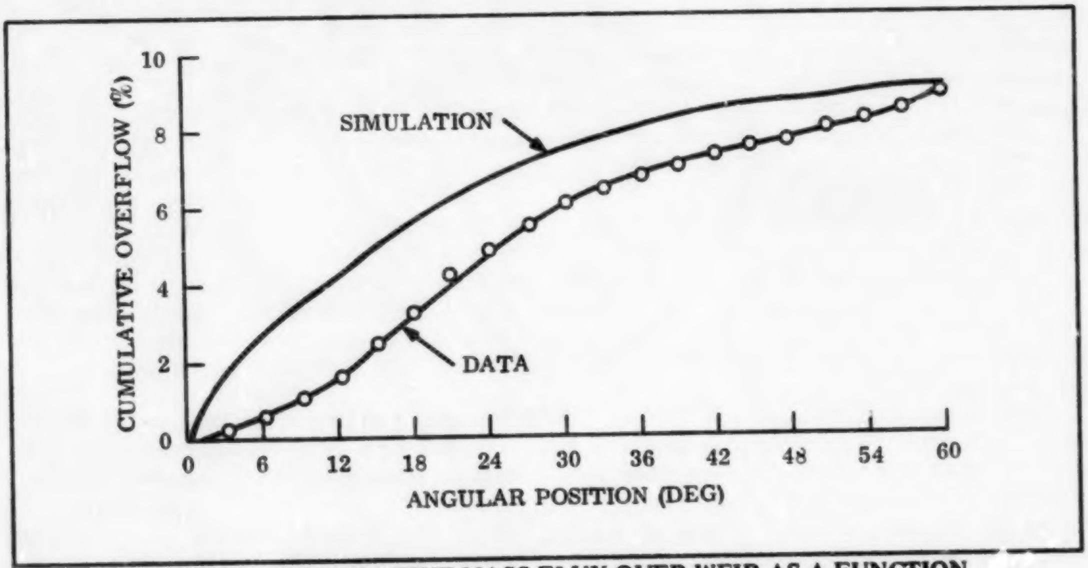

FIGURE 89 CUMULATIVE MASS FLUX OVER WEIR AS A FUNCTION OF ANGULAR POSITION

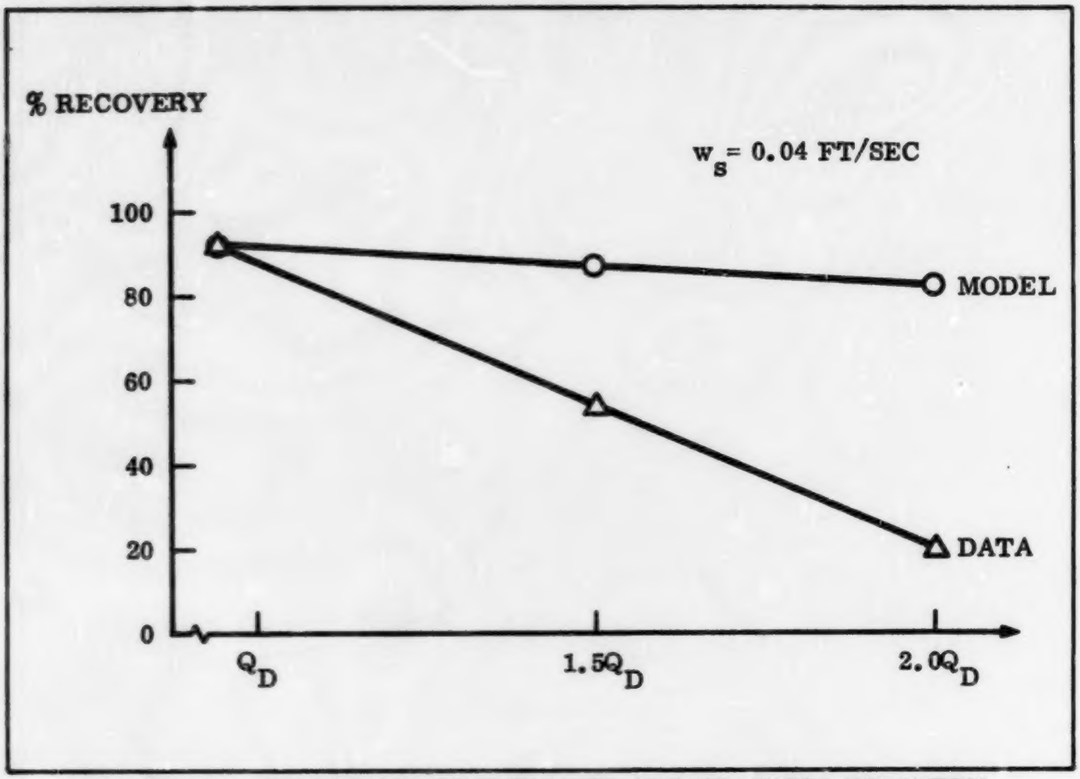

FIGURE 90 COMPARISON OF PREDICTED AND MEASURED RECOVERY EFFICIENCIES AT DISCHARGES GREATER THAN THE DESIGN VALUE 0.85 M^3/SEC (Q_D = 30 cfs)

diffusivity was adjusted to give the correct total amount of material discharge over the weir for the nominal case, as indicated in Figure 89.

Figure 90, Comparison of Predicted and Measured Recovery Efficiencies at Discharges Greater than the Design Value Q_D = 0.85 m^3/sec, (30 cfs) shows the predicted and measured recovery efficiencies at flow rates of 1.5 and two times the design flow rate of 0.85 m^3/sec (30 cfs). It is apparent that the computer simulation considerably underestimates the drop in recovery at the higher flows.

This is evidently the result of the poor representation of the lateral discharge, which becomes more critical as the flow rate is increased. At these high flows, large values of the radial velocity, *u*, are induced in the central region of the cross section, thereby sweeping a substantial amount of material over the weir. The present method for assigning the weir-induced cross-flow velocities, *u* and *w*, does not adequately account for these large cross-flows. Instead, most of the weir flow is withdrawn from the upper right-hand area of the cross section, where the concentration is lower, resulting in an under-estimate of the lost material.

At flow rates lower than the design discharge, the computer simulation should be substantially more accurate because the weir-induced cross-flows are then relatively less significant than the helical motion.

Calculated Results for Various Conditions

The computer model was exercised over a range of settling velocities and flow rates, to produce the parametric curves shown in Figure 91, Predicted Separation Efficiency Versus Settling Velocity at Several Flow Rates. These results show improvements in

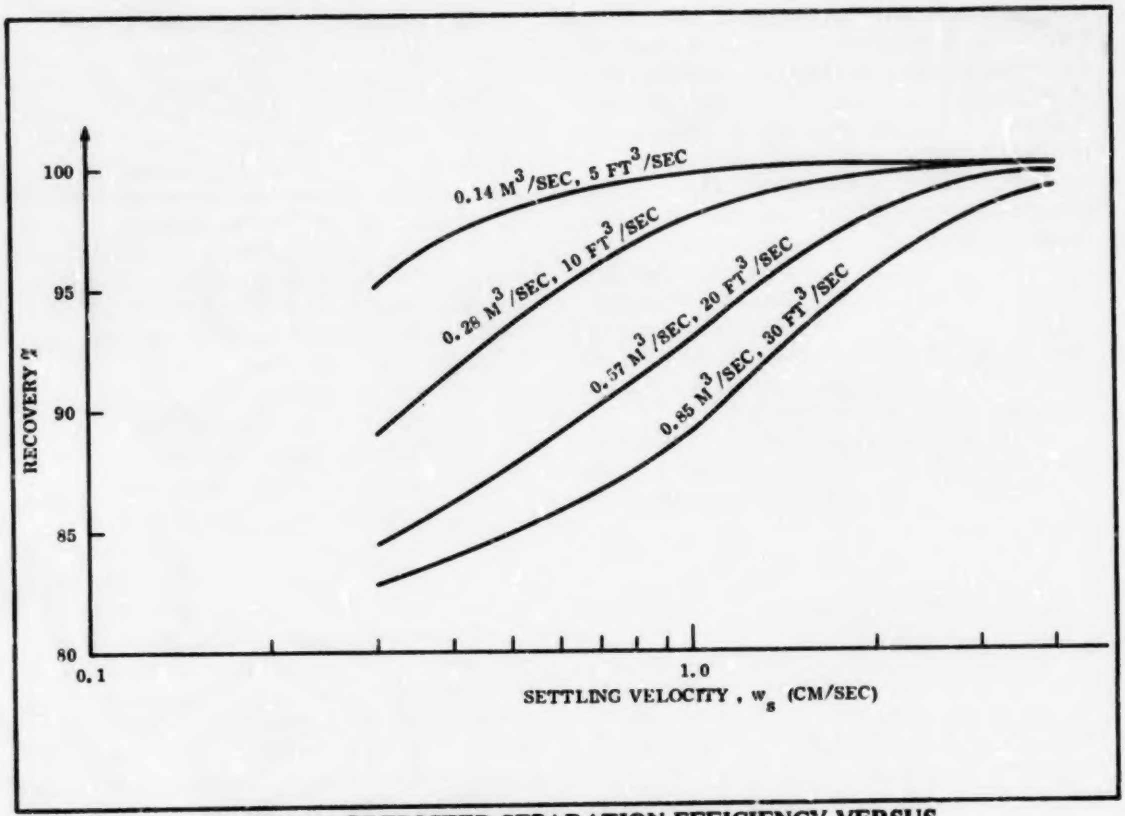

FIGURE 91 PREDICTED SEPARATION EFFICIENCY VERSUS SETTLING VELOCITY AT SEVERAL FLOW RATES

the recovery efficiency as the settling velocity is increased and the flow rate is reduced. Results for flow rates larger than the design discharge of 0.85 m^3/sec (30 cfs) are not shown because the model does not give reliable results at large flow rates, as explained in the preceding section.

An attempt was made to reduce the parametric curves in Figure 91 to a single-performance curve, through the use of an appropriate correlation. As has been noted, a significant parameter derived from the analysis for straight channels is the non-dimensional function, ϕ, defined in Equation (136):

$$\phi = \frac{w_s{}^2 \tau}{\epsilon} \quad ,$$

in which τ is the retention time.

$$\tau = \frac{L A_s}{Q_w} \quad ,$$

where

L is the arc length, A_s is the surface area, and Qw is the weir flow. Substituting for ϵ from Equation (132), and noting that $Qw = \bar{V}.A^c$ where A^c is the cross-sectional area:

$$\phi = \frac{w_s^2 \; L \; A_s}{\bar{V} \; A_c} \left(\frac{6}{k} \right) \quad \frac{1}{\bar{h} \; \bar{v} \sqrt{f/8}} \qquad (153)$$

For a fixed geometry, Equation (153) suggests that the performance should vary with the ratio of $w_s/\bar{V}$, which is the same behavior predicted from the non-dimensional settling parameter:

$$\phi = \frac{w_s \; A_s}{Q} \qquad (154)$$

Equation (154) was used successfully to correlate the results of the swirl concentrator tests.[8] This correlation also works for the present case, but only if the non-dimensional inlet concentration distribution is used. Under these conditions, the downstream development of the vertical concentration distribution – and hence the recovery efficiency – is basically a balance between the settling velocity and eddy diffusivity, as implied in the use of Equation (153) or (154). However, because of the long inlet transition section, significant changes in the initial concentration profile are expected as the inlet velocity or the settling velocity is varied. When these changes are incorporated, correlation of the results with either Equation (153) or (154) no longer results in a single universal curve.

A further important point is that in the swirl concentrator study,[8] Equation (154) was shown to represent the upper limit on recovery efficiency, ϵ, so that:

$$\epsilon \leqslant \frac{w_s A_s}{Q} \quad (155)$$

In the present case, this result is not applicable, and efficiencies greater than indicated by Equation (155) can result, especially at low flow rates and high settling velocities. The reason for this is that the inlet transition section also functions as a settling chamber under these conditions.

Additional numerical experiments were conducted to determine the importance of the bend radius on the performance of the helical separator. Using the same cross section, the outer radius of 17.4 m (57 ft) was increased by factors of two and ten. For these runs, the weir length was maintained constant by reducing the total angle of the bend, Θm, to 30° and 6° for these two cases, respectively. The results of these calculations for the design flow rate of $0.85 m^3$/sec (31.1 cfs) are summarized in Table 11, Recovery Efficiency at Various Bend Radii.

TABLE 11
RECOVERY EFFICIENCY AT VARIOUS BEND RADII

Radius (Initial Radius)	Recovery Efficiency
1	91%
2	89%
3	82%

These results show significant decreases in performance efficiency as the bend radius becomes larger. The decrease in recovery is a direct result of the reduced helical motion present in these configurations, since the other parameters were maintained constant.

Design techniques have been summarized in Section III.

NOMENCLATURE

A	Area; also constant used in one-dimensional flow solution
a	Channel width
B	Constant used in one-dimensional flow solution
B_1	Depth of scumboard below weir (Fig. 5)
B_2	Overflow height (Fig. 5)
C	Particle concentration
ϵ	Efficiency
$\underline{F}$	Froude number
$\vec{F}$	Particle flux vector
f	Darcy friction factor
g	Acceleration due to gravity
H	Head loss through orifice
h_a	$h(r)$ intercept (Eq. 22)
h_b	$h(r)$ slope (Eq. 23)
h_1	Channel maximum depth
h_2	Channel minimum depth
$h(r)$	Channel depth as a function of radius
k	von Karman constant
L	Weir length
n	Manning coefficient
$\vec{n}$	Vector normal to channel wall
P	Pressure
q	Lateral discharge
Q_o	Inflow rate
Q_s	Sludge withdrawal rate
R	Transformed coordinate r
r	Cylindrical radius coordinate
r_1	Channel inner radius
r_2	Channel outer radius
S	Scale factor
t	Time
U_o	Flow velocity at overflow
u	Radial velocity component

$\vec{V}$	Velocity vector
v	Longitudinal velocity component
V_f	Friction velocity
$\vec{V}_p$	Particle velocity vector
w	Vertical velocity component
w_e	Equivalent settling velocity
w_s	Settling velocity
Y	Vertical height above channel bottom
u_o	Scale length related to the roughness height
z	Cylindrical vertical coordinate
ZO	Fluid depth over the weir
Zr	Z/r
Zz	Z/z
ΔR	Increment in R
ΔZ	Increment in Z
$\Delta \Theta$	Increment in Θ
ζ	Fluid surface elevation
Θ	Transformed coordinate Θ
θ	Cylindrical angular coordinate
Θ_m	Channel angle maximum
ρ	Density
τ	Retention time
ρ_o	Bottom shear stress

REFERENCES

1. **T. M. Prus-Chacinski**, "Patterns of Motion in Open-Channel Bends," *Union of Geodesy and Geophysics*, Vol. 10, 9A, 1954, pp 311-318; also *Proceedings, Institute of Water Engineering, London*, Vol. 10, Aug. 1956, pp 420-426.
2. **T. M. Prus-Chacinski, and J. W. Wielogorski**, "Secondary Motion Applied to Storm Sewage Overflows," Symposium on Storm Sewage Overflows, Institute of Civil Engineers, London, 1967.
3. **J. G. Lloyd**, "Report on the Model Tests of the Nantwich Storm Sewage Spiral-Flow Separator 5/14B," Unpublished report by Mersey and Weaver River Authority, Warrington, CIRIA, London.
4. **J. A. Fox, and D. J. Ball**, "The Analysis of Secondary Flow in Bends in Open Channels," *Proceedings, Institute of Civil Engineering*, London, Vol. 39, March 1968, pp 467-477.
5. **V. T. Chow**, Open Channel Hydraulics, McGraw-Hill Book Company, New York (1959), p 200.
6. **W. E. Dobbins**, "Effect of Turbulence on Sedimentation," *ASCE Transcript*, Vol. 109, 1944, pp 629-656.
7. **T. R. Camp**, "Discussion of 'Effect of Turbulence on Sedimentation' by W. E. Dobbins," *ASCE Transcript*, Vol. 109, 1944, pp 660-667
8. **R. R. Boericke, et al**, "Mathematical Model of the Swirl Concentrator as Applied to Primary Separation of Sewage and Combined Sewer Discharges," Draft report submitted to American Public Works Association, by General Electric Co., June 15, 1974.
9. **R. J. Dalrymple, et al**, "Physical and Settling Characteristics of Particulates in Storm and Sanitary Wastewater," U.S. EPA Report No. EPA-670/2-75-011.

APPENDIX C
BACKGROUND INFORMATION ON THE HELICAL BEND

Report of C. H. Dobbie and Partners
by Dr. Prus-Chacinski

Experiments on the bends of open channels during the last 20 years have narrowed very considerably "the band of uncertainty." Prior to the time the series of experiments carried out at the Imperial College in London between 1950 and 1956[1,16,18] and the Russian experiments carried out about the same time[6,7,13] were completed, almost no information was available on this hydraulic phenomenon. Interest in the research on the bends of open channels has been revived in recent years and the experiments carried out in Karlsruhe are of particular interest.[2,3,14]

"The band of uncertainty" is however still considerable. The Russian studies and the most recent German studies were oriented towards the erosion in the bends of natural rivers and, therefore, the ratio of depth to width not much less than unity was experimentally investigated only in the Imperial College studies, and later by the studies oriented towards storm-sewage overflows.[19,20] Of interest have been recent experiments on stratified flow[5] where the ratio of depth-to-width was unity. What to date has not been achieved is a complete investigaion of the series of bends with different ratios of width-to-radius and with varying ratio of depth-to-width. The Russian studies are perhaps more complete in this respect than any others, but for deep, small channels their results are not well documented.

Considering the form of cross section and the nature of previous hydraulic bend studies, it would seem that virtually all forms of simple cross sections were investigated with the exception of the cross section with the deepest part at the inside bend – the basic form investigated by this (APWA) project. Therefore, the present study, apart from its value with regard to the design of combined sewer overflows, will also fill at least one gap in existing information on this subject.

Experimental or mathematical formulae which would describe the pattern of helical motion and its strength is open to speculation. In a small, smooth rectangular channel the expression which describes accurately the value of the bed angle for the fully-developed helical flow is one expressed by Wadekar[1] as:

$$\tan \alpha_0 = 25.4(^{d}/_{r_c})^{1/2}/R_e - C \qquad (1)$$

where "C" depends on the value of the secondary depth, that is the depth where the transverse velocity is nil; i.e., where $\alpha = 0$. The writer's equation:

$$\tan \alpha_0 = K^{W/r_c}\, R_e^{\,1/6} \qquad (2)$$

is a "blanket" expression which seems to provide a reasonable approximation for smooth channels in a wide range of depth-to-width ratio and of different cross sections. It is very likely that the same formula written in the form:

$$\tan \alpha_0 = K_1^{\,Wf/r_c} \qquad (3)$$

where "f" is the friction factor, may be the best approximation which would also cover rough channels. This has not yet been established by any experiments. The Russian approximation[6]:

$$\tan \alpha_0 = 11^{d/r_c} \qquad (4)$$

may be valid for the natural channels; again, it is a "blanket" expression covering many cross sections but mostly with small depth-to-width ratio. The Russian formula certainly overestimates the value of "α_0" in smooth laboratory channels. The writer has observed, however, during re-examination of his own experimental data[18] that in certain cases of small rectangular channel bends, where the bed was rough and "Re" reasonably large, the

Russian formula is a good approximation. It should be added that the Russian formula (4) can be easily derived from either formula (2) or (3): W = B + 2d. In shallow, wide channels, the influence of "Re" or "f" will be small, and as "B" (width) will tend to be constant, it is obvious that formula (4) is a "blanket" variation of formula (2) or (3).

Because the subject of helical flow is still not very well known, care must be practiced in accepting the published results of experiments and, particularly, of their interpretation. For example, it is difficult to accept without further study the helix pattern in the stratified flow at very low "Re," as reported in reference 5, Mode A. This applies, as well, to the statement in reference 2 and reference 10 that the strength of helical motion depends only on the ratio of depth-to-width. Obviously it must also depend on the ratio of width-to-central radius and on the resistance to flow. In certain cases control of the entry to the bend may be suspected, resulting in unacceptable experimental results. This is difficult to establish in some published references. A mathematical analysis has been attempted[1,6,7,9,12,13] but none of the results so far achieved seem to be of much help to the practical design. Recent studies on turbulence[21] by Yalin would seem to demonstrate the origin of the existence of helical motion in straight channels. The existence of helical multicellular flow in straight channels has been reported in several references, not quoted here, for a long time. Therefore, there has been some progress in the mathematical analysis. On the other hand, the general information on the behaviour of liquids, and particularly of water, at the molecular level, obviously most important in the boundary layers phenomena, is still, to say the least, incomplete. The recent opinions of physicists with regard to the present progress in this direction are rather pessimistic.[22]

The Main Overflow Chamber

a) The shape of the main chamber with the deepest part at the inside wall is a novelty, and to the writer's knowledge this shape has never been investigated. Some Russian studies included trapezoidal and triangular channels but, because the research was oriented towards the meanders of natural rivers, the deepest part was always at the outside bend. The triangular channel investigated by the writer and described in his PhD thesis[18] was also deepest at the outside wall.

b) The reasons for adopting the novel shape are as follows: It has been found by Wadekar[1] and confirmed by recent studies carried out under Professor E. Mosonyi at the University of Karlsruhe in Germany[2,3] that in a single bend the line of the maximum velocity which at the entry to a curved channel is at the inside wall, remains there only up to about 40 degrees to 60 degrees of the bend. Further, it crosses the channel and remains at the outside wall up to 180 degrees of the bend.

To the writer's knowledge, a bend longer than 180 degrees has not yet been investigated. Moreover, the region between 40 degrees and 60 degrees of the bend is where the bottom slow water is already at the top. In the writer's opinion, this region, in fact, occurs a little further downstream, perhaps at about 80 degrees of the bend. At the same region, a second smaller helix forms at the outer wall and grows bigger along the bend downstream. This is now firmly established, although there is still controversy with regard to the ratio of width-to-depth which may have an influence on the formation of the second helix.[2] In any case, at a region around 60 degrees of the bend the motion changes from that of a free vortex to a composite vortex. In the proposed novel shape of cross section, the line of maximum velocity will be kept at the inside wall for a greater length of the bend and so the upturning of the slow bottom water will occur further downstream. Therefore, the general condition of helical flow should be stable for a longer distance along the bend.

c) The relative strength of helical flow was approximated by the writer as

$$S = 10 \tan \alpha_0 \ \%$$

where $S = q_s / q$ or the ratio of the transverse unit discharge to the forward unit discharge and α_0 is the bottom angle of flow at the center line of the rectangular curved channel. The unit discharge is the discharge per unit width at the center line of the channel.

The above-mentioned recent German work carried out under Professor Mosonyi (Ref. 3) has confirmed the writer's approximation, except that S was integrated across the channel and therefore Mosonyi's S is only about 50 percent of the writer's S. Of course, α_0 changes appreciably across the bed. Also the position of the secondary depth, where the flow is purely circumferential, is not constant across the bed. In the proposed section, the mean value of α_0 should be slightly greater than the same value for a rectangular channel; but without experimental evidence it is not possible to predict the probable value. An attempt can be made of an estimate based on the approximation to a rectangular channel. Here the writer's expression for a rectangular channel may be applicable:

$$\tan \alpha_0 = 17.4 \quad W/r_C(R_e{}^{1/4}) \tag{5}$$

It is an open question as to what model scale should be applied in this kind of research as obviously neither Froudian nor Reynolds scales are applicable. A practical way of solving this difficulty is to apply in the model the same velocity as would be expected in a prototype. This has been established in the research on vortices. In this case velocity in the overflow chamber flowing full but not overflowing should be from 30.5 cm/sec (1.0 ft/sec) to about 76 cm/sec (2.5 ft/sec). Assuming the temperature of water to be about 20 degrees centigrade (68°F), the value of the Reynold number will vary between about 18,000 and about 45,000, approximately.

If the central radius is approximately 2.74 m (9.0 ft) and the wetted perimeter about 91.5 m (3.0 ft). The ratio W/r_c = 0.33, $(Re),^{1/4}$ will then vary between 108 and 146 and tan α_0 will vary between 0.55 and 0.36. Thus, the bottom angle α_0 will vary between about 29° and 20°. It is likely that in the proposed cross section, α_c will be slightly larger because the bed is sloping towards the inner wall, velocity at the outer wall will be appreciably smaller than at the inner wall, and the invert of the channel is round. However, when dip plates are inserted the bottom angle will become smaller. Therefore, the expected α_0 may very well vary between 30° and 20° at its maximum. The strength of secondary flow S, if it were a rectangular channel, would be then between approximately four and five percent. A comment is necessary. The secondary depth in a rectangular channel is about 0.3 of the total depth if the gradient of the transverse velocity is steep. If only the bottom half of the secondary depth is considered, then S in the bottom half will be very much greater and could be as much as 12 percent to 15 percent of the forward discharge. This should be sufficient to push the bottom bed load towards the inner wall. It will be necessary to establish the best position and the best length of the overflow weir and this is, of course, a purpose of the model study.

d) The adopted ratio for central radius-to-width was approximately 6.5 only because much research was carried out with the curved channels of a similar ratio. In addition, this type of curvature may be convenient in the practical design.

It should be added here that, to the writer's knowledge, there has been no systematic research which would vary the radius, the width and the depth in a really satisfactory manner; hence, the gaps in the present information are substantial. This should not affect unduly the proposed model.

e) There is a large volume of information with regard to the position and the depth of dip plates, or scum boards, (Reference 4 and many others). For this model the writer suggests the distance of about 3.81 cm (1.5 in.) from the wall and the "dip" depth of about 1.89 cm (0.75 in). It is very likely that the suggested distance from the wall and the "dip" depth must be increased. This depends on the relative importance of the floating material penetrating under the dip plates. The floating material is not very polluting but it is visually harmful.

f) The length of the bend has been recommended as 120 degrees but not less than 90 degrees. Ninety degrees is sufficient for the simple model but 120 degrees may be useful for a different type of overflow which will be described later.

The Inlet

a) The inlet as now adopted is an open channel transition 3.04 m (10 ft) long based on an idea of a long diffuser of five degrees. In the suggested design the open channel diffuser is followed by 1.52 m (5 ft) length of open channel of the same cross section as the main overflow chamber.

b) To the writer's knowledge the problem of stratification in storm sewage has never been properly investigated. The solids in storm water are seldom greater than 2,000 mg/l; the normal content is around 300 to 600 mg/l, or even less. BOD and ammonia are linked to the solids in a very complex manner. If the velocity in the incoming sewer is around 1.82 m/sec (6 ft/sec) it is probably not possible to say with any certainty whether the flow is stratified or not; this will depend on the content of solids and also on their size. In addition, there is a problem of flocculation; in fact, as far as the writer knows, the subject is still obscure. However, with a high content of solids it would be surprising if there were no stratification.

c) The problem of *waves* of discharge is further complicated by the well-known fact that storm discharge is seldom uniform. It occurs in the *waves* of high discharge lasting five to ten minutes, which may be followed by reasonably steady conditions of flow. Often one incident of overflow demonstrates two or even three *waves*. This means that the hydrograph of storm runoff may be quite complex. In long sewers the *waves* of the runoff are attenuated, but never completely. The result of these conditions is that the content of solids is extremely variable because each *wave* may contain more solids than in steady flow.

d) The intended purpose of the inlet is to decelerate the flow in a uniform manner and to direct the region of the maximum velocity to the inner wall of the main overflow chamber. The straight section downstream should result in reasonably steady conditions with regard to any stratification.

e) The helical flow in open channel bends with stratified liquids adds a further complexity which has been described in Reference 5. It has been found that the helical flow in the bends of open channels with two stratified liquids occurs in at least three modes:

1. If stratification is complete and velocity is low the heavy bottom liquid is almost free of helical motion and behaves as a *false bottom*. There is then no helical motion in the denser liquid but the helix in the lighter liquid was observed to be of the opposite nature than in the normal flow, that is, the top direction was towards the inner wall. Such conditions may not be bad for an overflow but probably they seldom occur, if ever, in sewers. The model observations carried out by the Mersey River Authority Hydraulic Laboratory have demonstrated good results with salty water at the bottom of the overflow chamber but the Reynolds number in the above experiments was always greater than Re = 3500, as quoted in Reference 5 for mode 1.
2. If the stratification is prominent and the velocity is greater, the heavier bottom liquid forms its own helix which mixes only to a small degree with the top helix of the lighter liquid. The heavy liquid tends to remain at the inner wall for at least 90 degrees of the bend. It is probable that such conditions occur in the stormwater curved overflows if the solids content is sufficiently large. The lighter liquid may demonstrate the presence of two helices after about 60 degrees of the bend. It is hoped that the model may provide some information on this subject.
3. If the stratification is less prominent or if the velocity is still higher, both liquids will mix to a large degree and only one helix occurs as in an ordinary non-stratified flow. But even then the heavier liquid is at the inner wall for at least 45 degrees of the bend. This case is probably common in the curved stormwater overflows if the content of the solids is average.

f) It is now an open question whether a curved overflow should be designed for conditions (2) or (3). The design for conditions (3) would require a short side weir starting at about five degrees of the bend and finishing at about 55 degrees of the bend. Design for conditions (2) would result in a longer weir, up to 70 degrees or 80 degrees of the bend. Again, experiments with the model should result in a reasonable compromise recommendation for the design. The model investigated in Reference 5 was small; the highest Reynolds number was only 9200. Therefore, the question of stratification is still far from being clarified.

g) The behavior of a model with steady flow will not reproduce the effect of the discharge *waves*. Such *waves* will invariably disturb the helical motion and they will decrease the efficiency of the overflow. However, this problem is common to all the types of stormwater overflow.

h) In view of the above discussion it is possible that the proposed novel cross section of the main overflow chamber may produce better results than any other cross section; this was an additional reason for the proposed novel cross section. But it is evident that the symmetrical cross section and the cross section deepest at the inner wall should also be investigated.

The Outlet

In British practice, a stormwater overflow passes to the treatment works 6 to 7 DWF, or sometimes even 8 DWF. It is, then, a relatively simple matter to design an outflow chamber in which the floating debris goes over the end weir and the outflow is controlled by the outflow sewer of such dimensions as are dictated by the downstream conditions. However, even with 7 DWF going to treatment, variations in the outflow discharge are observed, which are probably caused by floating material accumulating in the outlet chamber and temporarily decreasing the capacity of the outlet sewer. This, in turn, results in temporarily larger overflows. This effect is not very large but it does exist. The requirement of the APWA Research Foundation is to pass 3 DWF to the treatment works, and in such conditions the effect may be more serious. The design of the outflow chamber depends much on the dimensions of the incoming sewer; for large sewers it will be easier than for small sewers.

Alternative Design

The alternative design represented in Figure 92, Alternative Design for Future Investigation, may be an improvement as compared with a simple overflow. It would seem to be possible, practical, effective, and not particularly expensive.

The general concept is that, in addition to the main chamber, the side weir and the end outflow similar to those described already, three side pipes should be installed at the inner wall of the main chamber. These pipes are connected into a side sewer of small diameter which discharges into an end manhole and which is closed by a flapgate. The smallest flapgates obtainable in the United Kingdom are 7.62 cm (3 in.) in diameter.

A rough examination of discharges demonstrates that such a design will work safely if the inlet pipe is not smaller than about 60.5 cm (2.0 ft) diameter. Then the draw-off small sewer would be about 10.18 cm (4 in.) diameter and the off-take pipes could be either 7.6 or 10.8 cm (3 or 4 in.) diameter. The flapgate should then be balanced in such a way that it would open only if the inflow was almost 3 DWF, say 2.5 DWF. This would prevent the side pipes from silting.

The actual design may be different than that shown. For example, it would help if the invert of the end or foul sewer passing to the treatment works were approximately 15,24 cm (6 in.) lower than the invert of the main overflow chamber. Also, the small diameter side sewer could be straight, discharging directly without a flapgate.

The main factor in the above alternative is to avoid the silting up of the side pipes and of the small diameter collecting sewer. The flapgate should be balanced in such a way that the velocity in the side pipes is not smaller than 60.5 cm/sec (2 ft/sec). The alternative suggested in Figure 00 should be easier to design for large than for small inlet sewers. For example, if the inlet sewer were

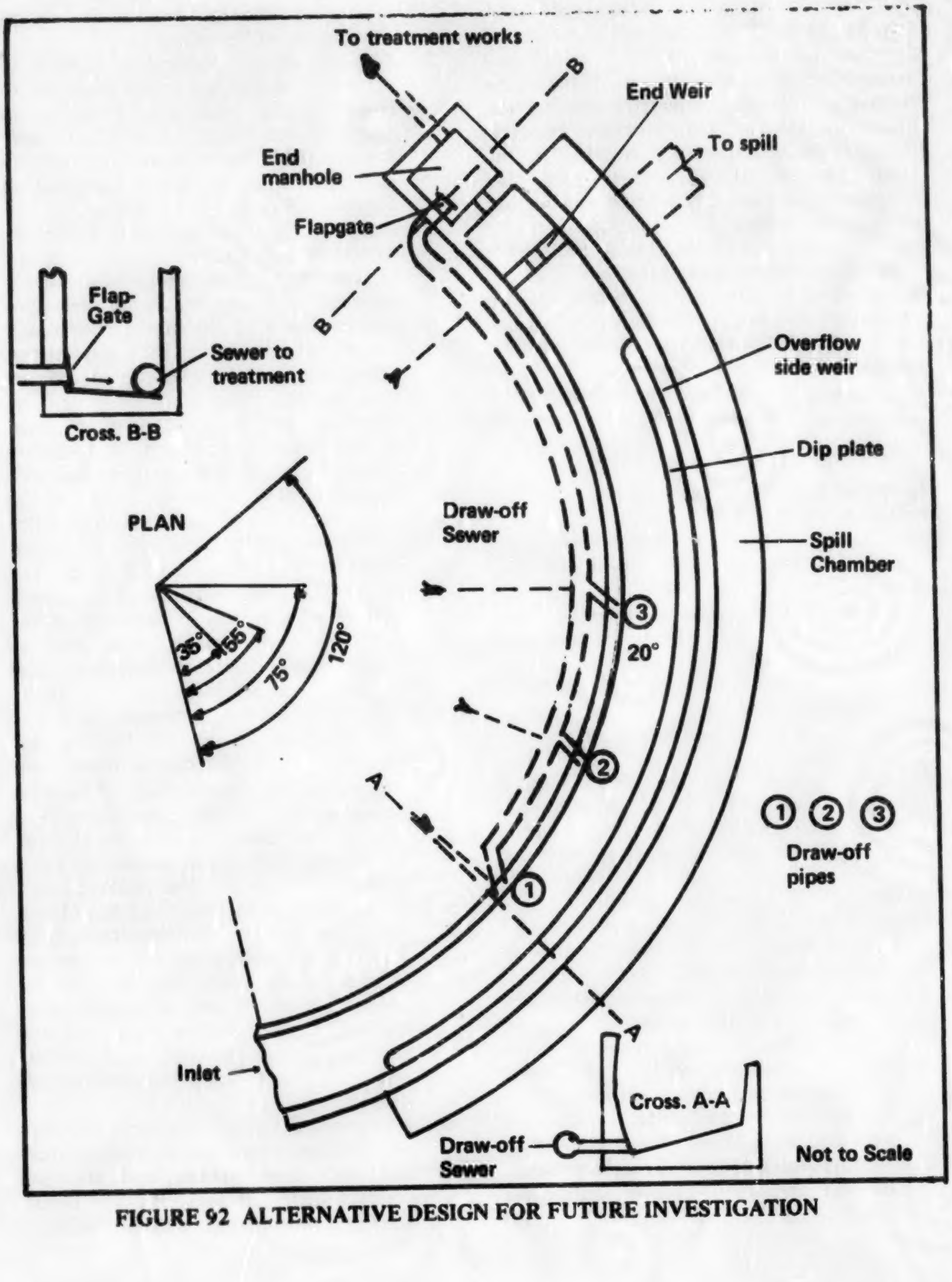

FIGURE 92 ALTERNATIVE DESIGN FOR FUTURE INVESTIGATION

90.5 cm (3.0 ft) diameter the draw-off sewer would be about 20.32 cm (8 in.) diameter and the side pipes could be 12.7 cm (5 in.) diameter. It is possible that with the above alternative, a simple symmetrical cross section similar to that in the Nantwich overflow might produce satisfactory results, but the sharp edges should be eliminated. It is also possible that the velocity in the main chamber could be increased.

It is recommended that the above possibilities should be investigated. It might be sufficient to have only two side pipes. The position of the side pipes and the position and the length of the side weir should also be investigated. The side pipes would discharge directly to the side spill channel but some means for collecting samples should be provided.

Review of Laboratory Techniques Known to the Writer

The list below is given in approximate order of time when the reference was published.

1. Shukry[15] has used the Pilot-sphere. Some of his results are open to doubt because it is evident that there was no proper control of the entry to the channel bend.
2. Malouf[16] used only the black dye – Process Black – and the local velocity was not measured.
3. Prus-Chacinski[17,18] used Process Black paint, small lighted floats, and the nylon threads for direction measurements, using an accurate protractor. Velocity was measured by a pitometer.
4. Wadekar[1] improved greatly on the methods of (2) and (3). In addition to Process Black paint he used droplets of Meridian-unity oil (S G 1.002) as a tracer for small velocities, and polystytene sand (1 mm dia. S G 1.06) as a tracer for larger velocities. For the direction inside of the channel, nylon threads and an accurate protractor were used.

   The surface direction and velocities were measured by a sophisticated method of photographing the surface wave patterns. He was able to observe accurately the direction of flow on the walls of his rectangular channel because it was all constructed of Perspex.®
5. The Russean researches known to date[6,7,13] have used methods similar to those described under (2), (3) and (4). In addition, the density flow effects were investigated,[13] demonstrating patterns, in general, similar to those described in Reference 5 case (3).
6. Fox and Bell[8] used nylon thread as direction indicators for velocity measurement. They used a heat-transfer recorder (not described) for velocities smaller than 9.15 cm/sec 0.3 ft/sec), and a multi-propeler or current meter with an ultraviolet light recorder (not described) for larger velocities.
7. Prus-Chacinski and Wielogorski[19] used Process Black paint and an accurate protractor, plastic sand, orange colored (S G 1.00), coal dust (particle size 0.1 to 1.0 mm), and polystyrene beads (S G 1.05) for the bed patterns, and nylon thread for direction inside of the channel. The plastic sand also demonstrated the general pattern of the helix in the body of the flow. Perspex® shavings were used to observe the surface flow direction. Local velocities were not measured.
8. The Mersey River Authority, with the cooperation of C. H. Dobbie and Partners[20], used the Process Black paint and potassium permanganate. Potassium permanganate was not satisfactory. The threads were used, as already mentioned. Local velocities were measured by a mini-current meter. For surface flow tracer, plastic beads were used. In addition the density flow was investigated by injecting the salty water colored by potassium permanganate upstream of the inflow. The results were most satisfactory but only if the injection point was very near to the bed. The analysis of overflow was carried out, using the conductivity meter.
9. Macagno and Alonso[5] measured velocities and densities with a constant temperature hot-wire anemometer and electrical conductometer, respectively. The signals were processed through an IBM DACS.

10. Francis and Safari[9,10] used tracers and sophisticated photographic and lighting equipment. For laminar flow they used TELCO powder (S G 0.9) with grain size 0.1 to 0.2 mm; turbulent flow droplets (quite large) were formed by the mixture of nitrobenzene, olive oil, and water (S G 1.0). The rectangular channel had glass windows in the walls. Local velocities were not measured. It is possible that the entry to their experimental channel was not free from helical motions.
11. Mosonyi and Gotz and Siebart and Musers[2,14] used the hot-film anemometer and a fibre-wire probe for the local velocity and local direction measurements. This procedure seemed to produce excellent results.

SYMBOLS USED

r_c	central radius of the bend in a rectangular channel
R_e	Reynolds Number
C	constant dependent upon depth
K	constant to describe strength of helical flow
W	wetted perimeter
f	friction factor
α_o	bed angle of
s	strength of helical flow
q_s/q	forward unit discharge
B	width of rectangular channel
d	depth of rectangular channel

REFERENCES

Only a short list of references which introduce some new observations will be quoted below. Otherwise, a long list of references is contained in the writer's PhD Thesis and in his paper (together with Wielogorski):

Secondary motions applied to Storm Sewage Overflows
Symposium at the ICE, London, 1967

1. G. T. Wadekar, *Secondary Flow in Curved Channels*, Unpublished PhD Thesis, Imperial College, London, 1956.
2. Emil Mosonyi and Werner Gotz, *Secondary Currents in Subsequent Model Bends*, International Association for Hydraulic Research, International Symposium on River Mechanics, Bangkok. January 1973.
3. E. Mosonyi and G. Meder, *Effects of Scale Distortion on Flow Properties in Model Meanders*, The Rehbock Laboratory for River Improvement, University of Karlsruhe, Germany, 1973.
4. P. Ackers, *A Theoretical Consideration of Side Weirs as Storm-Water Overflows*, Proceedings, Institute of Civil Engineering, London, Febraury 1957.
5. E. O. Macagno and C. V. Alonso, *Two-layer Density-Stratified Flow in an Open Channel Bend*, International Association for Hydraulic Research, Proceedings of 14th Congress IAHR, Paris, 1971
6. I. L. Rozovskii, *Flow of Water in Bends of Open Channel*, (Translated from Russian), The National Science Foundation, Washington, D. C., 1967 (The Russian original, Kiev, 1957).
7. A. K. Ananyan, *Fluid Flow in Bends of Conduits*, (Translated from Russian), Israel Programme for Scientific Translations, Jerusalem, 1965. (Russian original, Erevan, 1957).
8. J. A. Fox and D. J. Bell, *The Analysis of Secondary Flow in Bends in Open Channels*, Proceedings, ICE, London, March 1968.
9. J. R. D. Francis and A. F. Asfari, *Velocity Distributions in Wide, Curved Open Channel Flows*, Journal of Hyraulic Research No. 1, 1971.
10. J. R. D. Francis and A. F. Asfari, *Visualisation of Spiral Motion in Curved Open Channels of Large Width*, Nature, London, February,1970.
11. Yoshio Muramoto, *Secondary Flows in Curved Open Channels*, International Association for Hydraulic Research, Proceedings, 12th Congress IAHR, Paris, 1967.

12. E. Mastar, *The Effect of Bend on the Distribution and Development of the Macroturbulence Intensity in Open-channel Bends*, Proceedings, 12th Congress, IAHR, September 1967.
13. A. K. Ananyan, *An Approximate Theory of Secondary Flows at the Bend of the River Course*, Proceedings, 12th Congress IAHR, September 1967.
14. W. Siebert and R. Muser, *A Method to Determine the Vectors of the Average Velocity Field in Uniform Flow*, International Association for Hydraulic Research, International Symposium on River Mechanics, Bangkok. January 1973.
15. A. Shukry, *Flow Around Bend in an Open Flume*, Proceedings, American Society of Civil Engineers, Vol. 75, No. 6, June 1949.
16. K. M. Malouf, *The Movement of Detritus in Models of River and Channel Bends*, Unpublished PhD Thesis, University of London, 1950.
17. T. M. Prus-Chacinski, *Patterns of Motion in Open-channel Bends*, Union of Geodesy and Geophysics, 1954 10. 9A 3.1-318 also: Proceedings, Institute Water Engineering, London, August 1956, 10 pp 420-426.
18. T.M. Prus-Chacinski, *The Secondary Flow in a Meandering Channel*, Unpublished, PhD Thesis, University of London, 1955.
19. T.M. Prus-Chacinski and J.W. Wielogorski, *Secondary Motion Applied to Storm Sewage Overflows*, Symposium on Storm Sewage Overflows, Institute of Civil Engineers. London. 1967.
20. Mersey and Weaver River Authority under J. G. Lloyd, Chief Engineer with the cooperation of C. H. Dobbie and Partners, *Report on the Model Tests of the Nantwich Sewage Spiral Flow Separator (5/14B)*, Warrington, Lancashire, 1968, unpublished. Copies are with Mersey River Authority, Warrington, CIRIA, London, and C. H. Dobbie and Partners.
21. M.S. Yalin, *On the Formation of Dunes and Meanders*, 14th Congress of IAHR, September 1971.
22. J. Woodhead-Galloway, *Towards the Structure of Liquids*, New Scientist, London, 16th November 1972.
23. H. B. Fisher, *The Effect of Bends on Dispersion in Streams*, (University of California) Water Research, April 1969.
24. B. S. Thandaverswara and K. Seelharamiah, *Some Characteristics of Flow Arovnd 90° Open Channel Bend*, (Indian Institute of Science, Bangalore) Huile Blanche 26th January and September 1971.
25. L. Baviski and N. Owarkanali *Some Aspects of Sub-critical Flow in a 90° Open Channel Bend*, (Indian Institute of Technology, Bombay) paper No. 9, July 1970.
26. C. H. Yen and B. C. Yen, *Water Surface Configuration in Channel Bends*, J. Asce 97 HY 2, February 1971.
27. B. S. Thandaverswara and K. Seelharamiah, *Energy Loss in Open Channel 90° Bend*, (Indian Institute of Science) 4th Australasia Conference of Hydrology and Fl. Mech. (Monash University) November-December 1971.
28. E. Masian and V. Hutka, *Contribution to the Distribution of the Turbulent Exchange Coefficient Along the Waterstream Depth in Open Channel (Flow in Curved Section)*, Vodosoph, Prague, (In Czech language), March 1972.
29. A. I. deVriend, *Theory of the Viscous Flow in Curved Shallow Channels*, University of Technology in Delft, Department of Civil Engineering, 1972.
30. S. Fukooka and W.W. Sayru, *Longitudinal Dispersion in Sinuous Channels*, J. Asce HY 1, January 1973.
31. E. Massar, *Correlation Between the Velocities in Various Points of Water Flow in Straight and Curved Sections of Open Channels*, Slovak Ac. of Sc. Bratislava, Vodokospoh, (in Czech language) February 1968.